Cinématique, déformation et mise en place des laves

Sébastien Loock

N° d'Ordre : D.U. 1849

UNIVERSITÉ BLAISE PASCAL

U.F.R. Sciences et Technologies

ÉCOLE DOCTORALE DES SCIENCES FONDAMENTALES N°559

THÈSE

présentée pour obtenir le grade de

DOCTEUR D'UNIVERSITÉ

Spécialité : Volcanologie

par

Sébastien LOOCK

Diplômé de Master Recherches

Cinématique, déformation et mise en place des laves

Kinematic, deformation and lava emplacement

Soutenue publiquement le 05/09/2008 devant la commission d'examen composée de :

Jean-François LÉNAT	Université Blaise Pascal, Clermont Ferrand	Président
Chris KILBURN	Benfield UCL Hazard Research Centre, London, UK	Rapporteur
Hervé DIOT	Université de la Rochelle, La Rochelle	Rapporteur
Harry PINKERTON	Lancaster University, Lancaster, UK	Examinateur
Jérôme BASCOU	Université Jean Monnet, Saint Étienne	Examinateur
Benjamin VAN WYK DE VRIES	Université Blaise Pascal, Clermont Ferrand	Directeur de thèse

A ma Maman,

ABSTRACT

Kinematics and deformation in lava flows are addressed using three different approaches: descriptive volcanology, petrophysics and magnetism.

Pāhoehoe and ‘a‘ā are two terms used in volcanology, first used to differentiate lava surfaces, but then to describe two different emplacement styles. Pāhoehoe lavas emplace themselves as a lobe stacks that may coalesce. In contrast, ‘a‘ā lavas emplace en masse and form upper clinker by rupture crust of their. This crust can reach the flow base by roll-over caterpillar motion. As they have different modes of emplacement, they contain in their interiors several diagnostic features that make it possible to discriminate the type in old lava flows where surfaces are missing or covered. ‘A‘ā flows present clinker and highly deformed vesicles, whereas pāheohoe flows display slightly deformed vesicles, lobe stacks and particular zonations in vesicles and phenocrysts. These discriminatory characteristics allowed the attribution of lava types to several old lava flows. This has provided constraints on emplacement histories, particularly in the French Massif Central where some pahoehoe flows have been clearly identified.

Breccia associated with lava flows has been studied in detail, both in the field and in thin section. Detailed textural analysis, especially with scanning electron microscope (SEM) has revealed petrophysical information on breccia formation. These breccias include clinker (previously considered to be exclusive to ‘a‘ā lavas), fault cataclasites and peperites. The upper clinker are typical of ‘a‘ā flows, but lower clinker-like breccia can also develop in pāhoehoe flows according phreatomagmatism, or basal / lateral shearing. Peperites have phreatomagmatic features with more explosive textural patterns than clinkers. These breccia studies have revealed that phreatomagmatism is quite common during lava flow emplacement: the probability that a lava flow on its downslope movement encounters a water-saturated basement is quite high. This indicates that phreatomagmatic hazards associated with lava flows could be locally very significant.

A methodology for the correct use of Anisotropy of Magnetic Susceptibility (AMS) is proposed. This requires the determination of the AMS carriers and the AMS fabric time acquisition compared to the microlite fabric. This methodology has been applied to two lava flows to check the feasibility. The results show that AMS can be used confidently, with the methodology proposed. The results obtained are interpreted in terms of different emplacement scenarios. Interpretations include the establishment of a vertical qualitative velocity profile and the detailed reconstruction of the last emplacement stage of two lava flows.

A further improvement in understanding lava flow emplacement, with attendant hazard and aquifer knowledge improvement will be possible by continuing the investigation on the three topics on a broader range of lava flows, different compositions and environments.

RÉSUMÉ ÉTENDU

EN FRANÇAIS

INTRODUCTION

La cinématique étudie le mouvement des corps alors que la déformation correspond aux changements de forme ou de dimension produits dans un corps sous l'effet d'une contrainte. Ces deux processus sont directement liés et leurs études nous permettent de mieux comprendre la mise en place des corps particuliers que sont les coulées de lave.
Cette thèse est construite selon trois approches différentes qui permettent de préciser, autant que possible, les différentes caractéristiques associées à l'épanchement des laves. Ces trois approches seront traitées dans trois chapitres différents comme elles abordent des études et des méthodologies spécifiques.

CHAPITRE 1 :
DES COULÉES DE LAVE ‘A‘Ā ET PĀHOEHOE

Pāhoehoe et ‘a‘ā sont des termes hawaiiens utilisés en volcanologie moderne depuis 1953 (Macdonald) pour décrire, dans un premier temps, différentes morphologies de surface. Les coulées ‘a‘ā possèdent une surface rugueuse constituée de clinkers (ou scories) alors que les coulées pāhoehoe ont une surface lisse sans clinker. Dans un deuxième temps, cette distinction a permis de souligner l'existence de modes de mise en place différents : les coulées ‘a‘ā avancent de façon massive avec des clinkers se formant à leurs surfaces et basculant à leurs bases selon l'avancement de la chenille d'un tank, alors que les coulées pāhoehoe se forment par bourgeonnements successifs de lobes sujet à une inflation endogène.

L'attribution du terme ‘a‘ā ou pāhoehoe, significatif en terme de mise en place, est évident sur des coulées récentes où les morphologies de surface ont été préservées mais s'avère être compliquée pour des coulées anciennes comme celles du Massif Central Français à cause de l'érosion et du développement de sol masquant la surface originelle. Par conséquent, ce chapitre fait l'objet d'une synthèse bibliographique permettant d'associer aux termes ‘a‘ā et pāhoehoe des structures que l'on peut trouver à l'intérieur des coulées de lave refroidies anciennes comme récentes. Ainsi la présence de clinker, de vésicules déformées irrégulières

et l'absence de zonation en vésicules comme en phénocristaux se révèlent être typiques d'une lave ʻaʻā alors que la présence de lobes de lave, de fractures d'inflation, de vésicules sphériques à elliptiques, de mégavesicules et de tuyaux de vesicules, l'absence de clinker, et la présence d'une zonation en vésicule et en phénocristaux sont typiques d'une lave pāhoehoe.

ʻAʻā et pāhoehoe correspondant à deux modes de mises en place différents, ils correspondent ainsi à deux fluides ayant des propriétés rhéologiques différentes. Le parcours d'une lave étant assujetti à un trajet plus ou moins chaotique et à un refroidissement permanent, le taux de cisaillement ainsi que la viscosité apparente vont pouvoir évoluer et la lave pourra éventuellement passer du champ rhéologique pāhoehoe à ʻaʻā ou vice versa (Peterson & Tilling, 1980 ; Kilburn, 1981 ; Hon & al., 2003). Hon & al. (2003) ont réalisé un tel diagramme présentant l'évolution du taux de cisaillement en fonction de la viscosité apparente différenciant un champ pāhoehoe de ʻaʻā à partir de mesures effectuées sur des laves hawaiiennes. Ce diagramme a été appliqué qualitativement sur le champ de lave du Myvatn Fires émis par le volcan Krafla de 1724 à 1729 en Islande. Sur ce champ de lave, la morphologie de surface étant préservée, l'attribution ʻaʻā ou pāhoehoe est aisée. Des exemples de transitions ʻaʻā-pāhoehoe et pāhoehoe-ʼaʻā figées ont été étudiés. Les transitions ʻaʻā-pāhoehoe ont pu être expliquées en utilisant le diagramme de Hon & al. (2003) par une augmentation du taux de cisaillement le plus souvent associée à une augmentation de la pente et par une augmentation synchrone de la viscosité apparente due au refroidissement de la lave de surface. La transition pāhoehoe-ʼaʻā a, quant à elle, pu être expliquée par le bourgeonnement d'un lobe de lave à partir d'une fracture sur la coulée ʻaʻā permettant ainsi à la lave plus chaude, et donc moins visqueuse, circulant au cœur de la coulée ʻaʻā de s'épancher directement à l'air libre selon un taux de cisaillement moins important.

Les termes ʻaʻā et pāhoehoe ont ensuite été utilisés précisément dans différentes coulées du Massif Central Français afin de juger de leur applicabilité et de leur pertinence sur de telles coulées anciennes. La Chaîne des Puys se révèle être très largement dominée par des coulées de type ʻaʻā, localement connues sous le terme de *cheires*. Cependant deux coulées possédant les caractéristiques structurales communes aux coulées pāhoehoe ont été identifiées : la coulée F3 de Royat et la coulée des Grosliers.

La coulée F3 de Royat (ouest de Clermont Ferrand) ne présente pas de clinkers mais une structure en lobe, des fractures d'inflation, des vésicules elliptiques, des mégavésicules, ainsi qu'une croûte vésiculée et un enrichissement en phénocristaux en base de coulée ne laissant

aucun doute sur son appartenance au type pāhoehoe. Cette conclusion est par ailleurs corroborée de par l'existence d'un tunnel de lave à plusieurs croûtes vésiculées. L'utilisation de l'Anisotropie de Susceptibilité Magnétique (AMS) a par ailleurs révélé des directions de linéation (k_{max}) verticales à la périphérie d'un lobe de lave, témoignant ainsi de l'enregistrement de l'épisode d'inflation endogène de ce lobe.

La coulée des Grosliers (nord de Clermont Ferrand) ne présente pas de clinker à son sommet faisant penser, certes de façon moins certaine qu'à la coulée Royat F3, à une coulée de type paheohoe ou du moins à une coulée ayant une composante pāhoehoe.

D'autres coulées ont été étudiées dans le Massif Central Français et deux autres coulées pāhoehoe ont pu être mises en évidence : les coulées de Roca Neyra et de Jaujac.

La coulée de Roca Neyra (ouest d'Issoire) ne présente pas de clinker à son sommet, elle présente une undubitable accumulation de lobes de lave typique des coulées pāhoehoe.

La coulée de Jaujac (ouest d'Aubenas) ne présente aucune évidence de clinker mais a la particularité de présenter une structure en sill au sein même de sa coulée, signifiant ainsi une injection de lave plus tardive dans une lave en cours de refroidissement, ce qui est caractéristique du phénomène d'inflation commun aux coulées pāhoehoe.

Ainsi l'utilisation des données bibliographiques, accompagnée d'une expérience de terrain sur des laves récentes ont permis d'attribuer les termes ‘a‘ā ou pāhoehoe à des coulées anciennes et donc de préciser leurs modes de mise en place.

CHAPITRE 2 :
LES BRECHES ASSOCIÉES AUX COULÉES DE LAVE

Les brèches sont des roches formées par l'assemblage d'autres roches unifiées par une matrice consolidée ou non. De telles brèches peuvent être associées aux coulées de lave et, après de nombreuses études de terrain, se sont révélées être de deux natures différentes : les clinkers et les pépérites.

Les clinkers (ou scories) sont des fragments de lave associés communément aux coulées de type ‘a‘ā où ils se forment par fragmentation du toit refroidi de la coulée sous l'effet du cisaillement aux bordures (Walker, 1987 ; Hon & al., 2003). Ces clinkers se forment par

conséquent au toit de la coulée et vont pouvoir se retrouver à sa base selon le mode de déplacement de la chenille d'un tank comme évoqué plus haut.

Cependant, après l'étude de différentes coulées de lave, il s'est avéré, que des coulées de type pāhoehoe pouvaient également présenter des clinkers mais avec des morphologies différentes. Ces clinkers pāhoehoe ne peuvent pas se former par la rupture de la croûte car cette dernière est préservée sur de telles coulées et donc un autre mode de formation des clinkers doit être invoqué. Pour remédier à cette ambiguïté, des échantillons de clinkers provenant de différentes coulées 'a'ā et pāhoehoe ont été étudiés au microscope électronique à balayage (MEB) de la même manière que les études réalisées sur les cendres volcaniques (e.g. Heiken & Wohletz, 1985 ; Dellino & al., 1990 ; De Astis & al., 1997 ; Dellino & Kyriakopoulos, 2003).

Les coulées de type 'a'ā (Royat F1 et Blanzat) présentent des clinkers vésiculés confirmant bien leur formation à partir de la rupture de la croûte vésiculée. Ils présentent de grandes variations à petite échelle (centaine de microns) de l'intensité de déformation ce qui peut être relié aux grandes variations de taux de cisaillement existant dans la croûte vésiculée. Des textures diktytaxitiques similaires à celles des scories stromboliennes (Heiken & Wohletz, 1985) ont été observées et témoigne d'une fragmentation lavique. Ainsi, à partir de ces observations, nous retrouvons la façon « classique » de former les clinkers dans les coulées 'a'ā par rupture de la croûte vésiculée.

Les coulées pāhoehoe des Grosliers et de Roca Neyra ne présentent pas les textures observées dans les coulées 'a'ā mais de nombreuses particules adhérentes marneuses enlevées aux ultrasons. Ces particules témoignent de la fine fragmentation des marnes se situant sous les coulées de lave. Les fragments de lave ne présentent pas de formes irrégulières comme dans les coulées 'a'ā, mais des formes en bloc, des cassures conchoïdales ou des structures sphériques. La coulée de Roca Neyra a en outre la particularité de présenter des textures constituées par un emboîtement des microphénocristaux de plagioclase. Toutes ces figures ont déjà été rencontrées dans des dépôts phréatomagmatiques (e.g. Heiken & Wohletz, 1985 ; Dellino & al., 1990 ; De Astis & al., 1997 ; Dellino & Kyriakopoulos, 2003), par conséquent une origine phréatomagmatique a été également proposée dans le contexte des coulées de lave. En effet, en s'épanchant, une coulée de lave peut être amenée a rencontrer des terrains saturés en eau occasionnant ainsi une bréchification phréatomagmatique à sa base et ainsi générant des clinkers particuliers : des clinkers phréatomagmatiques.

Un autre type de clinkers est également présent dans la coulée de Royat F3, coulée présentant des caractéristiques pāhoehoe : des clinkers se sont formés par simple cisaillement à la base et

aux épontes de la coulée de lave générant ainsi des structures macroscopiques en écailles et des failles microscopiques.
Cette étude permet donc de montrer qu'il existe plusieurs façons de former des clinkers dans des coulées de lave de différents types. Ainsi les aquifères associées classiquement aux clinkers des coulées 'a'ā peuvent aussi se trouver dans des coulées pāhoehoe.

Les pépérites sont des brèches que l'on trouve classiquement dans les diatrèmes (racines d'édifices phréatomagmatiques), mais leurs présences ont également été révélées dans quelques coulées de lave en contexte désertique (e.g. Petry & al., 2007 ; Waichel & al., 2007). De telles brèches ont également pu être étudiées en Auvergne à Chateaugay, Pardines et Saint Gervazy dans un contexte autre que désertique. Ces coulées se sont épanchées sur un terrain marneux et présentent toutes des poches de pépérites à leurs bases. Les fragments de marne nourrissent la matrice de la brèche alors que la lave constitue l'essentiel des clastes. Ces clastes laviques présentent des figures de trempe et une analyse au MEB, comme pour les clinkers, a révélé la présence de clastes sphériques avec des cassures conchoïdales typiques du phrétaomagmatisme. Par conséquent, une origine phréatomagmatique doit être invoquée pour les laves étudiées. Comme pour la fragmentation phréatomagmatique des clinkers, ces coulées de lave ont vraisemblablement, au cours de leurs périples, rencontrées des marnes saturées en eau mais avec une teneur en eau plus importante permettant un phénomène plus explosif aboutissant à la formation des diapirs pépéritiques en base de coulée.

Ce chapitre a permis de mettre en évidence les différents phénomènes de bréchifications existants dans les coulées de lave permettant ainsi d'obtenir d'autres informations sur leur mode de mise en place et notamment sur la possibilité de rencontre d'une lave avec des terrain saturés en eau aboutissant à différentes intensités de phréatomagmatisme et donc à différents aléas associés.

CHAPITRE 3 :
L'UTILISATION DE L'ANISOTROPIE DE SUSCEPTIBILITÉ MAGNÉTIQUE (AMS) DANS LES COULÉES DE LAVE

L'Anisotropie de Susceptibilité Magnétique (ASM ou AMS en anglais) est un outil pratique, fréquemment utilisé dans les roches volcaniques pour obtenir, via des tenseurs, des informations sur la cinématique et la déformation des coulées de lave.
Cependant la relation entre le tenseur, et ses paramètres associés, avec les caractéristiques liées à la mise en place des laves n'est pas si évidente et une étude préliminaire de la fabrique magnétique s'avère nécessaire pour proposer une interprétation correcte.
Ainsi, afin d'utiliser correctement l'AMS, une méthodologie est présentée dans ce chapitre et pourra être appliquée à des contextes autres que volcaniques.
Pour savoir quelles sont les phases porteuses de l'AMS, des mesures de la température de Curie, des lames minces, des analyses chimiques des phases magnétiques ainsi que des diagrammes de FORC sont nécessaires. L'utilisation des diagrammes de FORC est préconisée vis-à-vis des diagrammes de Day & al. (1977) car ces derniers présentent un effet de somme. De cette manière, la mise en évidence de particules SD (single domain = monodomaine), tendant à biaiser la fabrique AMS (Rochette & al., 1992 ; Rochette & al., 1999) sera facilitée sur les diagrammes de FORC où l'influence de chaque particules est décelable.
Pour savoir quand est acquise la fabrique AMS, une comparaison entre un ellipsoïde de la fabrique AMS et un ellipsoïde de la fabrique microlitique permettra de situer cette acquisition vis-à-vis de la formation des microlites, connus pour se former tardivement lors du refroidissement de la lave (Hargraves & al., 1991).

Cette méthodologie a été appliquée à la coulée F2 de Royat sur un profil vertical. La fabrique AMS se révèle être portée par des titanomagnétites MD et PSD (multidomaines et pseudosingledomaines) sans présence de SD. La coïncidence entre les ellipsoïdes de fabriques AMS et microlites nous indique que la fabrique AMS a été acquise durant les derniers épisodes de déformations de la lave et que par conséquent tous les résultats et interprétations obtenus de l'AMS ne seront significatifs que des derniers soubresauts de la coulée.

Une attention particulière a été portée à la linéation magnétique (k_{max}) et au degré d'anisotropie (A). Des plongements de linéation supérieurs à 45° indiquent une surimposition d'un cisaillement pur vertical au cisaillement simple horizontal. Les imbrications du plongement de la linéation témoignent en fait d'une superposition de différents compartiments laviques. Ce qui est confirmé par l'occurrence de sauts du degré d'anisotropie en corrélation avec des changements inverses de sens de plongement de la linéation. Une telle succession des paramètres magnétiques a permis de proposer un profil de vitesse atypique où les sauts du degré d'anisotropie et les changements inverses du plongement de la linéation correspondent à des limites entre différents compartiments laviques. Une telle succession des paramètres magnétiques ne peut pas être expliquée par un épanchement sur un terrain ondulé, ni par une coulée de reflux, ni même par de multiples épisodes d'inflation (Walker & al., 1999 ; Cañón-Tapia & Coe, 2002) et la possibilité d'un empilement d'unités laviques ayant des propriétés rhéologiques différentes a été proposée et confortée par une étude la zonation des vésicules et des phénocristaux.

La méthodologie a également été appliquée à la coulée F3 de Royat sur un profil vertical. La fabrique AMS se révèle être portée, comme pour la coulée F2, par des titanomagnétites MD et PSD sans présence de SD. La fabrique AMS a aussi été acquise durant les derniers épisodes de déformations de la lave et, par conséquent, tous les résultats et interprétations obtenus de l'AMS ne seront significatifs que des derniers mouvements de la coulée.
Cette coulée a la particularité de présenter une linéation perpendiculaire à l'écoulement apparent de la lave dans un contexte de fabrique magnétique normale en l'absence de particules SD. En fait l'analyse des affleurements environnants a montré que cette linéation a bien marqué le mouvement de la lave, perpendiculaire à l'écoulement, s'expliquant par la formation d'un lobe terminal au sein duquel la lave a été étirée perpendiculairement à cause de son inflation. Par la suite, ce lobe a rompu et subi une déflation aboutissant à la formation de levées. Le surplus de lave a continué sa progression jusqu'à sa terminaison actuelle.
Ainsi, dans ce deuxième cas, une étude précautionneuse de l'AMS, nous a permis de reconstituer l'histoire de la mise en place du front de la coulée F3 de Royat.

Ce chapitre souligne l'importance de suivre une méthodologie précise pour réaliser une bonne interprétation de l'AMS. Cette procédure appliquée à deux coulées différentes nous a ainsi permis d'aboutir à différents résultats et différentes interprétations qui devraient se diversifier en étudiant d'autres coulées de la même façon.

CONCLUSIONS

Les trois approches traitées dans chaque chapitre ont permis de nombreuses améliorations sur la cinématique et la déformation des coulées de lave, permettant ainsi une meilleure compréhension de leurs mises en place. L'étude d'une coulée de lave dans chacune des ces approches apportera de nombreuses précisions. Tout d'abord, son style général de mise en place (ʻaʻā ou pāhoehoe) sera attribué. Puis la formation des éventuelles brèche permettra soit de préciser les propriétés rhéologiques de la lave ou alors en cas de phréatomagmatisme permettra de préciser le rapport eau-lave rencontré. Enfin, l'utilisation rigoureuse de l'AMS, selon la méthodologie proposée, permettra de proposer un profil de vitesse et de préciser les derniers mouvements de la coulée. Ces interprétations se révèleront être d'autant plus précises en poursuivant les recherches dans les trois thématiques présentées dans ce manuscrit.

CONTENTS

INTRODUCTION

Kinematics is the branch of mechanics that studies the motion of a body or a system of bodies without consideration given to its mass or the forces acting on it, whereas strain, or deformation corresponds to any change of form, shape, or dimensions produced in a body by a stress, without a breach of the continuity of its parts. These two aspects are directly linked, and could both contribute to our knowledge of lava flow emplacement.

Although lava flows are common in the geological record and erupted every year, their mechanisms and their history of emplacement remain a matter of debate. There are numerous parameters, which have a notable influence on their emplacement: there are internal lava parameters such as temperature, viscosity, chemical composition, rate of supply, crystal and bubble contents. Also, the external environment plays an important part, for example the substrate and the topography have a major effect.

The flow kinematics and deformation is recorded by structures and textures in the lava. In old lava flows, these features allow the determination of the relative importance of the above parameters on the flow emplacement.

I have constructed this manuscript in three different ways to consider lava structure to determine, as accurately as possible, the emplacement mechanisms of several old lava flows mainly from the French Massif Central but also from Iceland. These three approaches will be treated in three different chapters, as they will consider different approaches and thus different methodologies. However, these chapters are linked by the same emplacement styles and together will hopefully improve our knowledge in lava emplacement due to this multidisciplinary procedure.

The first chapter will discus the significance of ‘a‘ā and pahoehoe terms as currently used in modern volcanology to differentiate two main emplacement modes from active lava flows. This significance will be debated in old lava flows where surface information is not possible. The rheological links between the two terms will be considered, and in particular their relationships on a lava single flow field will be investigated.

The second chapter will consider the textural characteristics of lava breccia, and breccia formation associated with lava flows. These breccia include both clinker and peperite. The clinkers are known to be formed in a’a flows by the breakage of its solid surface under

torque but on our studied flows, this assumption needs to be revised. SEM imaging provides valuable information to study clinker / breccia especially in comparison to well-studied volcanic ashes. Also using SEM imaging lava flow-associated peperite formation will be discussed.

The last chapter considers magnetism with the Anisotropy of Magnetic Susceptibility (AMS) used on lava flows. This has been already performed by some authors, but here, I have emphasized that AMS usage requires a good methodology prior to interpret the obtained result and to propose accurate trustworthy interpretations. This methodological routine will be presented and performed on two lava flows from the Chaîne des Puys. The interpretation and discussion will allow us to illustrate different aspects of the kinematics and deformation for lavas.

In a conclusion, a synthesis of the main points of in this manuscript is proposed

Chapter 1:

Pahoehoe and ‘a‘a Lava Flows

INTRODUCTION

The Hawaiian terms pāhoehoe and ‘a‘ā are in widespread use in modern volcanology for classifying lava flows. Mostly and originally, they refer to surface structure and morphology but when considered in more closely, they can refer to two different lava flow emplacement modes and ultimately two different hazards to deal with.

In 1.1., I will study the relationships between pāhoehoe and ‘a‘ā to investigate not only surface structures but also other internal features such as inner geometric structures, vesicle zonation, phenocryst zonation, textural characterization and AMS (Anisotropy of Magnetic Susceptibility). Through this discussion I will discuss the important evidence allowing us to discriminate between the ‘a‘ā and the pāhoehoe, with particular interest on old lava flows where surface structures have been buried or eroded.

After having described the contrasts between the pāhoehoe and ‘a‘ā lavas, I will discuss in 1.2. the genetic relationships between pāhoehoe and ‘a‘ā. As numerous examples of lava transitions from pāhoehoe to ‘a‘ā have been described (e.g. Peterson & Tilling, 1980; Kilburn, 1981, Hon & al., 2003, Soule & Cashman, 2005), we will try to explain the origin of such a transition through a rheological approach, firstly through the literature and then on a new field example: a branch of the Myvatn lava flow field (Iceland).

In 1.3., I will apply conclusions from previous sections to help interpretation of lava flow emplacement in the French Massif Central. In this part I shall argue that pāhoehoe is extensively present in the Chaîne des Puys and also in the Limagne and the Ardèche provinces of the Massif Central. Its presence has implications for the type of eruptive activity to be anticipated if ever there is a reactivation of the volcanism.

1.1 PĀHOEHOE VERSUS ‘A‘Ā

1.1.1: Surface differences

Surface morphology provides the basis for classifying lava flows into pāhoehoe and ‘a‘ā (Macdonald, 1953), two Hawaiian terms introduced to describe the common lava types found on Mauna Loa and Kilauea. They apply equally to other lavas with silica contents less than about 50-55 wt % (Kilburn, 2000). Lavas with silica contents greater than 55 wt % are classified as blocky flows. Originally used to refer to the solidified lava flow surfaces, the terms were expanded to designate entire flows (Macdonald, 1953; Hon, 2003). Pāhoehoe flows are characterized by a smooth, billowy or ropy surface, and ‘a‘ā has a brecciated rough surface made of clinker (Macdonald, 1953).

1.1.2: Problems due to “old” lava flows

It is often tricky to associate many centuries to millions years old lava flows to one particular surface morphological type (pāhoehoe or ‘a‘ā), because the surface is can be eroded or covered. The intensity of the surface change depends on climatic parameters.

In the French Massif Central, lavas range from 6000 to several millions years old. The attribution of a flow to one particular surface morphological type is also tricky. In fact outcrops can be limited and several types of disruption will hide or modify the original surface of a lava flow. These disruptions include the cover of other volcanic products (other lava flows, pyroclastic mantles…), erosion in a temperate climate (which can be extensive in narrow valleys), the development of a thick soil on a plateau, and also anthropogenic intervention such as quarrying, stone removing for agriculture and urbanization.

Fortunately, pāhoehoe and ‘a‘ā flows not only differ superficially in surface textures, but also fundamentally in their emplacement mechanisms and thus in their internal structures (e.g. Kilburn, 1993 ; Polacci & al., 1999 ; Duraiswami & al., 2003). Thus criteria other than

surface texture can be used in the French Massif Central, these criteria will be visible on sections of the studied flows.

The attribution of the term pāhoehoe or ‘a‘ā for “old” lava flows is important, because a precise emplacement mechanisms deduced for such flows can be used when describing active flows (on which the pāhoehoe or ‘a‘ā nature is evident) in can eventually be used to forecast their behaviour.

Now I will present the different emplacement mechanisms of each lava flow type with the resulting geometry and then I will discuss the emplacement mechanism criteria that can also be used on lava flow sections.

1.1.3: Emplacement and geometric differences

1.1.3.1: Pāhoehoe flows

Pāhoehoe flows advance slowly (compared with ‘a‘ā flows) mainly with a lobe-by-lobe emplacement (a lobe being the smallest coherent package of lava, it also corresponds to a flow unit and the flow being the sum of all these lobes). The cooling surface of each lobe resists extensive tearing. The crust remains continuous around lobe margins and fronts. The initial thickness of a lobe is usually only a few decimeters (Kilburn, 2000). Rowland and Walker (1987) specify the minimum thickness in 3000 Hawaiian pāhoehoe flow units of about 3 cm and a median of 40 cm, whereas Self & al. (1998) have noticed lobes as thin as 2 cm. As all viscous flows are submitted to basal resistance, each lobe will progress via a rolling caterpillar-track motion (Merle, 1998; Lescinsky & Merle, in press). Because early lobes are thin, they are easily retarded by the crust and they will grow by an endogenous process through the mechanism of inflation (Hon & al., 1994). During inflation, pāhoehoe lobes can reach meter-scale thickness (Self & al., 1998) and spreading occurs by lava leaking out as small new lobes through breaks in the crust. Because of the dominant control of the crust on the emplacement, pāhoehoe flows are often considered as crust-dominated (e.g. Kilburn, 1993; Polacci & al., 1999; Duraiswami & al., 2003).
As a result, pāhoehoe fronts and margins soon develop as a complex of budding lobes, all of which are uplifted by newly arriving lava (Kilburn, 2000).

Meter-scale pāhoehoe lobes can coalesce laterally during inflation (Hon & al., 1994), producing sheets hundreds or even thousands of meters wide. Such immense sheets are also meters to tens of meters thick and range in length from hundreds of meters to perhaps as much as several tens of kilometers (Self & al., 1996, 1998).

Because of inflation, tumuli can develop and because of coalescence with endogenous growth, lava tubes often develop. The figure 1.1.1 shows the major flow structures of a pāhoehoe flow.

The smooth surface and thin initiation of pāhoehoe lobes suggest that fluid cores have Newtonian rheology (Hon & al., 1994).

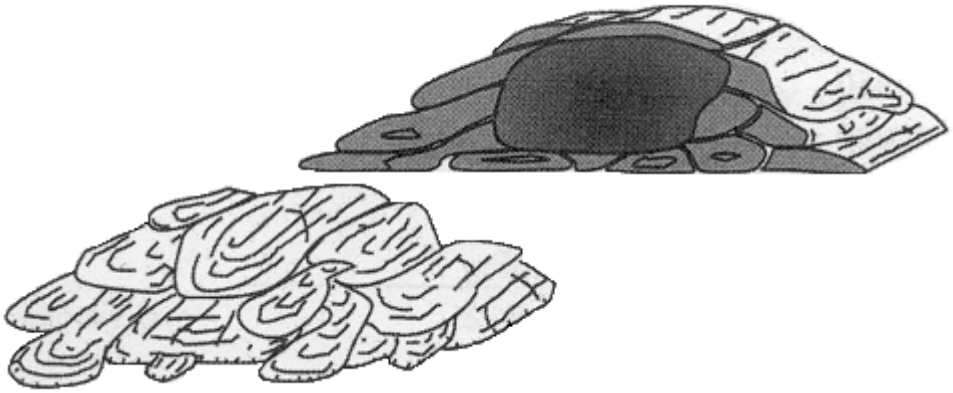

Figure 1.1.1: Major flow structures in a pāhoehoe flow that consists normally of a complex of intermingling lobes fed by lava from a tube system (Kilburn, 2000).

1.1.3.2: ‘A‘ā flows

‘A‘ā flows show simple evolutionary trends, their fronts tend to advance as single units, and it is rare for one part of a front to move far ahead of the body. Flow fronts rarely display a thickness less than 10 centimeters and they can reach 20 meters (Kilburn, 2000). They advance more rapidly in the down slope direction for a given thickness than pāhoehoe flows causing continuous disruption of the flow crust. This forms clinker and allows the exposed core to lose heat quickly. A note should be made about the term clinker; they are contorted and initially appear spinose but, during later stages of advance, the surface breaks to yield rounded and abraded rubble (Kilburn, 2000). Figure 1.1.2 shows the major flow structures of an ‘a‘ā flow.

Like pāhoehoe flows, ‘a‘ā flows advance with a rolling caterpillar-track motion. Witnesses of this motion are the clinker (formed at the top of the flow), which are present at the flow base.

It is possible that the pre-lava flow topography will accumulate clinker in hollows and nothing on topographic rises. So the absence of basal clinker will not inevitably indicate that the flow is not ‘a‘ā. Also, the upper clinker have to be always present, but in “old” lava flows this surface may be eroded. As the major control on emplacement is seen to be the core, ‘a‘ā flows are often called core-dominated (Kilburn, 1993; Polacci & al., 1999; Duraiswami & al., 2003). In fact, a characteristic feature of ‘a‘ā flows is core injection in the breccia (Duraiswami & al., 2003) but also the incorporation of breccia in the core (Crisp & Baloga, 1994; Duraiswami & al., 2003). It should be noted that under the upper rubble zone in ‘a‘ā flows there may be an upper vesicular subzone, which can lead to the formation of a crust and thus tumuli (Walker, 1991; Calvari & Pinkerton, 1998; Duncan & al., 2004) or lava tube formation (Calvari & Pinkerton, 1999).

The generally greater thickness of ‘a‘ā flows suggests flow interiors that possess a substantial yield strength (Hulme, 1974).

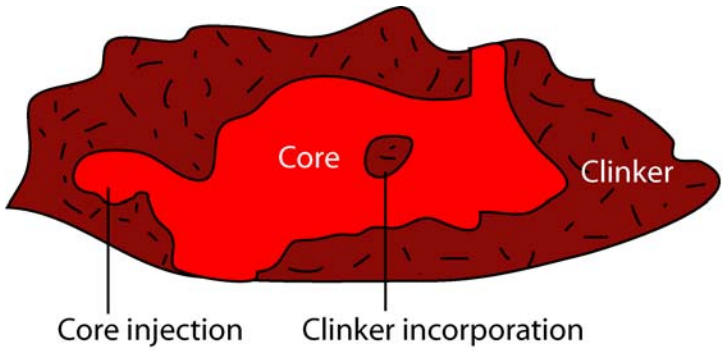

Figure 1.1.2: Vertical section displaying major flow structures in an ‘a‘ā flow.

From this discussion section on lava flow emplacement types, we can already associate a particular flow geometry to one type of emplacement (compare figures 1.1.1 & 1.1.2). Pāhoehoe flows are compound flows, they display lobe stacking and they are often associated with a lava tube system. ‘A‘ā flows tend to advance as single units and they are characterized by the presence of clinker.

1.1.4: Other criteria for emplacement differences

Several methods have been used to study lava flow emplacement, including the analysis of vesicles, mineralogical textures and Anisotropy of Magnetic Susceptibility (AMS). I will describe these three criteria.
In addition, other criteria have been used, such as structural analysis of folds (Bonnischen & Kauffman, 1987; Smith & Houston, 1994), deformed enclaves of two cogenetic magmas (De Rosa & al., 1996; Ventura, 1998) and columnar jointing deformation (Waters, 1960). These criteria can not be applied on the French Massif Central due to the scarce preservation of folds and the lack of lava flows displaying cogenetic enclaves.

1.1.4.1: Vesicle distribution

- Some remarks

Before discussing vesicle distribution, some aspects concerning the formation of vesicles should be evoked.
Vesicles in lava flows form when gas bubbles in silicate melts are trapped as the surrounding melt solidifies. Because the diffusion rate of gases in silicate melts is four orders of magnitude lower than the thermal diffusion coefficient of silicate melts, the thermal wave responsible for cooling and solidification of a flow can pass through the vertical thickness of a flow before a gas could diffuse through the same distance. Consequently, gases are trapped in the liquid as the solubility drops during cooling of the flow, and the exsolved gases will be concentrated in bubbles. The gases that begin to exsolve from a lava flow will generally still be exsolving as the magma temperature passes through the solidus, and the gas bubble will be frozen into the solidified liquid as a vesicle (Sparks, 1978; Aubele & al., 1988).
Assuming the first bubbles to be nucleated in a just vented lava volume as the original bubble population, this original population may be modified by continued bubble nucleation and growth (Aubele & al., 1988; MacMillan & al., 1989), crystallization-induced void production with cooling (Peck, 1978; Walker, 1989), bubble coalescence (Sahagian & al., 1989; Walker, 1989) and shear planes with cooling. The rise of bubbles in lava, (or their buoyancy) will be stopped when encountering a cooling front, but also earlier if the bubble is trapped in melt with a viscosity or yield strenght sufficient for inhibiting buoyant rise.
Thus, the vesicle population recorded in solidified lava flows is the integrated result of processes related to lava eruption, transport, emplacement and solidification. Consequently a quantitative analysis of pāhoehoe and ‘a‘ā vesicle distributions (size or deformation values)

will not necessarily distinguish just these two processes, but an amalgam of events and processes.

- *Pāhoehoe lobe vesicle distribution*

Different types of pāhoehoe lobes have been distinguished based on vesicle distributions. Walker (1989) used the term S-type pāhoehoe to describe lobes that were "spongy" with spherical vesicles distributed throughout but with higher concentration toward the center. Wilmoth & Walker (1993) and Self & al. (1998) used the term P-type to designate lobes containing pipe vesicles. P-type flows typically have dense interior and more vesicular exteriors, the exact opposite of S-type lobes. S-type lobes form with minimal inflation, whereas inflated lobes have the basic characteristics of P-type lobes, even when they lack pipe vesicles (Self & al., 1998).

An innovative paper was published by Aubele & al. in 1988 for explaining vesicle distribution mostly in pāhoehoe lobes called later the P-type. This work was based first, on observation and measurement of vertical sections of thin (< 10 m) basaltic lava lobes, which display a major upper vesicular crust, a minor lower vesicular crust and between the two, a dense zone. Following numerical simulations, a model was proposed assuming growth and rise of gas bubbles in cooling static lava. "As a bubble grows, it begins to ascend, and continues to ascend until it is overtaken by solidification progressing inward from either the upper or lower cooling surfaces of the flow" (Aubele & al., 1988).

A good description of vesicles distribution in a pāhoehoe inflated lobe is provided in Self & al. (1998). During inflation, a flux of fresh, bubble-laden lava is continually brought into the lobe (fig. 1.1.3b & c). After stagnation, for typical basalt viscosities, the remaining bubbles should rise to the surface within days to weeks (Aubele & al, 1988; McMillan & al., 1989; Manga, 1996), leaving a dense core (fig. 1.1.3d & 4). However, during the crystallization of this dense core, incompatible elements, including volatiles, concentrate in the residuum. Secondary vesiculation can cause this residuum to rise buoyantly as diapirs (Goff, 1996; Rogan & al., 1996). When these rising diapirs hit the base of the upper crust, they spread to form subhorizontal vesicle sheets (VSs) (Self & al., 1998) (fig. 1.1.3d). Vesicle cylinders can form near the base of flows that have thick upper vesicular crusts. Like horizontal vesicle sheets, vesicles cylinders are formed by diapiric rise of low density residuum (Goff, 1996) and should only be preserved after the flow has stagnated (Self & al., 1998) (fig. 1.1.4). In the

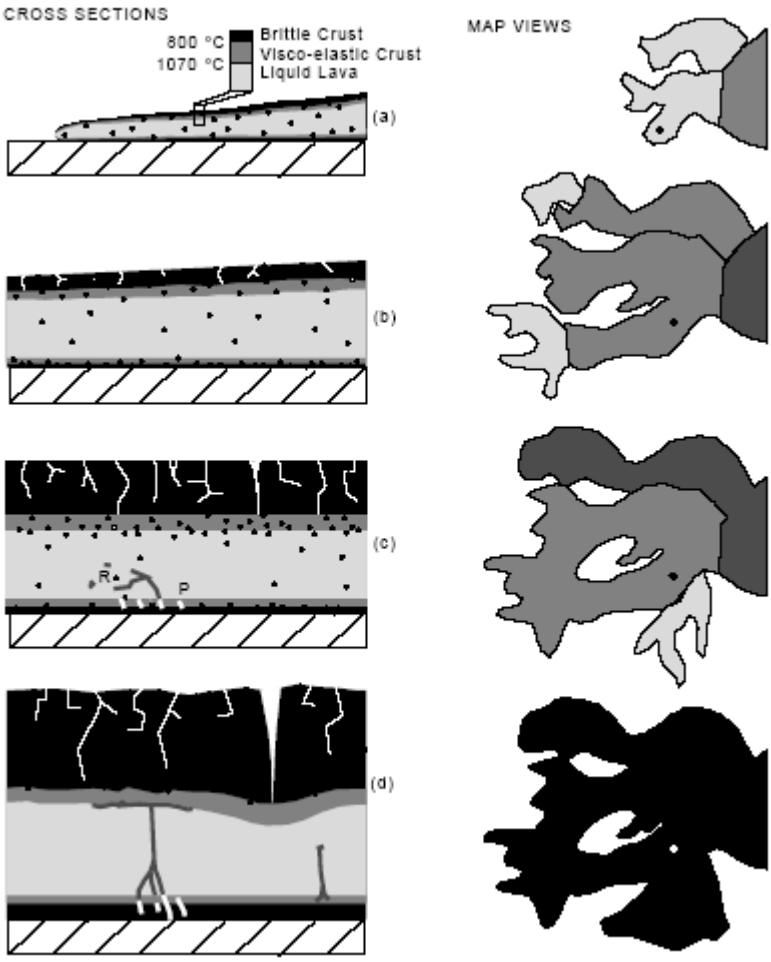

Figure 1.1.3: Cartoon of the development of an inflated pāhoehoe sheet flow (after Self & al., 1998). *On the left* are cross sections at a fixed location, and *on the right* are concurrent map views of the development of the flow field. The map location of the cross section is indicated by the *dot*. This cartoon applies equally to inflated pāhoehoe sheet lobes that range from 1–100 m in thickness and from <100 m to >10 km in lateral dimensions. The emplacement of a sheet lobe can take anywhere between days and years. In the cross sections the *shading* darkens with cooling, and in the map view it darkens with age. (*a*) A new lobe advances from right to left. Incandescent lava is exposed only at the very tip of the flow. (*b*) The lobe thickens by inflation as it extends. Bubbles from the moving lava are trapped in the crust, forming vesicles. The lower crust grows much more slowly than the upper crust. (*c*) Inflation continues. Depressurisation from the formation of a new breakout leads to a pulse of vesiculation within the liquid lava (Hon et al 1994). These bubbles are trapped to form a horizontal vesicular zone. Buoyant, vesicular silicic residuum (R) that rises from the lower crystallization front is disrupted and mixed into the flowing lava. Pipe vesicles (P) grow in the lower crystallization front. Some cracks in the upper crust become major clefts that reach the visco-elastic layer. (*d*) Flow stagnates. The remaining primary bubbles rise to the top of the flow in a few days to weeks. The vesicular residuum (R) is able to rise through the stagnant lava, forming horizontal vesicular sheets at the base of the upper crust. Cooling is enhanced around deep clefts. Note the complex plan form of a typical compound pāhoehoe sheet flow.

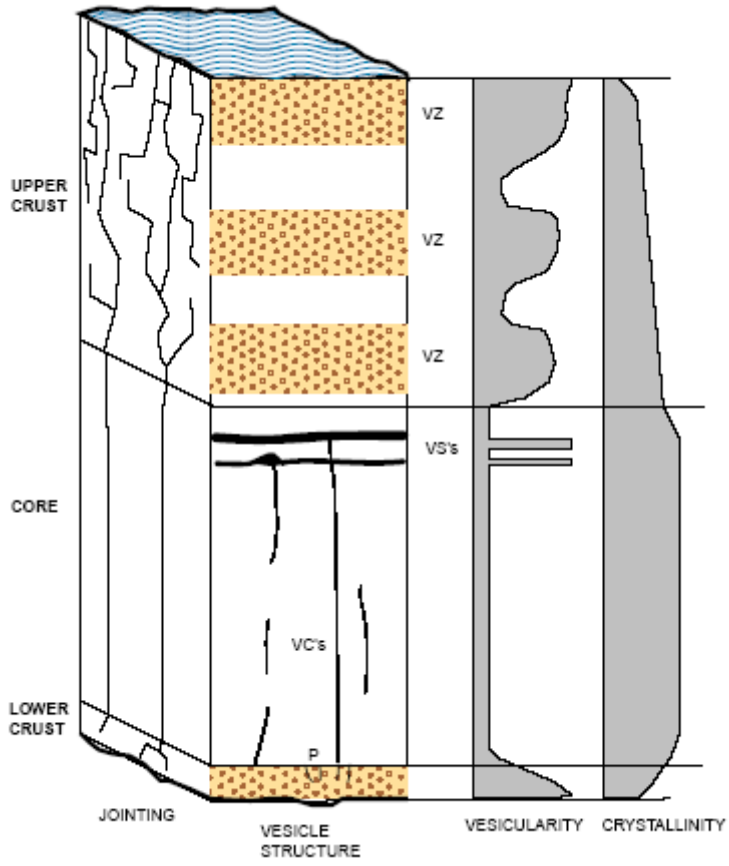

Figure 1.1.4: Idealized cartoon of the cross section through an inflated pāhoehoe lobe (after Self & al., 1998). The lobe is divided into three levels based on vesicle structures, jointing, and crystal texture. The upper crust makes up 40–60% of the lobe and the lower crust is 20–100 cm thick, irrespective of the total lobe thickness. *Upper crust*: Vesicular, often with discrete horizontal vesicular zones (VZs) that form during active inflation (see Figure 2*c*). Bubble size increases with depth. Prismatic or irregular jointing is found, sometimes equivalent to the entablature in thick lava flows. Petrographic texture ranges from hypohyaline to hypocrystalline (90–10% glass). *Core*: Very few vesicles. Porosity is dominated by diktytaxitic voids. Vesicles are mostly in the silicic residuum, which forms vesicle cylinders (VCs) and vesicle sheets (VSs). Holocrystalline (<10% glass). *Lower crust*: Nearly as vesicular as the upper crust, few joints, and 50–90% glass.

case of several time-spaced inflations in a lobe, several vesicular zones may be stacked in the upper crust (fig. 1.1.3 & 1.1.4).

As a result of inflation in pāhoehoe lobes, early-formed vesicles in the crust could be subjected to stretching and thus such vesicles could acquire an elliptical shape, whereas in the dense zone, vesicles will have spherical shapes.
In a section perpendicular to the downward propagation, an inflated pāhoehoe lobe presents an external concentric vesicular zone, thicker at the summit of the lobe, a smaller inferior vesicular zone and a more massive core in which vesicle sheets and vesicle cylinders can be present (fig. 1.1.5).

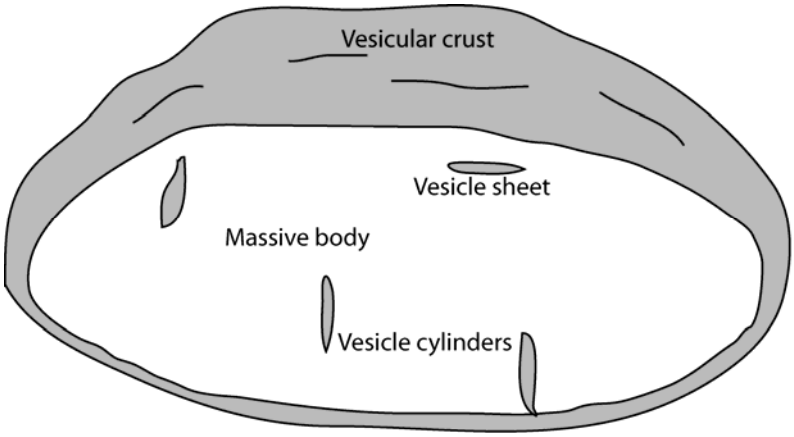

Figure 1.1.5: Typical vesicle distributions in a section through a pāhoehoe lobe. Grey areas are vesicular.

- *ʻAʻā flow vesicle distribution*

Studies on vesicle distribution in ʻaʻā flows are scarcer than those in pāhoehoe. They are limited to studies of the pāhoehoe to ʻaʻā transition and to near vent ʻaʻā flows.
The reason explaining this lack of interest can be pointed out for instance in the figure 2d *in* Cañón-Tapia & al. (1997). This figure shows several sections through ʻaʻā flows with structural features, but the authors were unable to sketch vesicles, in fact vesicles are so highly deformed that a foliation is present.
The same observations were made by studying vesicles through the pāhoehoe to ʻaʻā transition. Several authors have remarked that vesicles in pāhoehoe tend to be spherical in the core (see above), whereas those in an ʻaʻā core are commonly highly deformed (MacDonald,

1953; Polacci & Papale, 1997; Polacci & al., 1999). A more precise difference was noted by Cashman & al. (1999), "pāhoehoe vesicles are spherical to ellipsoidal and show little interconnection" while "'a'ā vesicles are highly irregular in shape, extensively interconnected" (fig. 1.1.6).

A particular vesicle distribution has been described in near vent 'a'ā lobes (fig. 1.1.7) showing a conspicuous pattern of concentric foliation. These vesicles are ellipsoidal to highly irregular in shape (Polacci & Papale, 1997; Cañón-Tapia & al., 1996). This near vent characteristic of such flows should be detectable in the field. Such flows are in close association with pāhoehoe flows, and they could also be considered as transitional flows (Polacci & Papale, 1997; Guest & Stofan, 2005).

No other particular vesicle distribution has been seen in 'a'ā flows but a vesicular crust can be formed in the context of tube feeding.

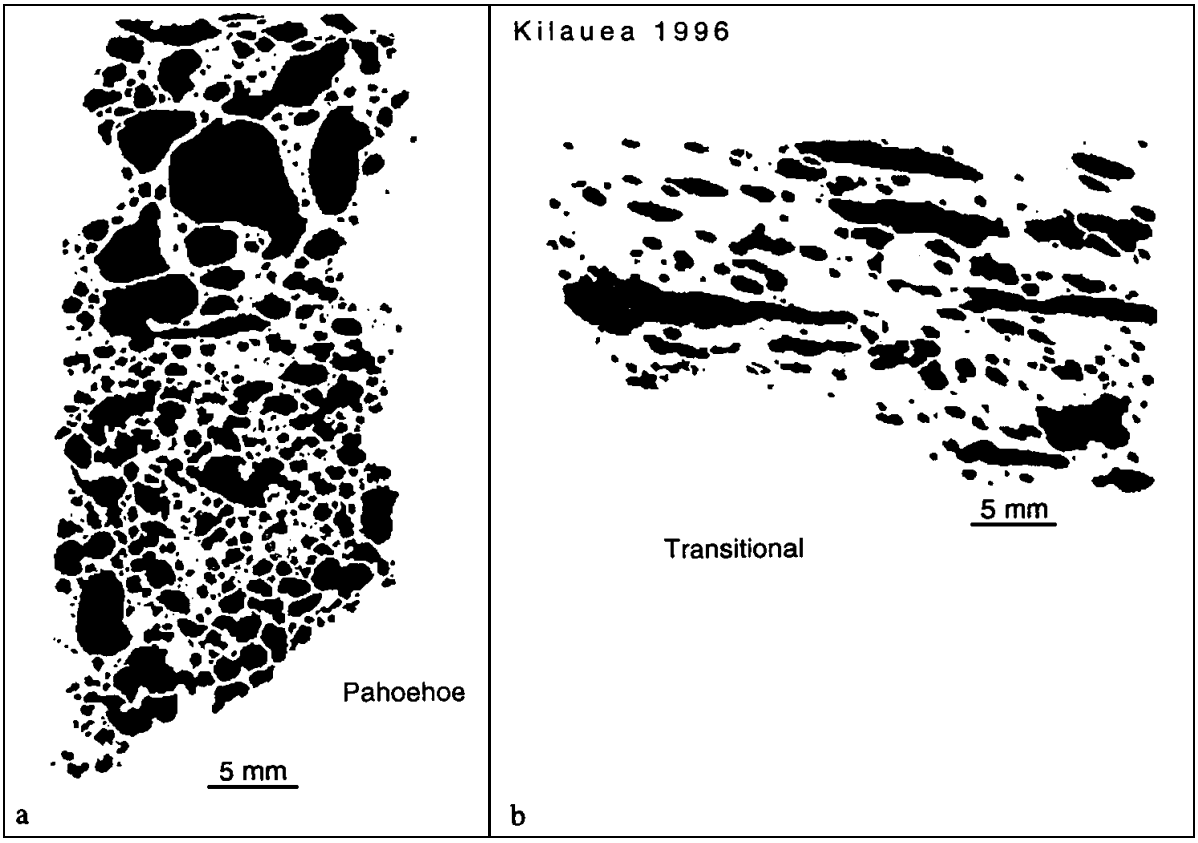

Figure 1.1.6: Binary images (vesicles as black features, glass plus microlites as white) in a pāhoehoe sample (**a**) and in a transitional sample (**b**). In the pāhoehoe sample vesicles tend to be little deformed, whereas they assume elongated and more deformed shapes in the transitional sample (Polacci & al., 1999).

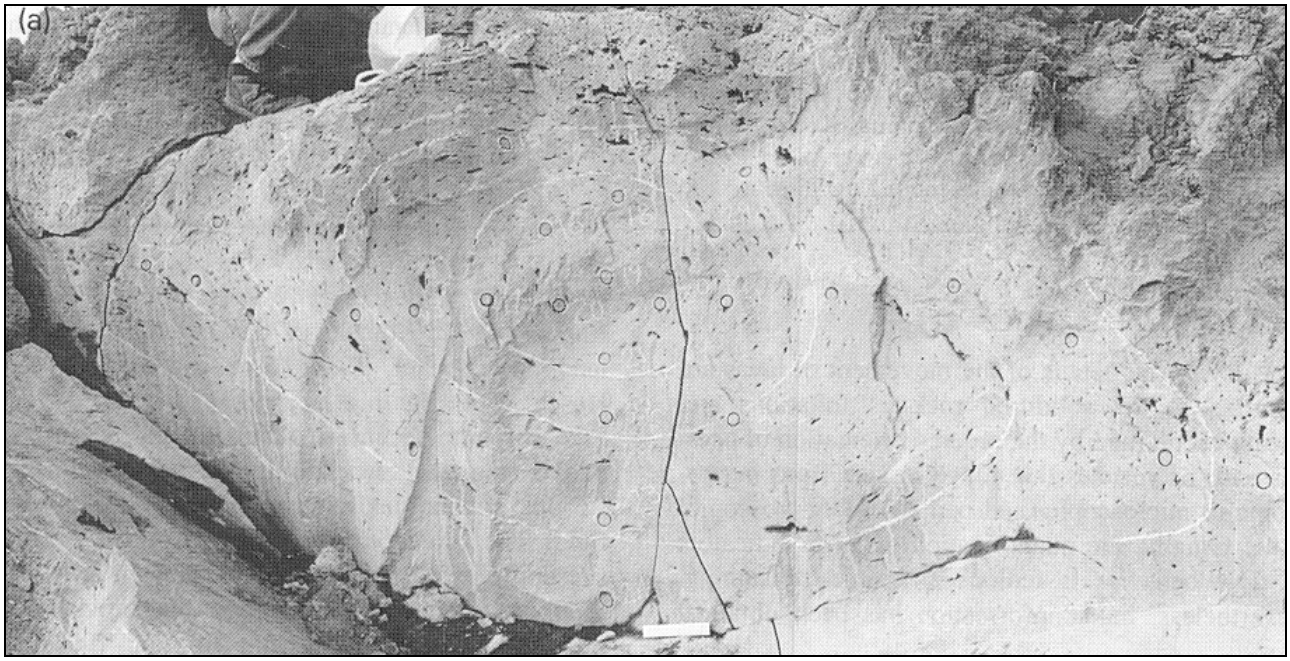

Figure 1.1.7: Photograph in near vent ‘a‘ā lobe showing concentric vesicle patterns. Scale bar is 15cm long (Cañón-Tapia & al., 1996).

As a conclusion, pāhoehoe lobes can be either the S-type (highly vesicular especially in the center) if inflation is limited, or the P-type with significant inflation. The P-type implies an upper and a lower vesicular zone, with in the middle a more massive zone (vesicle sheets and vesicle cylinders can be present). If several episodes of inflation occur, several vesicular zones will be stacked in the upper crust.

‘A‘ā flows, except for near vent ‘a‘ā flows and in tube feeding contexts, do not display clear vesicle distribution. In all cases, the vesicle deformation in ‘a‘ā flows will be greater than in pāhoehoe lobe.

The absence of rise structures and the scarcity of vesicle distribution in ‘a‘ā flows can be attributed to the existence of a substantial yield strength.

1.1.4.2: Textural characterization

The aim of this section is to discuss the possibility of linking pāhoehoe or the ‘a‘ā emplacement modes in a cooling lava to thin section textural observations.

A first approach toward this goal was performed by Sato in 1995. He has showed that the groundmass textures of surface samples from the 1778 AD pāhoehoe flow and the 1986 AD

‘a‘ā flow of Izu-Oshima volcano (Japan) differ in population density of plagioclase by about two orders of magnitude. The pāhoehoe lavas are coarser grained and have a population density of $10^{7.0}$ cm^{-3}, while the ‘a‘ā lavas are finer grained and have a population density of $10^{9.3}$ cm^{-3}. However, these results are very open to criticism. In fact, the author compares two different lava flows. The flows have different emplacement and crystallization histories. They do not have strictly the same chemical composition and the same topographic path. Furthermore, groundmass plagioclases have formed mostly at the end of the emplacement, when the lava has cooled and not when the lava was still active.

Polacci & al. (1999), proposed to look for textural characterization of the pāhoehoe-to-‘a‘ā transition in two Hawaiian flows. They have studied pāhoehoe and ‘a‘ā lava from the same flow. The glass is quenched melt so that original crystallization textures are preserved. Unfortunately, the absence of preserved glass in the ‘a‘ā has limited textural analysis of glassy areas to pāhoehoe and transitional morphologies. The results through thin sections display an increase in microlite crystallinity and crystal number density for pāhoehoe to transitional terms. In other words, microlite crystallinity and crystal number density is lower in pāhoehoe terms than in ‘a‘ā terms. The conclusion is the same as Sato (1995), but a question remains: when were the glass samples frozen?

Cashman & al. (1999) have collected hot samples in an active lava channel at Kilauea Volcano showing also a pāhoehoe-to-‘a‘ā transition during May 1997. To collect samples, they used a steel hammerhead suspended in the channel by a cable. This technique allowed sampling through ~1m of the flow, and samples are representative of the flow interior. All samples were water quenched immediately after collection for optimal glass preservation. In this way, there is no problem of late crystallization and they have true ‘a‘ā samples. Nevertheless, the conclusion remains the same: the groundmass crystallinity is greater in ‘a‘ā samples (fig. 1.1.8). The authors propose that this increase of groundmass crystallinity in ‘a‘ā lava was sufficient to generate a notable yield strength, so acquiring a Bingham rheology.

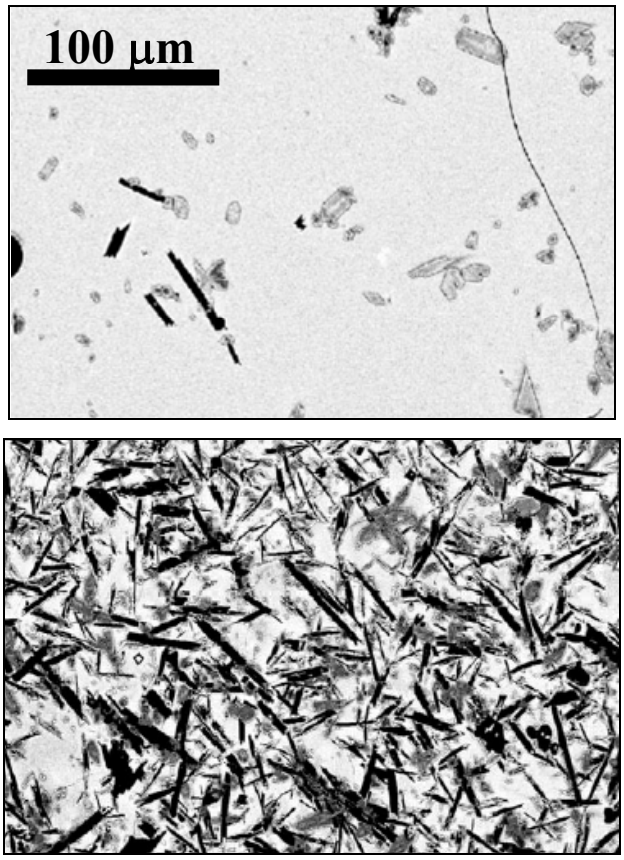

Figure 1.1.8: Typical BSE images on artificial quenched lava samples of the pāhoehoe (top) and the ‘a‘ā (bottom) type (Cashman & al. 1999).

For the “old” lava flows of the French Massif Central, the original glass (before lava cooling) was not preserved. Unfortunately nobody was present for quenching this lava. The only more preserved glass could be at the rims of the flow, or in the ‘a‘ā clinker, but incertitude on the relation emplacement and cooling will be still present.

Another criterion can be used rather than groundmass crystallinity: the mafic phenocrysts. These mafic phenocrysts are very interesting because they are present at the beginning of the lava flow, and they have a greater relative weight compared with plagioclase microlites. The study of these reveals that, in contrast with ‘a‘ā lavas, pāhoehoe lavas display a downward concentration of olivine (see also fig. 1.1.4) (Rowland & Walker, 1987, 1988; Walker, 1989) which is the result of the lack of a significant yield strength.

In conclusion, it is not evident to link pāhoehoe or ‘a‘ā emplacement mode to a thin section textural data in a cooling lava according to its groundmass crystallinity, because of the lack of original glass. Only quenched samples are significant. Nevertheless, a study of mafic

phenocryst zonation can be performed and if a downward concentration exists the lava could be considered as pāhoehoe.

1.1.4.3: AMS (Anisotropy of Magnetic Susceptibility)

AMS provides potentially a measure of the strain ellipse in a lava near the time of solidification. It can therefore be used to determine the flow regime.

The parameters are clearly described in detail in Chapter 2 and are the mean susceptibility k_m (k_m = kmax + kint + kmin / 3), the degree of anisotropy A (A= 100 (1 – $k_{min}/2k_{max}$ – $k_{int}/2k_{max}$)) and the magnetic fabric via the parameter U (U= ($2k_{int} – k_{max} – k_{min}$) / ($k_{max} – k_{min}$)) or T (T= (2 (ln k_{int} – ln k_{min}) / (ln k_{max} – ln k_{min})) -1) (the U parameter is used in this section as quoted by several authors but in chapter 3 we will promote the use of the T parameter).

Before using magnetic parameters the origin of AMS in the studied lava flow has to be verified. The magnetic mineralogy, its shape and its distribution need to be known

In the only study where the origin of AMS was strictly defined in lava (Bascou & al., 2005), it appears that magnetic grains (titanomagnetites) are interstitial, usually subhedral suggesting that the grains formed late in the crystallization history contrary to plagioclase microlites which constitute a flow-oriented silicate framework constraining the spatial distribution of interstitial titanomagnetite. The experimental studies of Hargraves & al. (1991) indicate that AMS can come from an anisotropy of distribution caused by a silicate "template". In other words, the magnetic fabric copies the mineralogical fabric. For other AMS studies, when quoted, this origin of AMS is used as an axiom. As the plagioclase microlites form mainly during cooling, AMS is expected to indicate the last phases of deformation (see 1.1.4.2).

Cañón-Tapia & Pinkerton (2000) perform an experimental approach for AMS in lava flows on melted samples of lava from Kilauea subjected to a range of strain rate and cooling histories. The results obtained have a great importance. Firstly, they show that the degree of anisotropy is a function of both the thermal and shearing history of a sample. "Additionally, lava subjected to complex shearing yields a lower degree of anisotropy even when high strain rates were imposed on it. These results lead to the conclusion that only the last phase of deformation is detectable using AMS and that high strain rates will not result in high degrees of anisotropy if either deformation ends while lava is still fluid or if the orientation of the maximum shear stress varies with time". Unfortunately in this paper, no thin sections were performed for confirming the behavior of plagioclase microlites.

It is thus very important to keep in mind that only the last phase of deformation is detectable using AMS.

Cañón-Tapia & al. (1997) studied the AMS of 22 basalt flow units over a vertical profile including S- and P- type pāhoehoe (see 1.1.4.1), transitional lava (toothpaste) and ‘a‘ā emplaced over different slopes in Hawaii. Unfortunately, the AMS origin of the 22 flows was not verified and some differences occur in several aspects of AMS.

‘A‘ā flows yield larger values of mean susceptibility (k_m) than pāhoehoe (fig. 1.1.9). However, due to the overlapping ranges of k_m, it is not possible to discriminate between lava types using k_m. The authors propose that the stronger k_m values of ‘a‘ā flows might be due to a more efficient mechanism, compared with pāhoehoe, for ingesting air or atmospheric water implying higher oxygen fugacities. However, a difference in k_m can be also attributed to differences in the magnetic population.

The degree of anisotropy (A) yield has also greater values for ‘a‘ā flows (fig. 1.1.10) attributed to greater deformation/shearing, but overlapping also occurs between the two types and it is thus tricky to discriminate the lava type according to A, especially as A can greatly vary on a flow section (see fig. 7 *in* Cañón-Tapia & al., 1997).

Finally, the magnetic fabric (U) displays on the vertical profiles several variations in the lineation field (U<0) and in the foliation field (U>0) whatever the lava type (see fig. 10 *in* Cañón-Tapia & al., 1997).

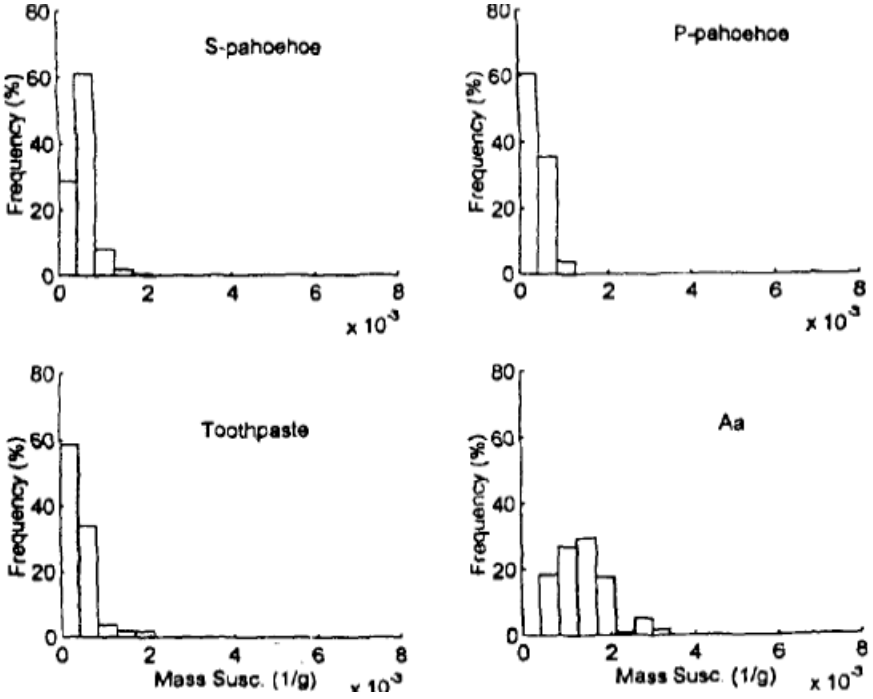

Figure 1.1.9: Relative frequency histograms of mass susceptibility (Cañón-Tapia & al., 1997).

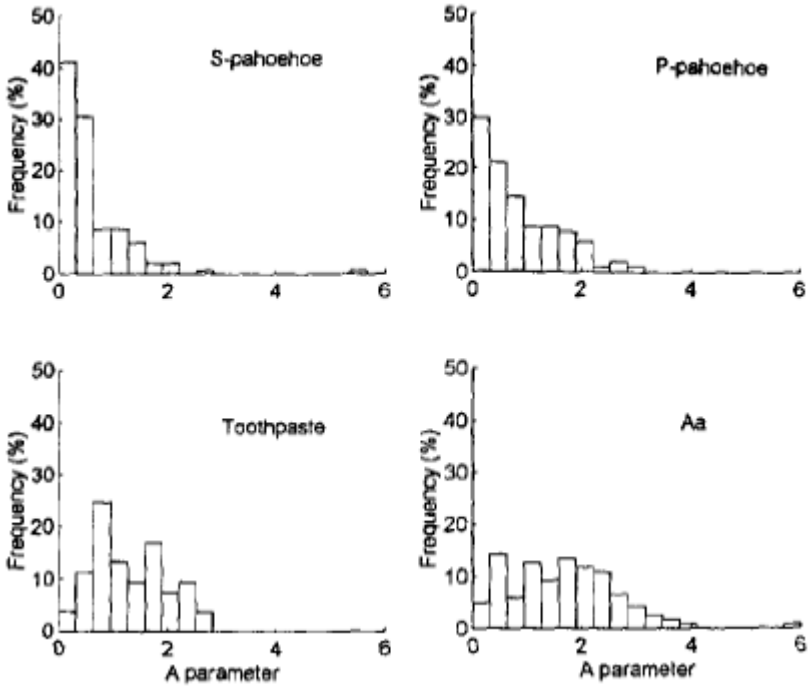

Figure 1.1.10: Relative frequency histograms of the degree of anisotropy (Cañón-Tapia & al., 1997).

So, the use of AMS in cooled lava is subjected to the same problem as the textural characterizations, this seems to be due to magnetic interaction with plagioclase microlites (that is why a detailed study of the AMS origin is needed), and because AMS will record the last phase of deformation. Even by looking at all AMS parameters, there is no clear difference between pāhoehoe and ‘a‘ā lavas. Thus AMS can not be used as a criterion for discriminating the lava type. Nevertheless, AMS will be used for investigating the late deformation phase as the late history of emplacement in Chapter 3.

1.1.5: Remarks on transitional flows

Until now I have considered only mafic lava flows as belonging to the pāhoehoe or the ‘a‘ā types. However, there is also a wide range of intermediate flow types between these two end-members, such flows are called transitional. Transitional flows are present along the pāhoehoe to ‘a‘ā transition (so are they between pāhoehoe and ‘a‘ā flows) and both types can also be found on a single flow.

Two transitional flow types are widespread in the literature: slabby pāhoehoe (Kilburn, 2000; Dance & al., 2001; Duraiswami & al., 2003) and toothpaste flow (Rowland & Walker, 1987;

Kilburn, 2000; Guest & Stofan, 2005). These two terms also designate surface morphology, which is often hard to see on "old" lava flows. Slabby pāhoehoe displays slabs with a smooth skin (a pāhoehoe skin) it corresponds to a first step in the fracturing process of the crust. On the other hand, a toothpaste flows display pulse buckles, pulse flaps and lateral shear zones allowing the formation of a lateral clinker (Rowland & Walker, 1987).

Transitional flows reveal numerous other types of morphology, and the most common transitional flow type displays a flow-top breccia composed of broken pieces of pāhoehoe crust, but this has no widely accepted name, unless it is equated to slabby pāhoehoe.

Whatever the type, transitional flows show some of the characteristics of both pāhoehoe and ʻaʻā flows (i.e. vesicularity zonation, clinker formation) and intermediate textures, deformation and AMS values.

A very interesting example is provided by the "sheet pāhoehoe" observed in the 1736 flows from the Montaña de las Nueces, Lanzarote (Solana & al., 2004). This flow appears to be a simple sheet flow without any lobes or lava tubes, so has ʻaʻā characteristics, but also it displays a massive core and a vesiculated crust, which is continuous and smooth, so it has pāhoehoe elements. Such flows would imply very fast emplacement with limited cooling before stagnation (see Solana & al., 2004).

1.1.6: Conclusions

In this discussion, we have seen that the pāhoehoe and ʻaʻā terminology first refers to surface morphologies. Unfortunately, this surface morphology is rarely preserved on "old" lava flows such as those from the French Massif Central. Fortunately, pāhoehoe and ʻaʻā terms also differ in emplacement mechanisms, which will procure several features in cross section for attributing to a lava the pāhoehoe or ʻaʻā emplacement modes.

Geometric and vesicular distributions give direct clues as to what type is observed. The clinker characterizes an ʻaʻā flow, but depending on the outcrop section or the erosion it can be hidden or eroded, so other criteria are required. Pāhoehoe flows are made of a lobe stack and lava tubes are frequent, whereas in ʻaʻā flow lobes and lava tubes are scarce. Due to the presence of a significant yield strength in ʻaʻā flows, the rise of vesicles is restricted. In contrast, pāhoehoe lobes have a vesicular crust and a massive core is present. Furthermore, the vesicle deformation is higher in pāhoehoe lobes than in ʻaʻā flows.

For completing these data, thin section analyses can be performed along a flow unit profile, if a downward increase in mafic phenocrysts occur, the lava has not a significant yield strength thus it is of the pāhoehoe type.

Interpretation of textures and AMS parameters will not permit the discrimination of a lava type, because of its late-stage acquisition.

1.2 PĀHOEHOE AND ‘A‘Ā RELATIONSHIPS

1.2.1: Pāhoehoe and ‘a‘ā relationships in the literature

Pāhoehoe and ‘a‘ā flows differ not only superficially by surface texture but also fundamentally in their emplacement mechanisms and thus in their internal structure (e.g. Kilburn, 1993; Polacci & al., 1999; Duraiswami & al., 2003). This allows us to attribute a pāhoehoe or ‘a‘ā type to lava flows that have the surface covered or removed, as often is the case in the French Massif Central. A lava flow can also change its emplacement mode during flow, thus a pāhoehoe flow will often evolve into an ‘a‘ā, and occasionally an ‘a‘ā flow can evolve into a pāhoehoe (Hon & al., 2003).

Peterson & Tilling (1980) first described the pāhoehoe-to-’a‘ā transition as an inverse relationship between the apparent viscosity of the lava and the shear rate applied to the flow. They proposed a dimensionless graph of apparent viscosity versus shear strain rate (fig. 9 *in* Peterson & Tilling, 1980) displaying a pāhoehoe field and an ‘a‘ā field separated by a transition threshold zone (TTZ). The diagram has been refined by Kilburn (1981) assuming pāhoehoe flows fed by near-Newtonian lava and ‘a‘ā fed by Bingham lava and the diagram has also been applied to Hawaiian lavas by Hon & al. (2003). The diagram (fig. 1.2.1) has also been used by Soule & Cashman (2005) as the basis for analogue experiments of the pāhoehoe to ‘a‘ā transition. We will also use qualitatively this diagram for explaining clinker formation because by crossing the transition threshold zone and going from the pāhoehoe field to the ‘a‘ā field clinker will be generated. We note that the transition threshold zone is quite broad because there are several transitional lava types between the pāhoehoe and ‘a‘ā poles.

Two processes can occur that lead to crossing the transition threshold zone and they can be linked:

1) The apparent viscosity can increase (red arrow on fig. 1.2.1): lava flows will cool and degas during emplacement and as they do so, the liquid viscosity increases and microlite content increases. Such an evolution from pāhoehoe to ‘a‘ā is described by Rowland & Walker (1987) (see also Chapter 2).

2) The shear rate can increase (blue arrow on fig. 1.2.1): this is a frequent occurrence in lava flows, it can increase, for example when a lava flow encounters a steeper slope (fig. 1.2.2) a contorted path, a narrower valley, or a more irregular topography (see also chapter 2).
Considerations concerning the crust rupture and the clinker formation will be discussed in chapter 2.

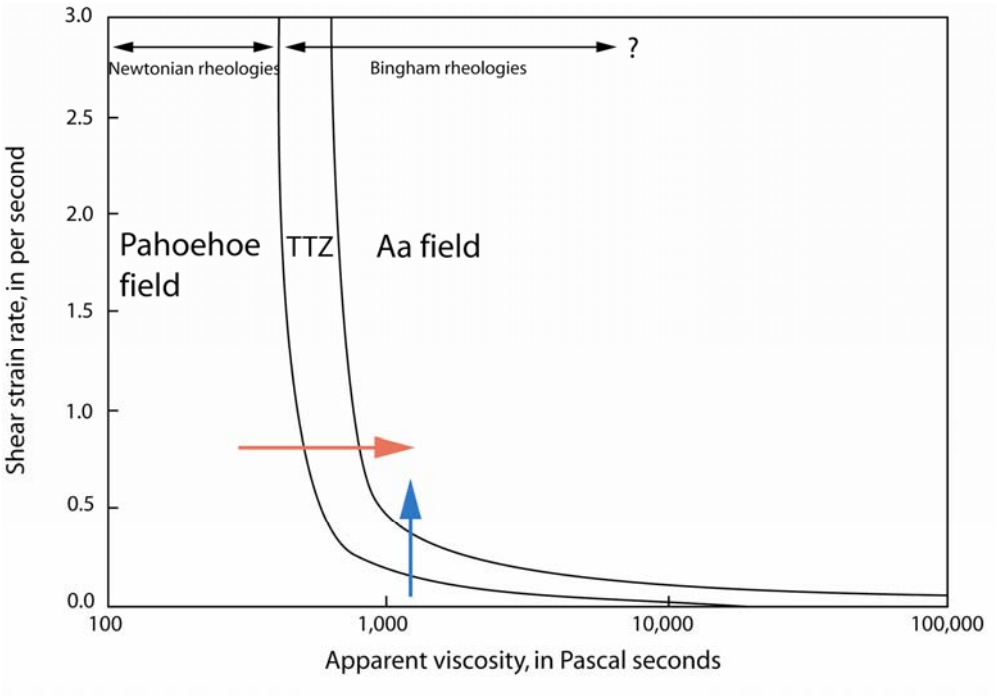

Figure 1.2.1: Diagram of shear-strain rate versus apparent Newtonian viscosity, showing the relationship of approximate stability fields for Hawaiian and ‘a‘ā lava flows and approximate transition threshold zone (TTZ) within Bingham rheology (simplified from Hon & al., 2003).

Figure 1.2.2: Pāhoehoe-to-'a'ā transition occurring in many small flows as they cascade down a steep slope at the base of Pulami Pali on the west side of the Pu'u 'O'o flow field in May 2002 (Hon & al., 2003).

1.2.2: The Myvatn fires lava flow field (Krafla volcano) as an example to discuss pāhoehoe and 'a'ā relationships

1.2.2.1: Geological setting

The Krafla volcanic system or central volcano is one of five fissure swarm-central-volcano complexes within the axial rift zone of N.E. Iceland (Bjornsson, 1985) (fig. 1.2.3) close to Lake Myvatn. The Krafla swarm is a 80–100 km long, 4–10 km wide zone of faults and fissures, with a central volcano, evidenced by a topographic high and caldera, just north of the swarm mid-point (Bjornsson, 1985; Gudmundsson, 1995, 1998). Rifting episodes, resulting from the build-up of tensional stresses due to spreading, occur every few hundred years and are accompanied by the intrusion magma and effusion of lava (Bjornsson, 1985; Gudmundsson, 1998).

The area around Mt. Leirhnjukur is a central volcano (fig. 1.2.4). About one hundred thousand years ago, this was the site of a volcanic cone that a large volume of pyroclastics and

underwent caldera collapse. The caldera has now filled with later volcanic material, so the landscape is flat. Underneath, there is a magma chamber at a depth of about 3 kilometres (Gudmundsson, 1995 & 1998).

Volcanic activity in Krafla is periodic. The magma chamber expands by magma pressure from intrusions, which raises the ground. The magma chamber boundary then suddenly fails and magma is injected northwards or southwards through dykes in a rifting episode. Part of the magma may reach surface to erupt. As the pressure in the magma chamber decreases, the ground subsides quickly. This process repeats itself at a few months interval over a few years running (Gudmundsson, 2008).

Eruptions began in 1724, in the Lake Myvatn area with a violent explosion, which created the crater Viti (The Inferno). A series of earthquakes and eruptions occurred in the following years near Mt. Krafla. The greatest eruption occurred in 1729 when lava ran from Mt. Leirhnjukur all the way down to Lake Myvatn. During the eruption, the lava ran around the church at Reykjahlid, which survived. After a dormant period of 250 years, a new series of volcanic eruptions ensued in the area around Mt. Krafla. These were the Krafla fires (1975–1984) that formed a lava flow field made of tholeitic lava (Gudmundsson, 2008).

During this PhD, I have worked on the South West branch of the Myvatn fires lava flow field, where it reached the Myvatn lake (fig. 1.2.4 & 1.2.5). This field work has lasted 2 weeks during August 2006 in collaboration with Thorvaldur Thordarsson (Edinburgh University). This fieldtrip was an opportunity to map this branch by determining surface types, or terms such as pāhoehoe, slabby pāhoehoe and ‘a‘ā lava and to map the occurrence of tumuli and tubes (fig. 1.2.5). In the field, particular attention was taken to explain the relationships between the different surface morphologies of a contemporaneous lava flow features in order to check the inferences provided in 1.2.1.

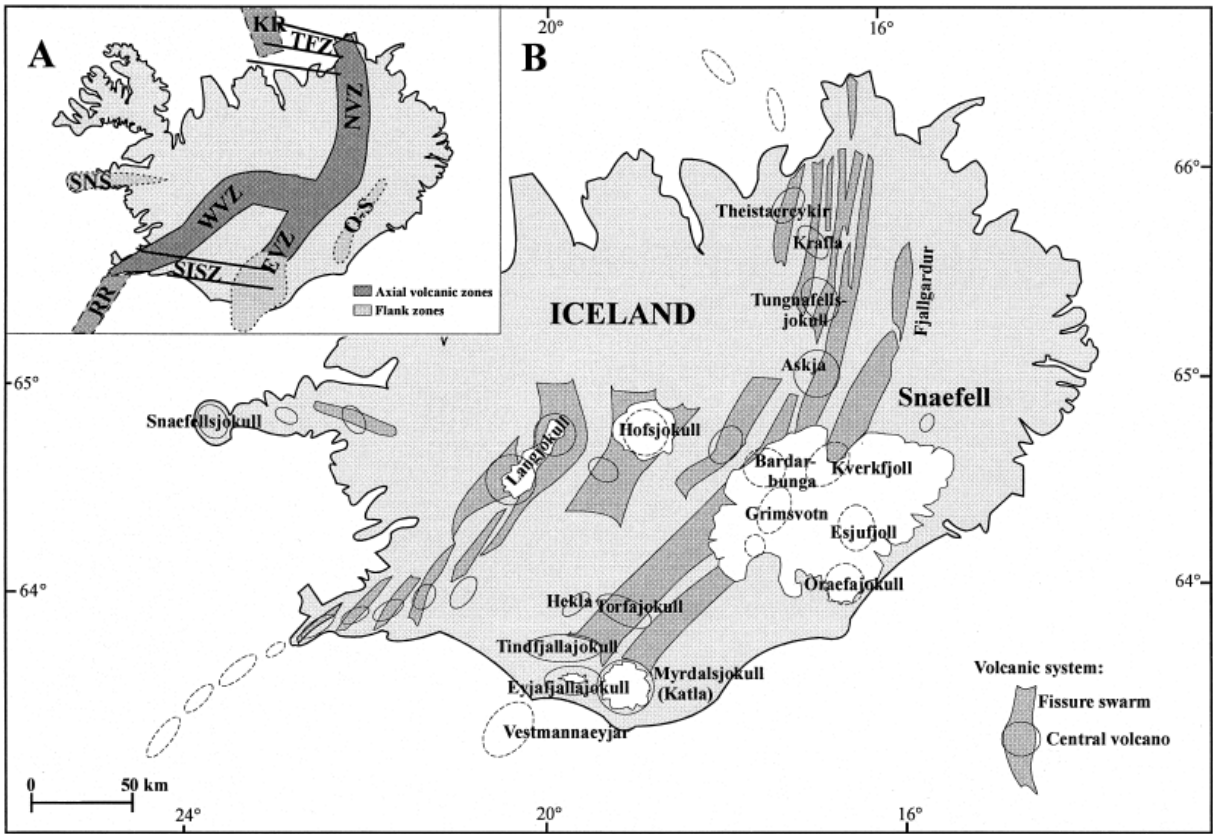

Figure 1.2.3: (A): Simplified tectonic map of Iceland, showing the neovolcanic zones—axial volcanic zones, flank zones and fracture zones. Abbreviations as follows: RR. Reykjanes Ridge, SISZ. South Iceland seismic zone, WVZ. Western volcanic zone, NVZ. Northern volcanic zone, EVZ. Eastern volcanic zone, TFZ. Tjornes fracture zone, KR. Kolbeinsey ridge, SNS. Snæfellsnes volcanic zone, O-S. Oræfajokull–Snæfell zone. (B): A selection of the recognised volcanic systems in the neovolcanic zones, which have been active in the Upper Pleistocene and postglacial period. (0.7 Ma). The locations of well-developed central volcanoes are marked, and all examples mentioned in the text are named. Stippled areas are fissure swarms, notably absent outside the axial volcanic zones (*from* Hards & al., 2000).

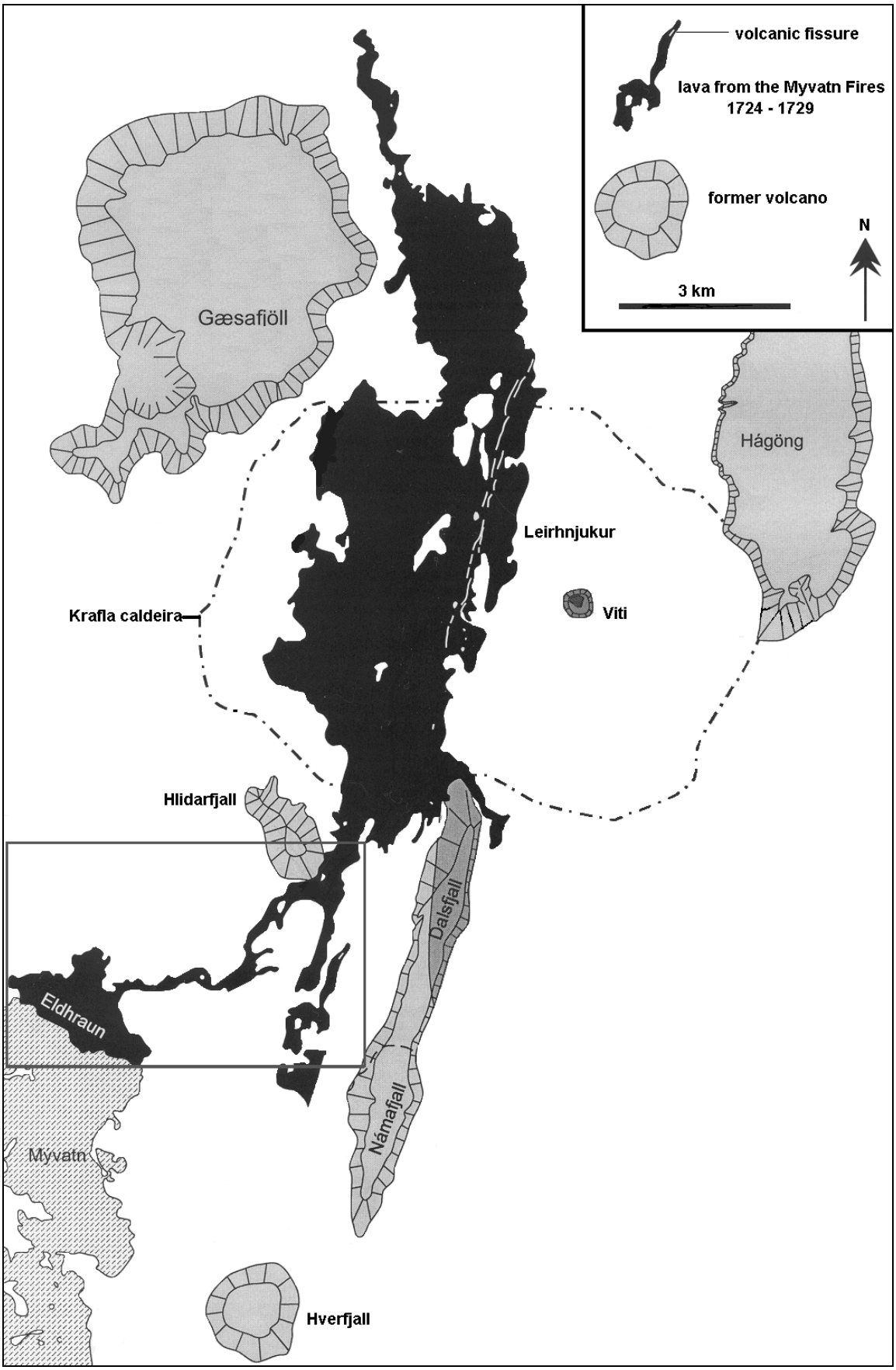

Figure 1.2.4: Map displaying the extension of the Myvatn Fires lava flow field (1724 – 1729) and its surroundings. The black box is the close up of fig. 1.2.3.

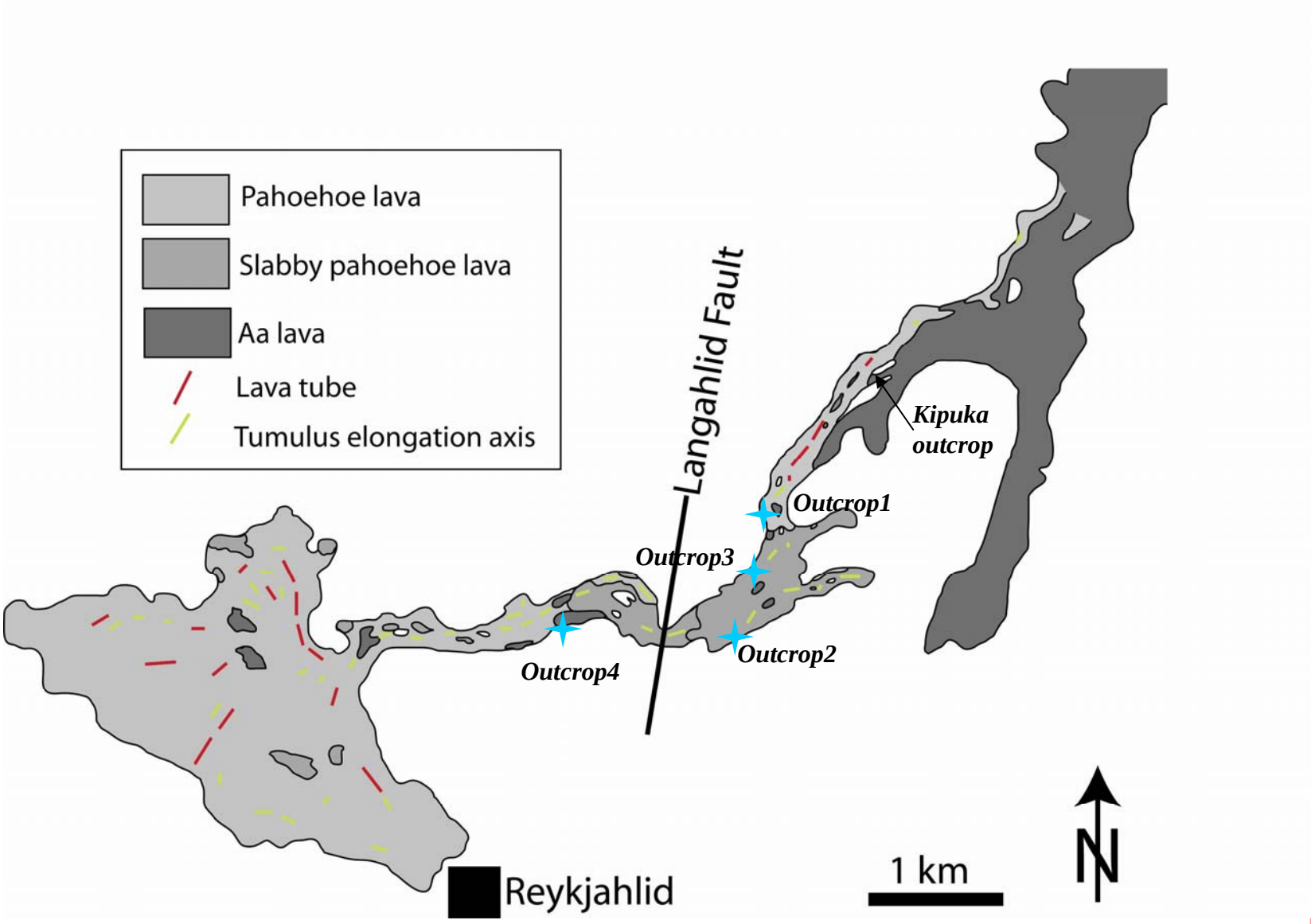

Figure 1.2.5: Map displaying the South East branch of the Myvatn Fires lava flow field (1724 – 1729): its different surface morphologies classification (pāhoehoe, slabby pāhoehoe and ‘a‘ā) and features interpreted from the surface features (tumuli and lava tube extents).

1.2.2.2: General pattern of the Myvatn fires lava flow field

The first stage in mapping a lava flow field is to classify the surface morphologies. It is evident in the field that we observed typical pāhoehoe (fig. 1.2.6) and ‘a‘ā (fig. 1.2.8) lavas. As the surface morphology has had only a slight vegetation colonization mainly due to lichens and the grey moss *Racomitrium*, the pāhoehoe – ‘a‘ā distinction is evident (see 1.1.1) and is of course corroborated by internal structures (see 1.1.3).

Nevertheless as noted in 1.1.5, pāhoehoe and ‘a‘ā are two end-members separated by a range of transitional terms. In the field, we can easily identify such a transitional terms, and we have identified slabby pāhoehoe according the criteria of Guilbaud & al. (2005).

A slabby pāhoehoe lava is a slabby-surfaced lava, characterized by a jumble of large tabular to curved pieces of pāhoehoe crust, dislocated and tilted-up on the flow surface (fig. 1.2.7a). Lava rise pits and inflation clefts are also common on these flows. The thickness of individual crustal slabs ranges from a few centimetres to several decimetres but is most commonly 20 to 50 cm and sometimes the slabs are imbricated. Smaller-sized rubble is often mixed in between the slabs as a minor component. The external surfaces of the slabs may be coherent and slightly spiny or convoluted with ropy features and stretched toes attached to the slab interior. Some slabs have undersides covered by numerous glassy protrusions typical of gas blister walls. In other cases scrape marks are present (fig. 1.2.7b) and many slabs have a reddish contorted base.

Figure 1.2.6: Surface of a pāhoehoe lava from the Myvatn fire eruption (outcrop 1, location on fig. 1.2.5), the flow is 12m wide and displays a smooth surface and inflation fissures.

Figure 1.2.7: a. Surface of a slabby pāhoehoe lava from the Myvatn fire eruption (outcrop 2), the flow is 10m wide and displays numerous pieces of pāhoehoe crusts that have been broken forming a non continuous surface. b. A more evolved slabby pāhoehoe lava (closer from the ‘a‘ā pole) displaying tilted pāhoehoe crust pieces with scrape marks are present (fig. 1.2.7b) and a reddish contorted base (outcrop 3).

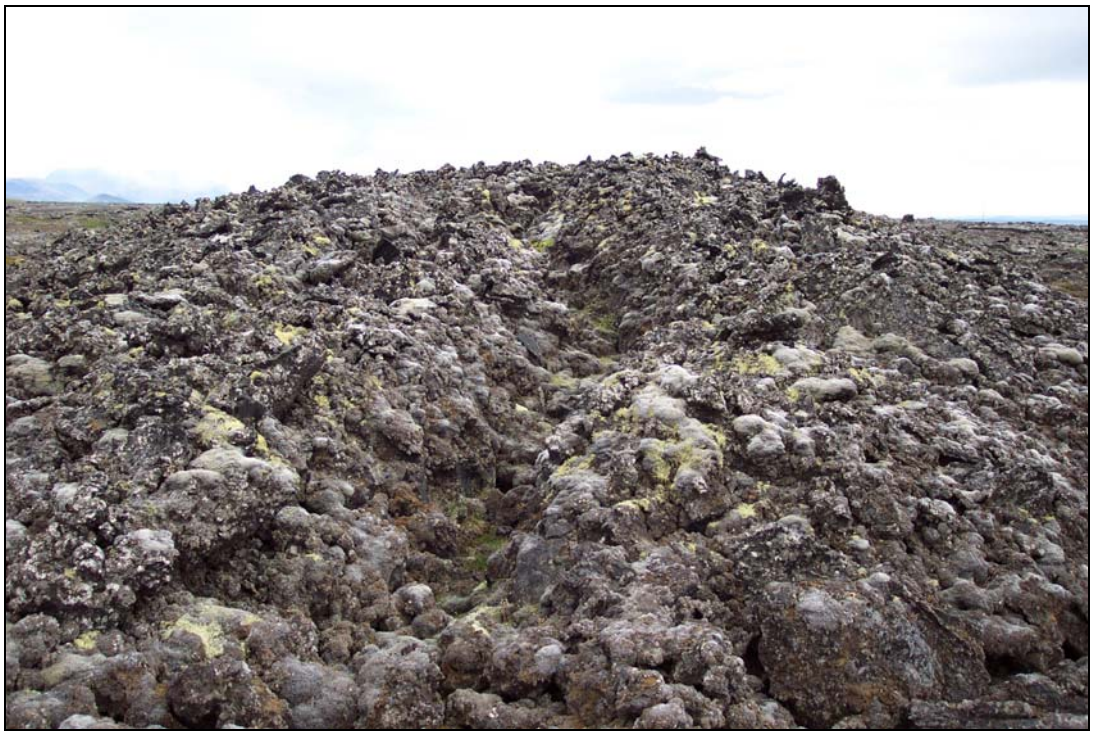

Figure 1.2.8: Surface of an ‘a‘ā lava from the Myvatn Fires eruption (outcrop 4), the picture is 10m wide and displays a clinkery surface.

As noted in 1.1 and as observed on the field (fig. 1.2.5), we have encountered lava tubes in pāhoehoe lavas and tumuli in both pāhoehoe and slabby pāhoehoe lavas confirming that the establishment of such structures is more frequent in less viscous pāhoehoe, rather than the more viscous ‘a‘ā ones.

1.2.2.3: Two close-ups on the Myvatn fires flow field underlining pāhoehoe and ‘a‘ā relationships

In this section we will discuss two examples of contemporaneous pāhoehoe and ‘a‘ā relationships, where we can explain the reasons for the variations. In fact, as the Myvatn Fire eruption lasted for 5 years, in the field we have several time-spaced lava flows, where there is not a simple rheological relationship but simply a more recent lava covering a former one. The two outcrop locations for synchronous lavas are indicated on fig. 1.2.5 by blue squares. We call the upslope one as the Kipukas outcrop as it is a lava tongue channelized between two kipuka (kipuka is an Hawaiian name used for an island of basement that has been isolated by lavas) and the downslope the Langahlid outcrop, which it is located on the Langahlid fault scarp.

1.2.2.3.1: The Kipukas outcrop

The Kipuka outcrop refers to a lava tongue between two kipukas that comes from a major ‘a‘ā lava field (fig. 1.2.9.a).

Most surprisingly, when issuing from the main ‘a‘ā lava flow, this tongue displays immediately a pāhoehoe surface (fig. 1.2.9.b). This is clearly evidence of an ‘a‘ā-to-pāhoehoe transition as previously described by Hon & al. (2003) (see 1.2.1). In the field, the origin of this pāhoehoe tongue, estimated from the ropey structure orientations, is located at a breakout in the middle part of the main feeder ‘a‘ā flow. In this middle part of the ‘a‘ā flow, i.e. the core, lava would have been less viscous than its clinkery surface or margins. Also, as the pāhoehoe tongue has not followed the main lava direction, and as ropey structures are preserved, we can also argue that the shear strain rate was lower than in the ‘a‘ā feeder flow. So according to field criteria, I propose that this ‘a‘ā-to-pāhoehoe transition was formed by a breakout allowing the fluidal core to extrude in direct contact with the atmosphere and with relatively low shear strain rates.

Down slope, this lava tongue has evolved into an ‘a‘ā lava. After the ‘a‘ā-to-pāhoehoe transition, we have just 40m further, a pāhoehoe-to-’a‘ā transition (fig. 1.2.9a & c). This second transition is also sharp: the continuous pāhoehoe surface is disrupted into slabs and in the space of a few meters these slabs are extensively broken to form clinker-like fragments (fig. 1.2.9.c). In the field an important parameter has changed at this transition point: the slope, or at least the surface slope. In fact, from its extrusion point to its transition point, the pāhoehoe tongue has a surface slope of around 3° and precisely at the transition point, its surface slope becomes around 10°. This break is correlated with the kipuka’s morphology. Thus, the transition has been triggered by a sudden slope increase, which indicates a probable increase in the shear strain rate.

In conclusion, even if this Kipukas lava tongue is small (110m long), it has recorded an ‘a‘ā-to-pāhoehoe transition and a pāhoehoe-to-’a‘ā transition. These transitions can be explained by rheological and kinematic parameters, such as the viscosity and the shear strain rate and the interpreted evolution between pāhoehoe and ‘a‘ā fields can be easily sketched in the Hon & al. (2003) diagram (fig. 1.2.10).

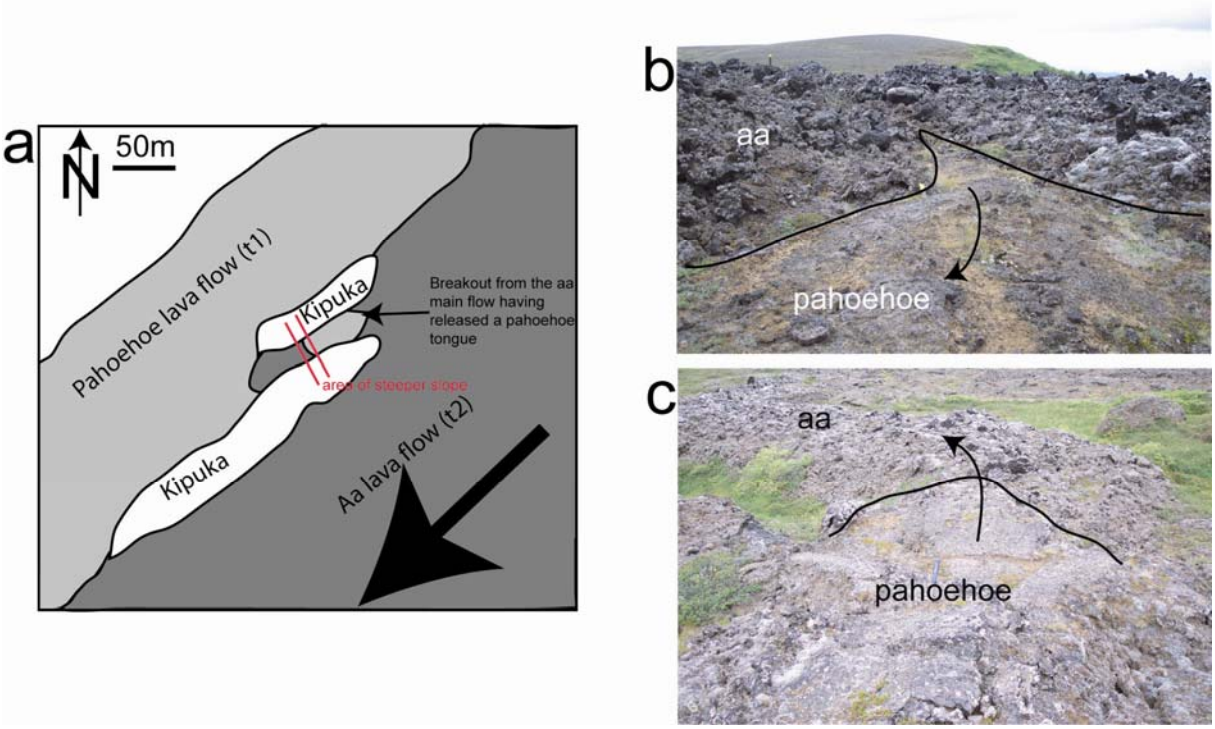

Figure 1.2.9: The Kipukas outcrop: **a**. map of the Kipukas outcrop displaying the lava tongue between two kipukas; **b**. The pāhoehoe tongue source issuing from a break in the ‘a‘ā lava (view toward North West); **c**. The same pāhoehoe tongue evolved into an ‘a‘ā tongue where the slope is steeper (10° as opposed to around 3° in the surroundings) (view toward South East).

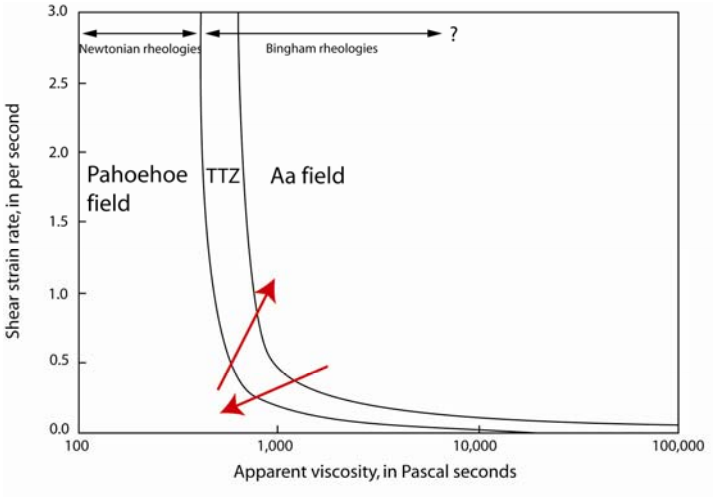

Figure 1.2.10: Sketched evolution of the Kipukas tongue on the Hon & al. (2003) diagram. See fig. 1.2.1 for a complete legend and see text for explanations.

1.2.2.3.2: The Langahlid outcrop

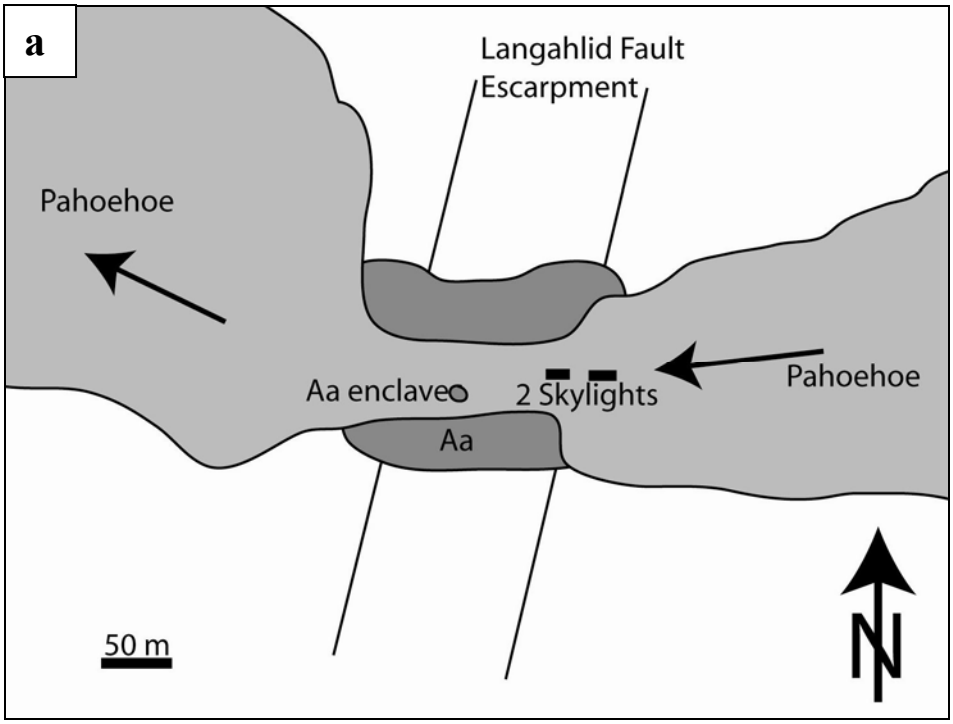
a
Langahlid Fault
Escarpment
Pahoehoe
Aa enclaveo
2 Skylights
Pahoehoe
Aa
50 m
N

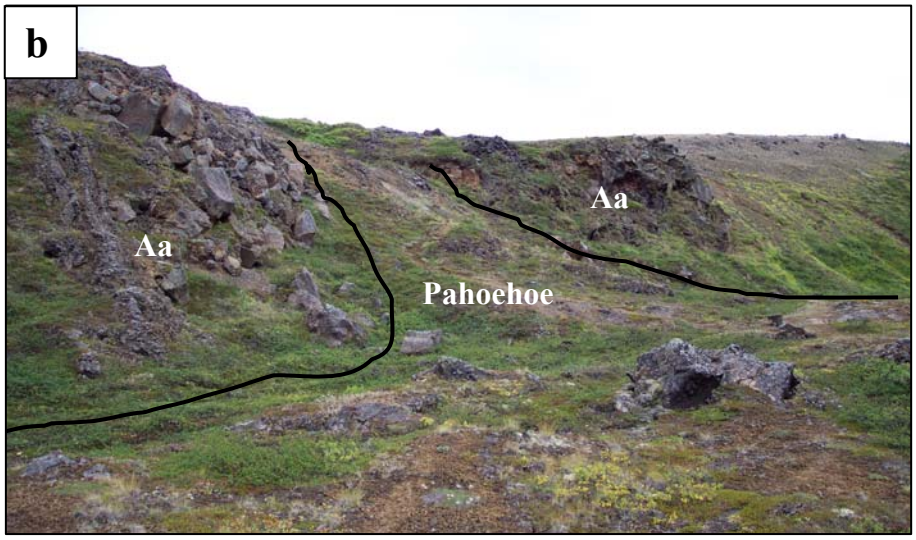
b
Aa
Aa
Pahoehoe

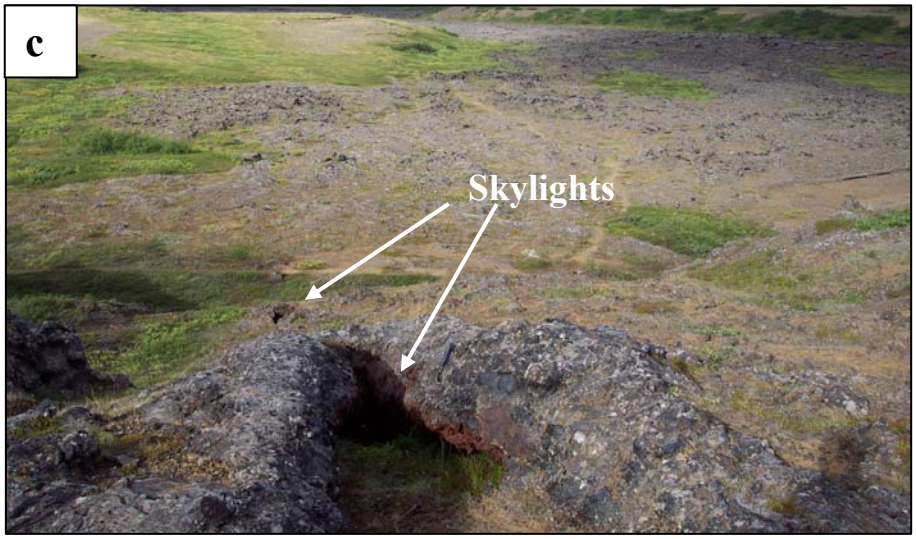
c
Skylights

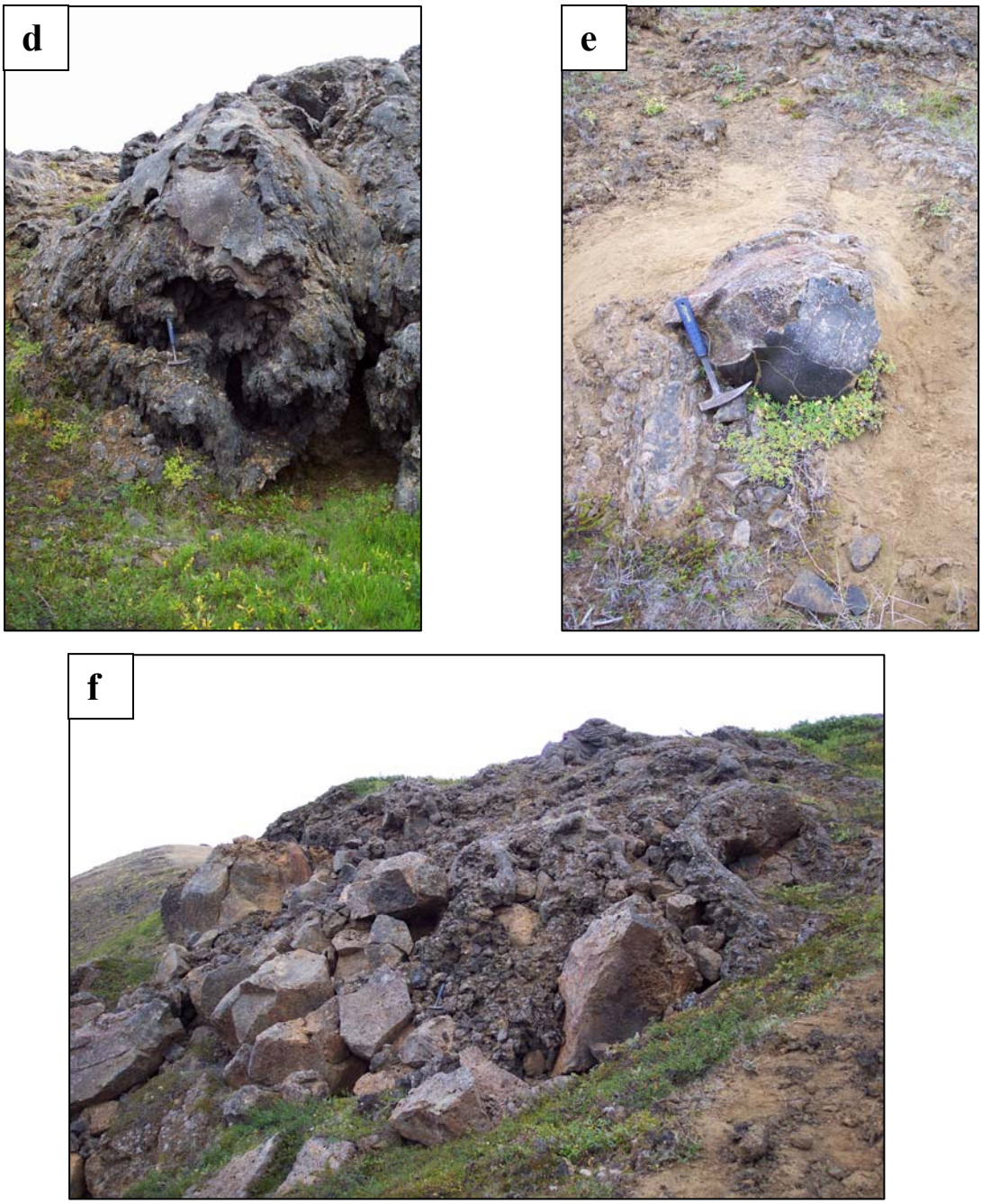

Figure 1.2.11: The Langahlid outcrop: **a**. Map of the Langahlid outcrop; **b**. Upward view of the Langahlid fault escarpment displaying pāhoehoe and ʻaʻā relationships; **c**. Down slope view from the top of the Langahlid fault escarpment displaying two skylights in the pāhoehoe lava showing a lava tube; **d**. In the middle of the fault escarpment, lava is falling by preserving its smooth pāhoehoe surface; **e**. Still in the middle of the fault escarpment there is a clinkery piece of an ʻaʻā lava, which has been enclosed and mantled by the later pāhoehoe lava; **f**. typical aspect of the ʻaʻā lava present on the sides of the fault escarpment.

The Langahlid outcrop refers to the area surrounding the NNE-SSW Langahlid normal fault escarpment (see 1.2.2.1).

Before reaching and falling down the escarpment, the lava flow displays a typical pāhoehoe surface and when overtopping the escarpment, a lateral zonation occurs: on the lava flow border there is ‘a‘ā lava whereas in the middle of the flow there is pāhoehoe lava (fig. 1.2.11.a, b, d & f). Hon & al. (2003) have observed on an active Hawaiian flow a pāhoehoe-to-’a‘ā transition when overtopping an escarpment (fig. 1.2.2) but here, the lava evolution does not seem to be so easily explained, as we are looking at the result of a 5 years-long eruption. On the fault escarpment ‘a‘ā lavas have clearly flowed before the pāhoehoe ones. Thus when the first amount pāhoehoe lavas reached the fault escarpment, there may have been the classical transition described by Hon & al. (2003), with the breaking of the vesicular pāhoehoe crust forming clinkers. Such a transition, as in the Kipukas pāhoehoe-to-’a‘ā transition is clearly and mainly due to the slope increase, generating a shear strain rate increase. This slope increase is stronger at the Langahlid outcrop, with a difference of 4° to 40°.

We have to explain, however, why pāhoehoe lava occurs on the fault escarpment to feed the pāhoehoe-dominated final flow front that reached the Myvatn Lake. The answer can possibly be found at the top of the escarpment with the occurrence of two skylights showing the existence of a lava tube (fig. 1.2.11 c). We can suggest a series of event where the pāhoehoe lava when first encountering the escarpment has indeed evolved into ‘a‘ā lava but then, with continuing flow from the vent, a tube network has developed before the escarpment. On the escarpment, due to the strong slope increase, the tubes have ceased and has thus released onto the escarpment a less viscous lava (thermally insulated before by the lava tube) that displays a chocolate-like fountaining (fig. 1.2.11 d) and ropy structures (fig. 1.2.11 e) even with the increase of the shear strain rate. In other words, the viscosity effect has predominated over the shear strain rate effect. This competition between of rheological parameters, was thus dominated at first by the shear strain increase to form at first ‘a‘ā lava and then the decrease in viscosity due to tube development has allowed the later extension of pāhoehoe lava.

This temporal evolution is also confirmed by the existence, on the escarpment, of an ‘a‘ā clinker having been mantled by the pāhoehoe lava released by the tube system (fig. 1.2.11 e).

In conclusion, as in 1.2.2.3.1 dealing with the Kipukas outcrop, we can also display the evolution of the rheological parameters at the Langahlid outcrop in the Hon & al. (2003) diagram (fig. 1.2.12). The arrow 1 refers to the first pāhoehoe-to-’a‘ā evolution whereas the arrow 2 refers to the preservation of pāhoehoe characteristics due to less viscous lava.

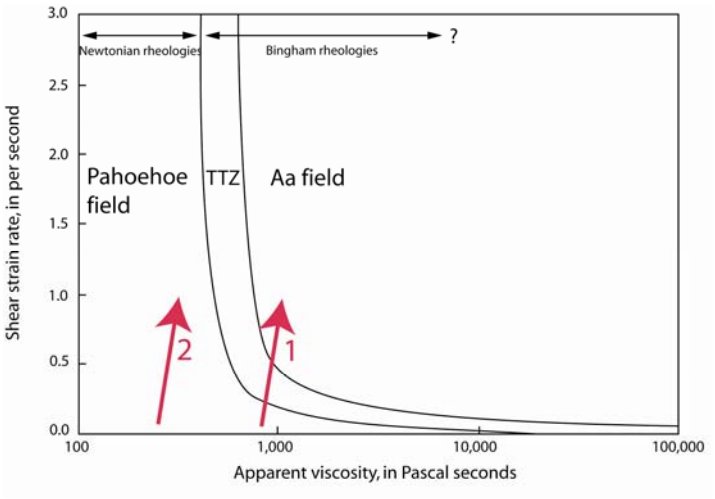

Figure 1.2.12: Sketched evolution of the Langahlid lava on the Hon & al. (2003) diagram. See fig. 1.2.1 for a complete legend and see text for explanations.

1.2.2.4: Conclusions

The Myvatn Fire lava flow field has allowed us to study the coexistence of pāhoehoe and ‘a‘ā lavas, but also transitional terms (slabby pāhoehoe in the studied case). It has also allowed us to discuss of this coexistence and the relationships due to two well-preserved areas. These two outcrops were significant in terms of slope increase revealing an increase in the shear strain rate. However both showed also the release from the lava core or lava tube allowing less viscous lava to flow over the surface. Simply, with the viscosity and strain rate, we have found suitable explanations for the lava facies variations. The use of the Hon & al. (2003) diagram, even if obtained for Hawaiian lava, has been used here and has been used to propose a suitable evolution of the lava between the pāhoehoe and the ‘a‘ā fields (fig. 1.2.10 & 1.2.12).

Nevertheless, in this location, we are conscious that we have used the evidence in our disposition, which have been relevant according Hon & al (2003) diagram. Other parameters, not guessable on a frozen lava flow field may have interacted such as the lava discharge rate, the chemical evolution, the roughness of the buried ground. It would be interesting to monitor closely a future eruption to test in more detail such possible parameters.

1.3: APPLICATION OF PĀHOEHOE AND ‘A‘Ā TERMS TO LAVAS FROM THE FRENCH MASSIF CENTRAL

1.3.1. Problems encountered and resolutions

As noted in 1.1.2, it is often tricky to associate many centuries to millions years old lava flows to one particular surface morphological type (pāhoehoe or ‘a‘ā) because the surface, the first criterion for attribution, is expected to be eroded and /or covered in a manner which depends on environmental parameters (see 1.1.2 for examples).

Fortunately, pāhoehoe and ‘a‘ā flows not only differ superficially in surface textures, but also fundamentally in their emplacement mechanisms and thus in their internal structures (e.g. Kilburn, 1993 ; Polacci & al., 1999 ; Duraiswami & al., 2003). Thus criteria other than surface texture can be used in the French Massif Central. These criteria have been already discussed in 1.1., and they include lava cross-section geometry, clinker formation, vesicle distribution and the mafic mineral distribution. In 1.1.4.3., we have supposed that the use of the AMS is not of a great interest; however we will discuss this point by the study of a lava flow (Royat F2). And in 1.1.4.2., we have pointed out that textural characterization can only be helpful when sampling glass on still active lava flow and thus will not be used by studying the Massif Central lava flows.

1.3.2. ‘A‘ā lava dominates in the Chaîne des Puys

The easiest way to recognize ‘a‘ā lava flow is by the occurrence of clinker (see definition in chapter 2) in a significant proportion at the flow top and eventually at the flow base. I use the

word ‘significant’ for the flow top as we will describe in the 2nd chapter two particular ways to form breccia at the flow base, that could be confused with ‘a‘ā clinker. As noted in 1.1.2., ‘a‘ā lavas will form clinker at their base and according a caterpillar motion, these clinkers can be moved to the flow base. In addition, as shown on fig. 1.1.2, some clinker pockets can be engulfed in the massive core. Thus, the occurrence of surface clinker in significant proportion will be sufficient to attribute the ‘a‘ā classification, whatever the outcrop size and the outcrop location in a flow section.

In the Chaîne des Puys, a local name *cheires* is used for describing irregular surface of lava flows consisting in a accumulation of clinkers. For these *cheires* the ‘a‘ā classification is clear. Thus, the more famous *cheires,* such as Saint Saturnin (≈ 8,000 years), Mazaye (≈ 15,000 years), Côme (≈ 12,000 years) and Louchadière (≈ 35,000 years) are typical ‘a‘ā flows (fig. 1.3.1 & see Boivin & al., 2004 for dating references). These are the only Massif Central lava flows where the ‘a‘ā surface has been well preserved.

For other lava flows, which are older, the surface morphology could have been removed, eroded or covered by later volcanic products or a thick soil and thus sections are needed to determine their type. Using sections, the Royat F1, F2 and F4 flows are classified as ‘a‘ā (see 2.1.4.1. for the flow map extension) (≈ 45,000 years), the Blanzat, the Argnat and the Egaules flows (≈ 40,000) (see 2.1.4.2. for the flow map extension) (see Boivin & al., 2004 for age determination references). Boivin & al. (2004) argue that lavas from the Chaîne des Puys are totally dominated by ‘a‘ā morphologies.

In fig. 1.3.2, we present a typical complete section of an ‘a‘ā flow by taking the example of the Royat F3 flow.

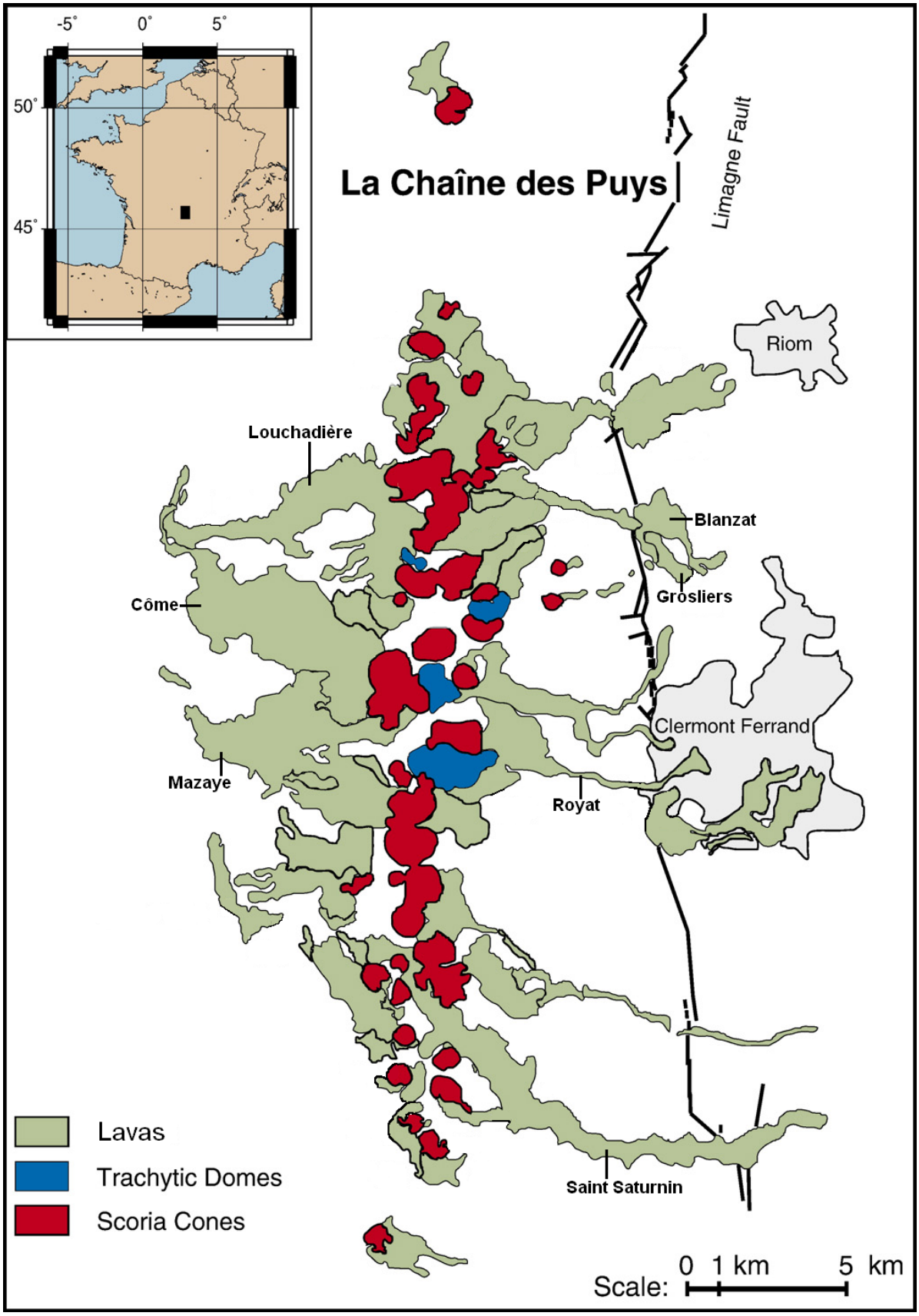

Figure 1.3.1: Simplified geological map of la Chaîne des Puys and location of the studied flows.

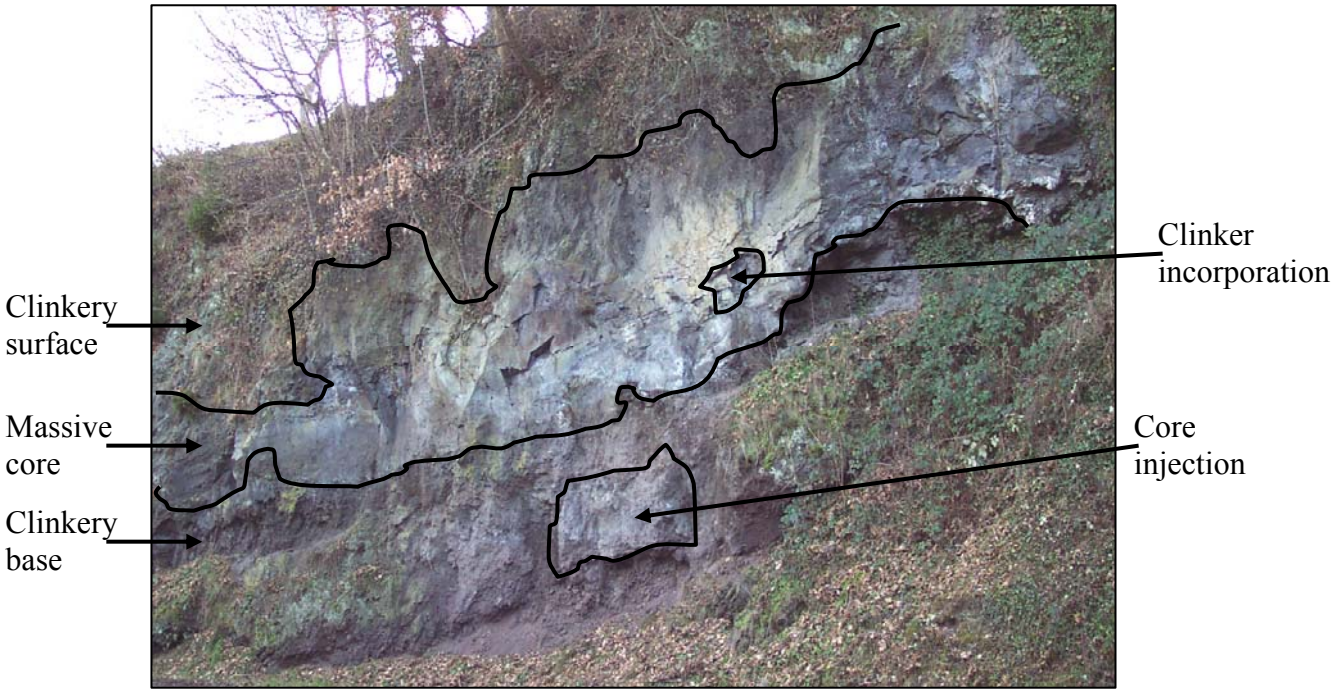

Figure 1.3.2: Cross section through the Royat F3 lava flow displaying typical ‘a‘ā morphology (compare with fig. 1.1.2) (the escarpment is 4m high).

1.3.3. Some pāhoehoe occur in the Chaîne des Puys

As explained in 1.3.2 the ‘a‘ā attribution to a lava flow is quite easy even if the outcrop available is quite small, if clinker is found. Things are not so easy for pāhoehoe determination and if the outcrop extension is small it may be impossible. According several criteria I have checked for pāhoehoe lava in the Chaîne des Puys, and I will present two examples displaying pāhoehoe characteristics: the Royat F3 flow and the Grosliers flow.

1.3.3.1. The Royat F3 lava flow

1.3.3.1.1. Presentation of the Royat F3 flow

The Royat F3 flow is a trachybasaltic lava flow emplaced about 45,000 ago (Boivin & al., 2004) from the Puy de Lacroix area as deduced by basement isobaths (Gagnière, 1980) (fig. 1.3.3 & see fig. 2.1.3a for a complete map of the Royat lava flows).

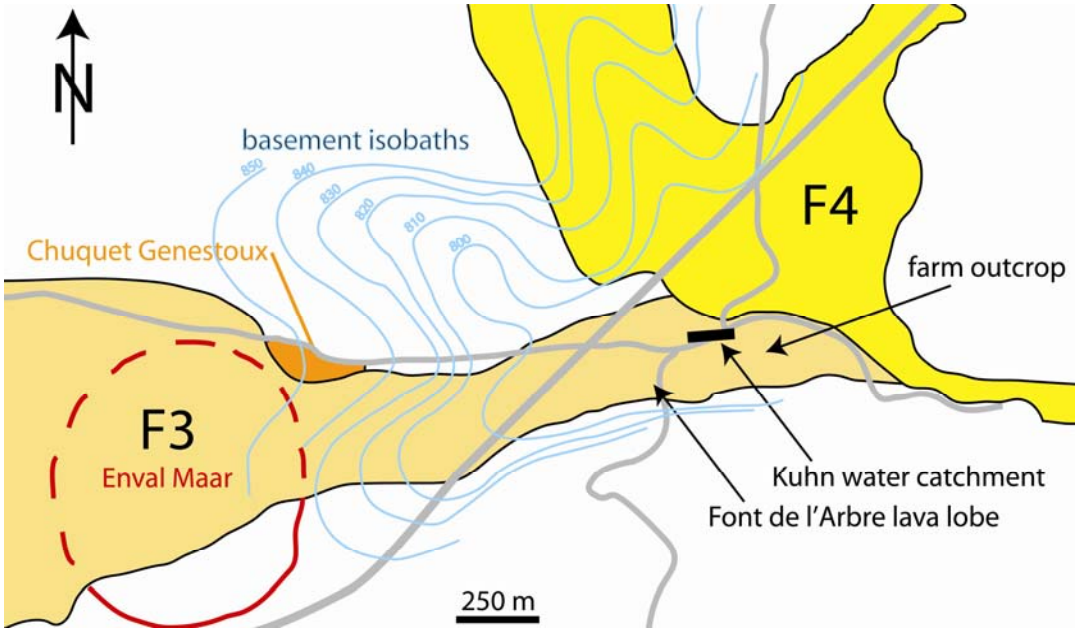

Figure 1.3.3: Map of the upper part of the Royat F3 flow with outcrop locations and the thalwegs having been used to guess its course.

1.3.3.1.2. Morphological evidences of a pāhoehoe flow

Two outcrops located in the small village of la Font de l'Arbre clearly reveal pāhoehoe emplacement evidence.

The Font de l'Arbre lava lobe

The first, the Font de l'Arbre lava lobe (fig. 1.3.4. and see location on fig. 1.3.3.) located on the Montrodeix road displays a typical pāhoehoe lobe morphology even if its base is not exposed. First and foremost, not a single clinker is present. The outcrop has a vesicular crust (see 1.3.3.1.3) and a massive core. In places, large vesicle pockets are formed. These are generally interpreted as being the result of bubble coalescence or gas accumulation under a cooled crust. One 35cm-long megavesicle is located under the vesicular crust (fig. 1.3.4.). These vesicle patterns are typical of a pāhoehoe emplacement (see 1.1.4.1.) and the formation of megavesicles is typical of an endogenous lobe growth: while the crust is cooling, the still hot and continually-fed core releases gas that accumulates under the crust.

The outer part of the outcrop also has radial fractures (fig. 1.3.4.). These fractures are not as regular as the cooling fracture forming columnar pattern, and they do not present any plumose structure associated to columns (Ryan & Sammis, 1978; DeGraff & Aydin, 1987;

Grossenbacher & McDuffie, 1995). In fact, these fractures are similar to those I have observed in the pāhoehoe tumuli of the Myvatn fire lava flow field and on other Icelandic shield volcanoes (Rossi & Gudmunsson, 1996). These fractures are also witnesses of endogenous growing of the cooling lava lobe still fed by fresh lava leading to the fracturing of the cooled vesicular crust.

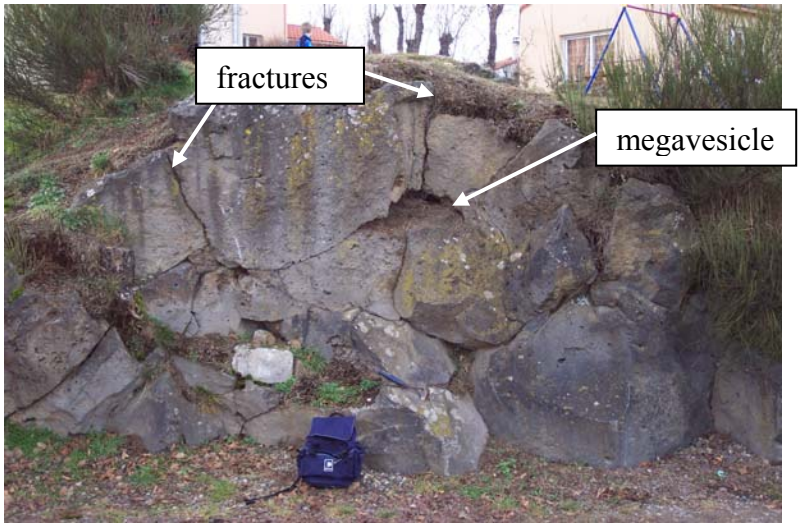

Figure 1.3.4: The pāhoehoe lobe of Font de l'Arbre (photo take before coring for AMS) with its endogenous associated fractures and one 35cm-long megavesicle.

The Kuhn water catchment gallery

The Kuhn water catchment gallery is a 50-m gallery located 10 m under the D68 (Frémion, 2001) (see location on fig. 1.3.3). Visits and study have been possible due to the Water Cleaning Center of Clermont Ferrand. This gallery curiously does not collect water directly from groundwater circulation in F3 but collects groundwater from the F2 flow through the altered granite regolith (Loock & al, 2007). Study of the catchment walls has revealed good evidence of a lava tube. Thus is the first lava tube described in the Chaîne des Puys to my knowledge.

Evidence includes:

(1) Non-penetrative grooves on the wall of the gallery-tube (fig. 1.3.5a) which correspond to the friction of still moving lava in the tube (Calvari & Pinkerton, 1998; Kauahikau & al., 1998, Calvari & Pinkerton, 1999).

(2) A smooth roof with beginning of smooth stalactites (fig. 1.3.5b) that are considered to form by remelting by gases accumulating below the roof (Kauahikau & al., 1998, Calvari & Pinkerton, 1999). Stalactites are quite small (a maximum size of 1.5 cm long has been measured), this can be explained by the fact that the lava tube roof is nearly horizontal and not conical, thus limiting the coalescence and the growing of speleothems.

(3) The roof structures reveal that it has not been constructed during one single lava flow. Rather, it has been subjected to at least three variations in the incoming lava influx resulting in the formation of a triple roof (fig. 1.3.5c): the first forming roof displays stalactites and the two other are observable under this by the occurrence of two vesiculated crusts. As noticed by Calvari & Pinkerton (1999), each roof probably corresponds to a feeding and spreading cycle of the tube. This cyclic process can be due to discharge rate variation, downward blocking, inflation at the lava flow front, or coalescence between several tubes (Calvari & Pinkerton, 1999). This last possibility can be in our case rejected as the F3 flow is well thalweg-constrained (fig. 1.3.3.) and thus the coexistence of at least two lava tubes appears to be implausible.

The fact that no clinker has been observed in the gallery even on sections cut for water trapment (where the excavators generally search for clinker), nor the Font de l'Arbre lobe outcrop strong indications of pāhoehoe lava. The tube-like structures and the inflation structures are also evidence that there was a main lava path channelized in a lava tube with lateral inflating lobes.

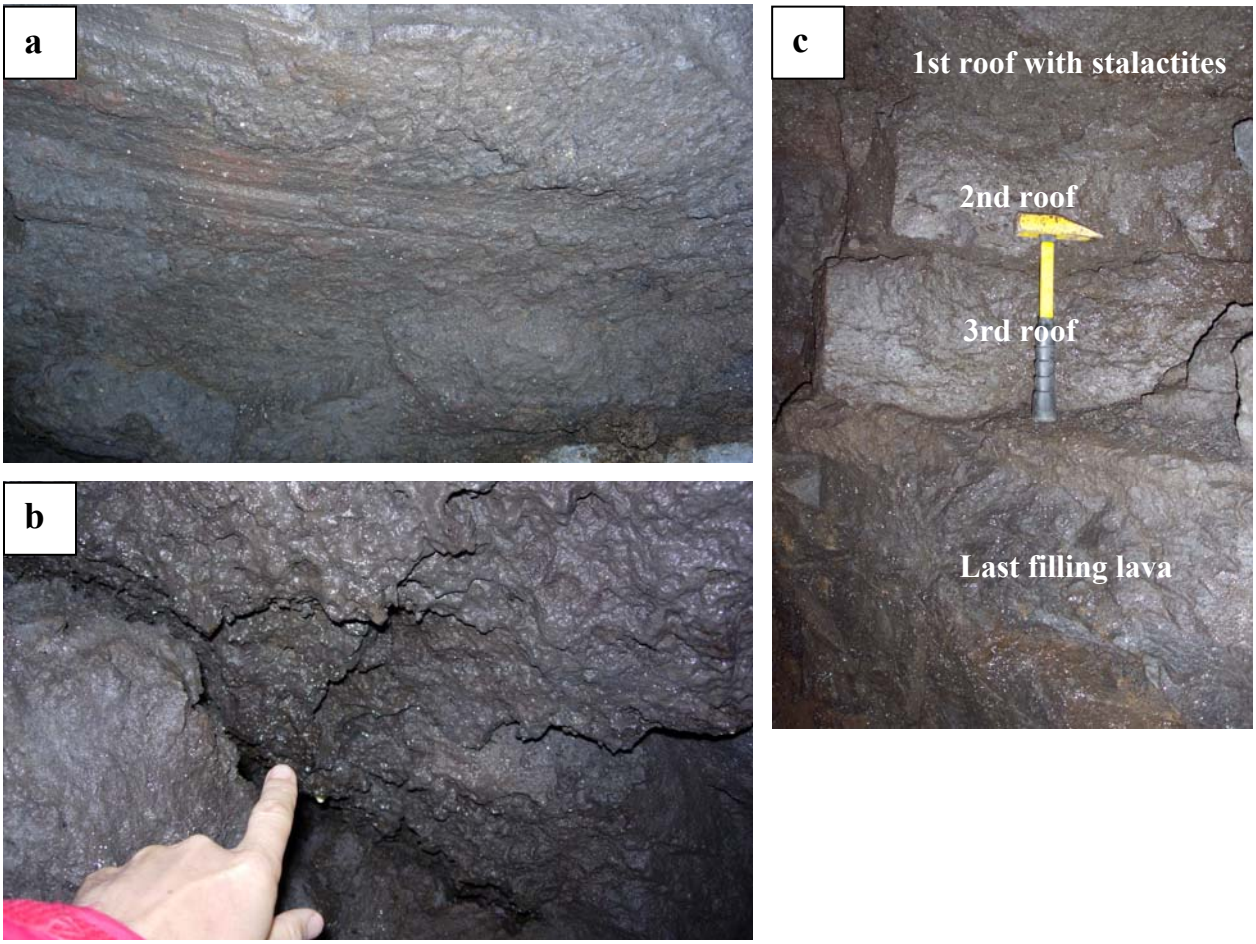

Figure 1.3.5: Different formations observed in the Kuhn water catchment gallery/tube: **a**. non-penetrative grooves on the sides of the gallery (picture is 15cm-high); **b**. stalactites present on the first tube roof; **c**. stack of the three tube roofs over the last lava fill (This is an artificial section done water trapment).

1.3.3.1.3. Rheological evidence of a pāhoehoe flow

Phenocryst zonation

As noted in 1.1. and as discussed by Self & al. (1998), a particular phenocryst zonation can be observed in pāhoehoe lobes. That is the reason why, in parallel with the AMS sampling on the Font de l'Arbre outcrop (see 1.3.3.1.4.), we have simply counted the number of phenocryst minerals (plagioclase, clinopyroxene and some olivines) on each thin section corresponding to an AMS core sample. These data are simply used to give a rough of idea of the phenocryst zonation as, of course, counting just refer to 2.2cm diameter disks. Results are given in Table 1.3.1. and displayed in fig. 1.3.6.

Results display a pattern revealing a slight downward enrichment of the number of phenocrysts, from 4 to 9 phenocrysts (table 1.3.1), which is in agreement with the upper part of the fig. 1.1.4 and which is in accord with a pāhoehoe rheology pattern (Self & al., 1998).

Site	Number of phenocrysts per section	Number of vesicles per section	A %	ΔA
0	5	19	0,350	0,378
1	6	12	0,593	0,341
2	6	19	0,424	0,166
3	4	20	0,634	0,135
4	4	19	0,517	0,038
5	6	6	0,623	0,072
6	4	5	1,345	0,193
7	5	5	0,926	0,028
8	6	0	0,480	0,280
9	6	0	0,517	0,114
10	7	0	0,787	0,143
11	6	0	0,623	0,403
12	7	0	0,427	0,093
13	9	0	1,429	0,044
14	8	0	1,897	0,017

Table 1.3.1: Evolution in the Font de l'Arbre outcrop of the number of phenocrysts and number of vesicles per section referring to thin sections associated with AMS core samples. Also the evolution of the degree of magnetic anisotropy (A) with its error bar. The drilling location is shown on fig. 1.3.6.

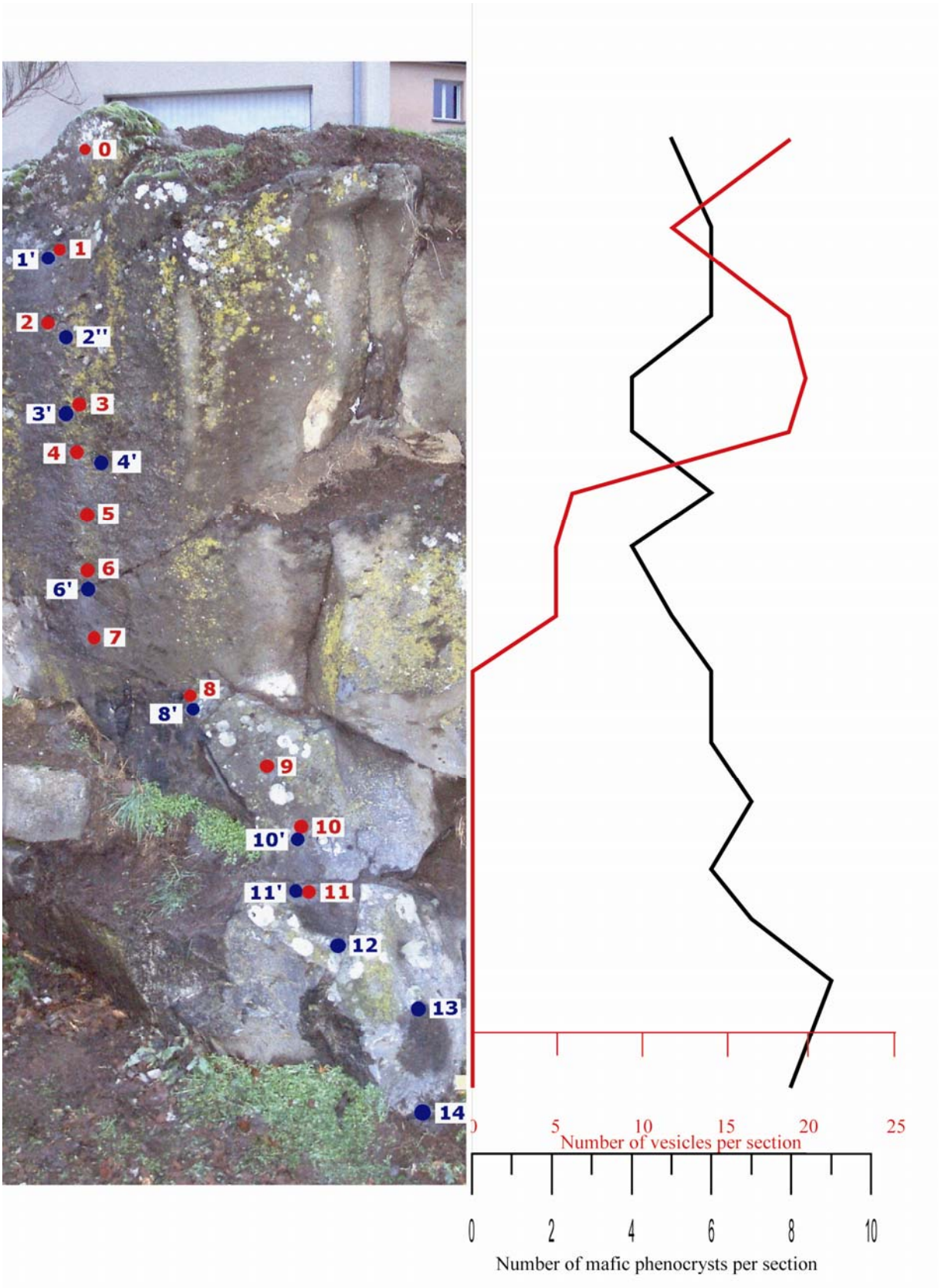

Figure 1.3.6: AMS sampling profile of the Font de l'Arbre outcrop and the corresponding evolution of number of phenocrysts and vesicles per each AMS thin section core sample.

Vesicles zonation

The vesicle zonation has been studied in the Font de l'Arbre outcrop, also simply by counting the number of vesicles on thin sections corresponding to AMS core samples. Results are reported in Table 1.3.1 and fig. 1.3.6.

We observe an upward enrichment in the vesicularity starting from 0 vesicle in the dense core to 20 vesicles in the vesicular crust. This is also in agreement with a pāhoehoe emplacement, where the vesicular crust has been preserved and not broken to form the 'a'ā clinkers (e.g. Self & al., 1998) (compare with fig. 1.1.4). The pattern is not perfect and there may be significant error, dependent on the approach. However if we stretch the results to the limit, we could speculate that the lowest value of 12 vesicles on thin section n°1 could be the result of a denser zone intercalated between two vesicular zones, each vesicular zones being linked to an inflation stage (Self & al., 1998).

An other vesicle zonation study has been performed in F3 on another outcrop close to a farm and thus called the Farm Outcrop (see location on fig. 1.3.3). This outcrop has allowed us to perform a more precise and continuous vesicle study on a constant plane. On this plane, a succession of thirteen 5×7,5 cm in size images was made on a vertical section (see fig. 1.3.7).

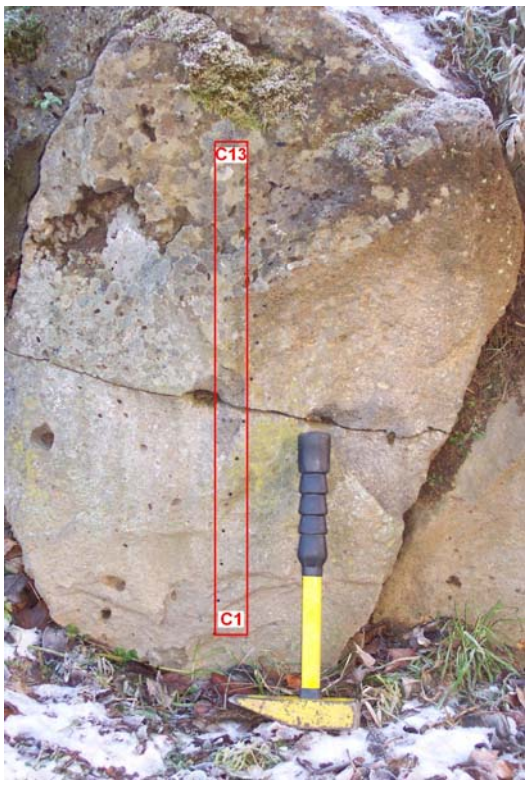

Figure 1.3.7: The farm outcrop and the vertical profile used for the study of the vesicularity.

Pictures were processed with the software ImageJ® : first they are converted into 8-bit images, then I drew the outline of vesicles, then I adjusted the threshold so that vesicles are black on white, I set the scale and the software analyzes particles from 50 pixels considered as ellipses. The results given are the number of vesicles per picture unit (5×7,5 cm), the apparent porosity (in %) (in fact I measure the porosity according a section plane and not on a volume), the average vesicle area (in cm^2), the long (l) and short (s) axis for each vesicles from which is calculated the average deformation D with $D = (l - s) / (l + s)$

Results are given on Table 1.3.2 and on fig. 1.3.8.

Snapshot	Apparent porosity	Number of vesicles	Average vesicle area	Deformation
C1	0,7	10	0,028	0,1546
C2	3,8	17	0,084	0,1056
C3	2,4	16	0,057	0,1678
C4	3,2	13	0,093	0,1964
C5	2,7	13	0,078	0,1470
C6	3,0	25	0,044	0,1389
C7	4,8	30	0,060	0,1603
C8	7,4	71	0,039	0,1435
C9	8,5	49	0,065	0,1336
C10	12,8	30	0,160	0,2244
C11	12,4	34	0,137	0,1912
C12	11,6	53	0,082	0,1507
C13	9,6	58	0,062	0,1556

Table 1.3.2: Vesicle measurements on the Farm outcrop using the ImageJ® software.

Like for the Font de l'Arbre outcrop, but with a more precise methodology, the apparent porosity is seen to increase upward (Fig 1.3.8a), the average vesicle area evolution tends also to follow this upward increase (fig. 1.3.8b). These patterns well reflect the observation of Aubele & al. (1988), also quoted in 1.1.4.1, that "as a bubble grows, it begins to ascend until it is overtaken by solidification progressing inward from either the upper or cooling surfaces of the flow". In our case, we are treating the upper cooling front as the base does not outcrop. The decrease in both apparent porosity and average vesicle area from C10 to C13 may be due to the interaction with this upper cooling front having prevented the ascent of bigger vesicles. The observed pattern of fig. 1.3.8a & b are also significant features of pāhoehoe (Self & al., 1998).

The evolution of number of vesicles (fig. 1.3.8c), in particular the C8 peak, is harder to interpret as there is no correlation with the apparent viscosity (fig. 1.3.8a) and average vesicle area (fig. 1.3.8b). Thus it could not be the result of a fresher lava input having led to the formation of another vesicular crust as described by Self & al. (1998). In fact, I think that it

may be a simple effect of a level where for an unknown reason vesicle coalescence was lower. The evolution of the vesicle deformation (fig. 1.3.8d) is also hard to interpret, as there is no particular trend, we can just say that at a centimetric scale we can have vesicle deformation, probably linked to the non constant inflation rate of a pāhoehoe lobe interacting with the downward cooling front. Nevertheless, the two studied outcrops have revealed the preservation of the vesicular crust and an upward increase in the porosity typical of a pāhoehoe lava (Self & al., 1998).

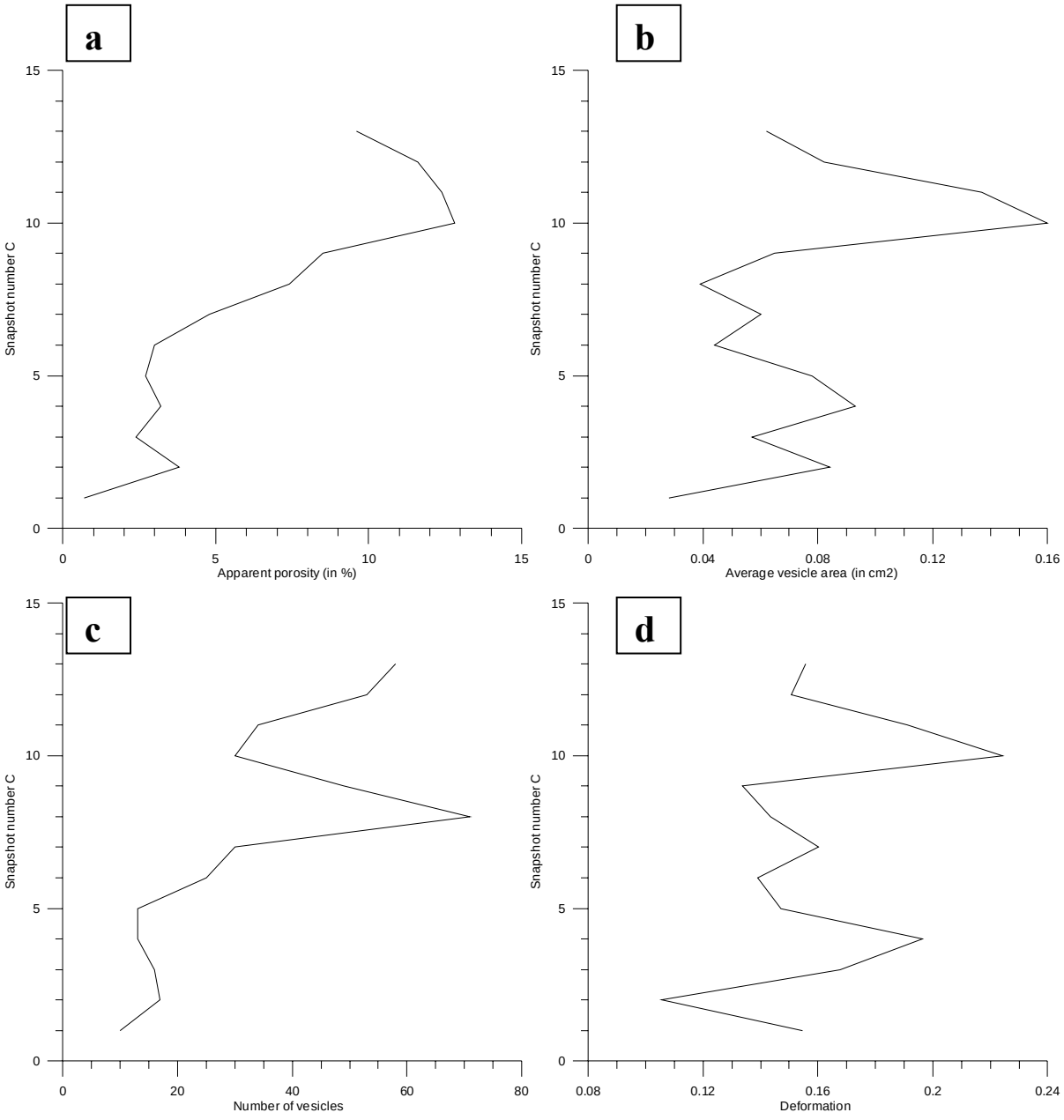

Figure 1.3.8: Diagrams showing the vesicle measurements along the farm outcrop: **a.** evolution of the apparent porosity (in %); **b.** evolution of the average vesicle area (in cm^2); **c.** evolution of the number of vesicles; **d.** evolution of the deformation.

1.3.3.1.4. Textural evidence of a pāhoehoe flow

AMS fabric

The AMS (Anisotropy of Magnetic Susceptibility) (see 1.1.4.3. for a general description of the approach to AMS and chapter 3 for detailed explanations) has been studied on the Font de l'Arbre outcrop where a vertical profile of 15 drill cores has been made (fig. 1.3.6). The results obtained are displayed on table 1.3.3, values of degree of anisotropy are also presented on table 1.3.1 and the evolution of the k_{max} azimuth is provided on fig. 1.3.9.

As noted in 1.1.4.3., the obtained AMS results are only significant for the last deformation stage during cooling. Like Cañón-Tapia & al. (1997), we have not found a particular trend concerning the evolution of the AMS parameters and especially the degree of magnetic anisotropy (A) confirming the fact that these parameters can not be used to check for pāhoehoe or 'a'ā lava types.

Nevertheless, the evolution of the k_{max} axis displays an interesting distribution (fig. 1.3.9). Samples 1 to 7 (outer rim of the lobe) display k_{max} axis having an ENE plunge, whereas samples 8 to 14 display a near vertical plunge (core of the lobe). The first group, in fact, has recorded the ENE emplacement direction of the lava flow (see fig. 1.3.3), whereas the second core group has recorded the vertical inflation growth of the lava lobe. Such a difference between the rim and the core is simply explained by the fact that the cooling crust will undergo lateral expansion due to the inner lobe lava influx after it has grained its AMS signature by solidifying. The lateral expansion will be restricted to the core, which with cooling will preserve the AMS inflation signature.

Thus it appears that the use of the k_{max} vectors, if they display vertical plunges, will reveal an inflation process and by this way a typical pāhoehoe emplacement.

No particular consideration has been accorded to the k_{max} vector associated with the n°0 outcrop, which is on the rim, as it displays a degree of anisotropy of 0,350 % with an error bar of 0,378% (Table 1.3.1 & 1.3.3).

Site, n	km 10^{-3} SI	km/m	k_{max}	Δk_{max}	Az $_{max}$	Inc $_{max}$	k_{int}	Δk_{int}	Az int	Inc $_{int}$	k_{min}	Δk_{min}	Az $_{min}$	Inc $_{min}$	A %	ΔA
0, 2	68,96	1,39	1,002	0,330	312,8	64,5	1,001	0,297	123,7	25,2	0,997	0,124	215,4	3,5	0,350	0,378
1, 2	73,71	1,46	1,004	0,188	67,5	0,8	1,001	0,188	158,3	44,6	0,995	0,013	336,7	45,4	0,593	0,341
2, 3	95,59	1,35	1,003	0,130	77,7	6,5	1,000	0,109	170,5	23,1	0,997	0,023	333,0	65,9	0,424	0,166
3, 2	68,37	1,45	1,004	0,042	57,9	7,0	1,001	0,083	150,1	17,4	0,995	0,045	306,9	71,2	0,634	0,135
4, 2	65,69	1,37	1,003	0,024	67,3	13,1	1,000	0,017	165,2	30,6	0,996	0,009	316,9	56,1	0,517	0,038
5, 2	65,07	1,26	1,004	0,02	72,2	11,2	1,001	0,043	183,7	61,7	0,995	0,015	336,8	25,7	0,623	0,072
6, 3	98,19	1,18	1,009	0,010	72,1	18,6	0,999	0,061	205,6	63,9	0,992	0,064	336,0	17,6	1,345	0,193
7, 2	69,45	1,26	1,006	0,001	76,2	28,1	0,999	0,015	229,7	59,1	0,995	0,014	339,9	11,7	0,926	0,028
8, 3	103,15	1,18	1,003	0,058	51,4	71,2	0,999	0,256	226,0	18,7	0,998	0,210	316,5	1,6	0,480	0,280
9, 2	57,09	0,96	1,003	0,034	309,5	79,6	1,000	0,064	71,4	5,6	0,996	0,089	162,3	8,8	0,517	0,114
10, 3	110,55	1,28	1,005	0,047	185,1	76,3	1,000	0,063	291,1	3,8	0,995	0,025	22,0	13,1	0,787	0,143
11, 2	55,87	0,93	1,004	0,197	210,9	80,0	1,002	0,182	79,1	4,2	0,994	0,072	342,8	11,2	0,623	0,403
12, 2	69,00	1,14	1,003	0,072	117,8	52,3	1,002	0,052	21,0	5,3	0,996	0,024	287,0	37,2	0,427	0,093
13, 2	65,08	1,09	1,010	0,010	101,4	78,3	1,002	0,010	210,3	3,8	0,989	0,000	300,9	11,1	1,429	0,044
14, 2	41,48	0,69	1,013	0,001	72,8	67,1	0,999	0,003	203,5	15,4	0,988	0,004	298,2	16,6	1,897	0,017

Table 1.3.3: AMS measurements on the Font de l'Arbre outcrop.

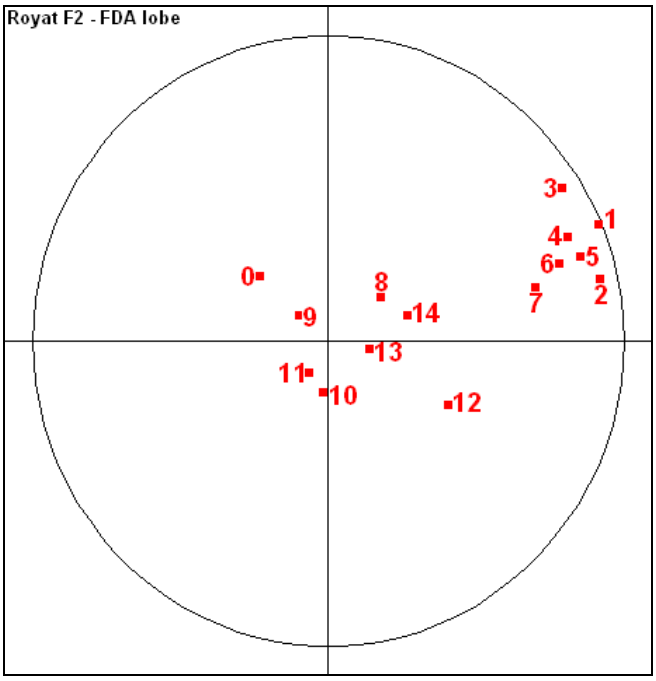

Figure 1.3.9: Equal-area projection (lower hemisphere) displaying distribution of the k_{max} vectors on the Font de l'Arbre lobe outcrop.

Microlite fabric

The microlite fabric has also been studied in parallel with the AMS study to check the whether the AMS fabric clearly represents the late stage of deformation in the Font de l'Arbre lava lobe (see 1.1.4.3. and chapter 3 for explanations).

Three thin sections are needed for the microlite image analyses (here vertical North-South, vertical East-West, and horizontal East-West). We have chosen a location in the outcrop where thin section sample is closest to AMS sample in order to reduce any lateral variation between the two subfabrics. This location is close to the AMS sample site 11 in the core of the lava lobe (see location on fig. 1.3.6).

As we had difficulty to isolate some microlites for their neighbours in thin sections, we used the intercept method of Launeau & Robin (1996) (see http://www.sciences.univ-nantes.fr/geol/UMR6112/index.html) (see also 3.1.2.2 & 3.2.3 for explanation).

Three different sectors, on each different thin section, have been submitted to the intercept procedure of Launeau & Robin (1996). The three microlite ellipsoid axes obtained are presented on fig. 1.3.10.

First and foremost, the three microlites fabrics are very close each other, thus indication good repeatability in the results. But, we observe surprisingly that kmax vectors are near horizontal on the contrary to the AMS fabric where kmax is near vertical (see Table 1.3.3 and fig. 1.3.9). Thus the inflation emplacement of the lava lobe is not confirmed in the core part of the lobe by the microlite fabric. In other words, the inflation episode recorded in the AMS fabric is not recorded in the microlite fabric. As microlites are known to be crystallized during the flow as evidenced by the quality of the fabric more or less in accordance with the real plane and direction of the flow, AMS fabric must be acquired after the microlite fabric, i.e. when the particles are locked each together and when the interstitial liquid is able to migrate and reorganize the interstitial magnetite. Thus the microlite fabric has recorded a NW direction which can be linked to the NW emplacement of the flow at this location (see fig. 1.3.3) and AMS record the inflation of the lobe. This is a very interesting case in which there is no concordance between the AMS and the microlite fabric underlining that, for making a good interpretation of AMS data, a fabric comparison is needed so to estimate the AMS fabric time acquisition (see 3.1.2.2.). More, Image Analysis is thus a relative more accurate method to investigate magmatic flow than AMS when a secondary fabric overprints this first one.

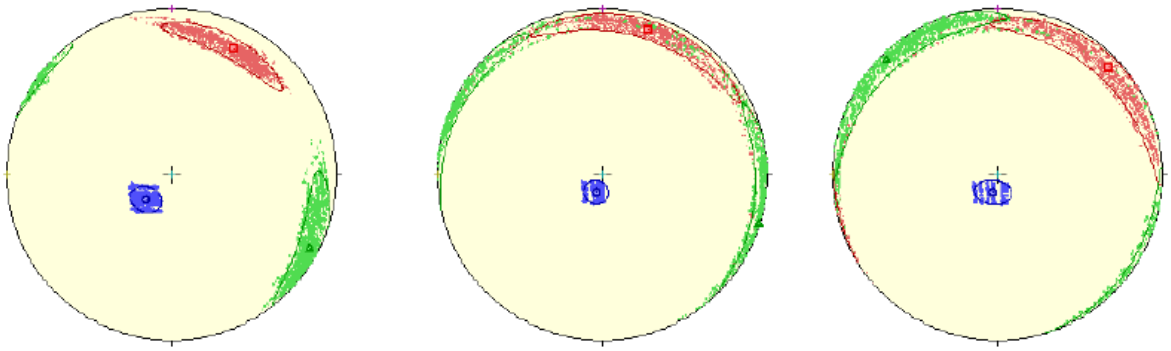

Figure 1.3.10: Three equal-area projections (lower hemisphere) displaying the microlites fabrics in three different thin section sectors in a sample close to the AMS site 11 located in the core of the Font de l'Arbre lava lobe (each dot represents a combination between 3 perpendicular images choosen among 16 images of thin sections. red dots are for kmax, green for kint, and blue for kmin).

1.3.3.1.5. Conclusions

The Royat F3 lobe has been subjected to a detailed study following different considerations for lava flow characteristics including; morphological evidence (inflation fissures, vesicular

crusts, multi-roofed lava tube) (1.3.3.1.2), rheological insights (phenocrysts and vesicles zonation) (1.3.3.1.3.) and textural insights (AMS and microlites fabrics) (1.3.3.1.4). Each method has led to the same conclusion: the Royat F3 flow is a pāhoehoe type flow.
The study of this lava was time-consuming but has the merit to confirm that there is at least one well document pāhoehoe lava flow in the Chaîne des Puys. It opens the possibility to find others, and to reappraise the lava emplacement conditions.
In the following sections, other pāhoehoe flows will be presented but in a more summary way, only considering morphological evidence.

1.3.3.2. The Grosliers lava flow

1.3.3.2.1. Presentation of the Grosliers flow

The Grosliers lava flow belongs to the Blanzat lava flow group, the extent of which is provided on fig. 2.1.3b. The flow is basaltic in composition and was erupted between 31,500 and 75,000 years ago (Boivin & al., 2004).It comes either from the Puy de Chaumont or the Puy du Petit Sarcouy. This flow hosts several springs and a water catchment gallery (the Grosliers gallery) has been dug at the contact between the flow and the crystalline basement.

1.3.3.2.2. Morphological evidences of a pāhoehoe flow

Like with the Royat F3 flow, no single clinker has been found at the top and in the core of the flow on the numerous outcrops. Nevertheless, clinkers occur at the flow base and the breccia is particularly well observed in the Grosliers gallery (see fig. 2.1.5b). As no clinker is present on the flow top, this basal clinker can not be formed simply by the caterpillar motion of an ‘a‘ā lava flow, which may have transported the hypothetical upper clinker to the flow base. In fact, as it will be explained in 2.1.5.2, this clinker is not formed by the classical ‘a‘ā brecciation, but rather by inflow phreatomagmatic fragmentation. The upper and inner clinker absence, also the preservation of an upper vesicular zone is typical of a pāhoehoe flow. Moreover, on the path leading to the Grosliers gallery, some subrounded lava formations (fig. 1.3.11) could be pāhoehoe lava lobes, even if no inflation structures have been observed.

Figure 1.3.11: The lava flow front of the pāhoehoe-like Grosliers lava flow displaying subrounded structures (1,5 m high) thought to be lava lobes.

1.3.4. Some pāhoehoe flows from the Massif Central

In this section, we will describe some lava flows displaying pāhoehoe evidence in the French Massif Central: one from the Limagne volcanic province (the Roca Neyra lava flow) and one from the Ardèche volcanic province (the Jaujac lava flow).

1.3.4.1. The Roca Neyra flow

1.3.4.1.1 Presentation of the Roca Neyra flow

The Roca Neyra flow belongs in age to the Limagne volcanic province. It is located to the west of the Issoire. The flow is basaltic in composition and has been dated at 3.6 My. And today it appears in relief inversion (Ly, 1982). We have mapped this flow, following it to a probable source at the Puy de Leyranoux (fig. 2.1.3c). In the fig. 2.1.3c we have also reported the actual and former hydrographic systems according to data from Thonat (1969). In 2.1.5.2, this flow has been the subject of a study of its basal clinker.

1.3.4.1.2. Morphological evidences of a pāhoehoe flow

As shown on fig. 2.1.3c, the Roca Neyra flow has flowed down a complex course with several confluences and even filled a valley going upstream. Despite the complexity, the lava flow displays over several outcrops the same pattern: a typical association of several lobes (fig. 1.3.12a & b). These lobes are decimetric to metric in diameter and they display a vesicular crust with a dense core. Vesicles of the crust are increasingly stretched as the outer rim is approached. Unfortunately a study using the ImageJ® software has been unsuccessful as the lava is quite altered (making vesicles hard to distinguish) and because it has been impossible to find a flat plane to make measurement on, as was the case for the Farm outcrop of the Royat F3 flow (see 1.3.3.1.3).

The lobes could be thought to be pillow lavas but they have no hyaloclastite material at the hypothetical pillow junction, so this hypothesis can be rejected. The columnar jointing clearly indicate that each lobe has emplaced as a single unit and the vesicle zonation also indicates inflation, with the stretching of the crust and the filling of the massive core, as is classically observed in pāhoehoe lava flow fields (see 1.1.3.1 & 1.1.4.1).

As for the Grosliers lava flow, no upper or inner clinker has been observed, but nevertheless a clinkery-like basal zone can be widely observed (see fig. 2.1.6a & b). These clinkers are not thought to have been formed by classical ‘a‘ā clinker mechanics but by a phreatomagmatic fragmentation (see 2.1.5.2).

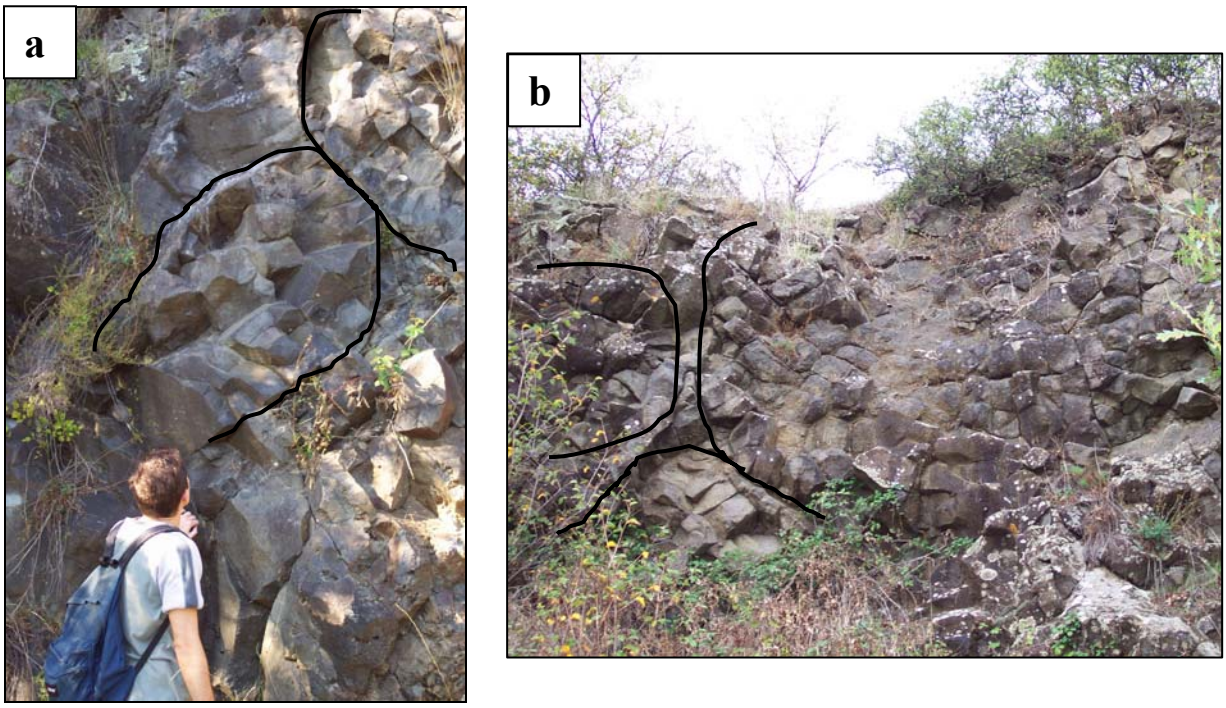

Figure 1.3.12: Two outcrops displaying the typical lobe association of the pāhoehoe-like Roca Neyra lava flow: **a.** at the Perrier cliff outcrop; **b.** at the Bergonne quarry outcrop (the escarpment is 5m high).

1.3.4.2. The Jaujac flow

1.3.4.2.1. Presentation of the Jaujac flow

The Jaujac lava flow belongs to the Ardèche volcanic province, it is located around Jaujac village 10km west of Aubenas. The lava flow has been erupted from the Coupe de Jaujac, a strombolian cone, and it is basaltic in composition. It has been dated at 15,000 years old (which is thus one of the youngest French lava flows), so that it is associated with the last of the third eruptive phases having affected the Ardèche province (Berger, 1973; Rochette & al., 1993; Berger, 2007). Despite its relatively young age, the lava flow displays lots of outcrop due to the highly active erosion of the Lignon river (fig. 1.3.13).

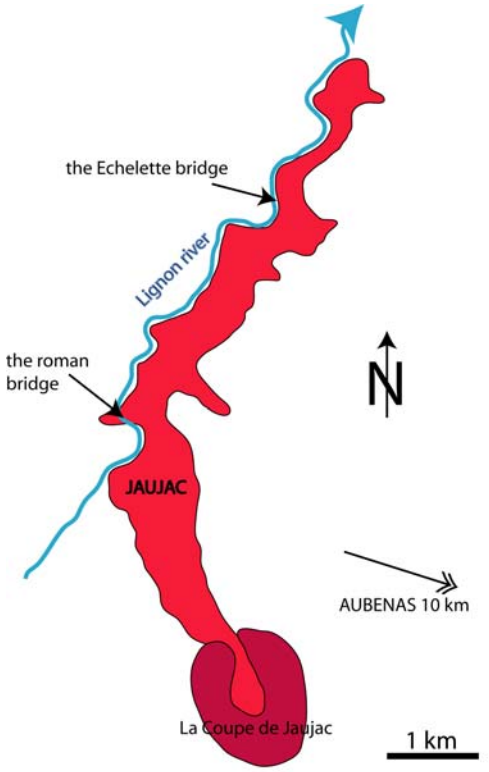

Figure 1.3.13: Extension of the Jaujac lava flow.

1.3.4.2.2. Morphological evidences of a pāhoehoe flow

First and foremost, on the numerous outcrops located on the Lignon river, no upper nor inner clinker have been noted. At the roman bridge outcrop (see location on fig. 1.3.13) the base of the flow; clearly outcrops and is in contact with the crystalline basement. There is no typical ‘a‘ā clinker at the base, but there is a blocky clinker in contact with the former Lignon

alluvium. This may have also formed by phreatomagmatic fragmentation (see 2.1.5.2). The upper, inner and lower clinker absence suggests the flow is a pāhoehoe.

The Echelette bridge reveals a highly interesting view over and extensive lava flow cliff, which displays a strange columnar succession as previously noticed by Berger (2007). Lava flows more than 10m thick are generally subject to a particular columnar succession. This is, from the base to the top: the lower colonnade with well developed perpendicular columns, the entablature with columnar bouquets of radiating columns, and the upper colonnade with vertical columns that are less well developed than in the lower colonnade (e.g. Ryan & Sammis, 1978; DeGraff & Aydin, 1987; Grossenbacher & McDuffie, 1995). In this case there is a repetition of such a stack. The structure can be interpreted as a sill, if the contacts between colonnades and entablatures are closely inspected (fig. 1.3.14). This sill displays its own lower and upper colonnade as its entablature and its termination is evident (fig. 1.3.14). Thus it appears that the Jaujac lava flow has had several lava pulses, so that a sill has developed in the formerly emplaced cooling lava. Such a phenomenon is in fact a classical inflation scenario, the process commonly invoked for pāhoehoe emplacement by Hon & al. (1994) (see 1.1.3.1).

In conclusion, both the absence of upper or inner clinker with the occurrence of a well-marked inflation stage revealed by a sill-like feature indicates that the Jaujac lava flow is a pāhoehoe lava.

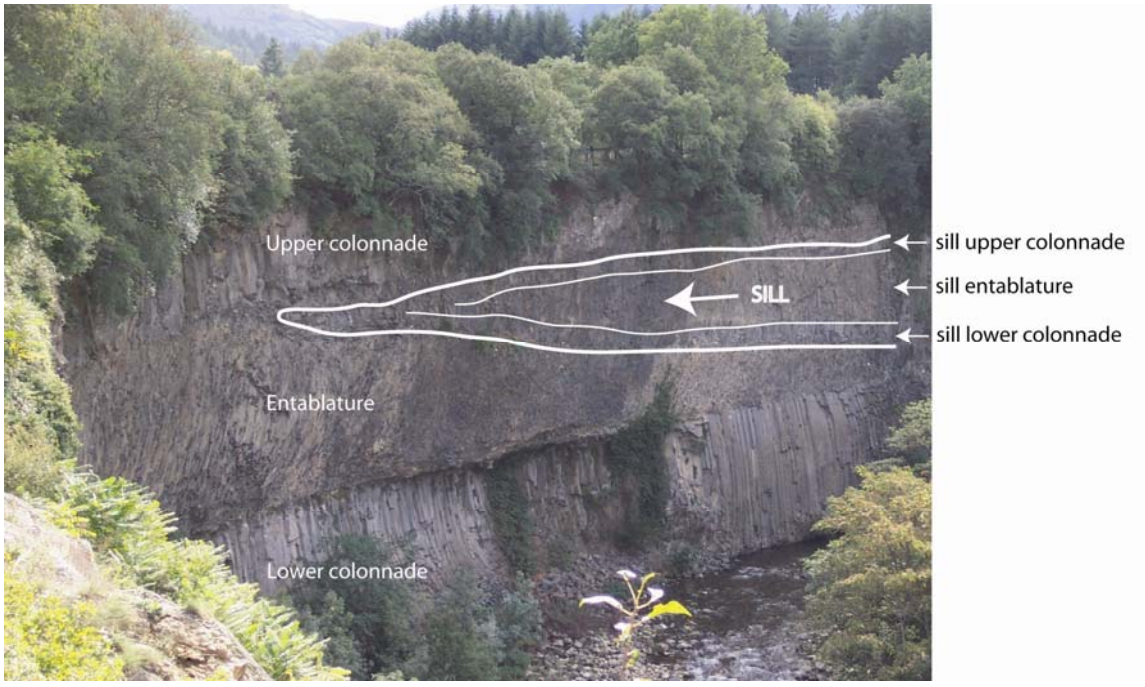

Figure 1.3.14: The Echelette bridge outcrop displaying a sill injection in the Jaujac lava flow (cliff is 20m high).

1.3.5. Conclusions

This section has tackled the problem of pāhoehoe or ‘a‘ā determination in lava flows were surfaces are buried or eroded. We have also explained the procedures that can be followed decide what type of flow type a lava is.

Identifying an ‘a‘ā lava is quite easy provided that clinker can be found in the lava flow. Determining with confidence a pāhoehoe type is more difficult: a lot of different considerations and observations have been has been made on the Royat F3 flow to check if it is really pāhoehoe. For the other lava flows, several key observations have allowed me to determine a pāhoehoe signature (upper and inner clinker absence, lobe stacking, inflation evidence…). But we have also to keep in mind, as noted in 1.1.5 that the pāhoehoe and ‘a‘ā terms refer to end members with several transitional flow types, the nature of which has been determined with surface features missing in our considered flows. These types are toothpaste lava and slabby pāhoehoe that may be more even more difficult to spot in older flows.

CONCLUSIONS

Pāhoehoe and ʻaʻā are terminology has been used since MacDonald (1953) to characterize Hawaiian lava flow surfaces. This simple classification was also relevant in terms of lava flow emplacement modes. This is because these two types will progress in different manners:

1. for pāhoehoe lavas mainly by lobe accumulation, lobe inflation and lobe coalescence and
2. for ʻaʻā by a massive emplacement with the upper clinker falling to the flow base via a caterpillar motion.

This difference in emplacement creates different structures and has helped us in determining the pāhoehoe or ʻaʻā nature of an old lava flows where the surface is hidden or lost.

The differences in emplacement will be revealed by the geometry of the lava flow section: a pāhoehoe flow will display an upper well-developed vesicular crust with little deformed vesicles, inflation features and lobe morphologies, whereas ʻaʻā flows will display an upper clinker zone, a massive core and most of the time a lower clinker zone. The core can display clinker incorporation, core injection in clinker and highly deformed vesicles. Pāhoehoe flows are also more fluid than ʻaʻā and thus a downward phenocryst enrichment can be detected. The AMS parameters do not help greatly in differentiating the flow types.

On active lava flow fields, several authors have noted the occurrence, for one single lava flow, of changes from the pāhoehoe surface morphology to ʻaʻā. This transition has been studied first by Peterson & Tilling (1980) and then by Hon & al. (2003) to explain observed ʻaʻā to pāhoehoe transitions. These authors proposed an interesting and useful diagram showing the evolution of the shear strain rate with the apparent viscosity. This displays a pāhoehoe and an ʻaʻā field with a transition zone where transitional lava can appear. These diagrams have been used so to solve transition observed in the 1724-1729 southwest branch of the Myvatn Fires (Iceland). In this field area, field parameters such as breakout location or slope can be linked to the Hon & al. (2004) diagram and thus can be used to explain the variations from pāhoehoe and ʻaʻā fields. This diagram works, even if it has been established for Hawaiian lava properties, but unfortunately it does not consider other parameters such as lava flux changes.

The French Massif Central was also subjected to numerous field studies with the aim to study the pāhoehoe or ‘a‘ā types.

In the Chaîne des Puys, the local term *cheire* corresponds to ‘a‘ā lava flows where the jumbled aspect of the upper clinker is preserved. Several cross sections in other lava flows have also revealed the abundant clinkery aspect typical of ‘a‘ā flow, allowing us to say that in the Chaîne des Puys, ‘a‘ā lava flows are largely predominant. Nevertheless a particularly well studied lava flow: Royat F3 has revealed pāhoehoe from considering geometrical evidence, phenocryst and vesicles zonation, and even AMS and microlites fabrics. These two fabrics have revealed a near vertical plunge of the maximum axis of fabric elongation (k_{max}), which can be linked to inflation occurring in the core of a lava lobe. Even if less deeply studied, as fresh outcrops are limited, the Grosliers lava flow also displays pāhoehoe geometrical evidence. Out from the Chaîne des Puys, other pāhoehoe-like lavas have been identified at the Roca Neyra lava flow (Limagne) where the lobe stack is evident and at the Jaujac lava flow (Ardèche) where a magnificent inflation feature (sill) is observable.

This chapter has considered the term of clinker to be most of the time typical of ‘a‘ā lava flows. However, as noted in the Grosliers and the Roca Neyra pāhoehoe-like lava flows, basal breccia can be formed in other contexts: other kinds of breccia can be found in lava flows and will be discussed in the following chapter.

REFERENCES

Aubele J.C., Crumpler, L.S., Elston, W.E., 1988. Vesicle zonation and vertical structure of basalt flows. J. Volcanol. Geotherm. Res. 35, 349-374.

Bascou, J., Camps, P., Dautria, J.M., 2005. Magnetic versus crystallographic fabrics in a basaltic lava flow. J. Volcanol. Geotherm. Res. 145, 119-135.

Berger, E., 1973. Le volcanisme récent de l'Ardèche. Paris Sud – Orsay PhD. 402pp.

Berger, E., 2007. Les Jeunes volcans d'Ardèche. BRGM Editions. 192 pp.

Bjornsson, A., 1985. Dynamics of crustal rifting in NE Iceland. J. Geophys. Res. 90, 10,151–10,162.

Bonnischen, B., Kauffman, D.F., 1987. Physical features of rhyolite lava flows in the Snake River Plain volcanic province, south-western Idaho. Geol. Soc. Am. Spec. Pap. 212, 119-145.

Calvari, S., Pinkerton, H., 1998. Formation of lava tubes and extensive flow field during the 1991-1993 eruption of Mount Etna. J. Geophys. Res. 103, 27291-27301.

Calvari, S., Pinkerton, H., 1999. Lava tube morphology on Etna and evidence for lava flow emplacement mechanisms. J. Volcanol. Geotherm. Res. 90, 263-280.

Cañón-Tapia, E., Walker, G.P.L., Herrero-Bervera, E., 1996. The internal structure of lavas: insights from AMS measurements I: near vent 'a'ā. J. Volcanol. Geotherm. Res. 70, 21-36.

Cañón-Tapia, E., Walker, G.P.L., Herrero-Bervera, E., 1997. The internal structure of lavas: insights from AMS measurements II: Hawaiian pahoehoe, toothpaste lava and 'a'ā. J. Volcanol. Geotherm. Res. 76, 19-46.

Cañón-Tapia, E., Pinkerton, H., 2000. The anisotropy of magnetic susceptibility of lava flows: an experimental approach. J. Volcanol. Geotherm. Res. 98, 219-233.

Cashman, K.V., Thornber, C.R., Kauahikaua J., 1999. Cooling and crystallization of lava in open channels, and the transition of pāhoehoe lava to ‘a‘ā. Bull. Volcanol. 61, 306-323.

Crisp, J., Baloga, S., 1994. Influence of crystallization and entrainment of cooler material on the emplacement of basaltic ‘a‘ā lava flows. J. Geophys. Res. 99, 11819-11831.

Dance, M., Hancock, P.L., Sparks, R.S.J., Wallman, A., 2001. Fracture and surface crust development in a Holocene pahoehoe lava flow on the Island of Tenerife, Canaries. J. Struct. Geol. 23, 165-182.

DeGraff, J.M., Aydin, A., 1987. Surface morphology of columnar joints and its significance to mechanics and direction of joint growth. Geol. Soc. of Am. 99, 605-617.

De Rosa, R., Mazzuoli, R., Ventura, G., 1996. Relationships between deformation and mixing processes in lava flows: a case study from Salina (Aeolian Islands, Tyrrhenian Sea). Bull. Volcanol. 58, 286-297.

Duncan, A.M., Guest, J.E., Stofan, E.R., Anderson, S.W., Pinkerton, H., Calvari, S., 2004. Development of tumuli in the medial portion of the 1983 ‘a‘ā flow-field, Mount Etna, Sicily. J. Volcanol. Geotherm. Res. 132, 173-187.

Duraiswami, R.A., Dole, G., Bondre, N., 2003. Slabby pahoehoe from the western Deccan Volcanic Province: evidence for incipient pahoehoe-’a‘ā transitions. J. Volcanol. Geotherm. Res. 121, 195-217.

Frémion, M., 2001. Captages de la Chaîne des Puys, Avis sur les mesures de protection : Siméoni, les Eaux, Kuhn, puits de la Vacherie et les Combes. Rapport pour le Service de l’Eau et de l’Assainissement de Clermont Ferrand, 93pp.

Gagnière G, 1980. Reconnaissance des ressources en eau souterraine des formations volcaniques à l'Ouest de Clermont Ferrand (Puy de Dôme). BRGM.

Goff, F., 1996. Vesicles cylinders in vapor-differenciated basalt flows. J. Volcanol. Geotherm. Res. 97, 19729-37.

Grossenbacher, K.A., McDuffie, S.M., 1995. Conductive cooling of lava: columnar joint diameter and stria width as functions of cooling rate and thermal gradient. J. Volcanol. Geotherm. Res. 69, 95-103.

Gudmundsson, A., 1995. Infrastructure and mechanics of volcanic systems in Iceland. J. Volcanol. Geotherm. Res. 64, 1–22.

Gudmundsson, A., 1998. Magma chambers modelled as cavities explain the formation of rift zone central volcanoes and their eruption and intrusion statistics. J. Geophys. Res. 103, 7401–7412.

Guest, J.E., Stofan, E.R., 2005. The significance of slab-crusted lava flows for understanding controls on flow emplacement at Mount Etna, Sicily. J. Volcanol. Geotherm. Res. 142, 193-205.

Guilbaud, M.N., Self, S., Thordarson, T., Blake, S., 2005. Morphology, surface structures, and emplacement of lavas produced by Laki, A.D. 1783–1784. *In*: Kinematics and dynamics of lava flows. Geological Society of America Special Paper (396). Geological Society of America, USA, pp. 81-102.

Hards, V.L., Kempton, P.D., Thompson, R.N., Greenwood, P.B., 2000. The magmatic evolution of the Snæfell volcanic centre; an example of volcanism during incipient rifting in Iceland. J. Volcanol. Geotherm. Res. 99, 97-121.

Hargraves, R.B., Johnson, D., Chan, C.Y., 1991. Distribution anisotropy: the cause of AMS in igneous rocks? Geophys. Res. Letters, vol 18. 12, 2193-2196.

Hon, K., Kauahikaua, J., Denlinger, R., Mackay, K., 1994. Emplacement and inflation of pahoehoe sheet flows: Observations and measurements of active lava flows on Kilauea Volcano, Hawaii. Geol. Soc. Am. Bull. 106, 351-370.

Hon, K., Gansecki, C., Kauahikaua, J., 2003. The transition from ʻaʻā to pāhoehoe crust on flows emplaced during the Puʻu ʻŌʻō-Kūpaianaha eruption. U.S. Geological Survey Professional Paper 1676.

Hulme, G., 1974. The interpretation of lava flow morphology. Geophys. J. R. astr. Soc. 39, 361-383.

Kauahikaua, J., Cashman, K.V., Mattox, T.N., Heliker, C., Hon, K., Mangan, M., Thornber, C., 1998. Observations on basaltic lava streams in tubes from Kilauea Volcano, Hawaii. J. Geophys. Res. 103, 27303–27324.

Kilburn, C.R.J., 1981. Pahoehoe and ʻaʻā lavas; a discussion and continuation of the model of Peterson and Tilling. J. Volcanol. Geotherm. Res. 2; 373-382.

Kilburn, C.R.J., 1993. Lava crust, ʻaʻā flow lengthening and the pahoehoe-ʼaʻā transition. In: Kilburn, C.R.J., Luongo, G. (Eds), Active Lava Flows: Monitoring and Modelling. UCL Press, London, 263-280.

Kilburn, C.R.J., 2000. Lava flows and flow fields. In: Sigurdsson, H. (Editor-in-chief), Encyclopaedia of volcanoes. Academic Press, Elsevier, 291-305.

Lescinsky, D.T., Merle, O., *in press*. Extensional and compressional strain in lava flows and the formation of fractures in surface crust.

Launeau, P., Robin, P.Y.F., 1996. Fabric analysis using the intercept method. Tectonophysics, 267, 91-119.

Loock, S., Celle-Jeanton, H., Bertrand, G., Van Wyk de Vries, B., 2007. The Tiretaine groundwater basin: volcanic and substratum regolith interactions (Chaîne des Puys, France). Poster at the IAH (International Association of Hydrogeology) meeting, Lisbon, Portugal.

Ly, M.H., 1982. Le plateau de Perrier et la Limagne du Sud : Etudes volcanologiques et chronologiques des produits montdoriens(Massif Central Français). PhD, Clermont Ferrand Univ., 180pp.

MacDonald, G.A., 1953. Pahoehoe, ‘a‘ā and block lava. Am. J. Sci. 251, 169-191.

MacMillan, K., Long, P.E., Cross, R.W., 1989. Vesiculation in Columbia River basalts. Geol. Soc. Am., Spec. Pap. 239, 157-167.

Manga, M., 1996. Waves of bubbles in basaltic magmas and lavas. J. Geophys. Res. 101, 17457-65.

Merle, O., 1998. Internal strain within lava flows from analogue modelling. J. Volcanol. Geotherm. Res. 81; 189-206.

Peck, D.L., 1978. Cooling and vesiculation of Alae lava lake, Hawaii. U.S. Geol. Surv., Prof. Pap. 935-B, 59pp.

Peterson, D.W., Tilling, R.T., 1980. Transition of basaltic lava from pahoehoe to ‘a‘ā, Kilauea volcano, Hawaii; field observations and key factors. J. Volcanol. Geoth. Res. 7, 271-293.

Polacci, M., Papale, P., 1997. The evolution of lava flows from ephemeral vents at Mount Etna: Insights from vesicle distribution and morphological studies. J. Volcanol. Geotherm. Res. 76, 1-17.

Polacci, M., Cashman, K.V., Kauahikaua, J., 1999. Textural characterization of the pāhoehoe-‘a‘ā transition in Hawaiian basalt. Bull. Volcanol. 60, 595-609.

Rochette, P., Bertrand, H., Braun, C., Berger, E., 1993. La province volcanique Pleistocène Supérieur du Bas-Vivarais (Ardèche, France) : propagation de fentes crustales en échelons ? C.R. Acad. Sci. Paris, 316 : 913-920.

Rogan, W., Blake, S., Smith, I., 1996. In situ chemical fractionation in thin basaltic lava flows: examples from the Auckland volcanic field, New Zealand, and a general physical model. J. Volcanol. Geotherm. Res. 74, 89-100.

Rossi, M.J.; Gudmunsson, A., 1996. The morphology and formation of flow-lobe tumuli on Iceland shield volcanoes. J. Volcanol. Geotherm. Res. 72, 291-308.

Rowland, S.K., Walker, G.P.L., 1987. Toothpaste lava: Characteristics and origin of a lava structural type transitional between pahoehoe and ‘a‘ā. Bull. Volcanol. 49, 631-641.

Rowland, S.K., Walker, G.P.L., 1988. Mafic crystal distributions, viscosities and lava structures of some Hawaiian lavas. Bull. Volcanol. 35, 55-66.

Ryan, M.P., Sammis, C.G., 1978. Cyclic fracture mechanisms in cooling basalt. Geol. Soc. of Am. Bull. 89, 1295-1308.

Sahagian, D.L., Anderson, A.T., Ward, B., 1989. Bubble coalescence in basalt flows: comparison of a numerical model with natural examples. Bull. Volcanol. 52, 49-56.

Sato, H., 1995. Textural difference between pahoehoe and ‘a‘ā lavas of Izu-Oshima volcano, Japan – an experimental study on population density of plagioclase. J. Volcanol. Geotherm. Res. 66, 101-113.

Self, S., Thordarson, Th., Keszthelyi, L., Walker, Hon, K., et al., 1996. A new model for the emplacement of the Columbia River Basalts as large inflated pahoehoe sheet lava flow fields. Geophys. Res. Lett. 23, 2689-92.

Self, S., Keszthelyi, L., Thordarson, Th., 1998. The importance of pāhoehoe. Annu. Rev. Planet. Sci. 26, 81-110.

Smith, J.V., Houston, E., 1994. Folds produced by gravity spreading of a banded rhyolite lava flow. J. Volcanol. Geotherm. Res. 63, 89-94.

Solana, M.C., Kilburn, C.R.J., Rodriguez Badiola, E., Aparicio, A., 2004. Fast emplacement of extensive pahoehoe flow-fields: the case of the 1736 flows from Montaña de las Nueces, Lanzarote. J. Volcanol. Geotherm. Res. 132, 189-207.

Soule, S.A., Cashman, K.V., 2005. Shear rate dependence of the pahoehoe-to-'a'ā transition : Analog experiments. Geol. Soc. of Am. 33, 361-364.

Sparks, R.S.J., 1978. The dynamics of bubble formation and growth in magmas: A review and analysis. J. Volcanol. Geotherm. Res. 3, 1-37.

Thonat, A., 1969. Les basanites noires de l'Est du Cézallier et la fossilisation de l'ancien réseau hydrographique de l'Allagnon. Rev. Sc. Nat. D'Auvergne, fasc 1-2-3-4.

Ventura, G., 1998. Kinematic significance of mingling-rolling structures in lava flows: a case study from Porri Volcano (Salina, Southern Tyrrhenian Sea). Bull. Volcanol. 59, 394-403.

Walker, G.P.L., 1989. Spongy pahoehoe in Hawaii: a study of vesicle-distribution patterns in basalt and their significance. Bull. Volcanol. 51, 199-209.

Walker, G.P.L., 1991. Structure, and origin by injection of lava under surface crust, of tumuli, "lava rises", "lava-rise pits", and "lava-inflation clefts" in Hawaii. Bull. Volcanol. 53, 546-558.

Waters, J.C., 1960. Determining direction of flow in basalts. Am. J. Sci. 258-a, 350-366.

Wilmoth, R.A., Walker, G.P.L., 1993. P-type and S-type pahoehoe: a study of vesicle distribution patterns in Hawaiian lava flows. J. Volcanol. Geotherm. Res. 55, 129-142.

Chapter 2:

Breccias Associated with Lava Flows

INTRODUCTION

A breccia is a rock made of the association of many rock pieces packed in a matrix that can behave as a brittle material. They are quite common in volcanic contexts and are famous for forming the Debris Avalanches Deposits (DADs), formations being the result of flank collapses common on stratovolcanoes. They are also formed by lahars, peperites and in intrusions. Wonderful outcrops of such DADs can be observed in the Auvergne area in locations such as Perrier, Le Cheix and Monton.

Breccias are also known to be associated with lava flow emplacement. As noted in 1.1.3.2 clinkers are known to be typical of ‘a‘ā flows. In this case breccias are formed by an association of clinker pieces with an ashy matrix. Such an ‘a‘ā breccia is often unconsolidated but sometimes, due to thermal welding, compaction of fines, cementation and mixing with fluid lava ban becomes strongly coherent.

During my numerous fieldtrips of my PhD, admittedly, I have encountered typical ‘a‘ā breccia in ‘a‘ā lava flows, but also other breccias occurring in pāhoehoe lava flows. That is the reason why I have decided in this second chapter to discuss in the first part the different ways to form clinkery breccia in lava flows, whatever their emplacement mode.

Another type of breccia has also been detected in the field is where the matrix was not of the volcanic ash type but rather of a marly morass with lavic clasts. Comparing them with the literature, they have similar characteristics to peperites, known to be formed, mostly in vent areas, related to diatreme structures. The occurrence of such breccias in the lava flows, and in particular associated diapiric structures has encouraged me to explain such a peperitic-like formation using structural and petrographic tools and will be the subject of the second part of this chapter.

2.1. CLINKER FORMATION IN BASALTIC AND TRACHYBASALTIC LAVA FLOWS

2.1.1. Introduction

Clinker are scoriaceous fragments commonly associated with ‘a‘ā flows. They initially appear as contorted spiny fragments, on cooling fluid lava surfaces, but during later stages lava advancement, the cooling surface breaks to yield rounded and abraded rubble (Rowland & Walker, 1987; Kilburn, 2000). Clinker is also a term used in the cement industry to characterize pieces formed after melting of a limestone and clay mix.

No studies that I have found have concentrated on clinker textures and their formation in basaltic lava flows. However, they are of special interest for at least two reasons: 1) understanding their formation will improve knowledge of lava flow emplacement conditions and kinematics 2) constraining their structure will improve knowledge of aquifers associated with lava flows as clinker is porous and separated by interstitial spaces (e.g. Kiernan & al., 2003) and thus allows groundwater to circulate.

2.1.2. The classical way to form clinker: lava fragmentation

In this section, we describe what is generally considered the classical way to form clinker. Basaltic lava flows were classified by MacDonald (1953) according to their surface morphology: if it is rough and fragmented (i.e. clinkery) the flow is ‘a‘ā and if it is smooth and continuous (i.e. clinkerless) the flow is pāhoehoe.

Pāhoehoe and ‘a‘ā flows differ not only superficially by surface texture but also fundamentally in their emplacement mechanisms and thus in their internal structure (e.g. Kilburn, 1993; Polacci & al., 1999; Duraiswami & al., 2003) allowing us to attribute a pāhoehoe or ‘a‘ā term to lava flows that have the surface covered or removed, as often in the French Massif Central. A lava flow can also change its emplacement mode during flow, thus a

pāhoehoe flow will often evolve into an ‘a‘ā, and occasionally an ‘a‘ā flow can evolve into a pāhoehoe (Hon & al., 2003).

Peterson & Tilling (1980) first described the pāhoehoe-to-’a‘ā transition as an inverse relationship between the apparent viscosity of the lava and the shear rate applied to the flow. They proposed a dimensionless graph of apparent viscosity versus shear strain (fig. 9 in Peterson & Tilling, 1980) displaying a pāhoehoe field and an ‘a‘ā field separated by a transition threshold zone (TTZ). The diagram has been refined by Kilburn (1981) assuming pāhoehoe flows fed by near-Newtonian lava and ‘a‘ā fed by Bingham lava and the diagram has also been applied to Hawaiian lavas by Hon & al. (2003). This diagram (fig. 1) has also been used by Soule & Cashman (2005) as the basis for analogue experiments of the pāhoehoe to ‘a‘ā transition. I will also use qualitatively this diagram for explaining clinker formation because by crossing the transition threshold zone and going from the pāhoehoe field to the ‘a‘ā field clinker will be generated. We note that the transition threshold zone is quite broad because there are several transitional lava terms between the pāhoehoe and ‘a‘ā poles (see below).

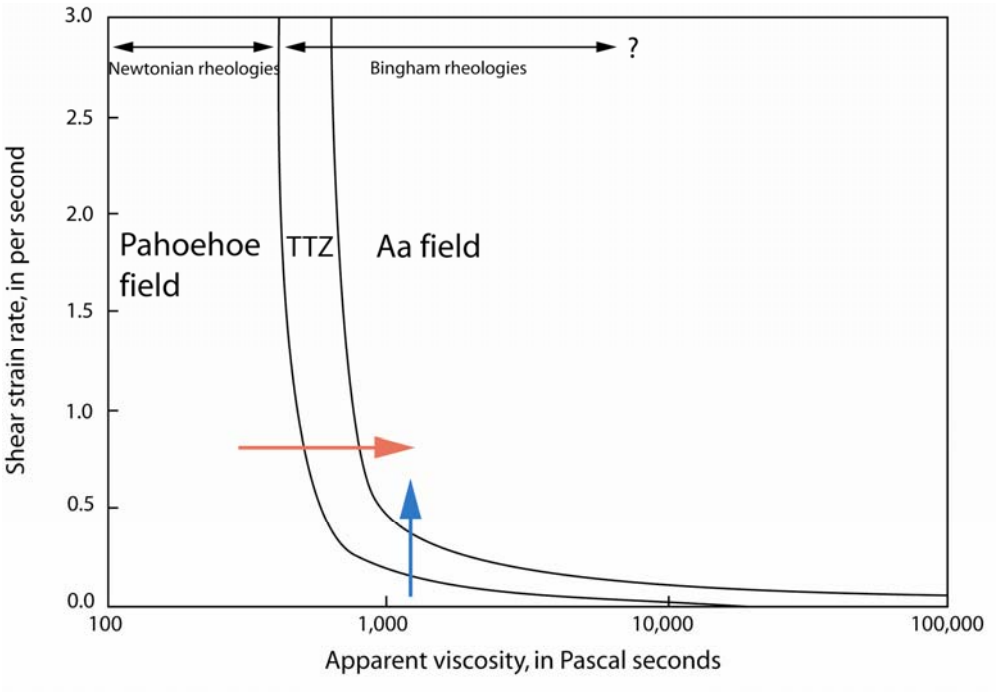

Figure 2.1.1: Diagram of shear-strain rate versus apparent Newtonian viscosity, showing approximate stability fields for Hawaiian and ‘a‘ā lava flows and approximate transition threshold zone (TTZ) within Bingham rheology (simplified from Hon & al., 2003).

Two processes can occur to cause a crossing of the transition threshold zone, and they can be linked:

1) The apparent viscosity can increase (red arrow on fig. 2.1.1): lava flows will cool and degas during emplacement and as they do so, the viscosity increases and microlite content increases. Such a process to evolve from pāhoehoe to ʻaʻā is suggested by Rowland & Walker (1987) and is illustrated in fig. 2.1.2. In a pāhoehoe flow the differential flow is accommodated by stretching and disruption of a thin skin (fig. 2.1.2.a). In this case, with cooling, a toothpaste lava will form (a transitional lava): rigid upper vesicular crust and lateral rims are formed. The rigid crust will undergo differential flow that is accommodated by shearing at the margins (fig. 21.2.b). This torque will generate the first clinkers at the contact between the lateral margins and the rigid crust. Continuing cooling, static levees will be individualized and breaking of the crust due to torque will migrate toward the center of the crust. Such a lava is called proximal-type ʻaʻā by Rowland & Walker (1987) (fig. 2.1.2.c). Finally, when the crust is totally disaggregated into clinker by torque and we will obtain a strict ʻaʻā flow, or a distal-type ʻaʻā flow according to Rowland & Walker (1987) (fig. 2.1.2.d). By this pāhoehoe – toothpaste - ʻaʻā transition clinker forms by torque.

2) The shear rate can increase (blue arrow on fig. 2.1.1): this is a frequent occurrence in lava flows, it can increase, for example when a lava flow encounters a steeper slope (see fig. 1.2.2 Hon & al., 2003), a contorted pathway, a narrower valley, or a more irregular topography. The upper vesicular rigid crust will be disrupted to form clinker as the interior reacts to the topography. If the shear rate increases progressively, another transitional lava type can occur: slabby pāhoehoe. If shear rate increases sharply, or by a jump, then the pāhoehoe to ʻaʻā transition can be very rapid (see fig. 1.2.2 Hon & al., 2003, where the slope increase is strong). By this pāhoehoe - slabby pāhoehoe - ʻaʻā transition, clinker is formed by simple disruption of the crust without necessarily any torque.
With torque, surface breaking, or a combination of both, it is important to note that clinker will form at the top and the sides of the lava flow but not at its base. Clinker can be transported to the ʻaʻā flow base by roll-over and caterpillar motion, but by the above processes it is never formed at the base. For clarity in the rest of this paper, I call this classical way to form clinker, by the term ʻaʻā fragmentation.

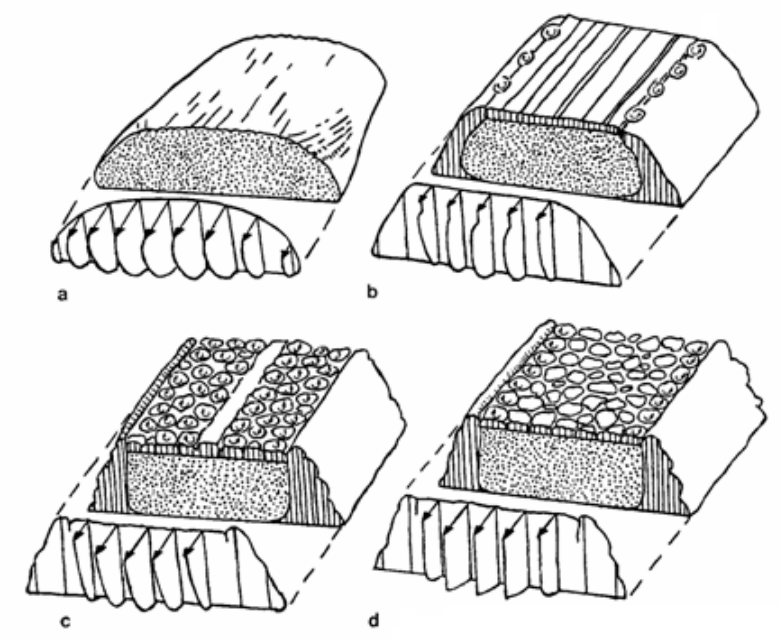

Figure 2.1.2: Schematic block diagrams of lobes of the four basaltic structural types in Hawaii showing velocity profiles. a. pāhoehoe, differential flow accommodated by wrinkling or wrinkling and disruption and rapid healing of skin; b. toothpaste lava, differential flow of rigid crust accommodated by shearing at margins forming the first clinkers; c. proximal type ‘a‘ā, differential flow causes tearing and rotation of the crust and also gradual outward movement, eventually to become attached to the levees; d. distal-type ‘a‘ā, plug flow of lava with loose clinker conveyed on surface. (Rowland and Walker, 1987).

Non ‘a‘ā clinker forming processes:

In the French Massif Central, I have observed three flows having pāhoehoe characteristics in cross section that have a basal clinker layer without any upper clinker layer, and that do have a non-disrupted vesiculated crust. This observation has led us to explore alternative ways to form clinker.

2.1.3. Methodology

I first did detailed outcrop descriptions of the flows and mapped them, to determine their general made characteristics. To compare with clinkers we believe to be formed by ‘a‘ā fragmentation we have also sampled basal clinker in two typical well constrained ‘a‘ā flows. We have sampled clinker of each flow and then studied fragment textures and morphology in hand specimen, binocular microscope and scanning electron microscope (SEM). When

adhering particles were observed on our samples, we put them for 30 minutes in a 50 to 60 Hz ultrasound bath.
As this is the first time to our knowledge that a SEM study has been performed on clinker, we have compared the obtained SEM images with those in the abundant literature concerning volcanic ash (Heiken & Wohletz, 1985; Dellino & al., 1990; Wohletz & Heiken, 1992; De Astis & al., 1997; Büttner & al., 1999; Dellino & al., 2001; Büttner & al., 2002; Dellino & Kyriakopoulos, 2003).

2.1.4. Geological setting

2.1.4.1. The Royat lava flows (F1 & F3)

The Royat lava flows belong to the Quaternary Chaîne des Puys volcanic province located to the west of Clermont Ferrand. They are four superimposed lavas (F1, F2, F3 & F4) dating from around 45,000 years that have been channelised into a narrow valley. The oldest lava flow (called F1) is the longest and the fourth (called F4) is the shortest. The flows have similar trachybasaltic compositions (Boivin & al., 2004). F1, F2 & F4 come from the Petit Puy de Dôme or the Travertin cone whereas F3 comes from the Puy de Lacroix (fig. 2.1.3.a).
The Royat F1 flow is a typical ‘a‘ā-type with a massive core and an upper and lower clinkery part (the upper part is missing on fig. 2.1.4.a) made of contorted and spiny clinkers. In contrast, the Royat F3 flow has pāhoehoe characteristics such as an upper vesicular part, vesicle pipes and no upper clinker. It has some sliver-shaped breccia at its base (fig. 2.1.4.b).

2.1.4.2. The Blanzat lava flows

The Blanzat lava flows belong also to the Chaîne des Puys. They consist of five lava flows (fig. 2.1.3.b), of which three have basaltic compositions (Grosliers, Blanzat and Egaules) and two are trachybasaltic (Féligonde and Mas d’Argnat) (Boivin & al., 2004). These lava flows have been erupted between 31,500 and 75,000 years BP (Boivin & al., 2004).
The Grosliers lava flow has pāhoehoe characteristics, such as stacked lobes, upper vesicular crust, and no upper clinkery part (see 1.3.3.2). Its base is clearly seen at the end of a water gallery (fig. 2.1.5.a) and has a 10-cm thick blocky clinkery layer. Groundwater gushes out at the contact with the underlying sandy and marly alluvium. The Blanzat lava flow is ‘a‘ā type,

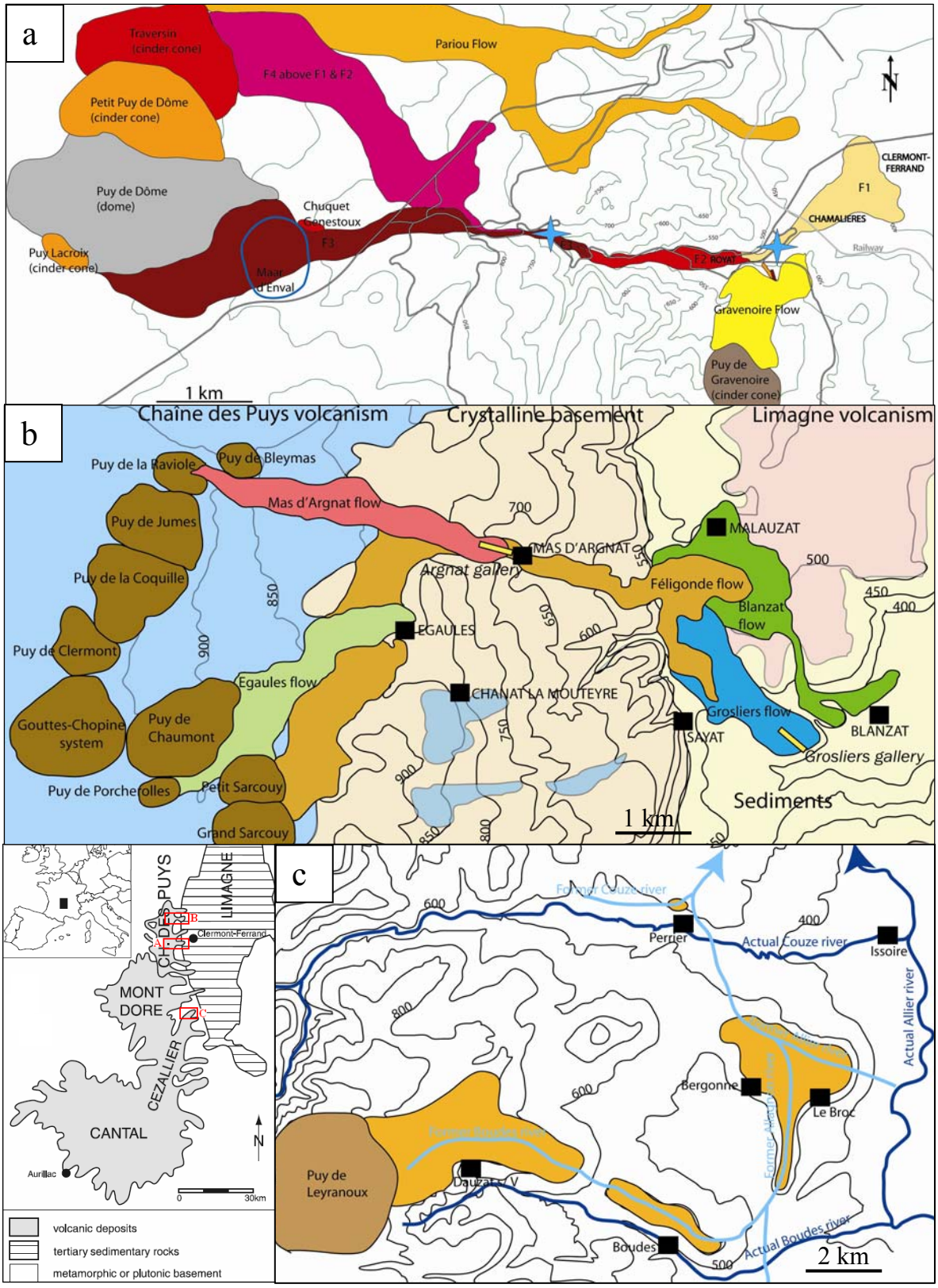

Figure 2.1.3: a. Map showing the Royat lava flows (F1 to F4) and surrounding lavas, the two blue stars indicate outcrop location of fig. 4b & 4c used for clinker sampling. **b**. Map showing the Blanzat lava flows, the two yellow lines indicate gallery emplacement where clinker was sampled. **c**. Map showing the pāhoehoe Roca Neyra lava flow and the contemporaneous hydrographic system, in comparison with the actual drainage.

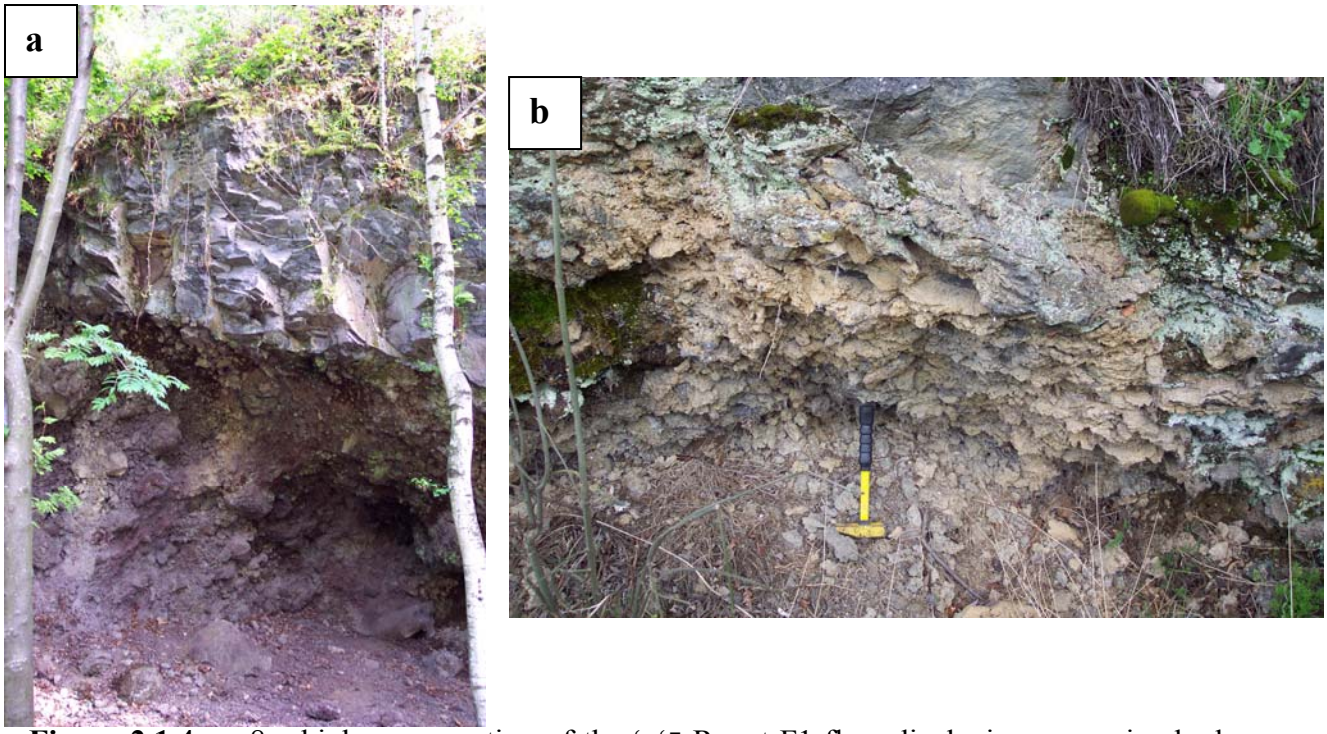

Figure 2.1.4: a. 8m-high cross section of the ‘a‘ā Royat F1 flow displaying a massive body over clinker; **b.** Base of the pāhoehoe Royat F3 flow displaying scales being detached to form clinker.

with upper and lower clinkery zones and a massive core, the spiny and contorted basal clinker has been sampled at the end of the Argnat gallery where groundwater is also extracted (fig. 2.1.5.b).

2.1.4.3. The Roca Neyra lava flow

In contrast to the other flows, the Roca Neyra flow does not belong to the Chaîne des Puys Province but to the older Limagne volcanic province to west of Issoire (Fig 2.1.3.c). The flow is basaltic in composition, has been dated at 3.6 My and today it forms an inverted relief (Ly, 1982). We have followed the outcrops of the flow and can trace it to the Puy de Leyranoux, a 2 km wide complex cinder cone (Fig 2.1.3.c). In figure 2.1.3.c we report the present and former hydrographic systems including data from Thonat (1969). The flow displays pāhoehoe characteristics (upper vesicular crust, lobe stacks and no upper clinker) (see 1.3.4.1). At Perrier the flows base outcrops and has a 30 to 60cm - thick clinkery layer (fig. 2.1.6.a & 6.b) where clinker have blocky and subrounded morphologies. This outcrop is located where the lava flow advanced up the Couze Pavin river, from the main Allier river channel (fig. 2.1.3.c).

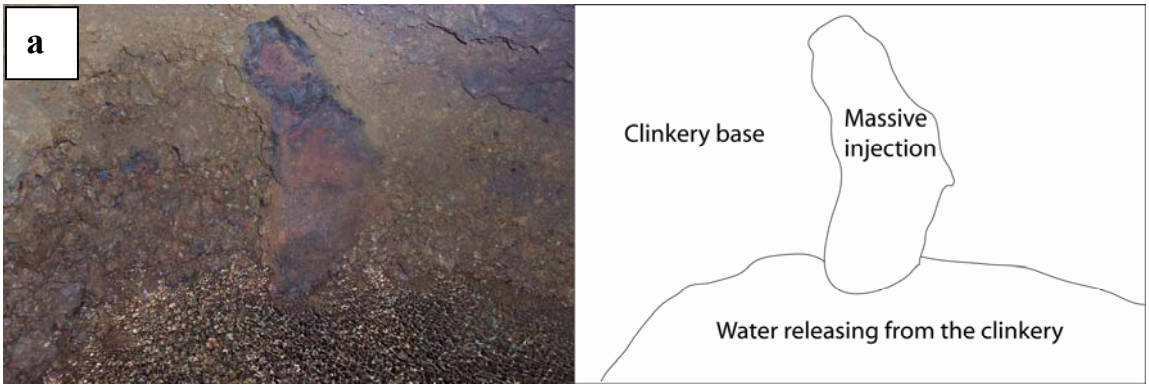

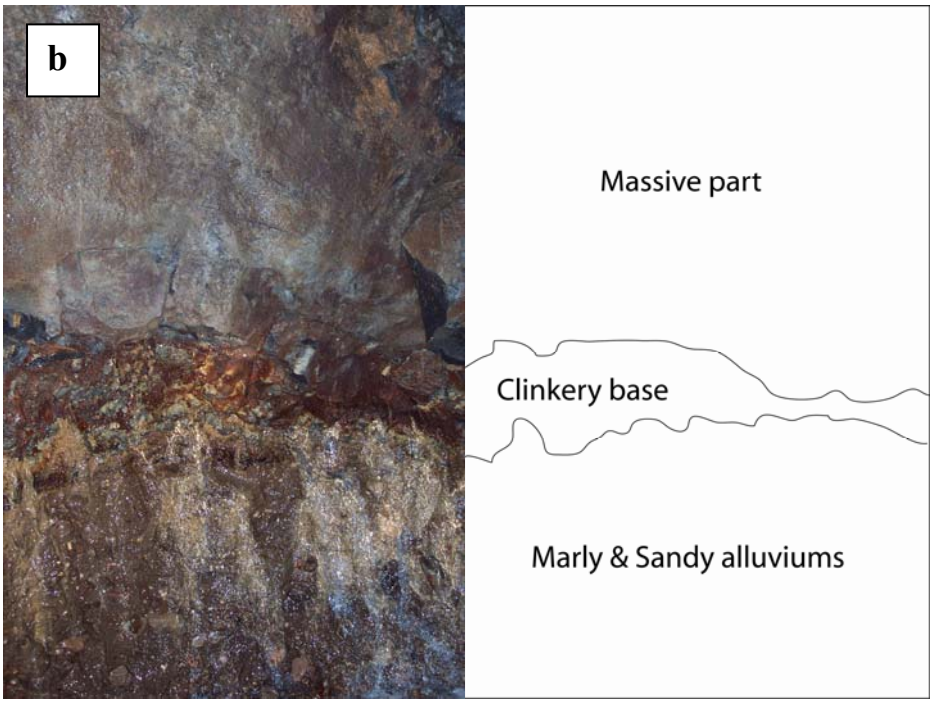

Figure 2.1.5: a. 50 cm-high image showing the clinkery base of the ‘a‘ā Blanzat flow and groundwater circulation; **b.** base of the pāhoehoe Grosliers flow displaying from top to bottom the massive core, a 10cm-thick clinkery layer with groundwater release and sandy/marly alluvium.

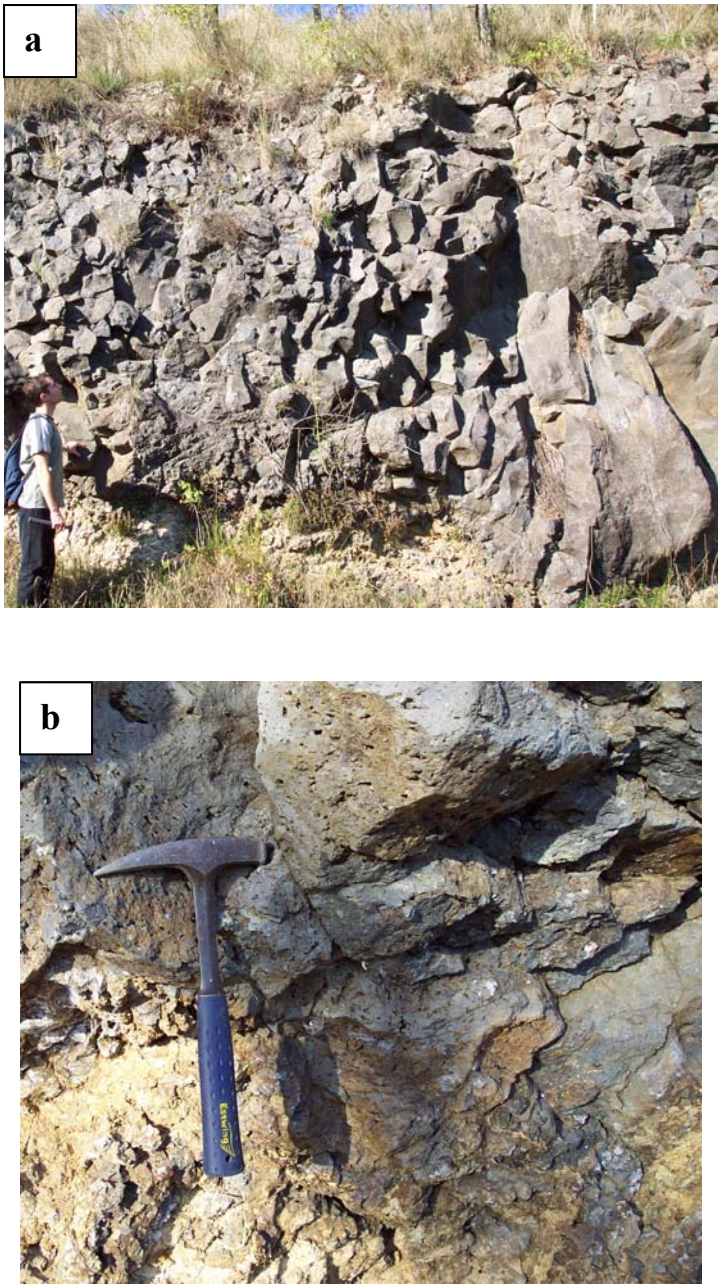

Figure 2.1.6: a. section of the Roca Neyra lava flow with its 30 to 80 cm-thick clinkery base; **b.** close up of the Roca Neyra flow base displaying the contact between the massive core and the basal clinker formation made of a mixing of blocky and subrounded clinkers and marly clasts.

2.1.5. Different ways to form clinker

2.1.5.1. ‘a‘ā fragment textures

2.1.5.1.1. Observations

We have considered first basal clinker samples from the typical ‘a‘ā flows of Blanzat (fig. 2.1.7) and Royat F1 (fig. 2.1.8). These clinker samples have vesicles (fig. 2.1.7 & 2.1.8) that could be linked to formation from the disruption of the upper vesicular crust. The clinker surfaces are not homogeneous (fig. 2.1.7.a & 2.1.8.a): some are rough (fig. 2.1.8.b), others are smooth (fig.2.1.7.b) and the rougher ones are more fractured. We interpret such a textural variation in a clinker sample as being due to differential deformation or torque rate between the inside and outside of clasts. The inner clast can be exposed by later breakage. Such an outer rough surface morphology had already been described in tachylite pyroclasts of a strombolian cinder cone at Lassen Peak (California). In our samples we have also found the diktytaxitic texture described by Heiken & Wohletz (1985) that consists of a network of finely crystalline glass-coated feldspar and pyroxene crystals separated by irregular vesicles (fig. 2.1.8.c). The clasts have many fractures, but we could not identify any distinct fracture plane family (e.g. fig. 2.1.7.a). Most fractures have no evidence of being synchronous, but are probably formed over the extended life of the clast from formation until final deposition. Fracture orientation is roughly parallel to the vesicle elongation plane (fig. 2.1.7.b).

2.1.5.1.2. Interpretation

‘A‘ā clinkers are probably formed by the disruption of a still-ductile cooling vesicular crust. We have found some clasts with tachylite and the diktytaxitic textures that are typical strombolian scoria features (Heiken & Wohletz, 1985). The ash coming from a cinder cone is known to be the result of magmatic fragmentation. Magmatic fragmentation is mostly provoked by the coalescing of bubbles and gas expansion due to rapid decompression forming fracture planes individualizing ash particles in dry conditions. In a lava flow this type of fragmentation is unlikely, although falling scoria can be incorporated during flow. Very glassy scoria fragments may be pyroclasts, while less grassy dyktytaxic pieces may be produced by slower cooling on the lava surface.

As an alternative to explosive fragmentation, fracture formation and clinker individualization could be done by fragmentation of the upper vesicular crust by torque and internal deformation. This fragmentation will also be ongoing as newly - formed clinker will interact together to create a progressive fracture formation. The existence of the diktytaxitic structure confirms that this fragmentation has occurred in dry conditions (Heiken & Wohletz, 1985). We propose to call this fragmentation in dry conditions *'a'ā fragmentation*.

2.1.5.2. Fragments in pāhoehoe basal breccia

2.1.5.2.1. Observations

Samples of this group come from the Grosliers and Roca Neyra pāhoehoe lava flows. We have observed many adhering particles that hide features, so samples were ultrasound-treated. These adhering particles are some micrometers long. Figures 2.1.9.d and 2.1.10.b display ultrasound-remnant adhering particles.

In the Grosliers lava flow, near-spherical glass fragments are present (fig. 2.1.9.a & 2.1.9.c). Some blocky glass fragments are also present in the Grosliers (fig. 2.1.9d) and the Roca Neyra flows (fig. 2.1.10.c). The blocky shapes are characterized by planar or conchoidal surfaces and spheres by conchoidal surfaces. These surface planes are independent of vesicles: the conchoidal plans do not follow the weakness plane formed by vesicle elongation in contrast to fragments in the 'a'ā flows (fig. 2.1.9.b compared with fig.2.1.7.b). Clinkers from Roca Neyra differ from the Grosliers lava flow clinkers, in that well-preserved pyroxenes are found (fig. 2.1.10a & 2.1.10b) and microphenocrysts of plagioclase have remained attached together (fig. 10d) even after ultrasound treatment.

2.1.5.2.2. Interpretation

Adhering particles are common in phreatomagmatic eruptions and are thought to collect when steam condenses inside the eruptive plume (Heiken & Wohletz, 1985; Dellino & al., 1990; De Astis & al., 1997; Dellino & al., 2001; Dellino & Kyriakopoulos, 2003). Spherical fragments have been previously obtained by experimental phreatomagmatic eruptions using Molten Fuel Coolant Interaction (Heiken & Wohletz, 1985; Wohletz & Heiken, 1992; Büttner & al., 2002) and have been found in natural phreatomagmatic deposits (Dellino & al;, 2001; Dellino &

Kyriakopoulos, 2003). They are thought to represent melt fragmentation in a ductile regime that is recorded during the expansion phase of magma-water interaction (Büttner & al., 2002). Blocky glass fragments have been also observed in Molten Fuel Coolant Interaction phreatomagmatic experiments (Heiken & Wohletz, 1985; Wohletz & Heiken, 1992; Büttner & al., 1999; Büttner & al., 2002) and are observed in natural phreatomagmatic deposits (Heiken & Wohletz, 1985; De Astis & al., 1997; Büttner & al., 1999; Dellino & al., 1990; Dellino & al., 2001; Dellino & Kyriakopoulos, 2003). The Roca Neyra microcryst structures are similar to phreatomagmatic deposits from a tuff ring near Clear Lake volcano (Heiken & Wohletz, 1985).

The Grosliers and the Roca Neyra lava flows clinker clearly display features that are indicative of phreatomagmatic fragmentation. Such ash is formed by the fragmentation of magma and also host rock due to a vibrating vapour film formed between the magma and the water-saturated rock (e.g. Wohletz & Heiken, 1992). A lava flow can also encounter water saturated ground, or stranding or running water. Phreatomagmatic fragmentation can occur in this situation. This is seen with rootless cones, and also with hyaloclastites formed when lava flows into the sea. This process, occurring at the lava flow base may form not ash but in the presented cases phreatomagmatic clinker. In fact, it seems that there is no particular difference between magma/water interaction textures and lava/water textures.

Clinker from Grosliers and Roca Neyra are different. It is quite possible that, like for explosive vent processes, the water/magma ratio can vary and thus the resulting products could display different features. We thus, look for possible water source differences between the two localities, and see if the change in fragmentation texture can be explained, through the local environment.

1. The Groslier flow, like the Blanzat flow, was emplaced onto a crystalline and previous lava flow basement. The Blanzat clinker does not display any phreatomagmatic features, and we propose that the water interaction for the Groslier flow occurred only when it reached a valley cut in marly and sandy alluvium (fig. 2.1.3.b). The alluvium was deposited by a small river (that still exists nowadays in the same area) and as they form the valley base that was probably water saturated when the lava arrived. Thus in this case, water is assumed to come from a small river and the water-saturated associated alluvium.

2. The Roca Neyra flow has flowed a different course and evolution. At the sample location, after having being channelized by the deep Allier river valley, the flow was thick enough to then flow up the palaeo Couze Pavin river (fig. 2.1.6.a). This was a larger river than the Grosliers, with a larger catchment area and coarser, thicker alluvium. In the Roca Neyra case,

the water can come from saturated alluvium, but there was probably a volumetrically more important input from the inflow, and probably damned Couze Pavin river. Moreover, hydrothermal minerals such as aragonite, calcite, gypsum and zeolites (phillipsite and chabazite) are only present in the basal clinker (Kieffer, 1967; Pégère, 2004) and to testify an important water presence during flow.

Thus, the amount of water encountered by the Roca Neyra flow was greater than that encountered by the Grosliers flow. The resulting different water/magma ratio may explain the differences in the phreatomagmatic clinkers obtained.

2.1.5.3. Shearing/faulting fragmentation features

2.1.5.3.1. Observations

Clinker samples from the pāhoehoe – like Royat F3 lava flow do not have the structures described for the previous pāhoehoe flows. This flow and others in Royat valley, have clear basal shear zones, where lava can be seen to be brecciated into angular fragments (fig. 2.1.4b). Small faults are clearly visible, with fault planes containing slickensides, fault zones having breccia, gauge, tension gashes, and Riedel shears. Such zones are not limited to the base of flows and can be seen in interiors, where zones of breccia are also seen. Even the upper parts of the Royat F4 flow have such breccia zones, and such structures are particularly common where intrusions of lava are injected into the top crust.

Clinker samples have scaly, flaky shapes and microfault planes are common (fig. 2.1.11.a & 2.1.11.b). These planes are marked with parallel striae and protrusions testifying to the movement having occurred on them (fig. 2.1.11.b). The features seen at outcrop and hand specimen are also seen in SEM images and in thin section, indicating a simple shear deformation at all scales. In some sections microlites even have CS textures.

2.1.5.3.2. Interpretations

The figure 2.1.4b clearly shows scale-shaped clinker being detached at the base of the flow, some clinkers are not totally individualized and are still linked with the flow base. Clearly there is in-situ clinker formation at the flow base, associated with the simple shear regime created by the flow of lava.

Such an in-situ brecciation at the flow base has not been described to our knowledge in basaltic lava flows but is a striking feature in the rhyolite lava flows described by Manley & Fink (1987) and Smith (1996). We have also observed major shear zones and brecciation on trachyandesitic flows on the Puy de Sancy, 80 km south of the Chaîne de Puys. Smith (1996) explained such basal breccia as a way to accommodate most of the basal shearing, while the main mass of lava is translated above as a plug. With basal cooling in any type of lava, the viscosity at the flow base will increase, the brittle transition will be met, and so faults and breccia can form. If the plug flow idea is correct it also indicates that the base of the flow has developed a *lower* resistance to deformation than the upper liquid body. This in turn indicates a shear softening at the brittle-ductile transition.

The occurrence of microfaults with protrusions and striae in Royat F2 clinkers indicates a differential movement between two rigid blocks. We suggest that once the flow is in contact with the ground, the first scale-shaped clinkers will be formed by shearing between the base and the cooled flow base, this process will continue as the flow is still moving and as the cooled base of the flow thickens, allowing more brecciation to follow.

The shear features are found in all Royat lava flows, be they ‘a‘ā or pāhoehoe, indicating that shear brecciation is a general process occurring in the lava flows. Such features can also be found on levee flanks (Linneman & Borgia, 1993) and in lava tubes. One important observation is that while such flakey clinkers can be found mixed with ‘a‘ā clinker, sometimes only flakey is found, or no clinker at all. This indicates that roll over does not always occur. This can only occur if the base of the lava is lubricated (Lescinsky & Merle 2005). Two possible lubrication processes are raised fluid pressures at the flow base by hydromagmatic activity, and propagation of high pressure fluidized zones along basal shear zones. Finally, the frictional heating produced in brecciation may help to retard lava cooling and prolong flow.

We can consider that the fragmentation processes proposed here can be linked together, for example when an ‘a‘ā flow presenting ‘a‘ā fragmentation encounters water, and maybe some structures can overprint or mix.

2.1.6 Conclusions

The multi-scale analysis of clinker samples coming from different basaltic flow bases has allowed us to propose three different modes of clinker formation.

1. ‘a‘ā fragmentation, which has generally been considered as the only way to form clinker. This type of fragmentation has been found in ‘a‘ā lava flows (Blanzat, Royat F1) by disruption of the upper vesicular crust either by an increase in the apparent viscosity or increase of the shear strain, or a combination of both. Clinker is first formed at the flow top and can appear at the base by a caterpillar roll-over process. These clinkers are characterized by non-synchronic fractures, a zonation of deformation and a diktytaxitic texture.
2. Phreatomagmatic fragmentation can also occur at the flow base, seen in the Grosliers and the Roca Neyra pāhoehoe flows. As in vent processes, different water/magma ratios can occur and thus several clinker morphologies can be created, including adhering particles, blocky shapes, spherical glass and the curious preserved attachment of plagioclase microphenocrysts. Such evidence clearly indicates that the fragmentation process will occur when a lava flow is encountering a water source and in particular when a lava flow follows river valleys.
3. Simple shear faulting fragmentation can also occur at the flow base (Royat F3) whatever the chemical composition of the lava flow due to increased strain, and strain rates. Clinkers formed by this way are flaky, have microfaults and are associated often with crushed fine material.
This is a first attempt to describe and classify clinker associated with basaltic lava flows. It has been proposed with detailed observations of only 5 lava flows, backed up with more summary observations on many other flows. The study could be extended to other compositions were we expect to find similar structures and textures.
Better knowledge of brecciation and the processes behind it can provide indications on the way lava flows deform and flow. Our observations indicate that all types of lava can form breccia internally, and that such breccia can provide evidence of conditions at the flow base and interior. Importantly the breccias show the importance of lava - water interactions and role of shear brecciation in a brittle regime. The observations suggest that a range of magma – water ratios may create a range of phenomena, like with hydrovolcanic explosions, and that such interactions may aid lubrication of the lava flow basal shear zone.
Variable breccia types have hydrogeological implications. In this study, a typical ‘a‘ā flow (Blanzat) posses an exploited aquifer in the basal clinker formed by ‘a‘ā fragmentation, this is in fact the classical context for exploiting aquifers associated with basaltic flows. But, the Grosliers flow, is typically pāhoehoe and nevertheless it posses also an exploited basal aquifer made by phreatomagmatic clinker. There is therefore a presently unexplored potential for exploiting aquifers in pāhoehoe flows especially as pāhoehoe are more abundant than ‘a‘ā flows (Self & al., 1998).

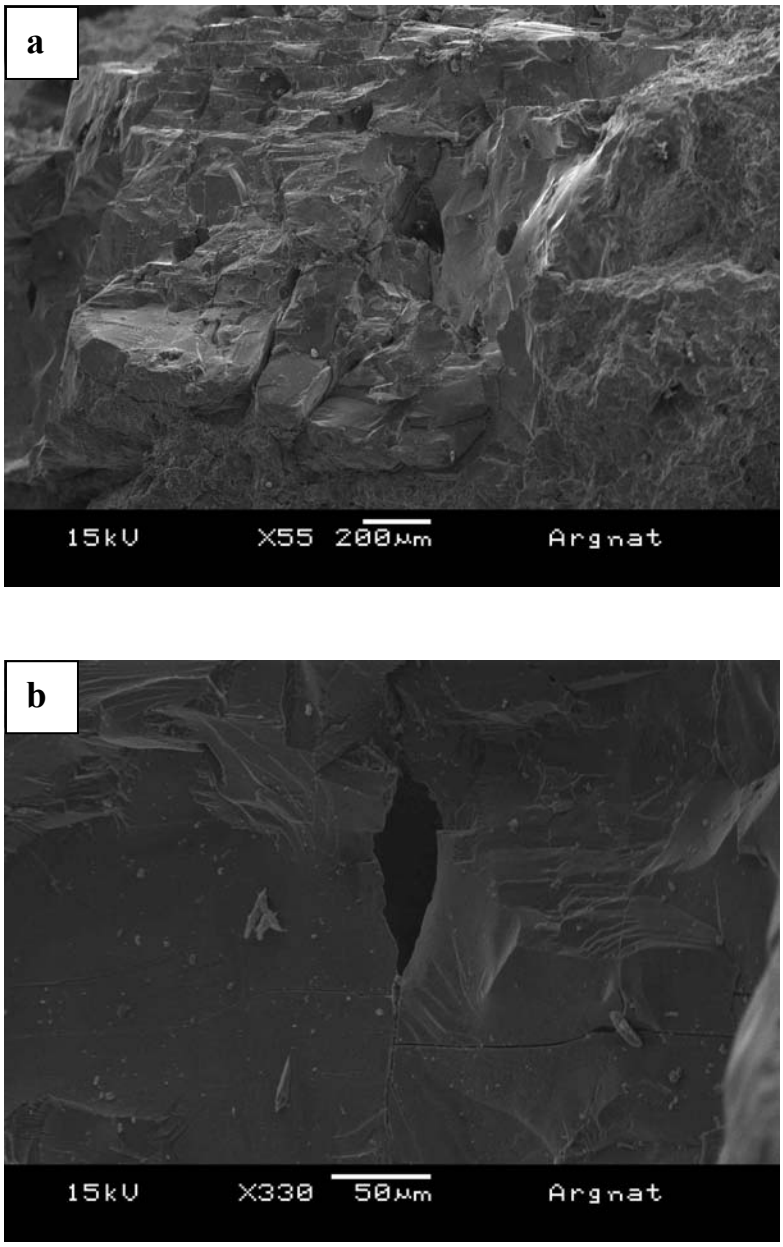

Figure 2.1.7: SEM images of basal clinkers coming from the ‘a‘ā Blanzat flow in the Argnat gallery; **a.** irregular aspect of the clinker surface; **b.** non synchronic fractures where one is crossing the elongation plane of the vesicle (see text for explanations).

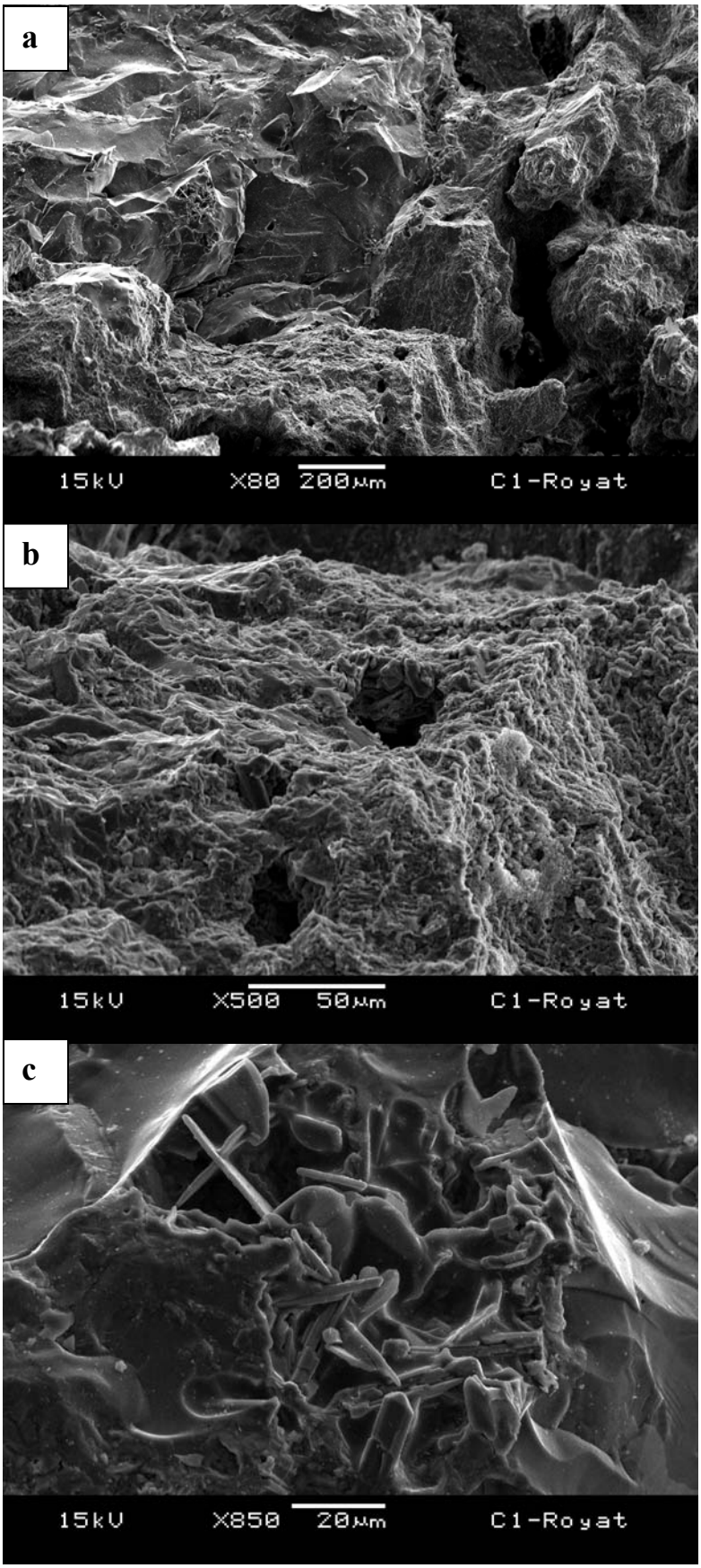

Figure 2.1.8: SEM images of basal clinkers coming from the ‘a‘ā Royat F1 flow; **a.** irregular aspect of the clinker surface; **b.** rough and vesiculated clinker surface; **c.** diktytaxitic texture (see text for explanations).

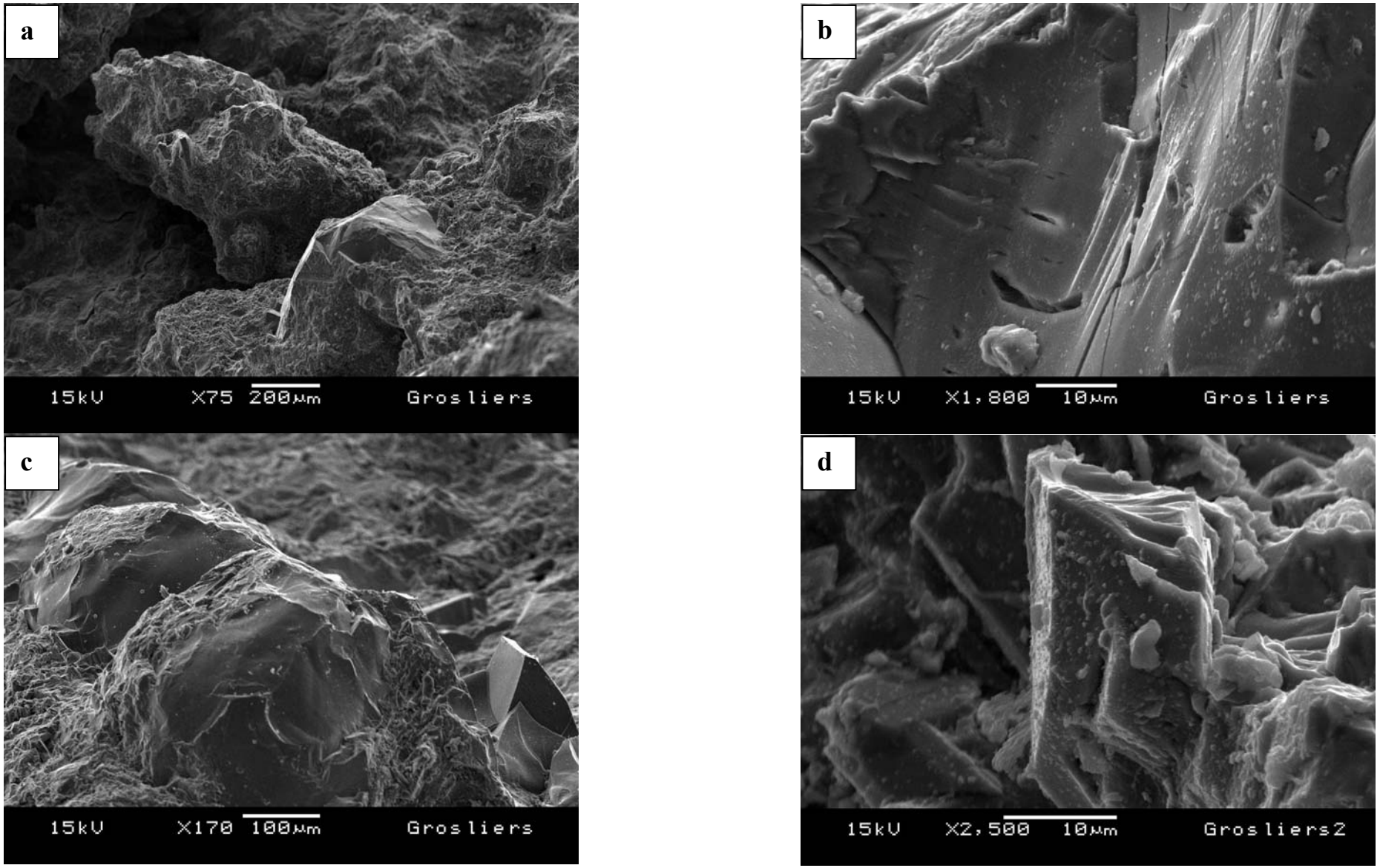

Figure 2.1.9: SEM images of basal clinkers coming from the pāhoehoe Grosliers lava flow in the Grosliers's gallery after 30 minutes ultrasound treatment; **a.** spherical glass fragment; **b.** close up of a conchoidal surface from a spherical glass fragment displaying a non alignment of vesicles and the conchoidal fracture plane; **c.** spherical glass fragments; **d.** blocky glassy shape with remnants of adhering particles (see text for explanations).

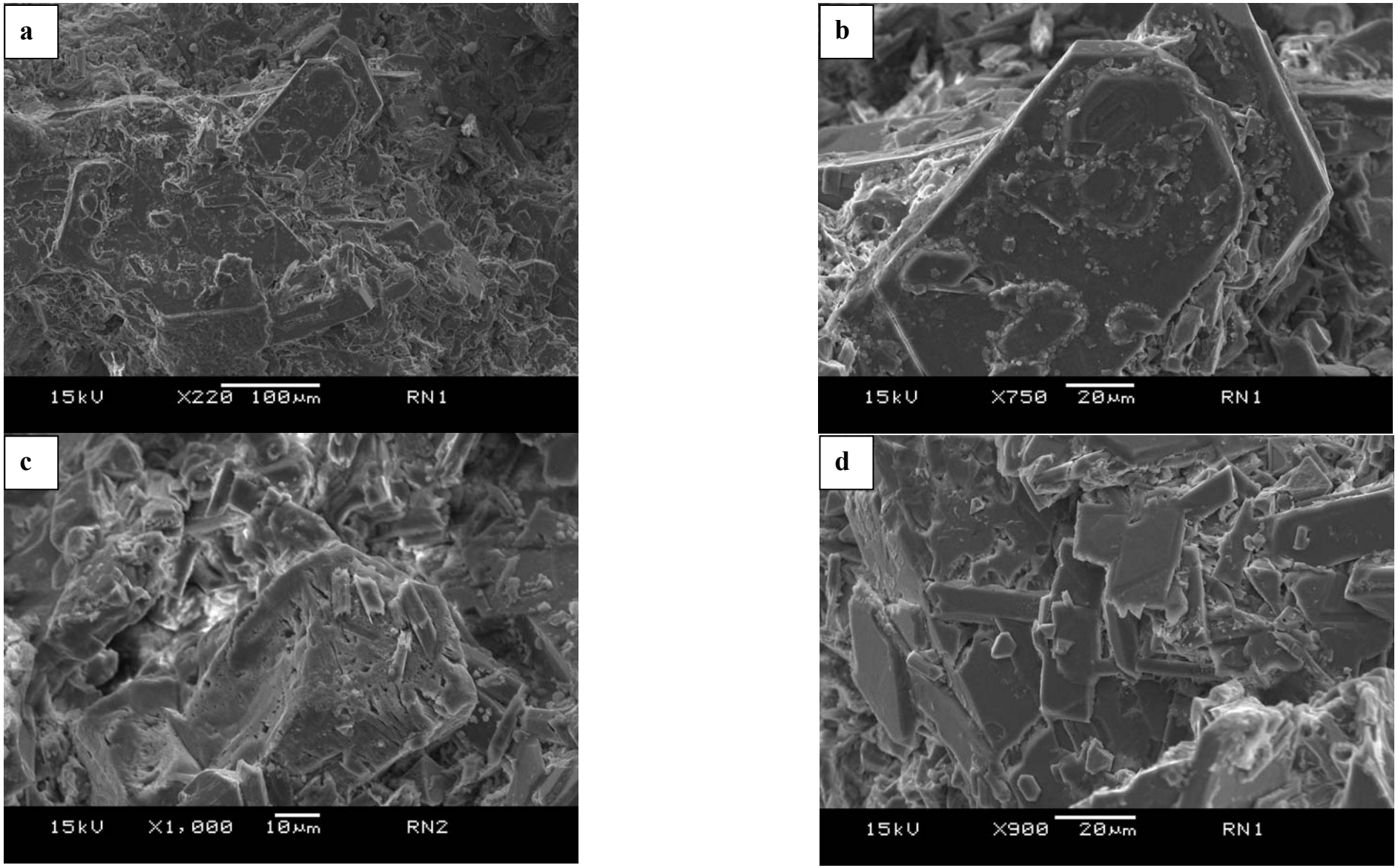

Figure 2.1.10: SEM images of basal clinkers coming from the pāhoehoe Roca Neyra flow at the Perrier outcrop; **a.** well preserved pyroxene; **b.** well preserved pyroxene with remnant adhering particles; **c.** a blocky glassy shape; **d.** microphenocrysts of plagioclase attached together (see text for explanations).

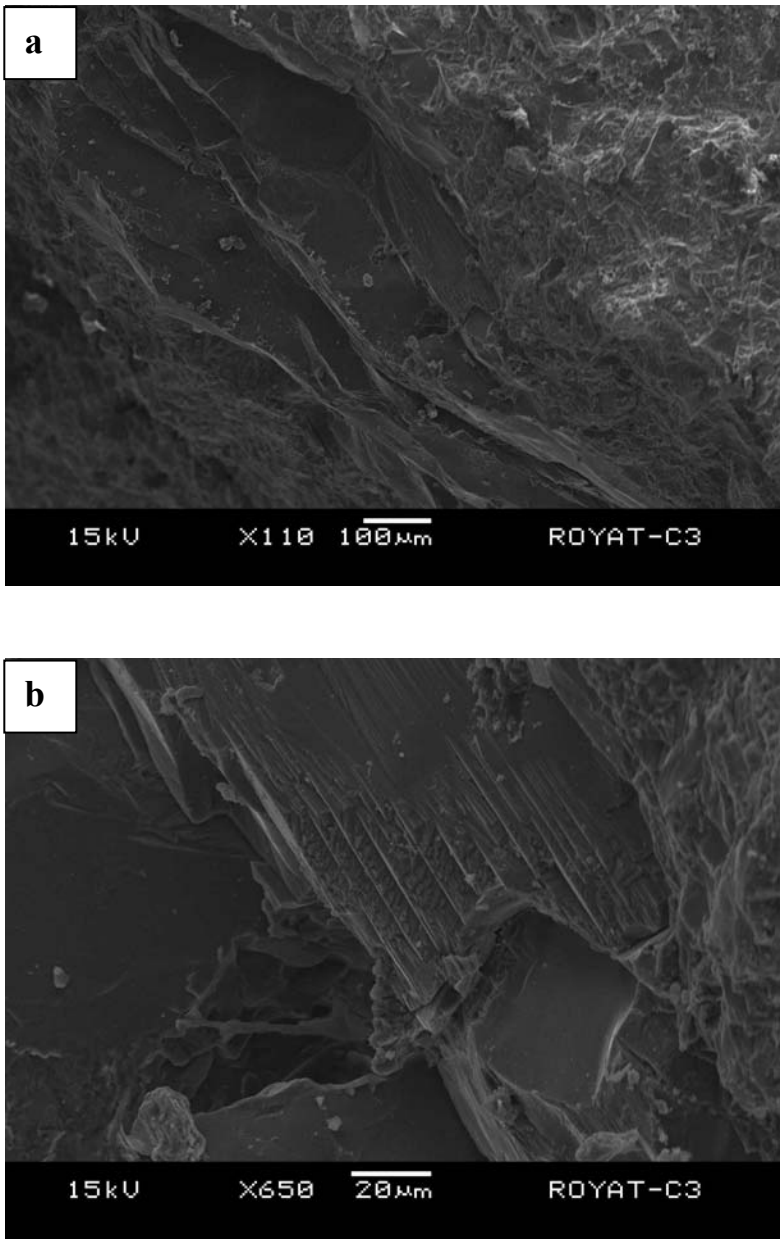

Figure 2.1.11: SEM images of basal clinker coming from the pāhoehoe Royat F3 flow; **a.** fault planes; **b.** close up of a fault plane displaying parallel striation and protrusions (see text for explanations).

2.2. WET PEPERITE FORMATION IN LAVA FLOWS

2.2.1. Introduction

2.2.1.1. Peperite definition

The term 'peperite' was used by Scrope (1827) to describe clastic rocks from the Limagne d'Auvergne region, that are mixtures of lacustrine sediments and basalt and which resemble ground pepper. The Limagne d'Auvergne is now the type locality for such rocks. The term 'peperite' is now most commonly used in a descriptive sense to refer to clastic rocks comprising both igneous and sedimentary components (e.g. Skilling & al., 2002). Brooks & al. (1982), White & al. (2000) and Skilling & al. (2002) defend the use of the term peperite in a genetic sense, as defined by White & al. (2000): *Peperite is a genetic term applied to a rock formed essentially in situ by disintegration of magma intruding and mingling with unconsolidated or poorly consolidated, typically wet sediments. The term also refers to similar mixtures generated by the same processes operating at the contacts of lavas and hot pyroclastic flow deposits with such sediments.*

2.2.1.2. Different types of peperite

Two main peperite types are known according the shape of the juvenile clasts:

1) Blocky peperite: the blocky clasts imply fragmentation of magma/lava in the brittle regime. Brittle fragmentation may affect earlier-formed juvenile clasts during and after mingling with sediments. Brittle fragmentation will be favoured when magma/lava viscosity is high and/or strain rates are high (Skilling & al., 2002). Most blocky clasts are presumed to form by

quenching and mechanical stresses, and by hydromagmatic explosions (Skilling & al., 2002). Quench fragmentation and hydromagmatic explosions require rapid transfer of heat to the pore fluid implying that insulating vapour films were not developed or not sustained.

2) Fluidal peperite: the fluidal clasts are fragmented in the ductile regime. According to Skilling & al. (2002), the only plausible explanation for this process is that vapour films along magma-sediment contacts prevented direct contact with the pore fluid. It is not clear how vapour films remain stable during intricate mingling and complex deformation of magma clasts. Processes inferred to give rise to fluidal clasts include fluid instabilities within vapour films (Wohletz, 1983), magma-sediment density contrasts (Donaire & al., 2002), host sediment vesiculation (Skilling, 1998) and hydromagmatic explosions (Busby-Spera & White, 1987). Surface tension and fluid-fluid shearing at the interfaces of mingling magma and fluidally behaving sediment must also promote fragmentation.

2.2.1.3. Peperite associated with lava flows

Peperites are mainly formed in vent locations in relation with phreatomagmatic features such as diatremes. They can also occur at the contact between intrusions (e.g. Schmincke, 1967; Kano, 1989; Boulter, 1993) and lava flows (Jerram & al., 2000; Jerram & Stollhofen, 2002; Martin & Németh, 2007; Petry & al., 2007; Waichel & al., 2007; Waichel & al., 2008) with sediments and many of other situations (see fig. 2.2.1 for a description of the widespread occurrence of peperite formation).

As stated in 1.1., peperites form at the contact with typically wet sediments. However dry peperites have been described associated with lava flows (e.g. Petry & al., 2007; Waichel & al., 2008). These dry peperites have been discovered only in two places: in the Parana flood basalts (South Brazil) (Petry & al., 2007; Waichel & al., 2008) and its African equivalent: the Etendeka province (Namibia) (Jerram & al., 2000; Jerram & Stollhofen, 2002). In these areas several basaltic lava flows have interacted with the underlying sand dunes in dry conditions. Figure 2.2.2 displays the different processes susceptible to have led to the peperite formation in such contexts (Petry & al., 2007).

Studies concerning wet peperite have aroused less interest than the dry ones, but one has been described in Western Hungary (Martin & Németh, 2007) and others also in the upper Parana complex when a wet climate had become dominant (Waichel & al., 2007).

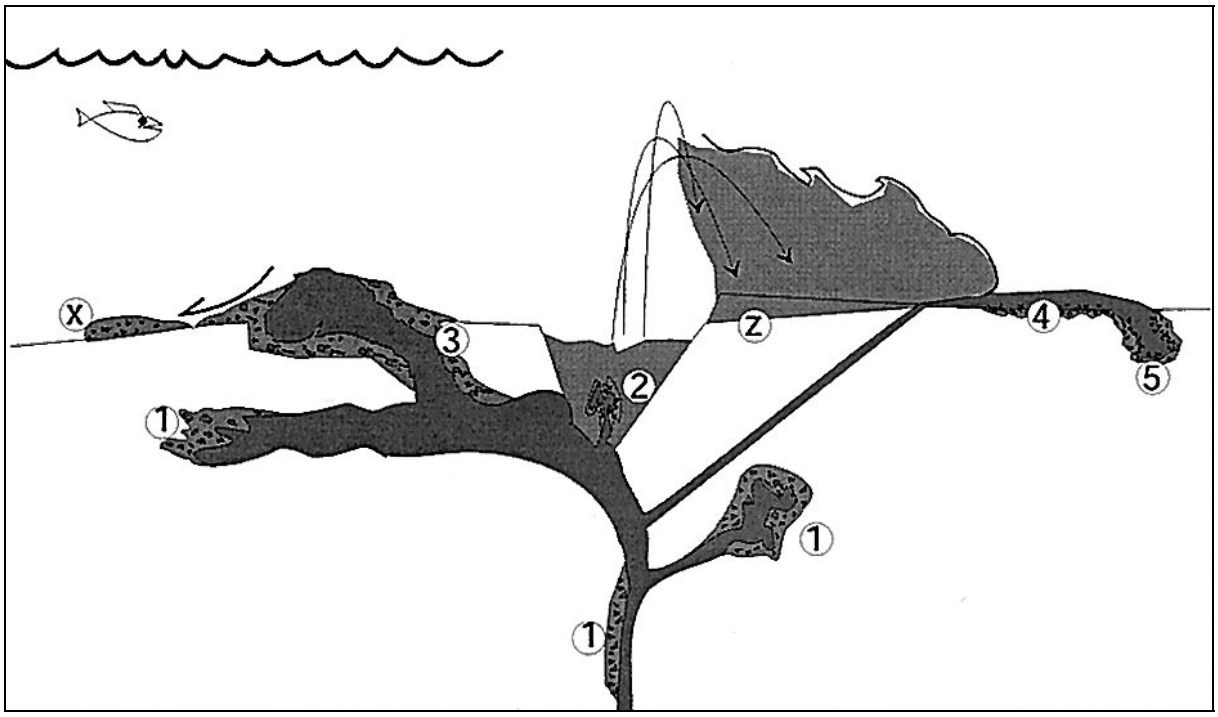

Figure 2.2.1: Schematic illustration of common sites of peperite development associated with: (1) dikes and other intrusions; (2) feeder dikes intruding vent-filling deposits; (3) partly-emergent intrusions; (4) base of lavas; (5) margins of invasive lavas. Other deposits, which are not considered peperites, are (x) slump or density current deposits derived from peperite; (z) fallout and pyroclastic density current deposits from explosive phreatomagmatic eruptions; lahar deposits (not shown)(*from* White & al., 2000).

2.2.1.4. Interests of such a study

The study of peperite in lava flows is important for several reasons:

1) peperites form essentially by interaction of a hot juvenile material with wet sediment or sediment-laden water, such a situation is very common at the vent but also along flow paths. Understanding the modes of peperite generation will improve our responses toward volcanic hazards.
2) peperites are also important for palaeoenvironmental reconstruction and relative chronology because its presence demonstrates approximate contemporaneity of magmatism and sedimentation (Skilling & al., 2002).
3) as peperites can be developed in wet sediments, they may be associated with hydrothermal alteration and/or mineralization (e.g. in sills: Boulter, 1993).

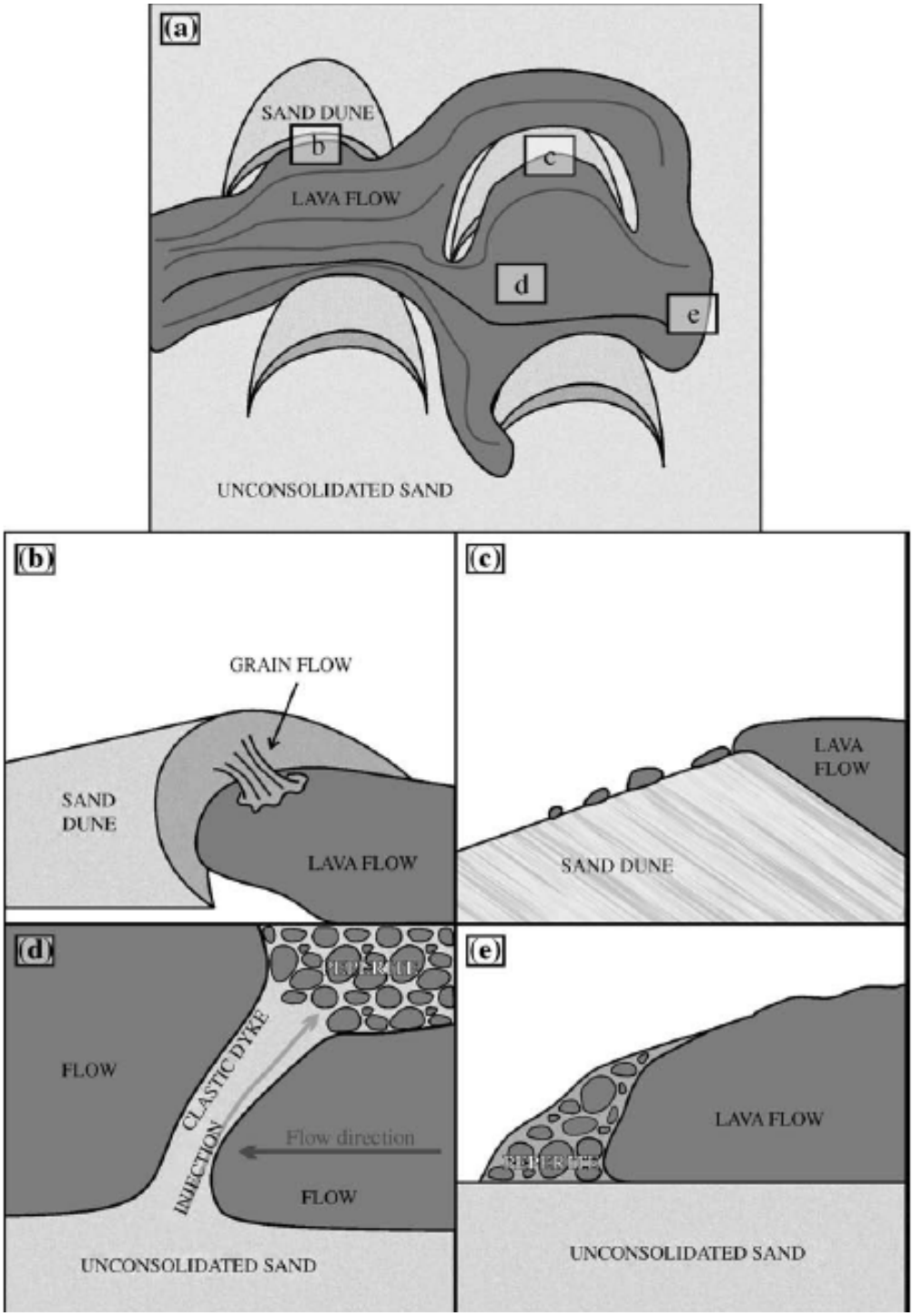

Figure 2.2.2: Schematic figure showing the different processes that lead to the formation of the volcanic-sedimentary interaction features as observed in the Serra Geral formation, Parana Basin, southern Brazil. **a.** The confinement of a flow (left) in the interdune and the partial cooling of the flow (right) leading to the injection of sand through fissures. **b.** Collapse of the dune inwards the flow (right) and formation of injection peperite (right). **c.** The final stage of formation of peperite, as the lava ceases to flow. **d.** Formation of filling clastic dykes with sand migrating over the flow. **e.** Incorporation of sand at the flow front (*from* Petry & al., 2007).

4) as lava flows may constitute water-exploited aquifers (e.g. Kiernan & al., 2003), the development of peperite in and/or at the base of flows will incorporate sediments into an aquifer, and could affect water quality.

2.2.2. Geological setting

We have studied three relief-inverted basanitic lava flows belonging to the Limagne volcanism in the French Massif Central: the Chateaugay, the Pardines and the Saint Gervazy lava flows. These flows have been studied because they have huge quarries that allow extensive internal investigation.

2.2.2.1. The Chateaugay lava flow

The Chateaugay lava flow is from the Miocene (Glangeaud, 1909; Aubert & al., 1973) and is located 10 km north of Clermont Ferrand where it constitutes a 9 km² plateau from 500 to 530 m.a.s.l., dominating the Limagne basin (fig. 2.2.3.b). This plateau is cut into at least 5 blocks separated by faults (fig. 2.2.3.b). The flow displays pāhoehoe characteristics (clinker absence and an upper vesicular crust with few-deformed vesicles). The flow comes from the place called “Champ Griaud” at the west of the plateau where remnants of a scoria cone can be observed (Noé, 2007). Basal flow contacts have not been observed, nevertheless, as seen on the road from les Mauvaises to Blanzat, the basement is made of marls (fig. 2.2.4.a). The flow is cut by the Fougerouse quarry in which 5 peperitic formations have been found. The flow forms also a non-exploited aquifer as shown by flooding in the quarry and springs occurring on the faults.

2.2.2.2. The Pardines lava flow

The Pardines lava flow is Pliocene and has been dated at 4.2± 0.3 My (Bout & al., 1966). It is located 5 km at the north-west of Issoire and forms a lava plateau around 600 m a.s.l. of 4 km², associated with two other summits above Sauvagnat Sainte Marthe and Saint Yvoine (fig. 2.2.3d). The Pardines plateau is also associated with later debris avalanche deposits emplaced around 2 My (Cantagrel *in* Poidevin & al., 1984; Lo Bello, 1988; Duffel, 1999). The alluvium deposits at the flow base indicate that it was emplaced in the palaeo-Allier river

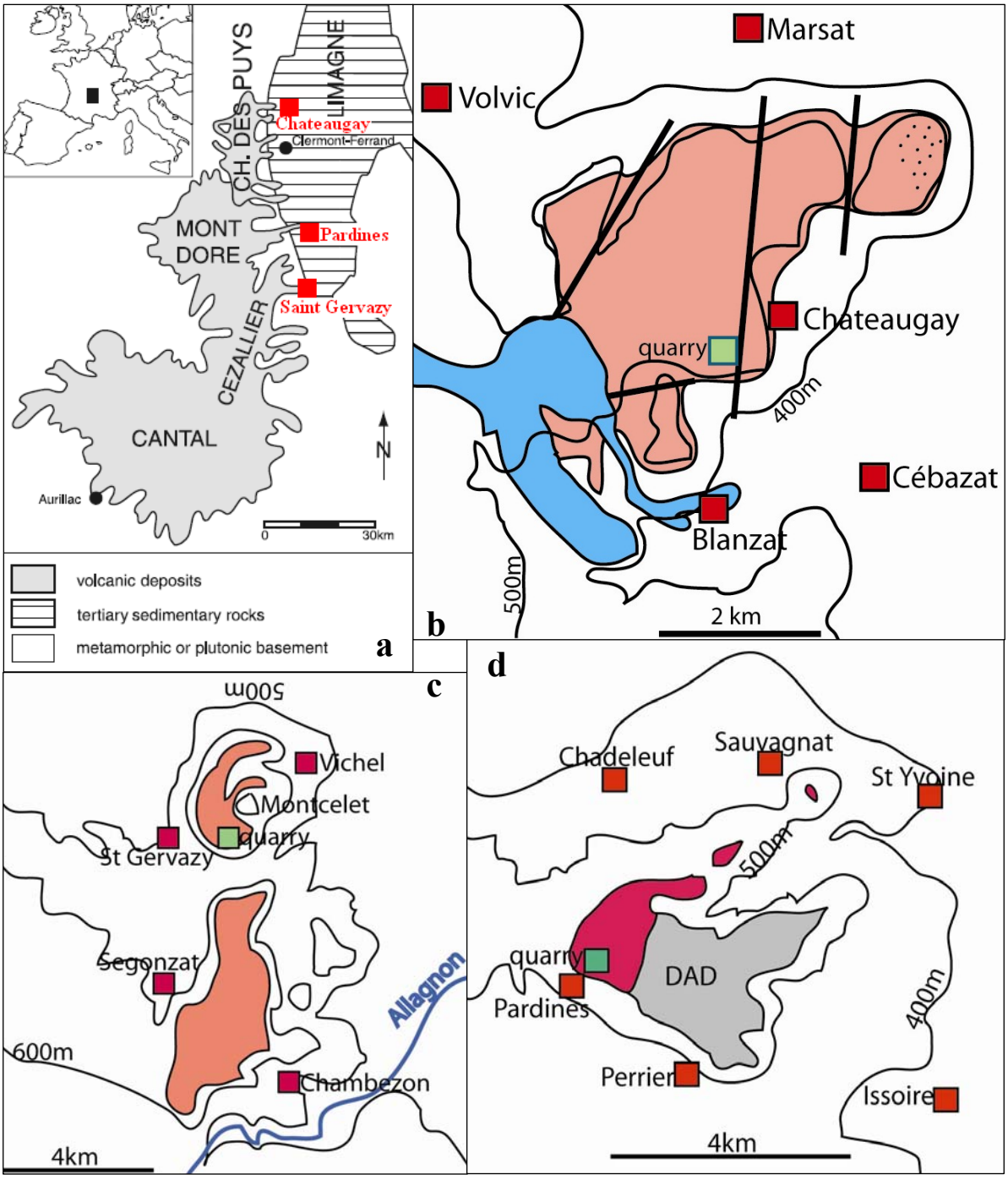

Figure 2.2.3: a. location of the three studied lava flows in the Limagne volcanic province; **b.** the Chateaugay basanitic flow extent displaying faults location and its source as the scoria-rich area (points) and later (Chaîne des Puys) volcanism as blue; **c.** the Saint Gervazy basanitic flow and its relationship with the Segonzat-Chambezon member that followed the palaeo-Allagnon course; **d.** the Pardines basanitic flow and its relationship with the later debris avalanche deposit (DAD) from Perrier.

(Pastre, 2002) and that the flow had a south-to-north course. Its vent source can not been identified as the area has been filled with many volcanic products coming from the Mont Dore and Cézallier volcanoes. The flow has been excavated by the C.T.P.P. quarry (Carrières Travaux Publics Pardines). The peperitic base associated with the substrata is observed and two peperite pockets are seen in the lava interior. The absence of clinker and the presence of vesiculated pipes reveal pāhoehoe characteristics. The flow has acted as an aquifer before destabilisation of the avalanche deposits (Vidal & al., 1996) as testified by the palaeo-piezometric groundwater elevation (fig. 2.2.5.a) and some present wet areas in the quarry.

2.2.2.3. The Saint Gervazy lava flow

The Saint Gervazy lava flow is from the lower Pliocene (Glangeaud, 1909; Thonat, 1969). It is located 15km south of Issoire and forms a 1,5 km² plateau (fig. 2.2.3.c). The flow is not associated with the Montcelet neck as the base of the neck is higher than the flow and as there is a thin sedimentary formation between the two (Thonat, 1969). The flow can be associated with the Chambezon flow as being the same according their elevation and having recording the palaeo-Allagnon course (Thonat, 1969) (fig. 2.2.3.c). Thus the flow comes from the South from a vent belonging to the Cézalllier volcanic zone or the Cantal stratovolcano. The flow is incised by the Chevalier quarry where two peperitic pockets are displayed. The contact at the base of the lava flow can not be seen as it is covered by a mass of fallen rock but nevertheless the marly basement can be observed at the quarry entrance where a fallen megablock lies over it (fig 2.2.6.a). As in the two other flows, there is no evidence of clinker and thus the flow seems to approach the pāhoehoe-type. The flow constitutes also an aquifer, and the water table can be observed in the quarry.

2.2.3. Macroscopic features

In the three quarries from the three lava flows, the peperites and the basanite flows were studied in the field, and then in hand specimen and in thin sections. These sections have displayed the same mineralogy in the lava flow and in the igneous clasts in the peperite except the presence of supplementary zeolite minerals in the clasts and in the marly matrix (fig. 2.2.4.f). These indicate that water has played a rule during the formation of peperites. Peperites consist of metric sub-spherical pockets made of an intermingling between the basanite and the marls. These pockets occur in the lower part of the flows and particularly one

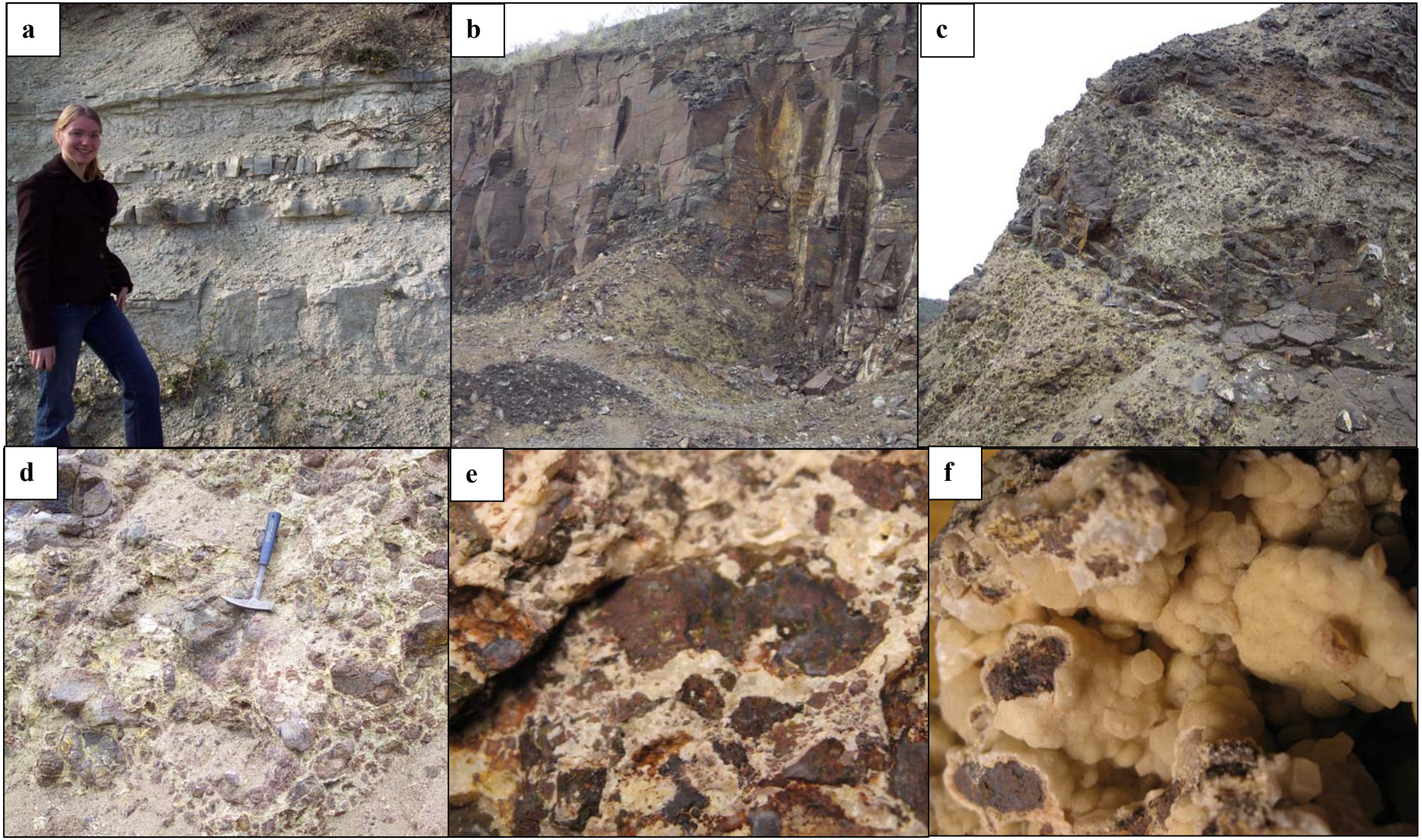

Figure 2.2.4: Several aspects of the Chateaugay lava flow: **a.** the marl sediments observed just south of the flow; **b.** peperitic pocket at the base of the flow (the cliff is 5m high); **c.** a peperite pocket close to the flow summit (picture is 4m high); **d.** fluidal aspect of the peperite with globular clasts; **e.** close up on the peperite showing the fluidal aspect (picture is 5cm long); **f.** abundant zeolite development in the peperite formation (picture is 8cm long).

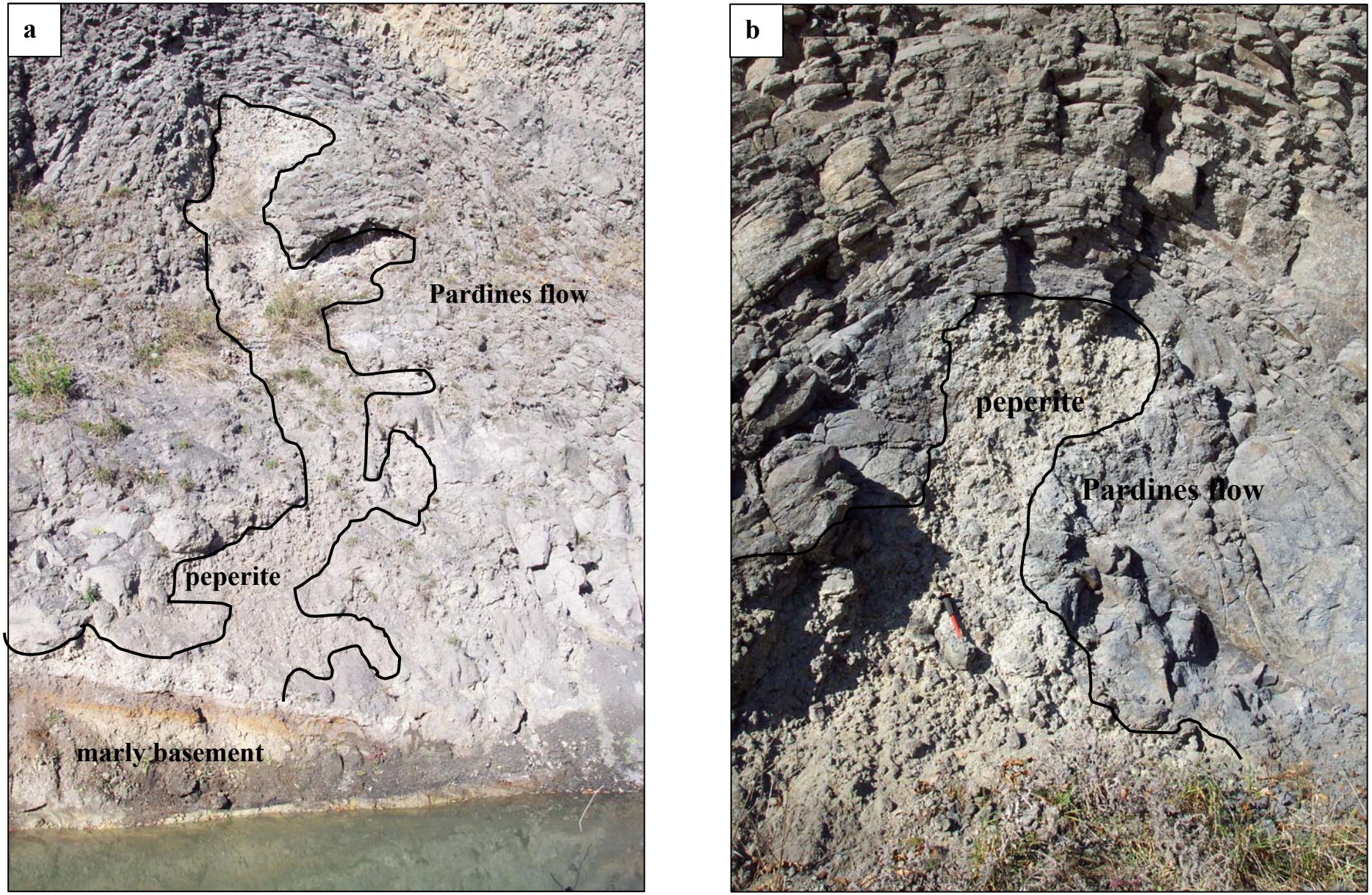

Figure 2.2.5: Several aspects of the Pardines lava flow: **a.** base of the flow displaying the marly basement which has been cooked, and rising peperite diapir (2 m high); **b.** another rising peperite diapir (1 m high) with concentric fractures in the surrounding in the flow.

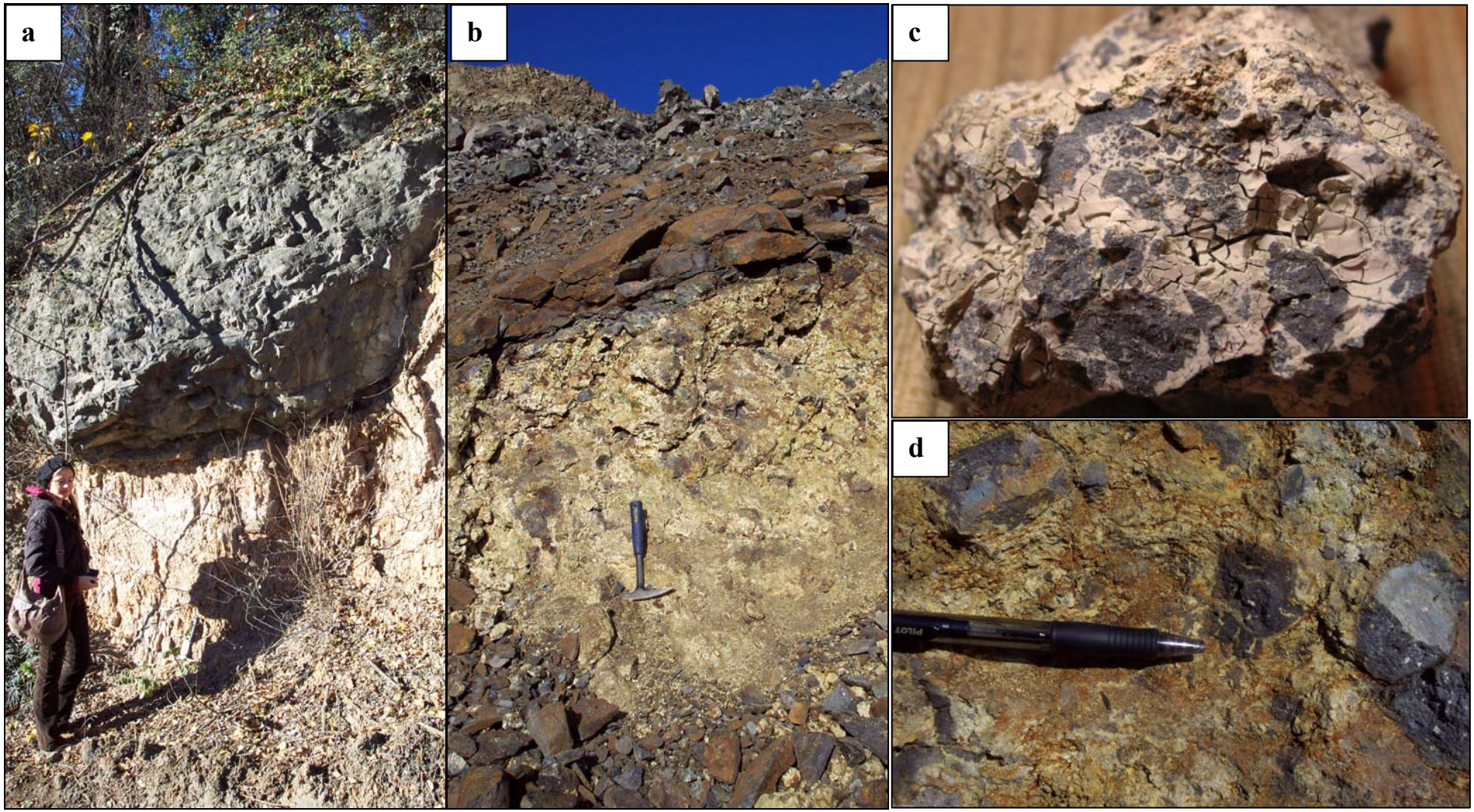

Figure 2.2.6: Several aspects of the Saint Gervazy lava flow: **a.** a megaclast of the flow having fallen on the marl basement; **b.** peperitic pocket at the flow base; **c.** close up the peperite displaying globular clasts typical of a fluidal peperite (sample 6cm long); **d.** other close up the peperite displaying a quenched basanitic clast with marly matrix infill.

pocket from the Pardines flow displays clear relationships with the basement (fig. 2.2.5.a). In Chateaugay, one pocket is close to the flow summit but has not reached the surface (fig. 2.2.4.c).

The basanite around the pockets has concentric fractures so that peperites appear to occupy diapiric-like bodies (fig. 2.2.4.b, 2.2.5.a, 2.2.5.b & 2.2.6.b). The shape of the volcanic clasts allows us to say that the peperites are fluidal at the macroscopic scale (see 1.2.). Clasts are subrounded and display enbayments (fig. 2.2.4.d, 2.2.4.e & 2.2.6.c). The figure 2.2.6.d displays a basanitic clast with radial fractures filled with the marly matrix, we interpret these fractures as being the result of the thermal contraction, sometimes this kind of fissures can give a blockier aspect to the clasts.

2.2.4. SEM features

To learn more about such peperitic textures, samples were analyzed on an SEM following the same reasoning as in the previous chapter concerning clinker formations. Several samples were taken from the Chateaugay and the Saint Gervazy peperites. We can easily observe the thermal contraction in the marls (fig. 2.2.7.a). According Waichel & al. (2007) such a feature testifies that marls were wet before the contact with lava. Moreover, the marly clasts display lots of crater features seeming to be formed by the impact of 50 to 200 micrometers basanitic clasts (fig. 2.2.7.a).

In the Saint Gervazy lava flow, near-spherical glass fragments are present (fig. 2.2.7.b& c) like those observed at the base of the Grosliers flow (previous chapter). Such morphologies have been previously obtained by experimental phreatomagmatic eruptions using MFCI (Molten Fuel Coolant Interaction) (Heiken & Wohletz, 1985; Wohletz & Heiken, 1992; Büttner & al., 2002) and have been found in natural phreatomagmatic deposits (Dellino & al., 2001; Dellino & Kyriakopoulos, 2003). They are thought to represent melt fragmentation in a ductile regime that is recorded during the expansion phase of magma-water interaction (Büttner & al., 2002). Moreover, on fig. 2.2.7.d, we can make out an oily skin structure having releasing conchoidal skin pieces. These can be observed everywhere on the samples (fig. 2.2.7.a& d).

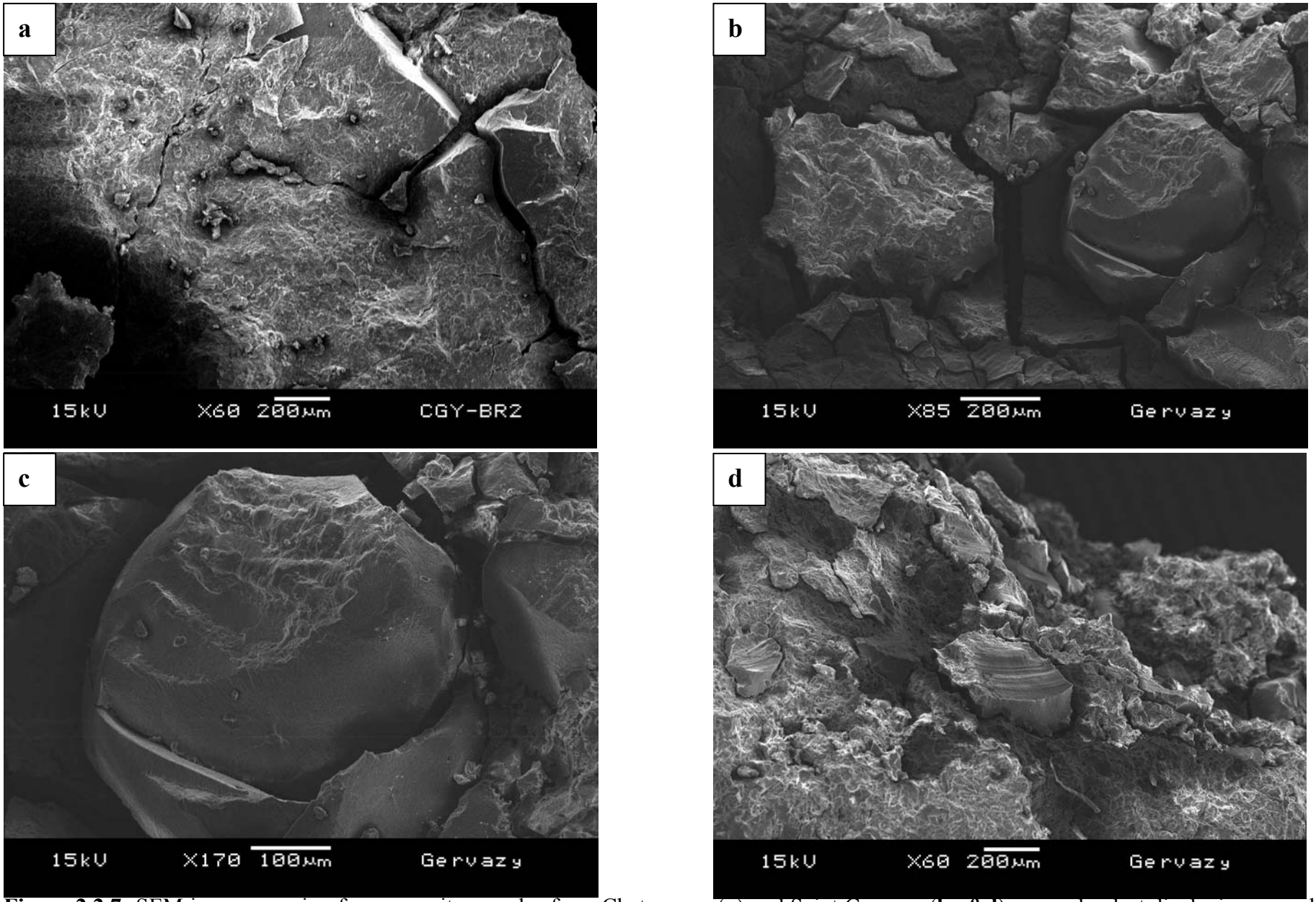

Figure 2.2.7: SEM images coming from peperite samples from Chateaugay (**a**) and Saint Gervazy (**b,c&d**); **a.** marly clast displaying quenching fractures and impact craters formed by less than 200 µm basanitic clasts; **b.** clasts of marls and a spherical glass; **c.** close up of the spherical glass displaying also an oily skin structure; **d.** an oily skin piece of glass over marly clasts.

2.2.5. Interpretation

Such peperitic pockets have been previously described in three contexts: the dry context of the Parana flows (Petry & al., 2007; Waichel & al., 2008), the wet context of the same flow (Waichel & al., 2007) and the wet context of the Hajagoshegy flow in Hungary (Martin & Németh, 2007)(fig. 2.2.8).

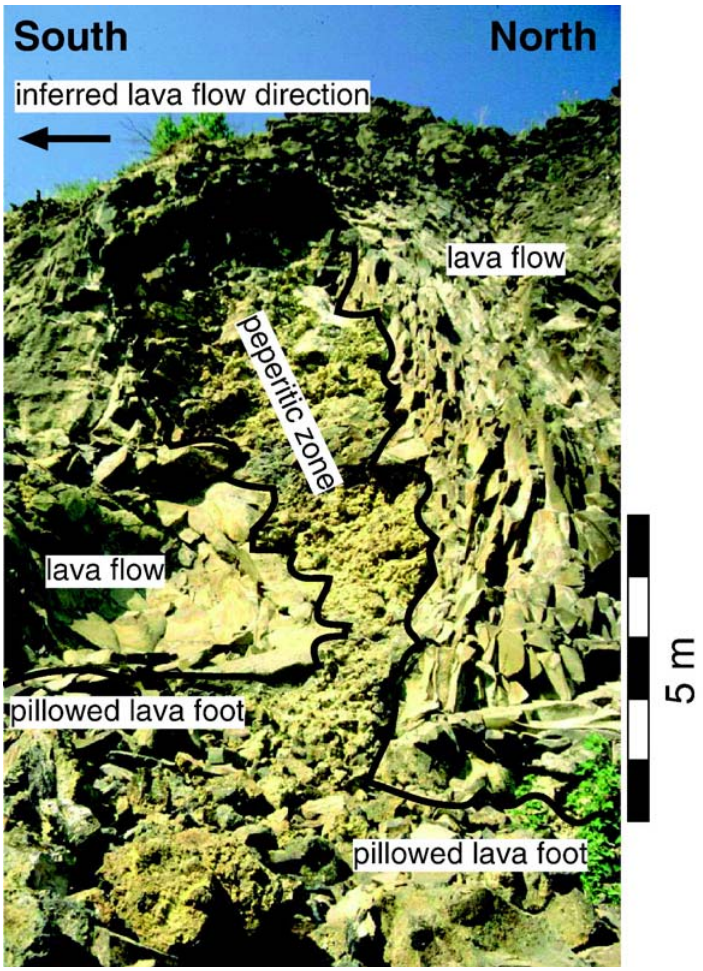

Figure 2.2.8: Globular peperite formed at the base of a lava flow at Hajagoshegy. The host sediment is fine inter-lava silt (*from* Martin & Németh, 2007).

Here we are clearly in the context of wet sediments as testified by the occurrence of quench fractures in the marly clasts (fig. 2.2.7.a) but above all by the presence of glass spheres (fig. 2.2.7.b& c, see 4.) and zeolites (fig. 2.2.4.f) in peperites. Thus the processes proposed by Petry al. (2007) in fig. 2.2.2 can not be applied here, and anyway marls are less fluidizable than dune sand in dry conditions.

The interaction between magma/lava with water or wet sediment is can be considered as molten fuel coolant interaction (MFCI) (Dullforce & al., 1976). The lava (fuel) is hot with temperatures causing the vaporization of water in the marly sediment interstices (coolant). The formation of a film of vapour at the fuel-coolant interface inhibits the rapid transfer of heat to the coolant. This effect, called Leidenfrost effect, is observed in experimental and natural volcanic settings (Waichel & al., 2007). Development of MFCI explosivity is dependent upon collapse of this vapour film (White, 1996; Waichel & al., 2007). Following Zimanowski & al. (1997) an explosive MFCI consists of a four-stage process: 1) a hydrodynamic mixing phase with premixing of water and melt under stable film boiling conditions; 2) a trigger phase with quasi-coherent quantitative vapour film collapse in the premix leading to direct contact between melt and water; 3) a fine fragmentation phase; and 4) a vaporization and expansion phase.

If MFCI has occurred, resulting peperites will display blocky textures resulting from the collapse of the vapour film and if they have formed during the persistence of this vapour film they will have fluidal peperite textures (Skilling & al., 2002; Waichel & al., 2007).

As basanitic clasts are mainly globular, being the fluidal type of peperite, we can attribute its formation to the same process as fluidal peperites: that is to say by the formation of a vapour film at the contact between marls and the basanite flows (Leidenfrost effect). The low permeability of fine-grained marly sediment is known to contribute to maintaining vapour films at the juvenile-clasts-sediment interface, facilitating the formation of fluidal peperites (Busby-Spera & al., 1987). Such fluidized peperite will rise in the still hot and viscous lava flow simply by a density gradient and will explain the typical pockets or diapir shapes seen in the quarries. Nevertheless, the weakness of the simple previous explanation is underlined by: 1) the occurrence of quenched marls (fig. 7a) and basanite clasts (fig. 6d) typical of blocky peperites; 2) the presence of spherical glass (fig. 7b&c) typical of phreatomagmatic explosions; 3) impact craters formed by 50-to-200 micrometer long igneous clasts in marls typical of projected products (fig. 7a), and 4) the absence of the finer grained fluidization zone around peperites as described in Martin & Németh (2007). We have also an explosive MFCI stage after the creation of the vapour film. We propose that the later destabilization of this film was responsible for the non preservation of the finer grained fluidal zone and appearance of quenched fractures in spherical glasses. Nevertheless, the explosivity was quite small as there is no evidence of radial fracture in the surrounding lava flows and as blocky shapes are common in the smallest clasts. Without having a concrete explanation, we propose that at first explosivity was restricted by the confining pressure of the overlying lava flow but also that

the explosivity may have strongly increased as such rising pockets experienced a strong decrease of the confining pressure, i.e. when it reached the top of the flow.

2.2.6. Conclusions

The study of three different Miocene-Oligocene basanites having flowed on the same marly ground has revealed the same peperitic features: peperitic diapirs in the base of the flow mingling the marly basement and the basanite material. Textures are mainly globular shapes so that such peperites can be called fluidal peperites. We have also evidence that the sediments were wet. This is seen from quenched structures in the marly and basanitic clasts and above all the occurrence of spherical glasses seen in the SEM and zeolites. The fluidal aspect of peperites was promoted by the development of a water film at the contact between the basanite flow and the water-saturated marls, forming the intimate mingling of both components. The resulting mixture was less dense than the overlying flow so diapiric rise occurred in the molten lava. Subsequent lava cooling produced concentric fractures around the diapir.

Nevertheless, the story is not so simple as there is also evidence of quenching and explosions (crater impacts and spherical glasses) indicating the MFCI existence at a small scales. The confining pressure seems to have counterbalanced the explosive expansion so that no radial fractures and injections appear around peperitic pockets.

This study has emphasized the occurrence of wet peperites in lava flows and such structures can be formed nowadays, so that a better understanding of such formation will help study of lavas encountering water, a very common situation. If such peperite can reach the surface of the flow, an explosive event can also be foreseen, as there will not be any confining pressure. We have also provided other arguments using SEM analysis of samples to assess the presence of water when the flow was emplaced. This can help reconstruction of palaeoenvironments. Finally, as the described lava flows are aquifers and as these aquifers are full of peperite pockets, there is also a pollution/alteration mechanism of the groundwater.

CONCLUSIONS

This chapter has described the different occurrences of breccia associated with lava flows revealing new interpretations on their formation and new implications concerning hazards related to lava flow emplacement.

Clinkery breccia has been revealed in several occurrences in both ‘a‘ā and pāhoehoe contexts. Classically, clinkers are formed by the fragmentation of the lava flow crust during ‘a‘ā emplacement. But the occurrences in pāhoehoe flows have showed that another formation possibility, which has been postulated after SEM imaging and comparison with volcanic ash: phreatomagmatic fragmentation, i.e. clinkers formed when the lava has encountered on its path a water-saturated area. Another clinker formation mechanism by shearing at the flow rims has been proposed from macroscopic evidence of shearing, cataclastic and fault breccias and from SEM-observed microfaults. These three different contexts need of course, to be developed and looked for in other lava flows to better constrain the rheologic parameters (shear strain rate and viscosity), water/lava ratio and the valley profile followed by the lava. Implications of these results will, as noted above, increase our knowledge in lava flow emplacement and their hazard mitigation and also improve our knowledge of potential lava flow aquifers where clinker, whatever their origin, could contain a water saturated area.

Peperitic-like breccias observed in three Limagne lava flows, emplaced above a marly basement, have displayed similar macroscopic features (diapir structures and clasts shape) and SEM features typical of phreatomagmatic ashes (such as impact evidence in marly clasts and near spherical glass fragments). So we have more evidence of phreatomagmatism occurring in lava flow, not leading to gentle-clinker formation but to peperitic-like structures. These represent an explosive hazard if peperitic diapirs could reach the flow surface. This suggests also another meeting of the lava with water, probably in a lacustrine, marshy context or on a marly soil. Other peperites observed in lava flows have revealed other mechanisms, but also susceptible by decompression to generate explosive hazard.

Finally, I would like to emphasize the great help brought by the SEM imagery to these breccia studies and that the SEM is useful for more than the restrictive volcanic ash descriptions so far prevalent.

REFERENCES

Aubert, M., Bouiller, R., Camus, G., Cochet, A., D'Arcy, D., Giot, D., Jeambrun, M., Roche, A., Bonhommet, N., 1973. Carte géologique à 1/50000 de Clermont Ferrand. BRGM.

Boivin, P., Besson, J.C., Briot, D., Camus, G., De Goër de Herve, A., Gourgaud, A., Labazuy, Ph., De Larouzière, F.D., Livet, M., Mergoil, J., Miallier, D., Morel, J.M., Vernet, G., Vincent, P.M., 2004. Volcanologie de la Chaîne des Puys, 4ème édition.

Boulter, C.A., 1993. High-level peperitic sills at Rio Tinto, Spain: implications for stratigraphy and mineralization. Trans. Inst. Min. Metall. 102, B30-B38.

Bout, P., Frechen, J., Lippolt, H.J., 1966. Datations stratigraphiques et radiochronologiques de quelques coulées basaltiques de Limagne. Revue d'Auvergne t.80, 207-231.

Brooks, E.R., Wood, M.M., Garbutt, P.L., 1982. Origin and metamorphism of peperite associated rocks in the Devonian Elwell Formation, northern Sierra Nevada, California. Geol. Soc. Am. Bull. 93, 1208-1231.

Busby-Spera, C.J., White, J.D.L., 1987. Variation in peperite textures associated with differing host-sediment properties. Bull. Volcanol. 49, 765-775.

Büttner, R., Dellino, P., Zimanowski, B., 1999. Identifying magma-water interaction from the surface features of ash particles. Nature 401, 688-690.

Büttner, R., Dellino, P., La Volpe, L., Lorenz, V., Zimanowski, B., 2002. Thermohydraulic explosions in phreatomagmatic eruptions as evidenced by the comparison between pyroclasts and products from Molten Fuel Coolant Interaction experiments. J. Geoph. Res. 107, 2277, 10.1029/ 2001JB000511.

De Astis, G., Dellino, P., De Rosa, R., La Volpe, L., 1997. Eruptive and emplacement mechanisms of widespread fine-grained pyroclastic deposits on Vulcano Island (Italy). Bull. Volcanol. 59, 81-102.

Dellino, P., Frazzetta, G., La Volpe, L., 1990. Wet surge deposits at La Fossa di Vulcano: depositional and eruptive mechanisms. J. Volcanol. Geotherm. Res. 43, 215-233.

Dellino, P., Isaia, R., La Volpe, L., Orsi, G., 2001. Statistical analysis of textural data from complex pyroclastic sequences: implications for fragmentation processes of the Agnano-Monte Spina Tephra (4.1 ka), Phlegrean Fields, southern Italy. Bull. Volcanol. 63, 443-461.

Dellino, P., Kyriakopoulos, K., 2003. Phreatomagmatic ash from the ongoing eruption of Etna reaching the Greek island of Cefalonia. J. Volcanol. Geotherm. Res. 126, 341-345.

Dellino, P., Isaia, R., La Volpe, L., Orsi, G., 2001. Statistical analysis of textural data from complex pyroclastic sequences: implications for fragmentation processes of the Agnano-Monte Spina Tephra (4.1 ka), Phlegrean Fields, southern Italy. Bull. Volcanol. 63, 443-461.

Dellino, P., Kyriakopoulos, K., 2003. Phreatomagmatic ash from the ongoing eruption of Etna reaching the Greek island of Cefalonia. J. Volcanol. Geotherm. Res. 126, 341-345.

Donaire, T., Sàez, R., Pascual, E., 2002. Rhyolitic globular peperites from the Aznalcollar mining district (Iberian Pyrite belt, Spain): physical and chemical controls. J. Volcanol. Geotherm. Res. 114, 119-128.

Duffel, H., 1999. Contribution géochronologique à la stratigraphie volcanique du Massif des Monts Dore par la méthode 39Ar-40Ar. DEA, Univ. Clermont Ferrand II, 56pp.

Dullforce, T.A., Buchanan, D.J., Peckover, R.S., 1976. Self-triggering of small-scale fuel coolant interactions : I. Experiments. J. Appl. Phys. 9, 1295-1302.

Duraiswami, R.A., Dole, G., Bondre, N., 2003. Slabby pāhoehoe from the western Deccan Volcanic Province: evidence for incipient pāhoehoe-'a'ā transitions. J. Volcanol. Geotherm. Res. 121, 195-217.

Glangeaud, P., 1909. Les regions volcaniques du Puy de Dôme. Bulletin des services de la carte géologique de la France et des topographies souterraines n°123, tome XIX, 180pp.

Heiken, G., Wohletz, K., 1985. Volcanic ash. University of California Press, Berkeley. 246pp.

Hon, K., Gansecki, C., Kauahikaua, J., 2003. The transition from ʻaʻā to pāhoehoe crust on flows emplaced during the Puʻu ʻŌʻō-Kūpaianaha eruption. U.S. Geological Survey Professional Paper 1676.

Jerram, D.A., Mountney, N., Howell, J., Stollhofen, H., Long, D., 2000. Death of a sand sea: An active aeolian erg systematically buried by the Etendeka Flood Basalts of NW Namibia. J. Geol. Soc. 157, 513-516.

Jerram, D.A., Stollhofen, H., 2002. Lava/sediment interaction in desert settings: are all peperite-like textures the result of magma-water interaction? J. Volcanol., Res. 114, 231-249.

Kano, K., 1989. Interactions between andesitic magma and poorly consolidated sediments: examples in the Neogene Shirahama Group, south Izu, Japan. J. Volcanol. Geotherm. Res. 37, 59-75.

Kieffer, G., 1967. Nouvelles observations géologiques et morphologiques sur la region de Perrier et le Nord du Cézallier. Revue d'Auvergne 81, 137-151.

Kiernan, K., Wood, C., Middleton, G.; 2003. Aquifer structure and contamination risk in lava flows: insights from Iceland and Australia. Environmental Geology 43, 852-865.

Kilburn, C.R.J., 1981. Pāhoehoe and ʻaʻā lavas; a discussion and continuation of the model of Peterson and Tilling. J. Volcanol. Geotherm. Res. 11, 373-383.

Kilburn, C.R.J., 1993. Lava crust, ʻaʻā flow lengthening and the pāhoehoe-'aʻā transition. In: Kilburn, C.R.J., Luongo, G. (Eds), Active Lava Flows: Monitoring and Modelling. UCL Press, London, 263-280.

Kilburn, C.R.J., 2000. Lava flows and flow fields. In: Sigurdson, H. (Editor-in-chief), Encyclopedia of volcanoes. Academic Press, Elsevier, 291-305.

Lescinsky, D.T., Merle, O., 2005. Extensional and compressional strain in lava flows and the formation of fractures in surface crust. Geological Society of America, special Paper 396: Kinematics and dynamics of lava flows: Vol. 396, pp. 163–179

Linneman, S.R., Borgia, A., 1993. "The Blocky Andesitic Lava Flows of Arenal Volcano, Costa Rica" in Kilburn, C. and Luongo, G. (eds), Active Lavas, UCL Press, pp 25-72.

Lo Bello, P., 1988. Géochronologie par la méthode 39Ar-40Ar de ponces quaternaries contaminées – Exemple des ponces du Mont Dore (MCF). Utilisation d'un laser continu pour la datation des minéraux individuels. Thèse 3ème cycle, Univ. Clermont Ferrand II, 180 pp.

Ly, M.H., 1982. Le plateau de Perrier et la Limagne du Sud : Etudes volcanologiques et chronologiques des produits montdoriens(Massif Central Français). PhD, Clermont Ferrand Univ., 180pp.

MacDonald, G.A., 1953. Pāhoehoe, ʻaʻā and block lava. Am. J. Sci. 251, 169-191.

Manley, C.R., Fink, J.H., 1987. Internal textures of rhyolite flows as revealed by research drilling. Geology 15, 549-552.

Martin, U., Németh, K., 2007. Blocky versus fluidal peperite textures developed in volcanic conduits, vents and crater lakes of phreatomagmatic volcanoes in Mio/Pliocene volcanic fields of Western Hungary. J. Volcanol. Geotherm. Res. 159, 164-178.

Noé, J., 2007. La mise en place de la coulee de Chateaugay (Puy de Dôme). Rapport de TER de Licence 3. USTL, Univ. Lille1. 22pp.

Pastre, J.F., 2002. The Plio-Quaternary fluvial deposits of the Allier & Loire basin. Field excursion September 12-14th, Fluvial Archives Group biennial meeting.

Pégère, G., 2004. Les péridots de Perrier. Le Cahier des Micromonteurs, 83: 21-23.

Peterson, D.W., Tilling, R.T., 1980. Transition of basaltic lava from pāhoehoe to ‘a‘ā, Kilauea volcano, Hawaii; field observations and key factors. J. Volcanol. Geoth. Res. 7, 271-293.

Petry, K., Jerram, D.A., de Almeida, D del P. M., Zerfass, H. Volcanic-sedimentary features in the Serra Geral Fm., Paranà Basin, southern Brazil,: Examples of dynamic lava-sediment interactions in an arid setting. J. Volcanol. Geoth. Res. 159, 313-325.

Poidevin, J.L., Cantagrel, J.M., G.U.E.R.P.A., 1984. Un site unique du Plio-Pleistocène en Europe: Le plateau de Perrier (Puy de Dôme). Revue Sc. Nat. D’Auvergne, 50, 87-95.

Polacci, M., Cashman, K.V., Kauahikaua, J., 1999. Textural characterization of the pāhoehoe-‘a‘ā transition in Hawaiian basalt. Bull. Volcanol. 60, 595-609.

Rowland, S.K., Walker, G.P.L., 1987. Toothpaste lava: Characteristics and origin of a lava structural type between pāhoehoe and ‘a‘ā. Bull. Volcanol. 49, 631-641.

Schminke, H.U., 1967. Fused tuff and peperites in south-central Washington. Geol. Soc. Am. Bull. 78, 319-330.

Scrope, G.P., 1827. Memoir of the Geology of Central France; Including the Volcanic Formations of Auvergne, the Velay and the Vivarais. Longman, Rees, Orme, Brown and Green, London, pp 79.

Self, S., Keszthelyi, L., Thordarson, Th., 1998. The importance of pāhoehoe. Annu. Rev. Planet. Sci. 26, 81-110.

Skilling, I.P., 1998. Mechanisms of globular peperite formation at Welgesien, Eastern Cape Province, South Africa. IAVCEI Int. Volcanol. Congress, Cape Town, Astracts p.56.

Skilling, I.P., White, J.D.L., McPhie, J., 2002. Peperite: a review of magma-sediment mingling. J. Volcanol. Geotherm. Res., 114, 1-17.

Smith, J.V., 1996. Ductile-brittle transition structures in the basal shear zone of a rhyolite lava flow, easter Australia. J. Volcanol. Geoth. Res. 72, 217-223.

Soule, S.A., Cashman, K.V., 2005. Shear rate dependence of the pāhoehoe-to-'a'ā transition : Analog experiments. Geol. Soc. of Am. 33, 361-364.

Thonat, A., 1969. Les basanites noires de l'Est du Cézallier et la fossilisation de l'ancien réseau hydrographique de l'Allagnon. Revue des Sc. Nat. D'Auvergne, 35, fasc 1-2-3-4.

Vidal, N., de Goër de Herve, A., Camus, G., 1996. Déstabilisation de reliefs d"érosion en terrain volcanique : exemples pris dans le Massif Central Français. Quaternaire, 7, 117-127.

Waichel, B.L., de Lima, E.F., Sommer, C.A., Lubachesky, R., 2007. Peperite formed by lava flows over sediments : An example from the central Paranà Continental Flood Basalts, Brazil. J. Volcanol. Geotherm. Res. 159, 343-354.

Waichel, B.L., Scherer, C.M.S., Frank, H.T., 2008. Basaltic lava flows covering active eolian dunes in the Paranà Basin in southern Brazil: Features and emplacement aspects. J. Volcanol. Geotherm. Res. In press.

White, J.D.L., 1996. Impure coolants nad interaction dynamics of phreatomagmatic eruptions. J. Volcanol. Geotherm. Res. 74, 155-170.

White, J.D.L., McPhie, J., Skilling, I.P., 2000. Peperite: a useful genetic term. Bull. Volcanol. 62, 65-66.

Wohletz, K.H., 1983. Mechanisms of hydrovolcanic pyroclast formation: grain size, scanning electron microscopy and experimental results. J. Volcanol. Geotherm. Res. 17, 31-63.

Wohletz, K., Heiken, G., 1992. Volcanology and geothermal energy. University of California Press, Berkeley, Los Angeles, Oxford. 432pp.

Zimanowski, B., Büttner, R., Lorenz, V., 1997. Premixing of magma and water in MFCI experiments. Bull. Volcanol. 58, 491-495.

Chapter 3:

Anisotropy of Magnetic Susceptibility (AMS) in Lava Flows

INTRODUCTION

The Anisotropy of Magnetic susceptibility is a widespread tool used in volcanic, plutonic, metamorphic, sedimentary rocks to understand strain related to emplacement and formation.
The interpretation of AMS will be different according the type of rock. Concerning volcanic rocks, and in particular with basaltic and trachybasaltic compositions, the AMS fabric is dominantly carried by ferromagnetic mineral phases such as magnetite, titanomagnetite, maghemite and hematite. Their presence will define the AMS ellipsoid characterization and will dominate the influence of diamagnetic or paramagnetic mineral phases.
The use of AMS is attractive as it can be quickly analyzed and samples are easily prepared, but interpretation of data is not so evident. Supplementary work is needed to fully characterize the AMS carriers and to determine when the AMS fabric is acquired so as to make valid, well-constrained interpretations. That is the reason why, as a first step, we will propose a methodology for using AMS in lavas based on AMS fabric identification. This includes determining the magnetic state of carriers (by using FORC diagrams) and AMS ellipsoid comparison with the microlite textures known to form during lava cooling.
After describing this methodology and the tools used, we will apply it to two lava flows from the Chaîne des Puys: the Royat F2 and F3 lava flows. We will extract data according to this methodology and use the information to reconstruct the kinematic and deformation history of these 45,000 years old flows. This will allow me to investigate their emplacement dynamics.

3.1. A METHODOLOGY FOR USING AMS IN LAVAS

3.1.1. Introduction

Lava flows are complex liquid-solid fluids with strong viscosity variations that cause complex emplacement scenarios (e.g. Self & al., 1998; Hon & al., 2003). Most studies consider lava flows as being relatively homogeneous during emplacement. Here, we look at the flow complexities in a valley-channelled lava flow near its front. The main tool used in this study is the Anisotropy of Magnetic Susceptibility (AMS), backed up by detailed mapping and structural analysis.

3.1.1.1: AMS definition

Magnetic susceptibility is simply the proportionality constant between the applied and induced magnetic field in a substance. The total susceptibility reflects the contribution of all phases within the material, i.e., ferromagnetic (s.l.), paramagnetic, and diamagnetic mineral phases. Theoretically, as long as the applied field is low, a linear relationship exists between H and M. The induced magnetization and the external magnetic field are linearly related, and so magnetic susceptibility can be defined by the ratio M/H. Both M and H are expressed in the same units (A/m in SI) and so magnetic susceptibility is a dimensionless quantity.
Ferromagnets and paramagnets align in the direction of the applied magnetic field (H), while diamagnets align opposite to H. Anisotropy of magnetic susceptibility results from the volume distribution of ALL the magnetic phases within the material (e.g., diamagnetic, quartz; paramagnetic, Fe-Mg silicates; ferromagnetic, Fe-Ti oxides) and thus, the alignment of the atomic moments of ALL phases within the sample (e.g., magnetite, shape anisotropy dominates while hematite crystalline anisotropy dominates), while volume percent of the various phases controls the magnitude of the bulk susceptibility (Tarling & Hrouda, 1993).
An anisotropy of magnetic susceptibility (AMS) measurement of one rock specimen results in an ellipsoid of magnetic susceptibility (k) defined by the length and orientation of its three

principal axes, $k_{max} > k_{int} > k_{min}$, which are the three eigenvectors of the susceptibility tensor (Tarling and Hrouda 1993). The long axis of the magnetic susceptibility ellipsoid k_{max} defines the magnetic lineation, while the short axis, k_{min}, defines the normal to the plane of the magnetic foliation.

3.1.1.2: Precautions to be taken when using AMS

The AMS-tensor is easily obtained and is linked through foliation to the emplacement history of all types of rock (e.g. Tarling & Hrouda, 1993). As noted by several authors (e.g. Borradaile, 1991; Rochette & al., 1992; Borradaile & Henry, 1997; Rochette & al., 1999), several precautionary steps should be taken when verifying the AMS-fabric crystal fabric link and the origin of AMS. These steps can be divided into two groups based on the questions: what mineral(s) carry the AMS and how/when is the AMS fabric developed? Once answered, the AMS can be confidently used as a petrofabric tool. This, combined with other textural and structural data, can provide evidence of deformation during emplacement. In addition, the steps used to answer the questions can themselves yield information about the lava flow conditions.

3.1.1.3: AMS parameters

In this chapter, we used the following parameters:

-The mean susceptibility: $km = (k_{max} + k_{int} + k_{min})/3$,

-the degree of anisotropy $A = 100 (1 - (k_{min} / 2k_{max}) – (k_{int} / 2k_{max}))$

-and the shape parameter $T = (2 (\ln k_{int} – \ln k_{min}) / (\ln k_{max} – \ln k_{min})) -1$.

If $T < 0$ the ellipsoid would be linear (prolate) and if $T > 0$ it would be planar (oblate).
The degree of anisotropy is a parameter quantifying the departure from the isotropic case. As shown by Cañón-Tapia (1994), the different ways to calculate the degree of anisotropy yield qualitatively equivalent results, differing only in their range of numerical values. In this work, we use the A parameter ranging from 0% (isotropic) to 100% ($k_{max} >> k_{min}$ and k_{int}).

The above formula allows us to have a direct comparison with results from another lava flow where a vertical profile was also performed (Cañón-Tapia & Coe, 2002).

3.1.2: AMS-Fabric relationship method in AMS interpretation methodology

3.1.2.1: AMS carrier determination

The first step in interpreting the nature of the AMS fabric is by fully documenting the magnetic mineral phases within the samples. Curie Temperature estimates provide a useful indicator of the magnetic phase or phases present within the rock (e.g. Cañón-Tapia, 2004; Hrouda & al., 2005; Bascou & al., 2005). Thin sections are also required to verify the main AMS carrier, define its shape, aspect ratio, concentration and the relationship with the other minerals. Chemical analyses of the main AMS carriers are done to check agreement with the Curie Temperature. Finally, establishing the domain state of the magnetic carrier provides important constraints on the reliability of the AMS fabric as a flow indicator, since SD-magnetite (single domain) have a reversed magnetic fabric, where k_{min} is parallel to the fabric and k_{max} perpendicular, while in MD (multi-domain) grains k_{max} lies within the fabric (Rochette & al., 1992 ; Rochette & al., 1999; Bascou & al., 2005; DeFrates & al., 2006).

3.1.2.2: AMS fabric-crystal fabric relationship determination

Once the main AMS carriers are known, the next step is to find out when and how the AMS fabric was acquired. Thin section examination and interpretation of shape preferred orientation (SPO) of each mineral phase will show when the growth of the AMS minerals occurred with respect to the other phases. In lava flows, during cooling, a well-developed microlite fabric generally forms, and this fabric is best compared with the AMS fabric (e.g. Cañón-Tapia & Castro, 2004; Bascou & al., 2005; Nkono & al., in press). This confirms the assumption that the silicate template controls the AMS fabric (Hrouda & al., 1971; Hargraves & al., 1991).

3.1.3: First Order Reversal Curve (FORC) interest

3.1.3.1: The magnetic domain theory

3.1.3.1.1: Magnetic domain definition and evidence

Ferromagnetic minerals (e.g. magnetite and hematite) display a spontaneous magnetization, but this magnetization would be modified if a magnetic field is applied, even if of very low intensity. This modification can be explained as the mineral is composed of areas called magnetic domains or Weiss domains in which the internal magnetization is saturated (Ms) but not necessarily with reference the external magnetic field. Such domains are on the order of micrometers to several hundred of micrometers but are greater than the atomic distance (e.g. Dunlop & Özdemir, 1997).

Magnetic domains can be visible according the Bitter technique (Bitter, 1932) by applying on the polished mineral a thin colloidal magnetite particle suspension with extremely reduced dimensions (<< 1 μm) (fig. 3.1.1).

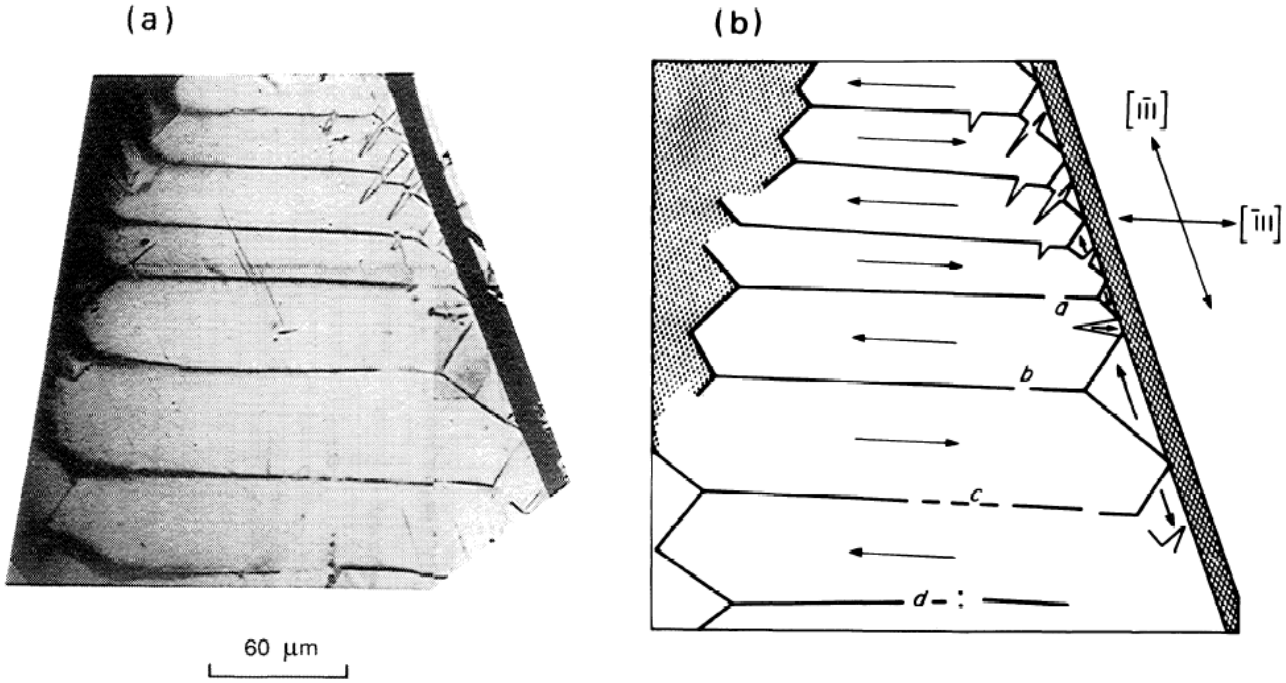

Figure 3.1.1: a. Magnetic domains observed on a magnetite crystal polished section {110}. **b.** Sketch of a. with inferred Ms directions in each domain. Domain walls between domains are emphasized according the Bitter (1932) technique. (*from* Özdemir & Dunlop, 1993).

3.1.3.1.2: Hysteresis curves

Under an increasing external magnetic field H, domains with magnetic orientation that are the same as the external field tend to increase at the expense of neighbour domains having a

different magnetic sense. For a sufficient applied field, all the magnetic moments are parallel to each other and magnetic saturation (Ms) is reached. During the decrease of the external field domains will not go back to the totally disordered arrangement, and when the field is removed, a residual magnetization remains (Mr). This is weaker than Ms. To offset this Mr magnetization (to return to the totally disordered state), an external field opposite to the initial external field should be applied, such a field is called a coercive field (Hc). If regularly varying the external field H between two values, positive and negative, we will obtain a closed magnetization curve, called hysteresis curve (fig. 3.1.2) (e.g. Mayergoyz, 1986).

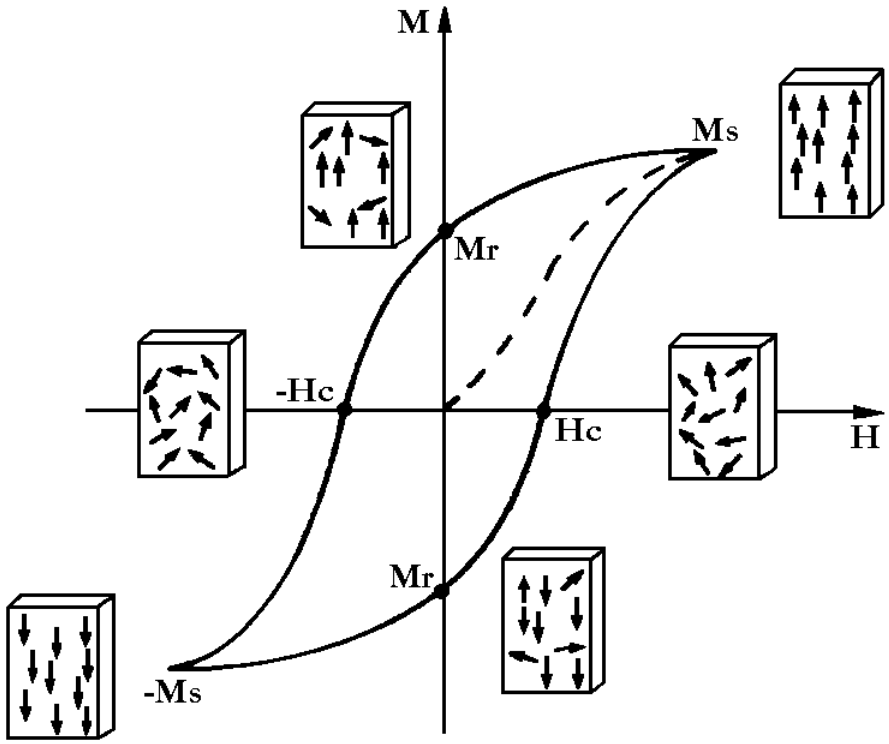

Figure 3.1.2: Ferromagnetic hysteresis curve showing the evolution of magnetization M with the external field H. Arrows correspond to magnetic domain orientation. Ms = saturation magnetization, Mr = remanant magnetization and Hc = coercive force or coercitivity of remanence.

3.1.3.1.3: Domain formation

Consider a crystal that is uniformly magnetized and having only one magnetic domain (Single Domain = SD). Surficial charges will be formed at the extremities or poles according magnetization and will have themselves a secondary magnetic field (demagnetization field). The energy associated with the surficial charge distribution is called magnetostatic energy.

This magnetostatic energy can be divided into two parts if the magnetization is shared in two magnetized domains (Multi Domain = MD) with two opposite directions. Thus, positive and negative charges will coexist, decreasing the spatial extension of the demagnetization field (fig. 3.1.3). This division in several domains (MD) can not indefinitely continue because the boundary between two domains (called a domain wall) requires energy to be produced and remained stable. Finally, an equilibrium in the number of magnetic domains will be reached for a given grain size (fig. 3.1.4).

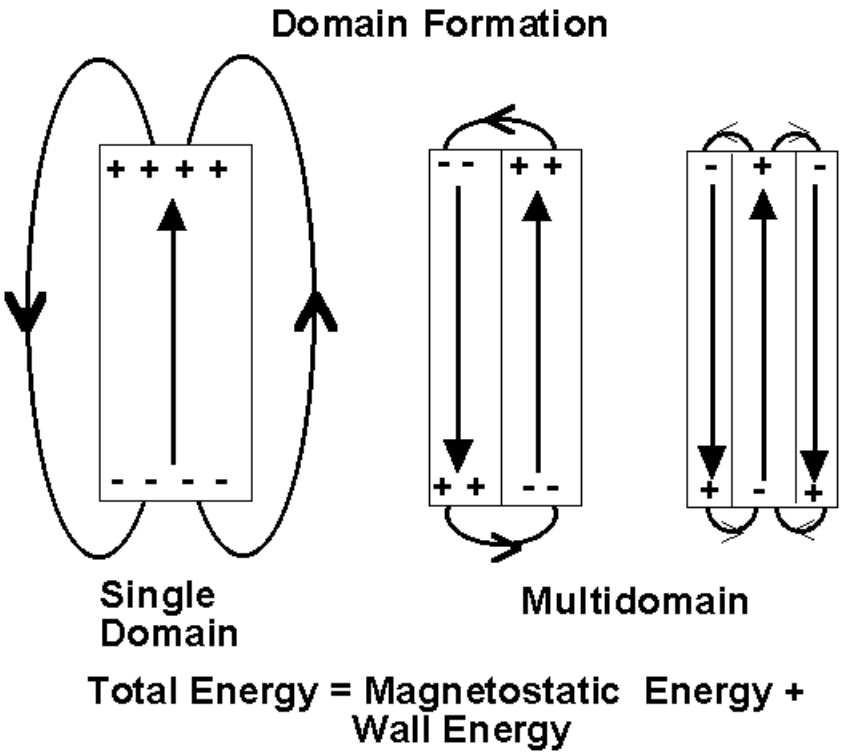

Figure 3.1.3: Formation of magnetic domains (IRM Minnesota).

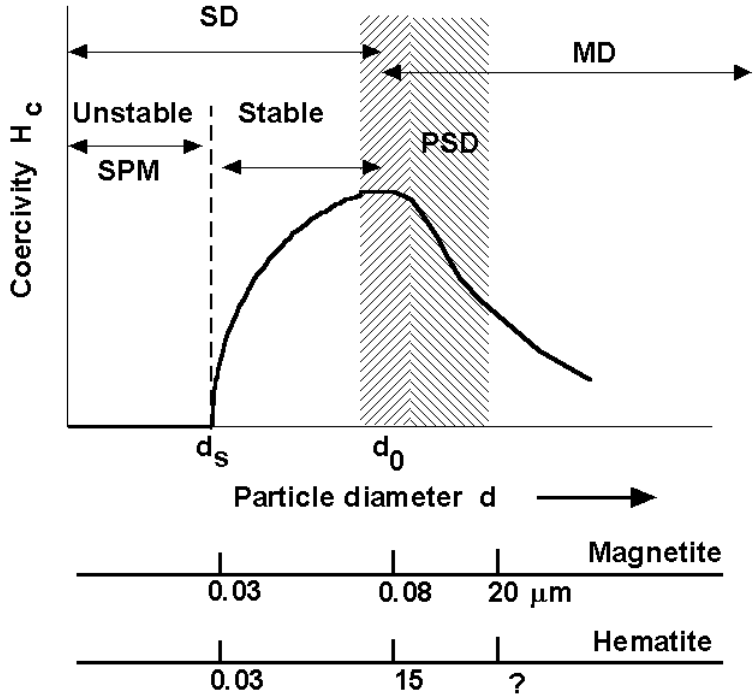

Figure 3.1.4: Evolution of the cœrcitive force Hc within magnetite and hematite grain size allowing the definition of different magnetic behaviours : super paramagnetic (SP), single domain (SD), pseudo single domain (PSD) and multi domain (MD).(IRM Minnesota).

Inspection of the figure 3.1.4 reveals that for a given magnetite or hematite grain size, an energy decrease will promote the establishment of one (SD) or several (MD) magnetic domains.

The distinction between SD and MD is evident on hysteresis curves as they do not have the same magnetic domain number (fig. 3.1.5).

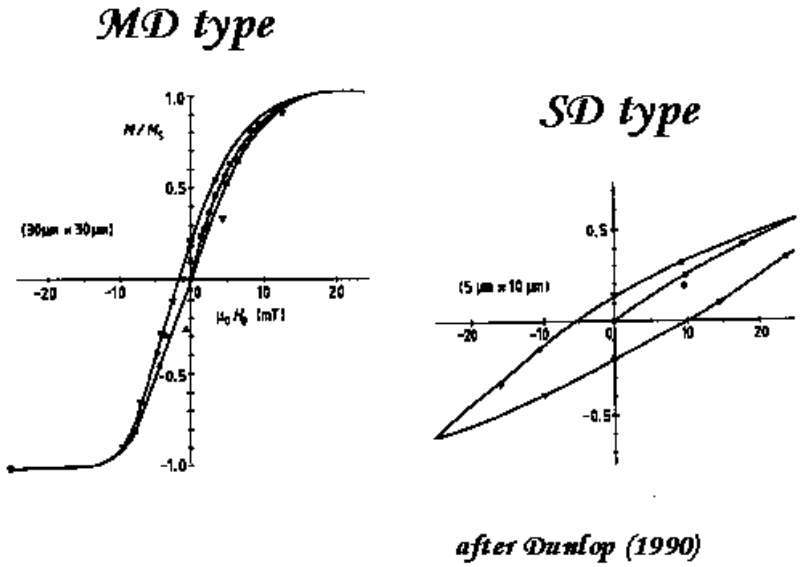

Figure 3.1.5: Examples of two hysteresis loops typical of a SD and a MD grain.

When the grain size decreases, a critical size will be reached when the grain will not be enough big to accommodate the presence of a domain wall. Under this critical size, the grain will contain only one domain (SD). A SD grain is homogenously magnetized to its saturation magnetization (Ms).

Change of the MD grain magnetization occurs during a wall translation, which is an energetically easy process and can be accomplished under relatively low external fields. Thus, a MD grain will display low coercitive values (Hc) (fig. 3.1.5). In contrast, the only way to change the SD grain magnetization is to turn the magnetization, an energetically expensive process and thus difficult. Thus, a SD grain will display a high coercitivity (Hc) (fig. 3.1.5).

The distinction between SD and MD is by this way evident. Nevertheless, small MD grains display a mixing between a SD (strong remanence) and MD (low coercitvity) and are called pseudo single domain (PSD) (fig. 3.1.4) (Dunlop, 1986).

Finally, the smallest magnetite or hematite grains display an unstable magnetization, i.e. a magnetization varying with the frequency of the external field, such grains are called super paramagnetic (SPM) (fig. 3.1.4) (Tauxe & al., 1996).

3.1.3.2: Magnetic domain state characterization

Before the development of FORCs (see 3.1.2.3), the way to characterize the magnetic domain state of a sample was its location on a Day diagram (Day, 1977). It simply consists on plotting a point in a Mr/Ms versus Hcr/Hc diagram (Hcr is for the coercitive remanence).

As previously noted by Pawse & al. (1996) and Tauxe & al. (1996), such a diagram reflects the average of the whole magnetic grain population. Thus, if we have a mixture of different magnetic populations, the point on the Day plot will be simply an average of the grains and not necessarily reflect the grains present (e.g. a mixing of both SD and MD signatures could give a PSD signature).

This can be considered as of a low degree of interest, but the presence of SD particles is important as it will tend to alter the normal AMS fabric, because of their reverse magnetic contribution (Rochette & al., 1992 ; Rochette & al., 1999). So, a good AMS data interpretation requires a check for the possibility of encountering SD magnetites. This is the reason why we are not satisfied in using Day plot only (Day, 1977), but use another tool: FORC.

3.1.3.3: FORC definition

FORC is an acronym for First Order Reversal Curves. The use of these curves and their relative diagrams has been started by Pike & al. (1999) and Roberts & al. (2000).
A FORC diagram is calculated from a set of partial hysteresis curves (see Mayergoyz, 1986). The measurement of a FORC starts with the saturation of the sample in a high positive field. The field is afterwards decreased to the reversed field Ha, and the FORC is the magnetization curve measured from Ha back to saturation. A set of FORCs is obtained by repeating this measurement for different values of Ha. At the applied field Hb on a FORC starting from Ha the magnetization is denoted as M(Ha, Hb), where Hb >Ha. The FORC distribution ρ(Ha, Hb) is then defined as the mixed second derivative:

$$\rho(Ha, Hb) \equiv -\partial^2 M(Ha, Hb) / \partial Ha\, \partial Hb \quad (1)$$

where ρ(Ha, Hb) is defined for Hb >Ha. It became convenient for plotting the FORC distribution to use the coordinate system {Hc = (Hb - Ha)/2, Hu = (Ha + Hb)/2} instead of the original {Ha, Hb}. As Hb >Ha, Hc > 0, and the FORC diagram is plotted as a contour plot in the right-hand half plane with Hu and Hc as the vertical and horizontal axis, respectively. The Hc coordinate is referred to microcoercivity. Further details about the derivation of eq. (1), the change of the coordinates and basic interpretation of the resulting FORC-diagram details can be found in Pike et al. (1999).

3.1.3.4: A comparison between the Day plot and FORC diagram

In order to have a concrete comparison between insights provided by the Day plot and FORC diagram a set of 4 samples from four different locations have been analyzed on the Micro Vibrating Sample Magnetometer of the CEREGE, Institute, Aix en Provence, France. This allows us to obtain Mr, Ms, Hc and Hcr data, as FORC diagrams for 100 hysteresis loop integrations.
Samples come from the Royat lava flows (F2, F3 and F4) (see a general description of these flows in 2.1.4.1 and on fig. 2.1.3) and from the chilled rim of pillow lava in the Prady lava flow (fig. 3.1.6). The Prady lava flow is, according its relief inversion, linked to the Limagne volcanism and it forms the plateau of Creste village, 20 km west of the Issoire. The Prady lava flow (PL) is basaltic in composition and flowed from west-to-east. At its eastern termination the lava spilled into a maar-lake, and produced pillow lavas (fig. 3.1.6). We have chosen to sample the pillow lava, because it is likely to contain the finest magnetite size population.

Figure 3.1.6: Examples of pillow lavas from the Prady lava flow (PL). Hammer for scale.

The magnetic parameters needed for a Day plot are provided on Table 3.1.1. and the Day plot is displayed on fig. 3.1.7.

	Mr (μAm²)	Ms (μAm²)	Hcr (mT)	Hc (mT)	Mr/Ms	Hcr/Hc
F2	55,07	366,4	10,49	4,306	0,1503	2,43613562
F3	59,37	473,9	10,82	4,229	0,1253	2,55852447
F3FDA	32,03	209,2	13,80	4,886	0,1531	2,82439623
F4	163,30	949,5	29,25	13,380	0,1720	2,18609865
PL	33,10	50,81	79,75	56,050	0,6514	1,42283675

Table 3.1.1: Magnetic parameters required for a Day plot (1977).

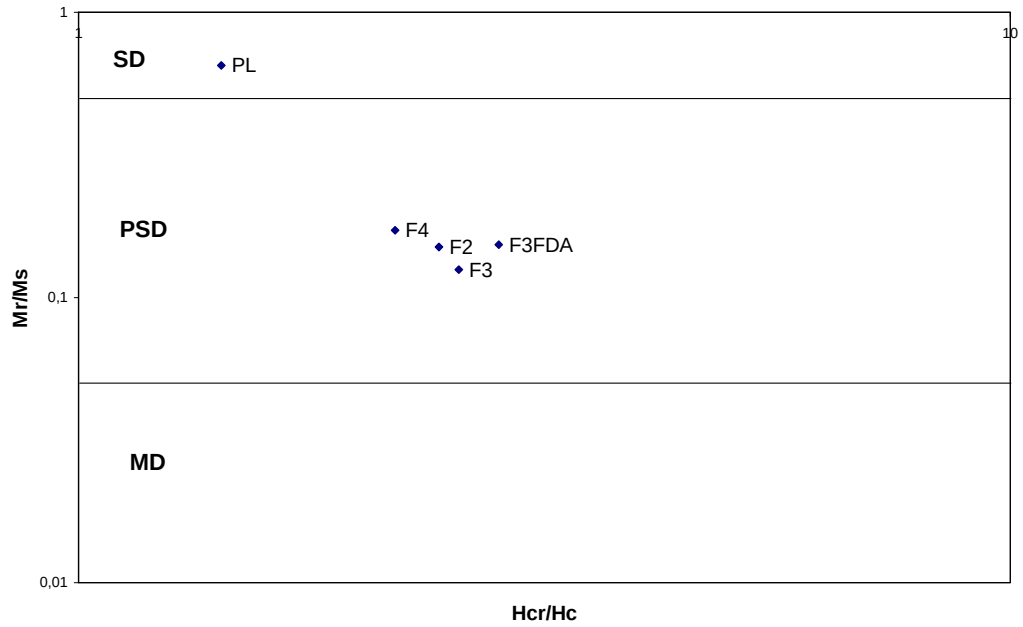

Figure 3.1.7: Day plot (Day, 1977) displaying the location of each lava sample. Field delimitation is from Dunlop (1986) and DeFrates & al. (2006).

All samples from the Royat flows are in the PSD field the Prady pillow lava plot in the SD field (see fig. 3.1.7).

FORC diagrams for these samples are provided in fig. 3.1.8., their interpretation is possible mostly due to the works of Pike & al. (1999), Roberts & al. (2000). A general summary of morphology interpretation is then given:

- convergence of the inner contours around a central peak indicates the absence of SD particles
- contours diverging away from the origin are interpreted as a manifestation of MD particles
- asymmetry of the inner contours around a central peak, indicating a small amount of PSD particles

Thus, applying these observations to our studied samples, we argue that F2, F3 and F4 display an evident MD population with varying traces of PSD (varying dissymmetric diagrams). Prady (PL), in contrast, clearly presents the SD signature.

A concordance between FORC and Day plots is observed for PL but this is not the case for F2, F3 and F4. In fact, FORC diagrams indicate abundance of MD and the presence of PSD, whereas the Day's diagram reveals only the presence of PSD. Thus, this example of the Day plot confirms its summing up effect, which reduces the ability to discriminate the magnetic grain size, while the FORC diagrams do distinguish all types.

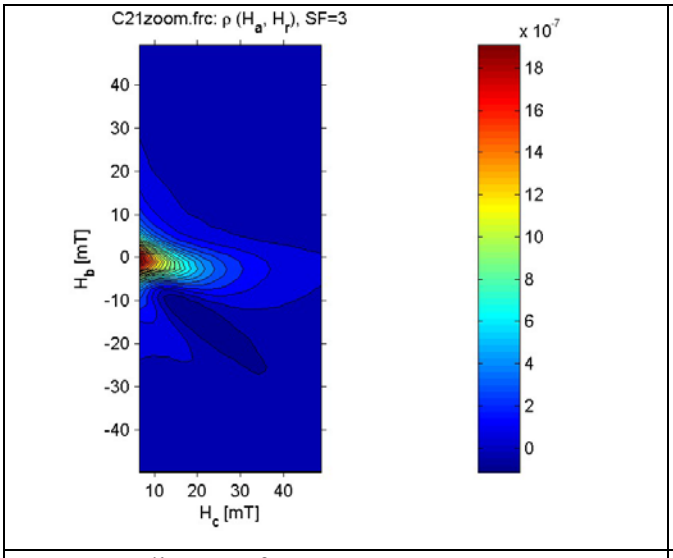

a. FORC diagram from F2

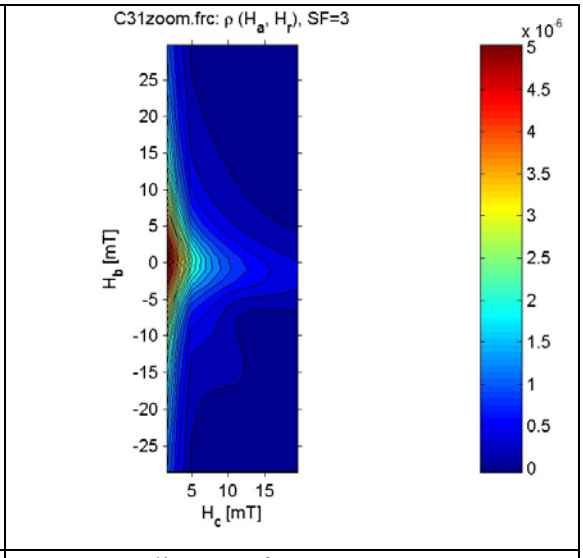

b. FORC diagram from F3

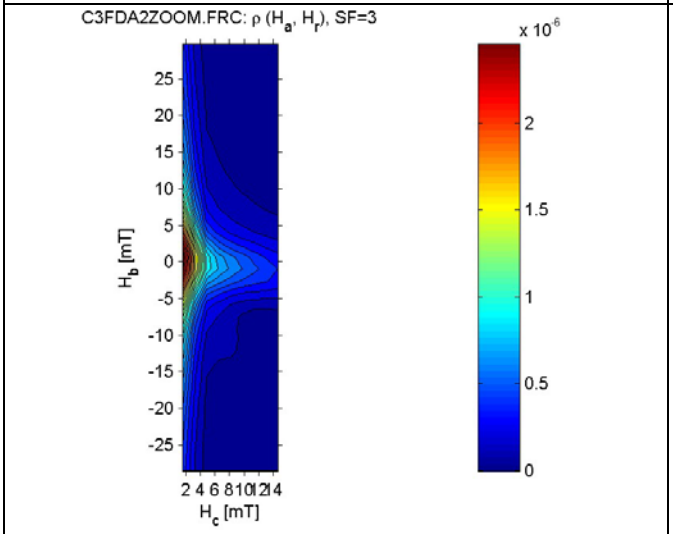

c. FORC diagram from F3FDA

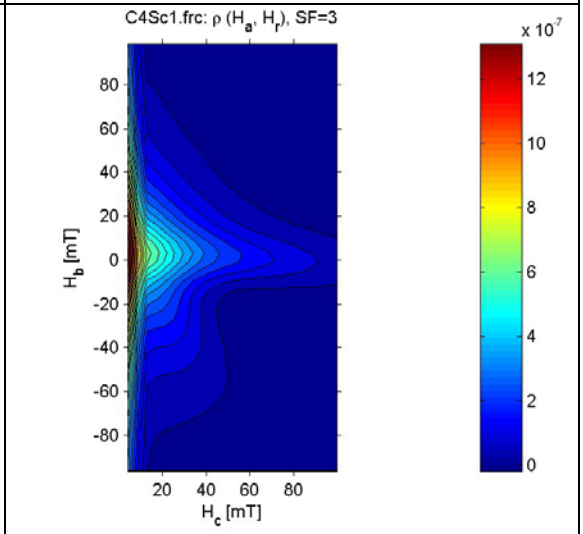

d. FORC diagram from F4

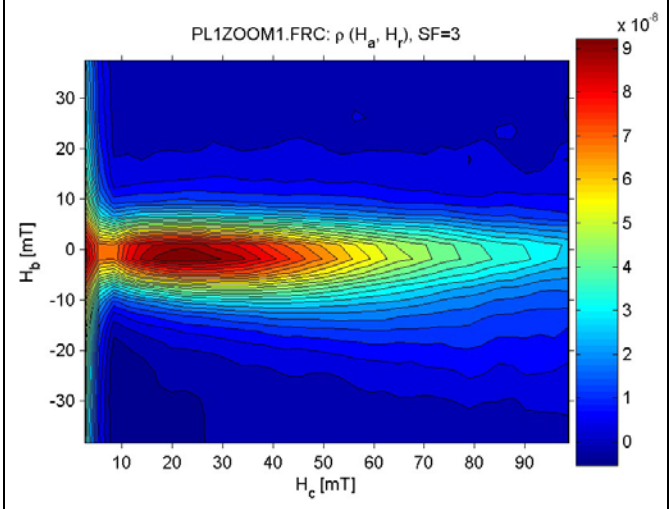

e. FORC diagram from PL

Figure 3.1.8: FORC diagrams obtained for each sample from the Royat lava flows (F2, F3 and F4) and the Prady pillowed lava (PL).

3.1.3.5: A FORC profile in a lava flow: example of the Royat F2 flow

As noted in 3.1.2.1, SD-magnetites (single domain) have a reverse magnetic fabric, where k_{min} and k_{max} are perpendicular, while MD (multi domain) have k_{max} parallel to the fabric (Rochette & al., 1992 ; Rochette & al., 1999) (e.g. Bascou & al., 2005; DeFrates & al., 2006). The presence of SD, therefore will lower and bias the AMS fabric and its ellipsoid orientation. We have also underlined in 3.1.3.4, the fact that the best manner to determine the presence of SD is the use of FORC diagrams. In this section, we discuss the sampling methodology to perform in a lava flow section to have a representative FORC information of the whole flow (since FORC analysis is time and money consuming). For this we have made a sample collection for FORC measurements on a vertical profile of the Royat F2 flow (see information about this flow in 3.2.1). The vertical sampling was performed in 6 locations (A, C, F, M, Q & U) and the relative FORC diagrams are provided in fig. 3.1.9.

The results obtained display a relative homogeneous pattern for each FORC diagram along the flow. In fact, we observe contours diverging away from the origin, which is classically interpreted as a manifestation of MD particles (Roberts & al., 2000). Furthermore, the slight asymmetry of the inner contours around a central peak indicates a small amount of PSD particles (e.g. Bascou & al., 2005). So we have on this flow (see 3.2) a persistence of the MD signature with a few PSDs, but no SD evidence and thus no likelihood of a biased AMS fabric.

It is probable, even if not observed in this study, that a sampling at the extreme flow base and the flow top, where magnetites are quenched and thus of small size, that the FORC signature will be different than the major inner part of the flow, with a finer magnetite population and probably some SD occurrences.

Because of the homogenous response of the test lava flow, we suggest the magnetite population is generally homogenous for lavas. Thus for the other lava flows sampled (Royat F3 (3.3. & 3.4.1)), we have analyzed just one sample for one FORC diagram. In these lavas no top or bottom rim has been drilled.

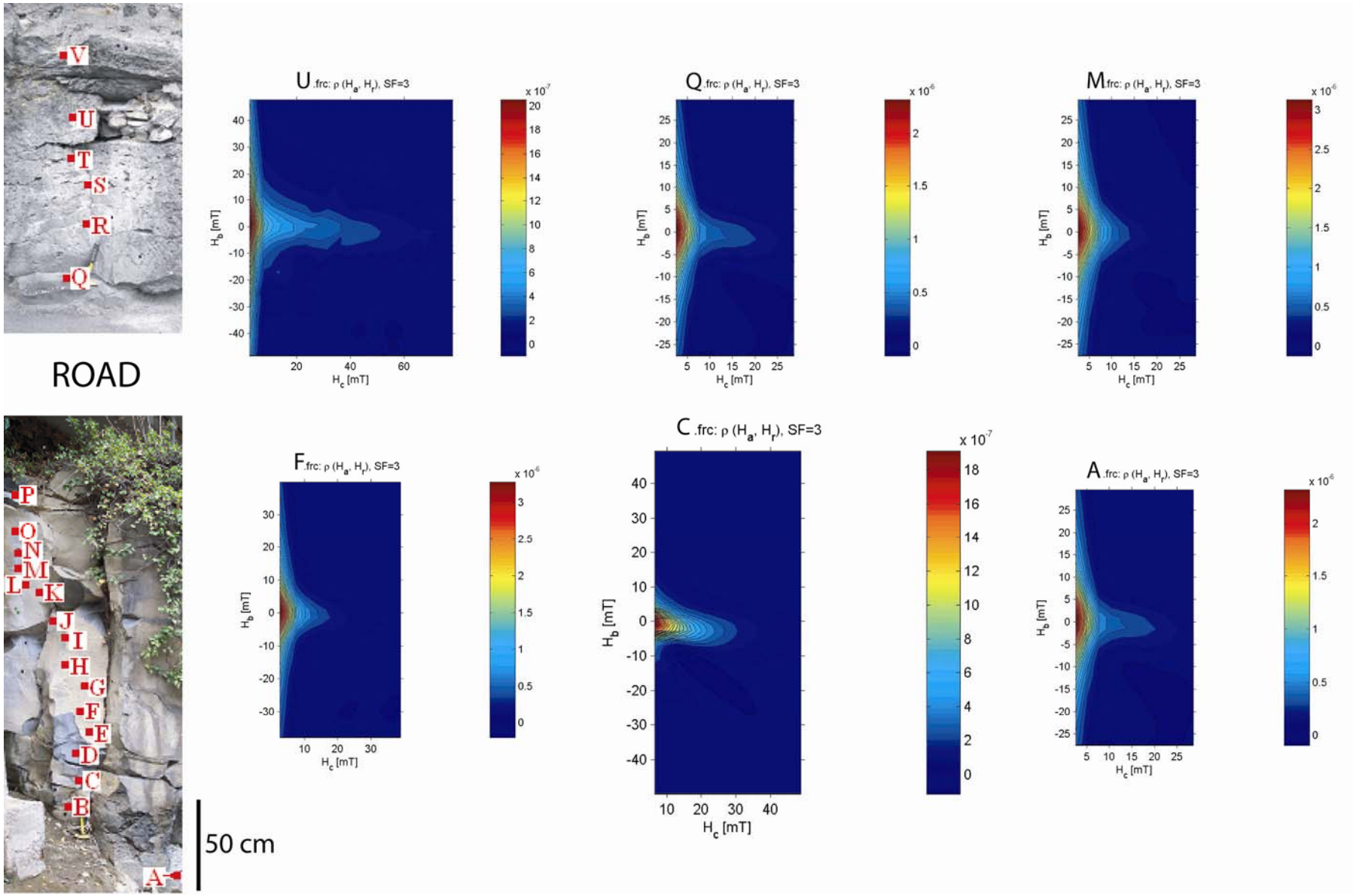

Figure 3.1.9: FORC diagram evolution (samples A, C, F, M, Q & U) on a lava flow section (Royat F2 flow) (see also 3.2)

3.2. APPLICATION OF THE AMS METHODOLOGY TO THE ROYAT F2 FLOW

3.2.1: The Royat F2 flow

The area around the city of Clermont Ferrand has been affected by volcanic activity repeatedly in the Quaternary, as well as receiving tephra falls from the Chaîne de Puys. The town is sited on a maar and volcanic neck (ca. 150,000 years ago). At about 70,000 years ago, there was a major lava flow eruption from the Gravenoire volcano (Goër de Herve & al., 1993; Boivin & al., 2004). At 45,000 years ago four trachybasaltic flows ran down the Tiretaine valley to the city outskirts (Boivin & al., 2005). At about 8,000 years ago, trachy-andesitic flows descended to the north side of Clermont-Ferrand from the Pariou volcano (Boivin & al., 2004) (fig. 3.2.1).

As previously explained in 2.1.4.1, the Tiretaine lava flows are four superimposed lavas (F1, F2, F3 & F4) that have were chanalized into the narrow valley. The first emitted lava flow (called F1) is the longest and the fourth (called F4) is the shortest. These flows have similar trachybasaltic compositions (Boivin & al., 2004). F1, F2 & F4 came from the Petit Puy de Dôme or the Travertin cone whereas F3 came from the Puy de Lacroix (fig. 3.2.1).

The outcrop studied is located close to the end of the F2 lava, which is 6km long (fig. 3.2.1 & 3.2.2a). The main outcrop is 5m high above and below a street in Royat (fig. 3.2.2b & 3.2.9a). The top of the flow is preserved, but the base is not exposed. However, we know we have sampled very close to the outcrop base, as only 10m away, it is seen in the Grotte de Laveuses. (fig. 3.2.3b & 3.2.3e). The base seen in this cave is a platy basal layer about 1 m thick (fig. 3d). This platy layer is observed low in the study outcrop. Thus, the outcrop provides a near complete vertical section of the F2 flow for AMS study.

From mapping, we observe that the lava flow has a general westward flow direction. This direction is confirmed by grooves orientated N065, 18° towards the East, located under a vesiculated roof (fig. 3.2.3a). The lava flow is close to a pāhoehoe, as indicated by the

presence of vertical vesicle pipes (fig. 3.2.3c), vesicle zonation (Table 3.2.3 & fig. 3.2.8j), the limited occurrence of clinker at the base and top (fig. 3.2.3b) and the presence of lateral lobes. Figure 2b sums up F2 characteristics.

Twenty-two samples (cylinder cores of 2.5 cm in diameter and >10 cm long) were drilled using a gasoline-powered drill. They were orientated using both solar and a magnetic compass.

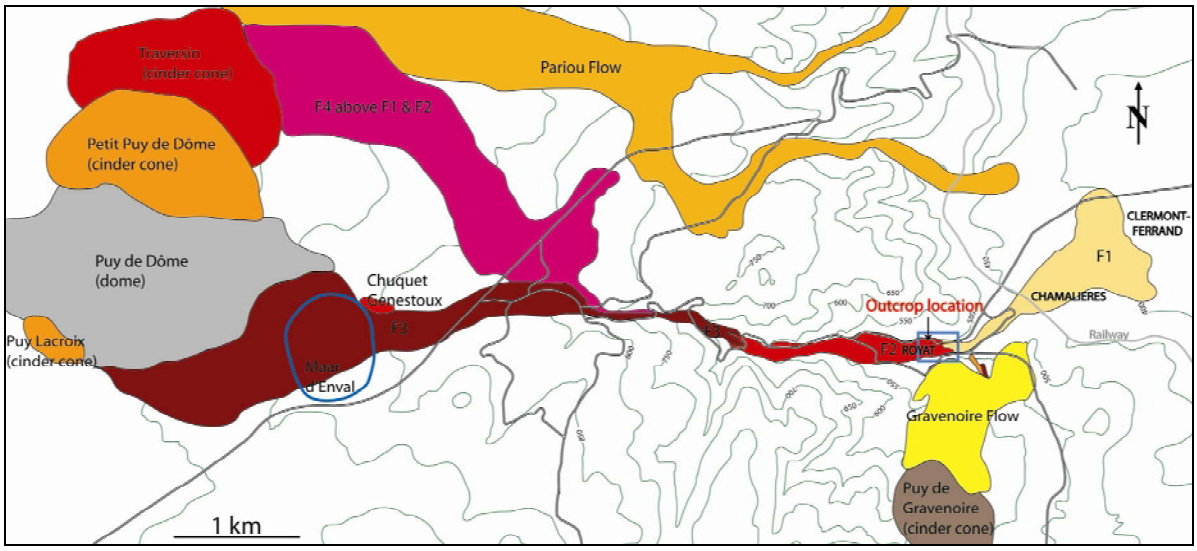

Figure 3.2.1: Map showing the Tiretaine lava flows (F1 to F4) and surrounding lavas, the outcrop location in F2 is indicated by a black arrow. The square shows the close-up map on fig. 3.2.2a.

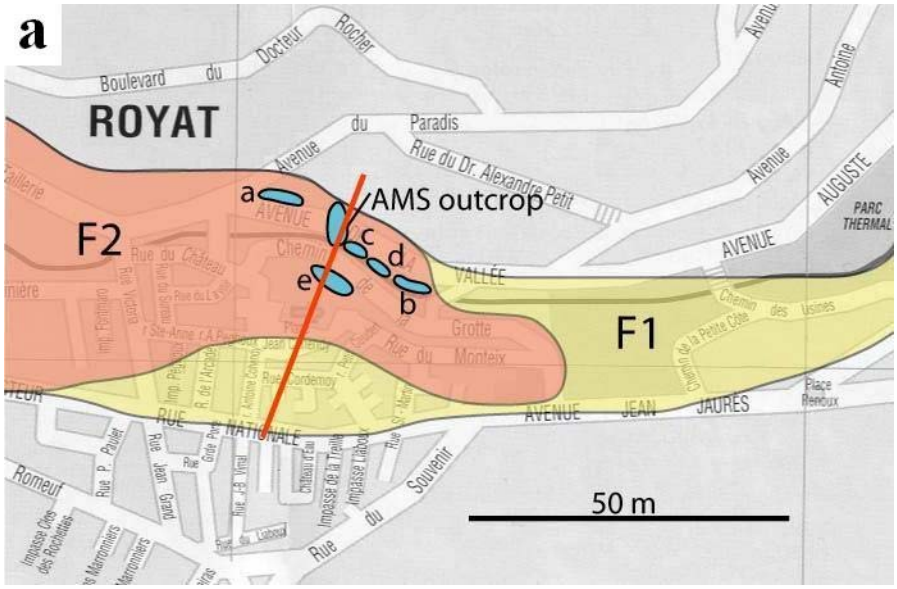

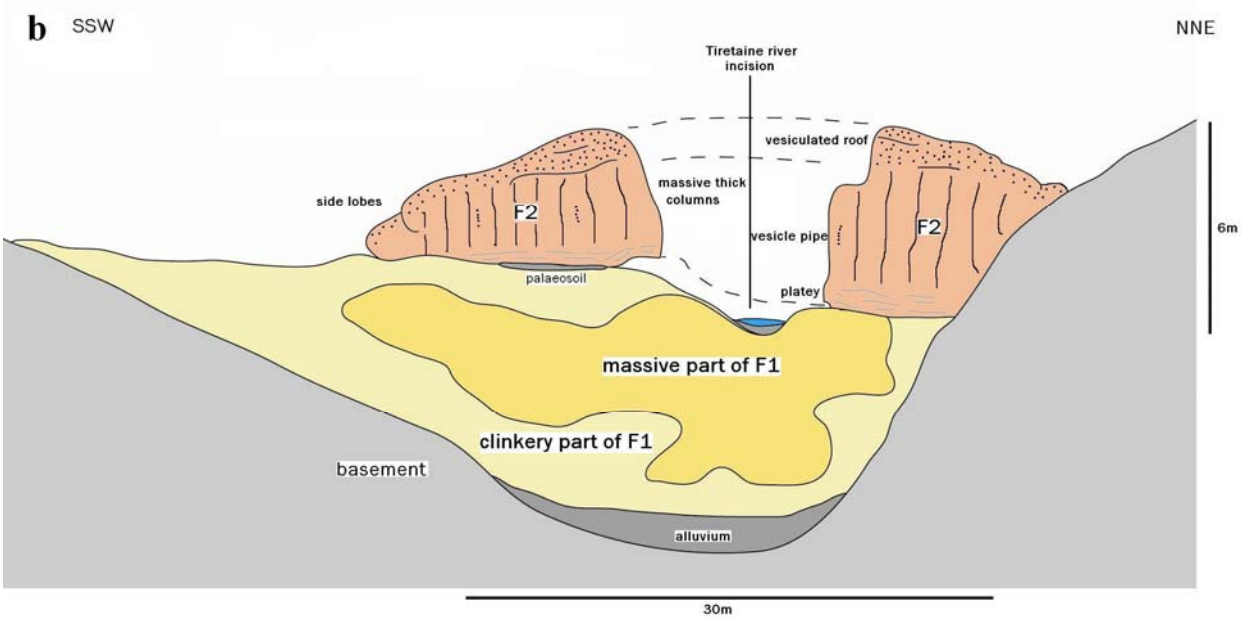

Figure 3.2.2: a. Detailed map showing the studied F2 Tiretaine flow with the main outcrop sampled for AMS and others (a to e) used for textural and structure analysis. Description of these outcrops is provided on fig. 3.2.3. The red bar represents the cross section profile of fig.3.2.2b - **b**. cross section (shown on fig. 3.2.2a) displaying the lava flows F1 and F2, and summarizing structural observations on F2.

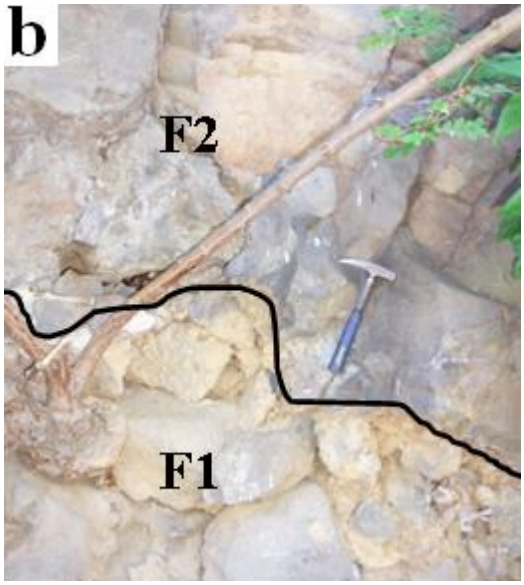

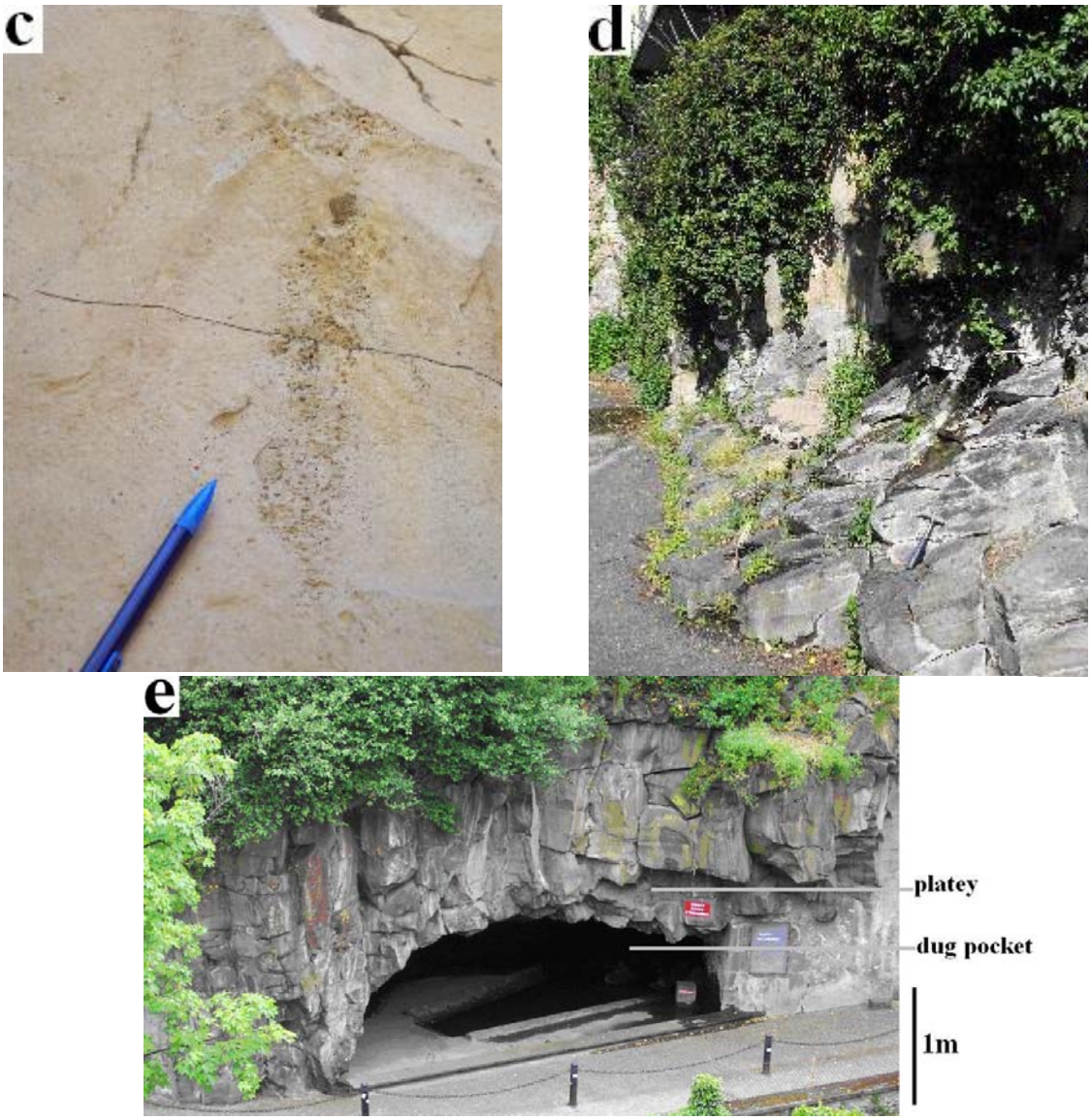

Figure 3.2.3: Outcrops near the main profile, their location is provided on fig. 3.2.2b. a: Grooves under a vesiculated roof with a N065,18°E direction. b: contact displaying the base of F2 with scarce clinker lying over the clinker-rich top of F1. c: a vesicle pipe in F2 indicating a low viscosity interior flow typical of pāhoehoe (e.g. Self & al., 1998). d: the platy zone of F2 close to its base. e: The base of F2 where an F1-clinker pocket has been dug out. Platey zone can be seen above the cave, which wraps around cave, but becomes horizontal just 1 m above roof.

3.2.2: The AMS carriers

3.2.2.1: Curie Temperature

We carried out two measurements from two different samples of continuous thermomagnetic curves (K-T curve) at high temperature using a furnace (CS-3) in an Ar atmosphere coupled to a KLY-4 Kappabridge on cylinder cores from F2. Representative thermomagnetic curves are displayed on fig. 3.2.4a&b.

The thermomagnetic curves are not reversible and are similar to those from Bascou & al. (2005) from the upper and lower part of the Saint Thibéry lava flow (French Massif Central). A rapid decrease in susceptibility occurs between 90°C and 120°C on fig. 4a, but is less constrained on fig. 4b. These Curie Temperatures indicate that the main Fe-Ti oxide phases are Ti-rich titanomagnetites (Nishitani, 1981; Dunlop & Özdemir, 1997). By considering the conventional expression of titanomagnetite ($Fe_{3-x}Ti_xO_4$) with $0 \leq x \leq 1$, microprobe analyses of titanomagnetites give $x \approx 0.7$, which is in good agreement with the observed Curie Temperature (O'Relly, 1984). On continued heating, we note an irreversible slight decrease of susceptibility around 460°C and at 550°C. The interpretation of this is less evident, but like Bascou & al. (2005), we propose that this could indicate the presence of metastable titanomaghemite corresponding to low-temperature oxidation of titanomagnetite. Nevertheless, the main Fe - Ti oxide phase and, by inference the AMS carrier, is titanomagnetite with $x \approx 0,7$.

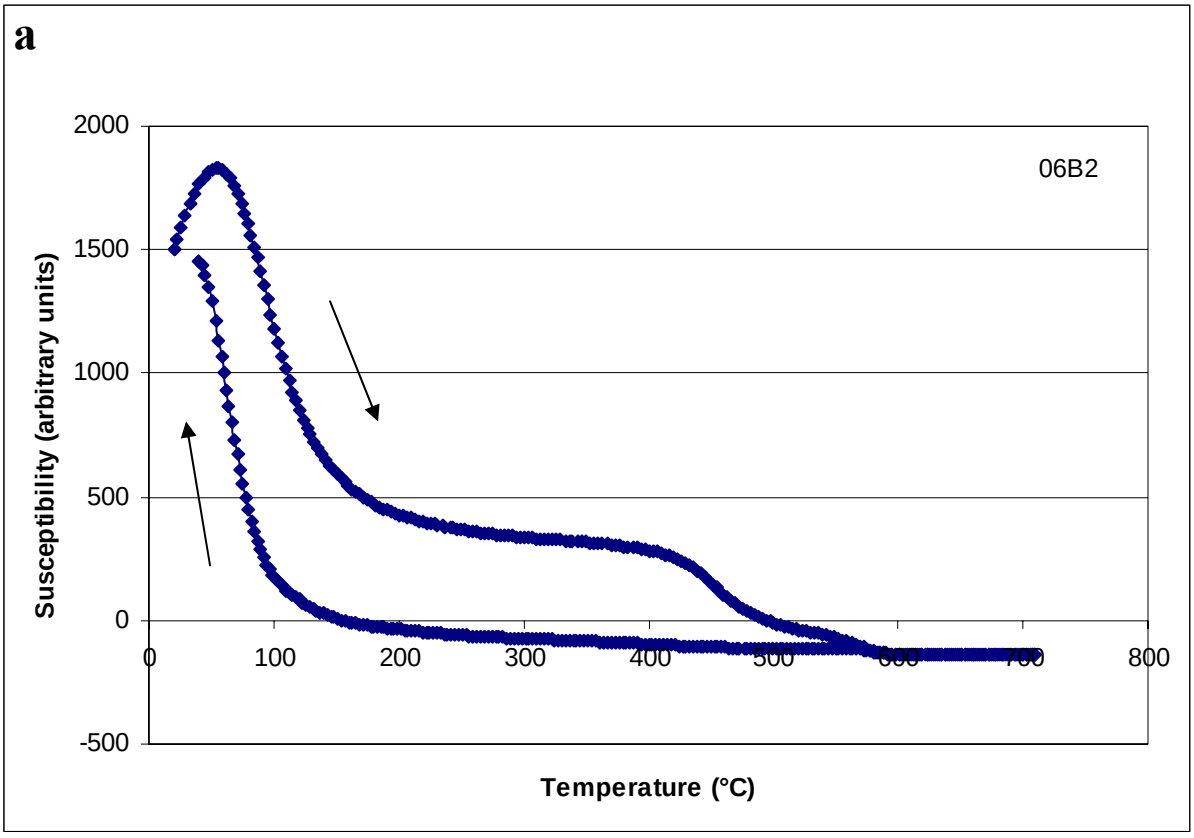

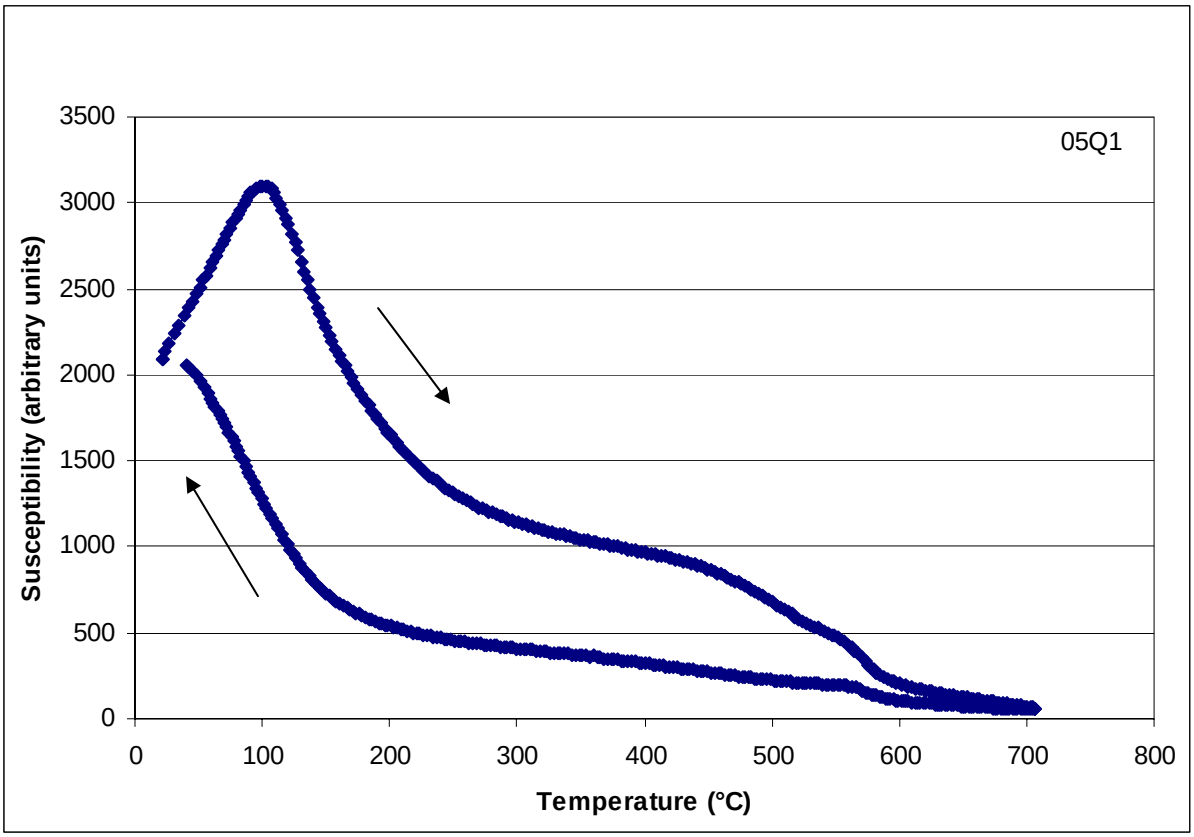

Figure 3.2.4: Representative thermomagnetic curves at high temperature from: **a.** the B site (sample 06B2) and **b.** the Q site (sample 05Q1).

3.2.2.2: Thin section investigation

The SEM image displayed on fig. 3.2.5a is representative of all 35 thin sections studied in F2. It shows a good contrast between white titanomagnetites and the other matrix components. The image shows that the titanomagnetite population is not homogenous. Crystals are often skeletal with a wide size range (from some microns to 100µm) and variable aspect ratio (from 1,2 to 2,7). Microprobe analyses performed on the microphenocrysts gave only titanomagnetite, with none of the suspected titanomaghemite detected.

As the lava flow is only 45,000 years old, it is unlikely that the flow is significantly altered, nevertheless we have checked the possibility of any later alteration or weathering, which could have biaised the preservation of the primary magnetic signature (e.g. Ade-Hall & al., 1971; Krasa & Herrero-Bervera, 2005). First thin section examination on both optical and electronic microprobe have not revealed presence of any alteration halos around the Fe-Ti oxide phases suggesting that if alteration occurred, it is very weak. To check this, a microprobe colour composite has been performed on a thin section (see fig. 3.2.5b and its

legend for the channel inputs) to ensure that magnetic elements have not migrated during a hypothetic alteration episode. The figure 3.2.5b reveals that titanomagnetites are chemically homogenous, so that they appear turquoise blue. There is no release of either titanium or iron, and thus no evidence of any fluid modifying the magnetic mineralogy.

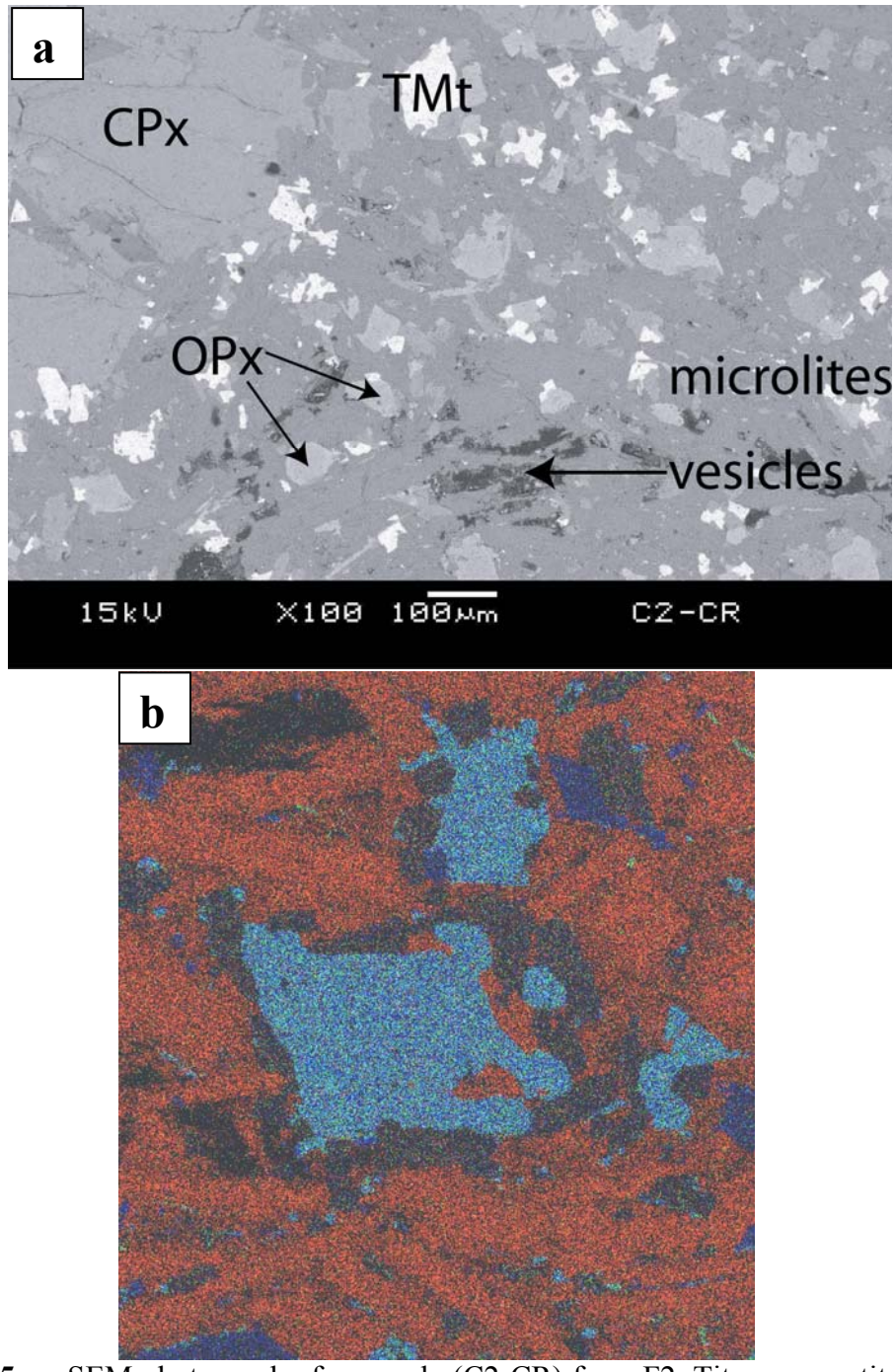

Figure 3.2.5: a. SEM photograph of a sample (C2-CR) from F2. Titanomagnetites (TMt) are white; **b.** microprobe chemical colour composite of a thin section area (C2-F2, 200×210µm) from F2: the green channel is for Titanium, the blue for iron and the red for aluminium. Thus titanomagnetite appears as turquoise blue (blue + green), while pyroxenes appear as blue and microlites as red.

3.2.2.3: Magnetic state of the AMS carriers

To determine the magnetic domain state of the AMS carriers we have used first-order reversal curves (FORCs) like Bascou & al. (2005), rather than using the Day plot (Day & al., 1977) as DeFrates (2006). This is because the use of the Day plot will give a point summing the whole magnetic state of titanomagnetite in the sample. This point will be located in a PSD-SD or MD field and could be the result of a mixed population. FORCs are expressed by contour plots of a two dimensional distribution function (Pike & al., 1999; Roberts & al., 2000) and the examination of these contours reveals the presence of PSD-SD or MD titanomagnetite even in case of mixing (see also 3.1.3.4). FORC measurements (100 FORCs per measurement) were performed on six sample locations: sites A, C, F, M, Q and U from F2 (see location on fig. 3.1.9) using the Micro Vibrating Sample Magnetometer of the CEREGE, Institute, Aix en Provence, France. Hb is a measure of magnetostatic interactions while Hc provides indirect information about the magnetic domain structure.

As detailed and discussed in 3.1.3.5, FORC diagrams display similarities in shape in 6 samples of the vertical section. On diagrams from figure 3.1.9, contours diverge away from the origin, which was interpreted by Roberts & al. (2000) as a manifestation of MD particles. There is a weak asymmetry of the inner contours around a central peak, indicating a small amount of PSD particles (e.g. Bascou & al., 2005). The absence of any convergence of the inner contours around a central peak indicates the absence of SD particles. So, in F2, there are mostly MD and some PSD titanomagnetites. This is also in agreement with the size range of visible titanomagnetite from 1 to 100µm in the thin sections. The absence of SD particles (the smallest) is important because, when present, they tend to alter the normal fabric, because of their reverse magnetic contribution (Rochette & al., 1992 ; Rochette & al., 1999). Thus, the magnetic fabric in F2 can be considered as normal (k_{max} is parallel to the silicate fabric flow direction) and is not weakened by SD presence.

Moreover, on the six measured FORC-samples, Mr/Ms values range from 0,14 to 0,16 and Hcr/Hc values range from 2,38 to 2,49 such values in a Day diagram (Day & al., 1977) will fall in the PSD field due to the effect of one Day point for the whole magnetic population. It underlines thus the interest of using FORC diagrams, which in our case have clearly emphasized the presence of mostly MD and some PSD.

3.2.2.4: AMS-Fabric conclusions

The main AMS phases are titanomagnetites with x ≈ 0.7. They display a large size and shape range, so the population is heterogeneous. They are MD and PSD particles, so that there is a normal magnetic fabric signature.

3.2.3: The AMS behaviour

The relationship between the silicate fabric (Hargraves & al., 1991) and the AMS tensor was tested by comparing microlite fabric found from image analysis and the AMS fabric. Three thin sections are needed for the image analyses (here vertical North-South, vertical East-West, and horizontal East-West). We have chosen a location in the outcrop where the thin section sample is closest to an AMS sample in order to reduce any lateral variation between the two subfabrics. This location is close to the AMS sample site E (see location on fig. 3.2.9a). While a block sample would have been preferable for this, the outcrop is too massive to allow such sampling. As we had difficulty to isolate some microlites from their neighbours in thin sections, we used the intercept method of Launeau and Robin (1996) (see http://www.sciences.univ-nantes.fr/geol/UMR6112/index.html). This is based on an analysis of the boundary orientation of objects (obtained by filtering and thresholding the digital images obtained using a colour CCD mounted on a binocular, 5× magnification and a rotating polarizer stage microscope of Fueten (1997), (see http://craton.geol.brocku.ca/faculty/ff/ff1.html). We chose this method rather than the inertia shape tensor method, based on an averaging of orientation and shape parameters of each object, due to the microlite distinction confusion.

The results are displayed on fig. 3.2.6 and table 3.2.1. The main axis orientations of the two tensors (AMS and microlites) coincide. Thus, the two tensors have recorded the same deformation direction. According to fig. 1 & 2a, the trend of the k_{max} axes are parallel to the lava flow course and thus the tensors reflects in fact the flow direction. This suggests that, in this case (see 7.3 for generalization to the 22 samples), the k_{max} axis is the indicator of the flow direction. Given the overall consistency between the AMS and microlite data, we have not considered the imbrication of the magnetic foliation as used in dykes by several authors (e.g., Geoffroy & al., 2002; Callot & Guichet, 2003). The relative elongation of the main axes and, as a consequence, the degree of anisotropy, are not similar and reflects the different shape aspect ratio between titanomagnetites and microlites (see 3.2.4).

Iron-titanium oxides usually crystallize late in basaltic melts at low pressure (e.g. Hill & Roeder, 1974), but here, from thin section observations (fig.3.2.5) the titanomagnetites have crystallized before the full growth of plagioclase microlites as they display sub-euhedral morphologies. As the tensor axes are similar, we suggest that the flow was active during the growth of microlites. The plagioclases thus control the distribution/orientation of the AMS subfabric.

Finally, with the AMS verification process, we are confident that the AMS results given in section 7 show the late stage of the flow deformation of F2. This stage is compatible with results from experimental deformation of natural melted lava (Cañón-Tapia & Pinkerton, 2000).

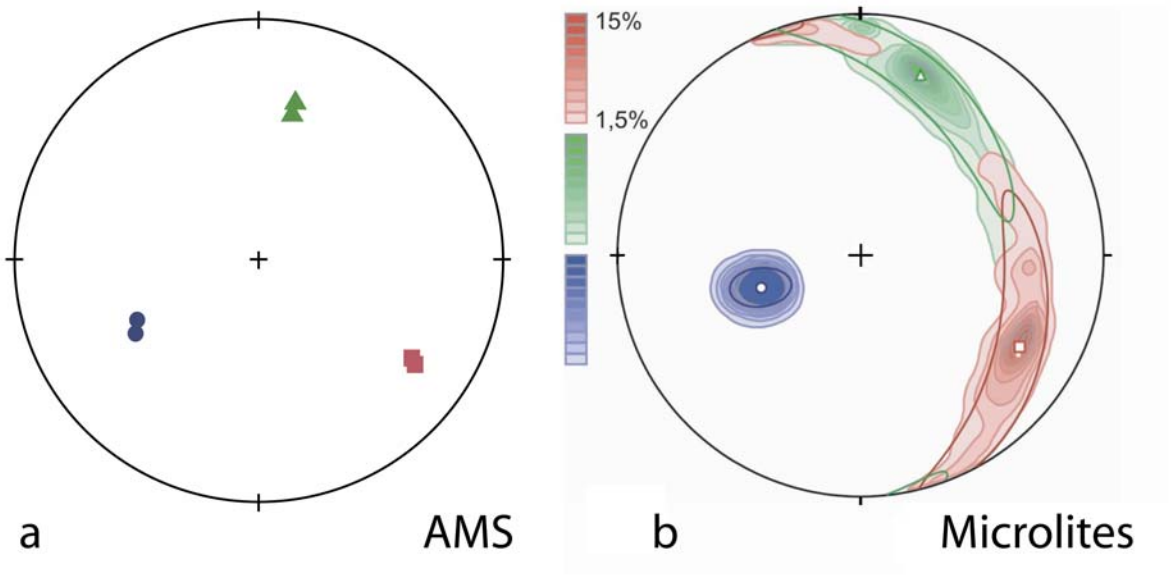

Figure 3.2.6: Equa area projections (lower hemisphere) of the AMS subfabric: **(a)** and the microlite subfabric **(b)** at E, in F2. Contours in **(b)** display the confidence interval. Squares are k_{max}, triangles k_{int} and circles k_{min}.

		k_{max}			k_{int}			k_{min}			Aniso.
Subfabric	Name	$k_{max\ relative}$	Az_{max}	Inc_{max}	$k_{int\ relative}$	Az_{int}	Inc_{int}	$k_{min\ relative}$	Az_{min}	Inc_{min}	A
AMS subfabric	E	1.014	123.2	25.5	1.000	13.0	36.0	0.986	239.8	43.2	2.130
Microlite subfabric	Em	1.134	120.1	25.3	1.072	18.5	23.1	0.823	251.7	54.6	16.446

Table 3.2.1: Comparison between the AMS and the microlite subfabrics.

3.2.4: Remarks on the significance of the degree of anisotropy

It is generally assumed that the values of degree of magnetic anisotropy is directly linked both to the magnetic mineralogy and the shear strain of the flow (e.g. Hrouda, 1982; Rochette & al., 1992). As we know the likely magnetic phases controlling the AMS, we can discuss the second part of this assumption.

In low concentration suspensions, i.e. without substantial interactions, and for a population of particles with a single aspect ratio, the development of a shape fabric is theoretically cyclic during simple shear. Integration of the equation giving the general motion of a particle (Willis, 1977) yields the critical shear strain γ_T corresponding to one complete rotation of the particle (Fernandez & al., 1983): $\gamma_T = 4\pi / (1-K^2)^{1/2}$ with $K=(n^2-1)/(n^2+1)$ with n = particle aspect ratio. The degree of anisotropy A (the fabric intensity D *in* Ildefonse et al., 1992 and Arbaret et al., 1996) reaches a maximum value of $A = n^2$ when the fabric is parallel to the shear direction (Ildefonse et al., 1992). The shear strain at which the maximum intensity is reached is given by $\gamma_C = \gamma_T/4$.

The F2 titanomagnetites display for the visible elements from thin sections variable n from 1.2 to 2.7, and if we consider independently each extreme subpopulation, maximum values of A would be between 1.44 and 7.29%. This explains the low degree of anisotropy values reached on F2 of between 0.9% and 3.0% (see Table 3.2.2). Also the γ_C will be between 3.2 and 4.8. We also note here, when considering a microlite fabric with n=7.5, that A will reach 56.25%.

If we consider a range of variable aspect ratios and interactions between them, there must be a departure from theoretical curve (Arbaret & al., 1996), and a stabilisation of the fabric (e.g. Launeau 2004). Thus, the relationship between the degree of anisotropy and the shear strain is biased. On fig. 3.2.5, we observe that titanomagnetites interact with clinopyroxene pheno- and microphenocrysts, as well as with orthopyroxene microphenocrysts. This indicates that there was an early fabric of mafic phases. Then, as plagioclase microlites appear after titanomagnetite and pyroxene, interactions with this latter phase (see 3.2.3) will overprint any previous AMS fabric. The fabric finally arrived at is a combination of both, dominated by the plagioclase lath fabric element.

Lastly, we have also to consider, as in most lava flows, a pure shear component (e.g. Merle, 1998) may be present during the stabilization of the magnetic fabric. This may be due to flow thinning or inflation.

3.2.5: AMS results and interpretation

Figure 3.2.9a displays the vertical AMS profile on F2 under and above the road. Sample A is the lowest, below which is the very platey near-base of the flow. Sample V is the highest and is taken very near the surface crust of the flow. F2 is vesicle-rich from points R to V in the upper part of the flow and lower down it is massive, with very few isolated vesicles.

3.2.5.1: Mean susceptibility Km

The variation of the bulk susceptibility is displayed on fig. 3.2.9b. The bulk susceptibility ranges from 77.86×10^{-3} SI in P to 31.57×10^{-3} SI in R. Such variations cannot be explained by vesicularity changes, thus we have to consider that the distribution of titanomagnetites can not be considered as a simple trend as previously observed in other lava flow sections (Cañón-Tapia & al., 1997; Cañón-Tapia & Coe, 2002).

3.2.5.2: Shape parameter T

The evolution of the shape parameter (fig. 3.2.9c) displays several switches from the lineation field to the foliation field. These changes are modest as, the ellipsoids have low degree of anisotropy: from 0.915% and 3.023%. Such variations from the lineation to the foliation field were also observed on lava flow sections studied by Cañón-Tapia & al. (1997).

3.2.5.3: Eigenvector orientations and plunge

Values of azimuths and inclinations of the eigenvectors (table 3.2.2 and in fig. 3.2.7 & 3.2.9d) show a relatively good agreement with the westward flow direction of F2 as previously observed in 3.2.3. (alignment of K_{max} azimuth). Thus the AMS tensor has recorded the flow deformation over the whole F2 section and again (see 3.2.3) we consider the k_{max} azimuth as the indicator of the flow direction and not the magnetic foliation used in dykes by several authors (Geoffroy & al., 2002; Callot & Guichet, 2003).

K_{max} plunge directions (fig. 3.2.9d) switch from eastward to westward and some are steep (over 45°). This is the first time, to our knowledge, that more than one switch of the k_{max} axes has been reported. Single k_{max} axes switches from the upper and the lower flow parts are commonly observed (Bascou & al., 2005). These opposing dips are interpreted as being due to

the velocity profile characteristic of a roofed lava (Cañón-Tapia, 1996). During flow cooling, the roof thickness increases and the vertical velocity profile evolves as a function of time. Modelling of strain within lava flows (Merle, 1998 & 2000) showed that for a roofed flow or a tunnel, strain evolves toward a central low strain area of highest velocity. Clearly, then, F2 must have a more complicated history.

A first explanation would be a succession of several lava units each undergoing a basal and top shear. According this explanation, we have to suppose that a sample close to the F2 base (under the sample A) has to display a westward k_{max} dip direction (fig. 3.2.9d). In this way, the contact between each lava unit will be located where there is a k_{max} dip change from westward (top) to eastward (bottom) that is to say between S&T, O&P, K&L, E&F and A&B.

A second possibility would be an inhomogeneous flow with rheological steps. These variations may be attributed bulk compositional zones in the flow, volatile loss, as well as differential crystallization.

A third possibility is that the lava has occasional upstream flow events.

A fourth possibility is that the flow is wavy, and the vertical profile is recording the progressing lateral set of undulations. We will discuss these possibilities in 3.2.5.5.

The inclination of k_{max} can locally be greater than 45°, that is to say greater than the incremental elongation axis dip in simple shear. The largest value is located at L, where the inclination reaches 61.2° (Table 3.2.2). Such values can also be found in other flows (e.g. Cañón-Tapia & al., 1995; Walker & al., 1999; Cañón-Tapia & Coe, 2002; Cañón-Tapia, 2004) but have not always received any interpretation. Mostly, it has been assumed that lava flows are mainly submitted to simple shear, but k_{max} dips greater than 45° suggest pure-shear. Thus, here lava flow emplacement results in a combination of simple shear and pure shear. In our case, the simplest way to obtain k_{max} dips greater than 45° is by vertical pure shear elongation. Such stretching can occur when a lava flowing into a larger valley is entering in a narrower valley or filling a flow front: in both cases it will thicken. The two possibilities are combined for F2, as the Royat valley narrows at the outcrop and as F2 is close to its termination (fig. 3.2.2). The pure shear may have affected the whole flow section to different degrees to combine with the simple shear flow deformation. The simple shear can have different gradients in a single simple lava flow (e.g. Merle, 1998) and thus the lava will appear to have already a zoned AMS pattern. In this way, places where simple shear is relatively low will preserve the pure shear signature i.e. k_{max} values greater than 45°.

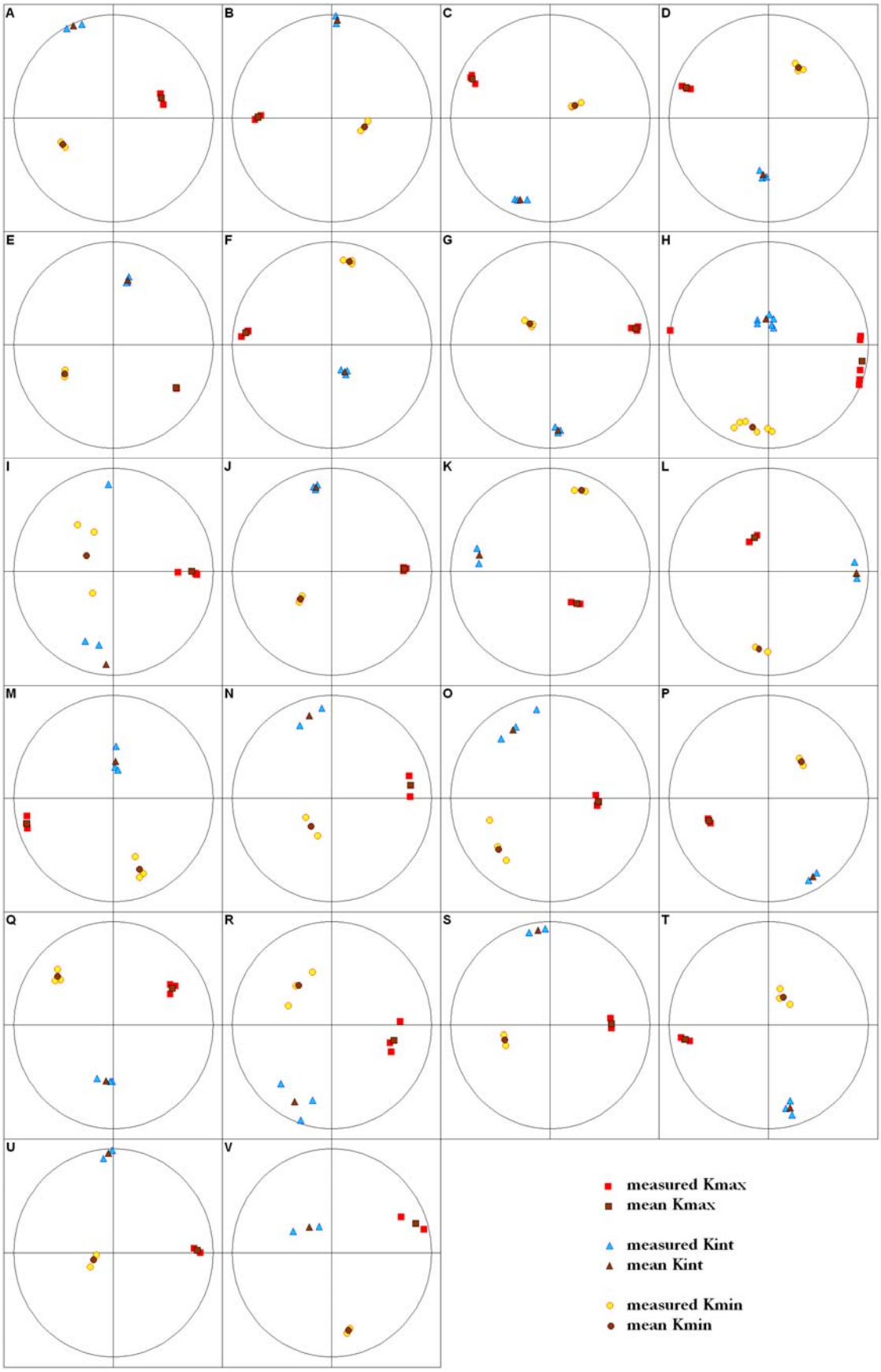

Figure 3.2.7: F2 stereograms of the anisotropy of magnetic susceptibility. Equal-area projection (lower hemisphere).

			k_{max}				k_{int}				k_{min}							
Site, n	km 10^{-3} SI	Δkm 10^{-3} SI	k_{max}	Δk_{max}	Az $_{max}$	Inc $_{max}$	k_{int}	Δk_{int}	Az int	Inc $_{int}$	k_{min}	Δk_{min}	Az $_{min}$	Inc $_{min}$	T	ΔT	A %	ΔA
A, 2	76.17	0.01	1.020	0.005	69.70	47.0	1.002	0.007	336.2	3.3	0.978	0.002	243.2	43.0	0.176	0.006	2.943	0.056
B, 2	68.52	0.06	1.016	0.003	270.4	27.1	1.001	0.005	2.8	4.9	0.984	0.007	102.4	62.3	0.054	0.002	2.349	0.042
C, 3	72.58	0.02	1.015	0.004	295.9	14.6	1.000	0.004	201.2	16.9	0.985	0.004	64.1	67.4	0.030	0.001	2.134	0.036
D, 3	74.98	0.03	1.014	0.005	289.5	13.6	0.999	0.004	185.9	44.4	0.987	0.004	32.3	42.3	-0.084	0.003	2.052	0.035
E, 3	73.97	0.02	1.014	0.000	123.2	25.5	1.000	0.002	13.0	36.0	0.986	0.001	239.8	43.2	0.018	0.000	2.130	0.008
F, 3	64.86	0.03	1.014	0.003	277.6	13.9	1.003	0.002	153.2	66.4	0.983	0.003	12.4	18.6	0.316	0.007	2.003	0.023
G, 3	65.89	0.01	1.013	0.003	79.7	13.9	1.002	0.002	174.6	18.5	0.985	0.004	314.9	66.5	0.162	0.004	1.970	0.023
H, 6	67.33	0.02	1.014	0.004	99.5	5.4	0.999	0.007	355.2	69.3	0.987	0.006	191.5	19.9	-0.104	0.005	2.071	0.046
I, 3	43.03	0.01	1.015	0.014	89.9	22.5	0.996	0.072	184.6	11.3	0.989	0.069	299.4	64.6	-0.456	0.020	2.217	0.376
J, 3	60.18	0.01	1.016	0.001	88.3	27.6	0.999	0.001	348.6	17.7	0.985	0.002	229.9	56.3	-0.087	0.001	2.392	0.010
K, 2	61.04	0.02	1.016	0.005	139.8	57.2	1.000	0.009	281.7	26.9	0.984	0.004	20.9	17.5	-0.015	0.001	2.352	0.052
L, 2	45.41	0.05	1.009	0.005	334.3	61.2	0.999	0.007	89.0	13.1	0.992	0.007	185.2	25.4	-0.163	0.009	1.344	0.032
M, 3	77.49	0.01	1.006	0.003	255.0	10.8	0.999	0.023	5.1	60.3	0.995	0.022	159.0	27.2	-0.238	0.034	0.915	0.047
N, 2	60.79	0.03	1.010	0.014	81.8	21.3	1.001	0.031	344.8	18.6	0.989	0.023	216.3	62.1	0.146	0.026	1.472	0.119
O, 3	52.02	0.01	1.010	0.003	93.1	50.8	1.000	0.051	335.0	21.4	0.990	0.049	231.0	31.8	-0.025	0.008	1.448	0.155
P, 2	77.86	0.07	1.021	0.001	249.9	36.9	1.005	0.004	149.7	13.2	0.975	0.003	43.4	50.1	0.321	0.007	3.023	0.026
Q, 3	61.79	0.02	1.021	0.005	58.9	31.6	1.000	0.009	187.3	45.3	0.980	0.006	310.0	28.2	0.018	0.001	3.013	0.072
R, 3	31.57	0.01	1.010	0.026	102.0	35.7	1.001	0.069	204.9	18.6	0.990	0.049	317.2	49.0	0.094	0.037	1.420	0.243
S, 2	45.02	0.02	1.010	0.004	88.5	38.4	1.000	0.008	352.0	8.2	0.990	0.004	251.9	50.7	0.015	0.001	1.544	0.032
T, 3	39.27	0.02	1.011	0.004	260.6	16.3	0.999	0.011	165.3	18.5	0.990	0.012	29.5	64.9	-0.167	0.013	1.601	0.049
U, 2	45.70	0.03	1.009	0.003	88.6	16.8	1.002	0.007	356.6	5.7	0.989	0.008	248.0	72.3	0.247	0.013	1.346	0.029
V, 3	56.07	0.02	1.014	0.034	70.3	14.4	1.001	0.034	311.9	61.6	0.985	0.001	167.2	24.1	0.097	0.014	2.117	0.215

Table 3.2.2: AMS measurements and parameters on F2. n is the number of cuttings for each core sample that have been measured.

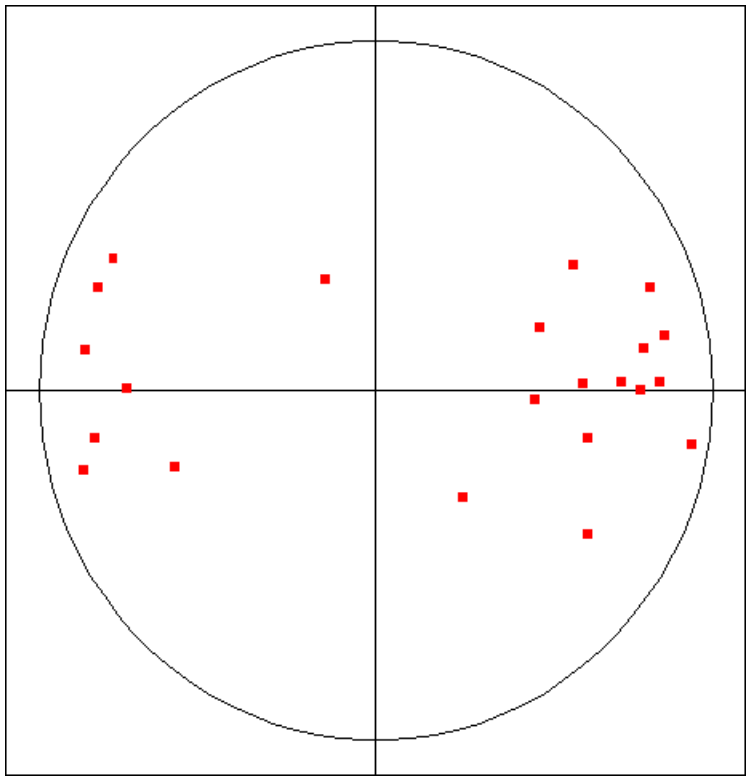

Figure 3.2.8: F2 stereogram of the k_{max} axis on the 22 samples drilled all over the outcrop. Equal-area projection (lower hemisphere).

3.2.5.4: Degree of Anisotropy A and interpretation

Values of degree of anisotropy (table 3.2.2, fig 3.2.9e) are low (A varies between 0.915% in M and 3.023 in P) and could be explained by the low aspect ratio of titanomagnetites. The values of the degree of anisotropy tend to increase toward the top and base of F2. At these sites, cooling is most rapid and thus inward-flow cooling propagation may quench textures before the degree of anisotropy has been stabilized by the latter interactions and subfabric overprinting as explained in 3.2.4. Thus, close to the lava edges, the degree of anisotropy may not have been stabilized and displays higher values, as previously noted by Cañón-Tapia and Pinkerton (2000) on experimental lava flows. However, in the central part of F2, the degree of anisotropy has probably been stabilized and thus variations can not be explained by different shear strains.

Two well constrained breaks of A are located between K and M (2.352 to 0.915% in 12cm) and between O and P (1.448 to 3.023% in 17cm). Another break is less evident between Q and R (3.013 to 1.420% in 30cm) where the distance and the error bars are greater. This less

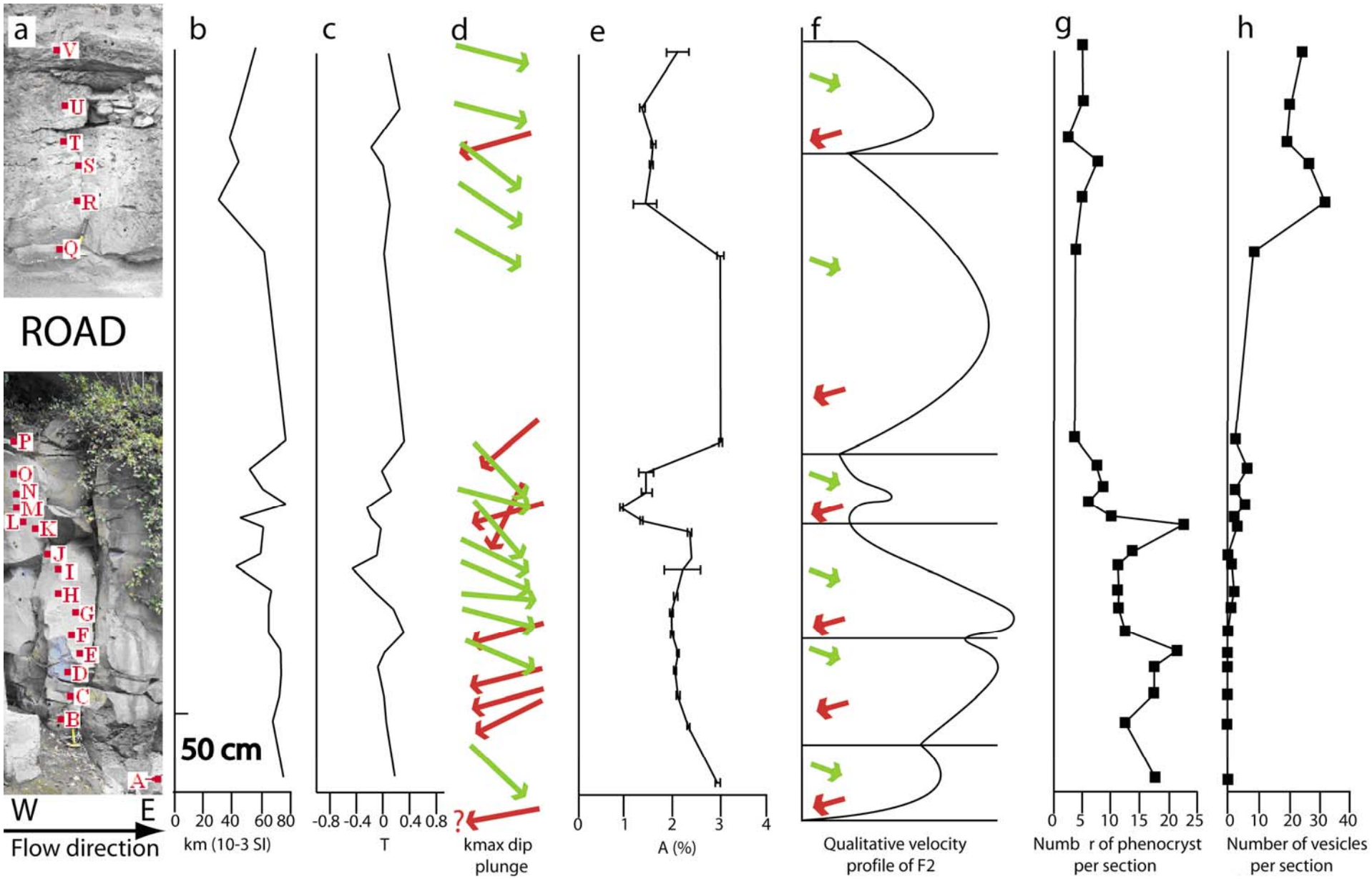

Figure 3.2.9: a. The 5m-high outcrop on F2 with the core locations – **b.** Evolution of the mean susceptibility – **c.** Evolution of the magnetic shape parameter – **d.** Evolution of the k_{max} dip plunge – **e.** Evolution of the magnetic degree of anisotropy – **f.** Qualitative velocity profile deduced from fig.3.2.9d & 9e – **g.** Evolution of the number of phenocrysts per section – **h.** Evolution of the number of vesicles per section.

evident break can be simply the result in differential titanomagnetite development as it is located at the contact between the vesiculated and no-vesiculated part of F2.
The two well-constrained breaks are both located at k_{max} switches (compare fig. 3.2.9d and 3.2.9e). This indicates that there is a heterogeneity plane located in the lava flow, which could be either a separation between two lava units of the flow or an inhomogeneous flow displaying a rheological threshold due to chemical or crystallization differences.
Whatever the case, each lava flow unit or rheological part displays its own signature and that the passage from one unit to another can be potentially detected by a break in A if the signature is sufficiently different.
Leading from the variations of k_{max} plunge directions and the degree of anisotropy, we propose a qualitative velocity profile of F2 during the late stage of deformation (fig. 3.2.9f).

3.2.5.5: Rheological insights and interpretation

The possible rheological variations of F2 have been investigated from the evolution of vesicle and mafic phenocryst number density along the same vertical profile as AMS measurements. On each core sample a thin section was made for counting. The counting is thus done on a circular area 2.2cm in diameter. We are conscious that this method could have large errors, as the studied surface is small, but we consider it is sufficient for finding vesicle and phenocryst *trends* and is also adequate for a direct comparison with AMS parameters (table 3.2.3, fig. 3.2.9g & 3.2.9h). The results are also backed up by direct observation on the outcrop where vesicles and mafic phenocrysts are picked out by the weathering surface.
There is a simple vesicle pattern, with upper vesiculated crust and a massive core (fig 3.2.9h). The classical lower vesiculated crust of Aubele & al. (1988) is absent here, as we cannot see the F2 base, but it is also not present in other nearby outcrops.
The evolution of the phenocryst number is not so simple. Mafic phenocrysts are more concentrated in the lower part of the flow, indicating probable settling. However, this downward enrichment does not follow a regular trend (fig 3.2.9g). Direct observations at outcrop show also this heterogeneous pattern. In fact, the downward phenocryst-enrichment is not constant and can display locally an impoverishment. Such a pattern can not be acquired by simple settlement in a lava flow. We propose that this variation is the combination of an inhomogeneous magma (with phenocryst gradients in the conduit) and the long flow history down a complicated lava channel and tube system.

Site	Number of phenocrysts per section	Number of vesicles per section	Degree of magnetic anisotropy A (%)
A	18	0	2.943
B	14	0	2.349
C	18	0	2.134
D	18	0	2.052
E	21	0	2.130
F	14	0	2.003
G	13	1	1.970
H	13	2	2.071
I	13	1	2.217
J	15	0	2.392
K	22	3	2.352
L	12	2	1.344
M	9	5	0.915
N	11	2	1.472
O	10	6	1.448
P	7	2	3.023
Q	7	8	3.013
R	8	31	1.420
S	10	26	1.544
T	6	19	1.601
U	8	20	1.346
V	8	24	2.117

Table 3.2.3: Number of phenocrysts and vesicles per section 2.2cm in diameter. The change in the degree of anisotropy is also provided for direct comparison.

In section 3.2.5.4., using changes in k_{max} plunge directions and the degree of anisotropy, we located four heterogeneity planes between A&B, K&L, O&P (plunge direction and degree of anisotropy changing), S&T (only plunge direction change) and Q&R (only break of the degree of anisotropy). For each plane we checked for correlations with the vesicle and phenocryst number density variations.

- The heterogeneity between Q&R displays no significant variation of phenocrysts, but does for the vesicle numbers: from 31 in Q to 8 in R. Thus this boundary may have a rheologic relationship.
- The contact between K&L displays no significant difference in vesicularity, but does in the concentration of phenocrysts: from 22 in K to 12 in L, this indicates a possible rheology difference, if the change is within error.
- Vesicularity decreases from 6 in O to 2 in P and the number of phenocrysts for 10 in O to 7 in P. We consider that such variations might be correlated to a rheological change, but are small compared with probable errors.
- No vesicles appear in A or in B, but phenocrysts decrease from 18 in A to 14 in B. This difference is so small as to provide no clue to a rheological change.

- Between S&T, variations also occur: phenocrysts decrease from 26 to 19 and vesicles from 26 to 19.

Thus, it appears that heterogeneity planes deduced from AMS do in some cases correlate with vesicle and phenocryst number changes that could have a rheological explanation.

In fact, several hypotheses are possible:

1) Irregular topography: Wavy flow: The lava flow has been emplaced on very irregular topographic path, which could have led to heterogeneous flow behaviour. Wavey flow patterns may have been produced. However, in the field we have not any proof for this. On the contrary, while the basal platey area of the flow wraps around topographic obstacles, it becomes subparallel over a short vertical distance. In addition, other outcrops do show gas pockets and horizontal fracture levels. This is evidence that wavy behaviour is not present.

2) Uphill flow: This is an intriguing possibility. Flow uphill could occur if the lava was thickening at a blocked flow front. A breakout higher on the flow could also create upward drainage. In addition in-flow from the top, for example, could sink and flow back under the main flow. Such flow can be observed in blocked stream channels, but we do not know if it is possible in lava. It is, however, a process worth further consideration. It would indicate that inflation of a flow is more than a static layering up of lava inside the crust.

3) Multiple inflation episodes: Another hypothesis could be invoked: the possibility that the lava flow has undergone several inflation or feeding stages. Such an explanation has been invoked by Walker et al. (1999) and Cañón-Tapia and Coe (2002) to explain vertical variations of degree of anisotropy and AMS imbrications in the >45 m- thick Birkett lava flow (Columbia River, USA). In our case, F2 is only 5 – 6 m thick, allowing us to perform denser sampling. F2 does not display individual vesicular layers as on the Birkett. Some disruptions can be seen in the F2 vesicular zone (fig. 3.2.9a), but they are discontinuous. Vesicularity (fig. 3.2.9h), and field observations do not display strong breaks in porosity or vesicle concentrations like those on fig. 3 *in* Walker et al. (1999). So we cannot say that in our case, F2 has undergone several lava pulses, because each pulse would have developed its own vesicular layer. Moreover, Cañón-Tapia and Coe (2002) proposed for the Birkett lava flow that each edge of a new lava input, (i.e. the upper and lower rim subjected to intense shear with the cooled lava) would display a peak in the degree of anisotropy. This is clearly not the case here (see fig.3.2.9e), where there is a break in the degree of anisotropy but not a peak.

Finally, Walker & al. (1999) have pointed out, for the Birkett, that the magnetic fabric in the vesicular part (upper) and the non vesicular (basal) part have but ONE plunge direction reversal due to ONE symmetric k_{max} plunge direction reversal. In fact, they propose that the level at which injection will occur is always located at the same place, in the middle of the previous still viscous lava, (i.e. in the former no-shear zone separating opposite k_{max} dips). For F2, we have more than ONE reversal, and it would be difficult to imagine that the hypothetical new input of lava could occur randomly in the cooling lava. Thus, from the above observations, we consider that F2 has not been emplaced by a simple inflation model.

4) Multiple rheological layering: Due to the variable downward phenocryst-enrichment and the above correlations between AMS breaks and possible rheological variations, we propose that F2 is a heterogeneous flow displaying rheological variations linked to initial variations. It is important to remember that this AMS-evidenced structure is recorded only at a very late stage in the lava flow history. Simply, the AMS ellipsoid records the last incremental motion of flow. The F2 profile is made of at least 5 parts that we interpret as having different rheological conditions. It is possible that if a denser sampling was done, more rheological units might be obtained. F2 is made of several parts and not several stacked flow units, because there is no evidence of contact where break of degree of anisotropy occurs and there are not several vesicular layers or 'cryptozones'. Such a layered structure could develop by differential flow within the lava along its path, as units with slightly different viscosity flow at different rates, this process could be achieved partly by 'viscous fingering' (Anderson et al. 2006). Fig. 3.2.10 summarizes this conceptual point of view according data presented in this paper.

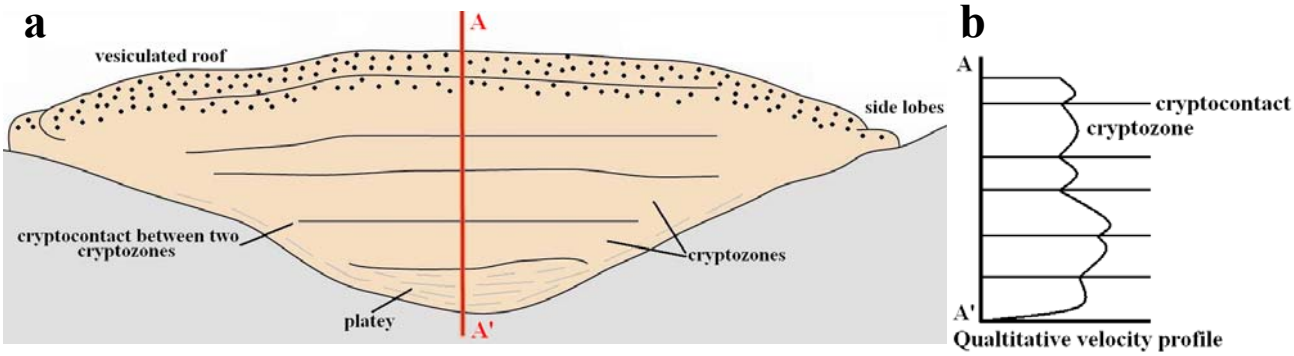

Figure 3.2.10: a. Conceptual section of a lava flow displaying structures found from field, AMS, structural and textural data. 'A'Ā' represents the vertical section of fig. 3.2.9b – **b.** Qualitative velocity profile of the same lava flow.

3.2.6: Conclusions

In this study, we have illustrated a methodology for the interpretation of lava flow deformation based on soundly constrained AMS and structural / textural observations. The AMS method requires as a first step determination of the main AMS carrier, and a subsequent step to find when the AMS subfabric was acquired. Once these are known, AMS results can be interpreted in the context of other data. We propose that such a procedure should be done every time AMS is used in a new context.

We have applied this methodology to the Tiretaine F2 lava flow from Chaîne des Puys. Firstly, this methodology has allowed us to show that the main AMS carriers are MD and PSD titanomagnetites ($x \approx 0.7$) with irregular size and shape. The absence of SD particles is important, because it means no 'inverse' magnetic fabrics are produced. Secondly, we have demonstrated that the AMS subfabric was acquired during the last stage of deformation of the lava flow. The AMS has a pure shear component and a stabilized simple shear strain component.

We have interpreted each AMS parameter, with a special attention to the k_{max} plunge direction and the degree of anisotropy. Both reversals in k_{max} correlated with breaks in the degree of anisotropy and they indicate the existence of heterogeneity planes separating different lava units. The k_{max} plunge direction greater than 45° indicates a vertical pure shear stretching. From the results we propose a qualitative velocity profile displaying a complex pattern. Uncertainty remains as to the origin of the compartmentalization. Lava waves are discounted due to other evidence. Upslope flow may be possible, but we have no evidence to support it. Multiple punctuated injections, like that proposed for the Birkett flow (Cañón-Tapia & Coe, 2002), are unlikely due to the lack of horizontal vesicle zones.

A layering of several subtly distinct rheological units is our preferred explanation. This interpretation is supported by the vesicle and phenocryst number densities that show subtle correlations with AMS variations. The flow may have individualised such subtle rheological units or 'cryptozones', during magma ascent or during flow the channel and tube system.

Whatever the final explanation for the variations here, the work shows that strain can be variable in a small single flow. Our profile is denser than any yet produced, and further fine-

scale investigation may provide even more rheological complexity. The results indicate that lava flows can have very complex internal flow organisation that will lead to complex variations in flow behaviour. A greater understanding of this will be required if lavas are to be successfully modelled for hazards. In addition, a better understanding will be needed if the use of lava flows as evidence of source conditions and eruption reconstruction is to be successful.

3.3. APPLICATION OF THE AMS METHODOLOGY TO THE ROYAT F3 FLOW

3.3.1: The Royat F3 flow

As previously noted in 1.3.3.1.1, the Royat F3 flow is a trachybasaltic lava flow erupted 45,000 ago (Boivin & al., 2004) by the Puy de Lacroix area as deduced by basement isobaths (Gagnière, 1980) (fig. 1.3.2 & see fig. 2.1.3a for a complete map of the Royat lava flows). The upper part of the flow was already studied in 1.3.3.1.1 on the Font de l'Arbre lava lobe displaying evidence of pāhoehoe emplacement.

In this section, we will present AMS results on a complete cross section of the F3 lava flow, down valley of the Font de l'Arbre outcrop, opposite a laybye on the D68 road (the outcrop location is provided by a star on fig. 2.1.3a). This outcrop was also already discussed in 2.1.5.3, and revealed shearing/faulting fragmentation features leading to a clinker formation in a pāhoehoe-like lava flow.

The outcrop consists of a 2m-high section with from the base to the top: the basal sheared clinker, the massive lava body, which becomes more vesicular toward the top, and finally an upper clinker zone formed in-situ by the classical pāhoehoe crust beginning to break up (see chapter for information about clinker formation).

Sixteen samples (cylinder cores of 2.5 cm in diameter and >10 cm long) were drilled and orientated using a solar and magnetic compass in the same manner as for 1.3.3.1 and 3.2.

3.3.2: The AMS carriers

3.3.2.1: Curie Temperature

We carried out a susceptibility versus temperature experiment (K-T curve) at high temperature using a furnace (CS-3) under Ar atmosphere coupled to a KLY-4 Kappabridge instrument (Agico, Czech Republic) on one cylinder core from F3, at the H location (sample 07H2) (fig. 3.3.1).

The thermomagnetic curves, as for the Royat F2 flow (see 3.2.2.1), are not reversible and are also similar to those from Bascou & al. (2005) from the upper and lower part of the Saint Thibéry lava flow (French Massif Central). The steepest decrease in susceptibility occurs between 80°C and 150°C. These low Curie Temperatures indicate that the main AMS phases are Ti-rich titanomagnetites (Nishitani, 1981; Dunlop & Özdemir, 1997). By considering the conventional expression of titanomagnetite ($Fe_{3-x}Ti_xO_4$) with $0 \leq x \leq 1$, microprobe analyses of titanomagnetites give $x \approx 0.7$, which is in good agreement with the observed Curie Temperature (O'Relly, 1984). We also note an irreversible slight decrease of susceptibility around 550°C. The interpretation of this is less evident, but like Bascou & al. (2005), we propose that this could indicate the presence of metastable titanomaghemite corresponding to low-temperature oxidation of titanomagnetite. Nevertheless, the main AMS carrier is represented by stable titanomagnetite with $x \approx 0,7$.

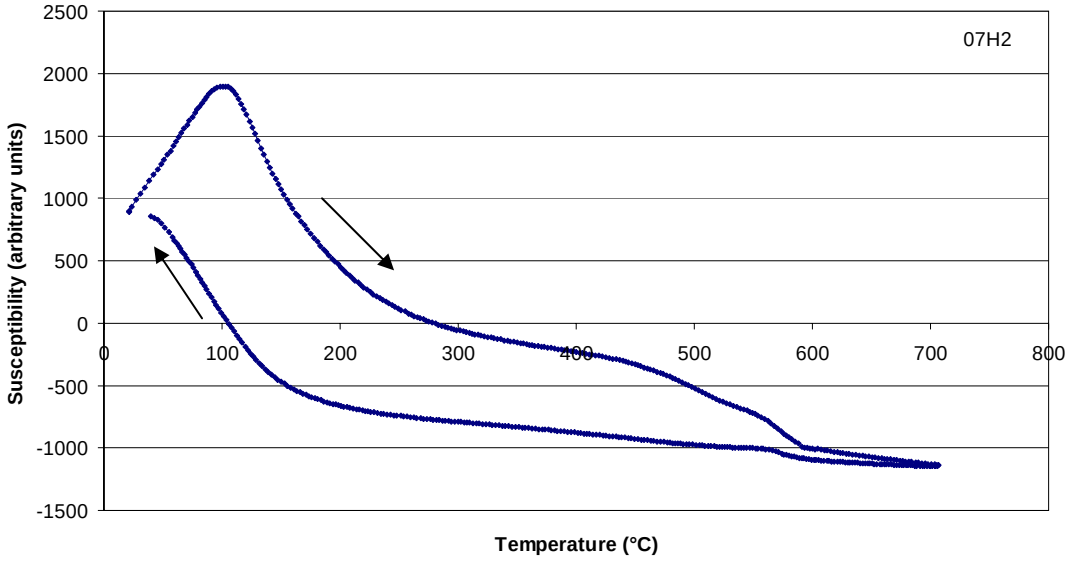

Figure 3.3.1: Thermomagnetic curve at high temperature from the H site (sample 07H2).

3.3.2.2: Thin section investigation

The SEM image displayed on fig. 3.3.2a is representative of all the 21 thin sections made on F3. It shows a good contrast between white titanomagnetites and the other matrix

components. The image shows that the titanomagnetite population is not homogenous. Crystals are often skeletal with a wide size range (from some microns to 100µm) and variable aspect ratio (from 1,3 to 2,5). Microprobe analyses performed on the microphenocrysts gave only titanomagnetite, and none of the suspected titanomaghemite was detected.

As for the Royat F2 flow (see 3.2.2.2), this lava is 45,000 years old and nevertheless we have checked the possibility of any later alteration, which would have biaised the preservation of the magnetic signature (e.g. Ade-Hall & al., 1971; Krasa & Herrero-Bervera, 2005). First thin section examination on both optical and electronic microprobe have not reveal presence of any red alteration halos, meaning that if alteration had occurred it is very weak. To further check this, a colour composite has been made on a thin section on the microprobe (see fig. 3.3.2b and its legend for the channel inputs) to assure that magnetic elements have not migrated during an hypothetic later episode. The figure 3.3.2b reveals that titanomagnetites are homogenous on a chemical point of view, so that they appear turquoise blue and that there is no release of either titanium or iron and thus no evidence of a fluid modifying magnetic mineralogy.

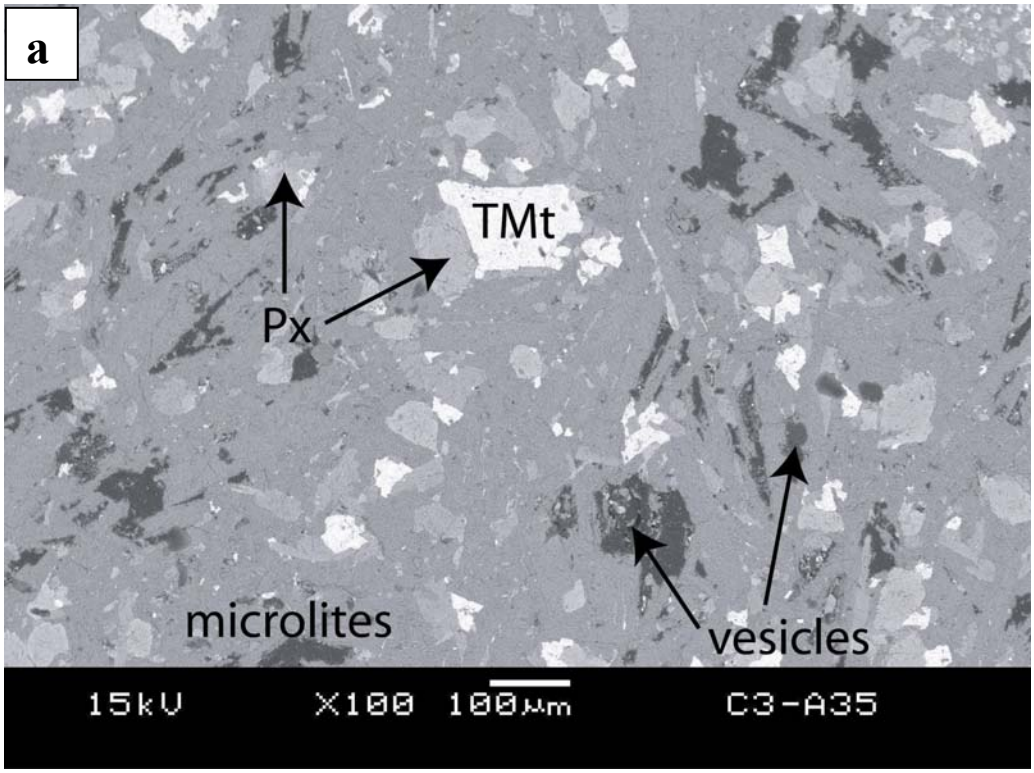

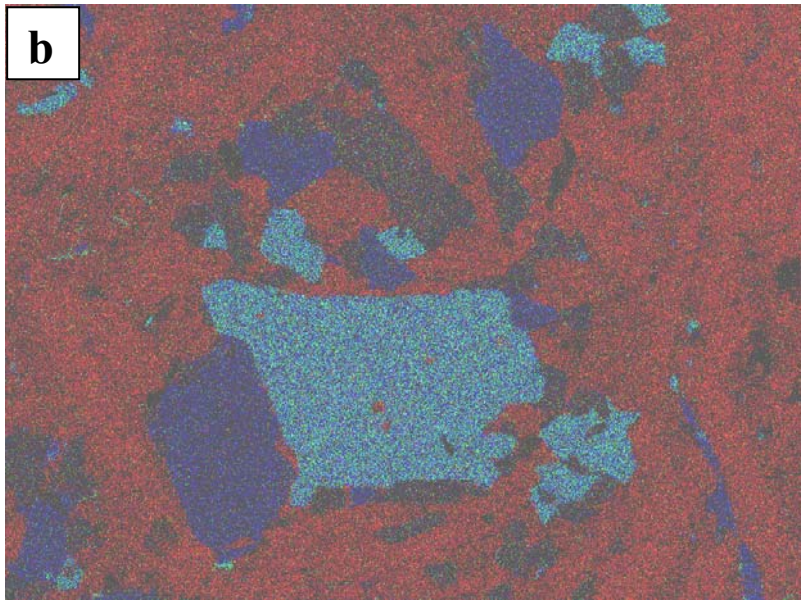

Figure 3.3.2: a. SEM photograph of a sample (C3-PL) from F3. Titanomagnetites (TMt) are white; **b.** microprobe chemical colour composite of a thin section area (C3-PL) from F3: the green channel is for Titanium, the blue for iron and the red for aluminium. Thus titanomagnetite appear as turquoise blue (blue + green), while pyroxenes appear as blue and microlites as red.

3.3.2.3: Magnetic state of the AMS carriers

As in 3.2.2.3, in the Royat F2 flow, to determine the magnetic state of the AMS carriers we have used first-order reversal curves (FORCs) like Bascou & al. (2005), because the use of the Day plot will give a point summing the whole magnetic state of titanomagnetite in the sample (see 3.1.3.4). FORC measurements (100 FORCs per measurement) were performed on two sample locations: sites B and K (see location on fig. 3.3.6) using the Micro Vibrating Sample Magnetometer of the CEREGE, Institute, Aix en Provence, France. Hb is a measure of magnetostatic interactions while Hc provides indirect information about the magnetic domain structure.

On diagrams from figure 3.3.3, contours diverge away from the origin, which was interpreted by Roberts & al. (2000) as a manifestation of MD particles. There is a weak asymmetry of the inner contours around a central peak, indicating a small amount of PSD particles (e.g. Bascou & al., 2005). The absence of any convergence of the inner contours around a central peak indicates the absence of SD particles. So, in F3, there are mainly MD and some PSD titanomagnetites. This is also in agreement with the size range of visible titanomagnetite from 1 to 100 μm in the thin sections. We remember that the absence of SD particles (the smallest)

is important because, when present, they tend to alter the normal fabric, because of their reverse magnetic contribution (Rochette & al., 1992 ; Rochette & al., 1999). Thus, the magnetic fabric in F3 can be considered as normal (k_{max} is parallel to the silicate fabric flow direction) and is not weakened by SD presence (this was also the same case in F2, see 3.2.2.3).

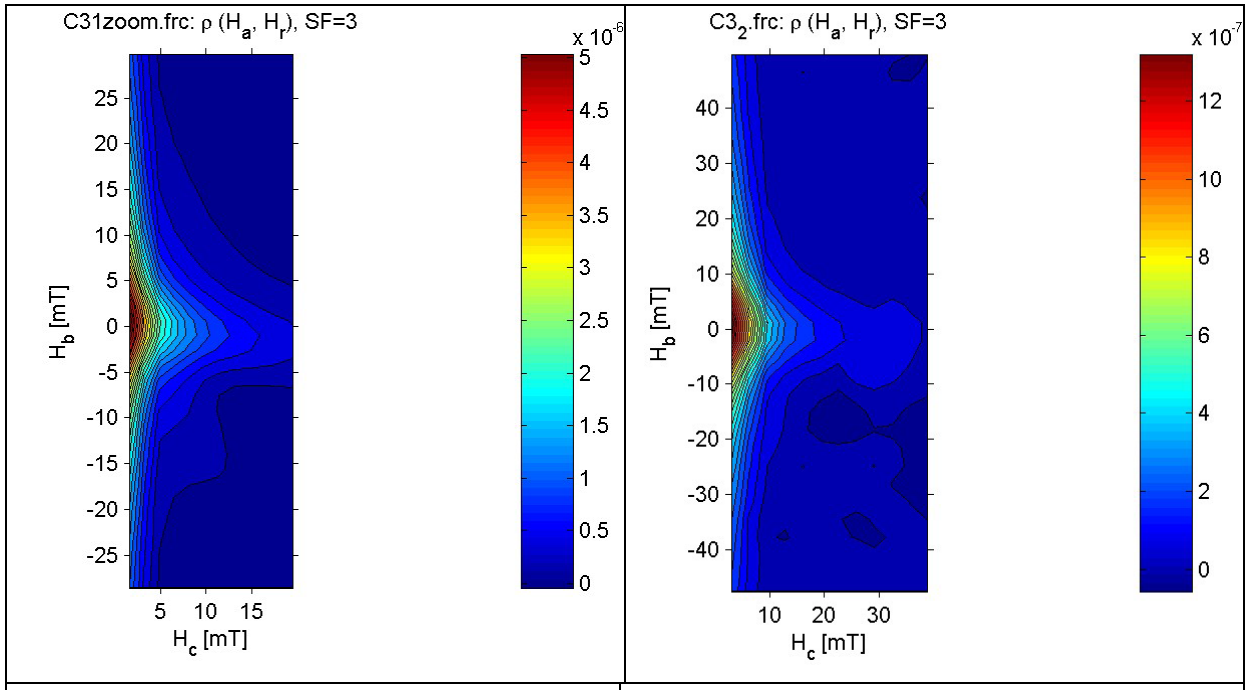

a. FORC diagram from sample B | **b.** FORC diagram from sample K

Figure 3.3.3: FORC diagrams obtain for two samples of the Royat F3 flow at the D68 lay-by outcrop.

3.3.2.4: AMS-Fabric conclusions

The main AMS phases are titanomagnetites with x ≈ 0.7. They display a large size and shape range, so the population is heterogenous. There is no evidence of alteration. They are MD and PSD particles, thus there is a normal magnetic fabric signature. We can also note, that the results obtained are quite similar to those of the Royat F2 flow (see 3.2.2.4) which can be linked to a similar magma input feeding system even if those two lavas do not come from the same vent (see 3.2.1 and fig. 3.2.1).

3.3.3: The AMS behaviour

As previously noted in 3.1.2.2 and 3.2.3, the relationship between the silicate fabric (Hargraves & al., 1991) and the AMS tensor was tested by comparing the microlite fabric found from image analysis and the AMS fabric. Unfortunately, in contrast to F2, we have not succeeded in collecting the three thin sections needed for the microlite fabric procedure (see 3.2.3). Nevertheless, to make up for this lack, we have considered the previous microlite and AMS results obtained for F3 at the Font de l'Arbre outcrop (see 1.3.3.1.4). The obtained result in this location (see fig. 1.3.10), has clearly showed that the microlite fabrics are close to the AMS ellipsoid. This confirms that AMS has well recorded the late stage of deformation consistent with microlite formation.
We assume that there are no AMS versus microlite fabric variations between the Font de l'Arbre and the D68 car park outcrop.

3.3.4: The AMS results and interpretation

3.3.4.1: Mean susceptibility Km

The variation of the bulk susceptibility is displayed on table 3.3.1 and on fig. 3.3.5b. The bulk susceptibility varies from 62.13 in F to 199.2×10^{-3} SI in G. Parallel measurements of the core sample weight has allowed us to calculate the mass susceptibility variation (K_m/m) from 1.71 to 2.36×10^{-3} SI/g. So vesicularity can not explain variations in K_m, but we have to consider that the distribution of titanomagnetites can not be considered as a simple trend as previously observed in other lava flow sections (Cañón-Tapia & al., 1997; Cañón-Tapia & Coe, 2002). The bulk susceptibility displays numerous variations at a small scale (F and G are 6 cm apart, see fig. 3.3.5b). Such variations are hard to interpret and may be related to strong vertical variations in the titanomagnetite content.

3.3.4.2: Shape parameter T

The evolution of the shape parameter (fig. 3.3.5c) displays several switches from the lineation field to the foliation field. This may not be significant as the ellipsoids have low degree of anisotropy: from 1.8% to 3.4%. Such variations from the lineation to the foliation field were

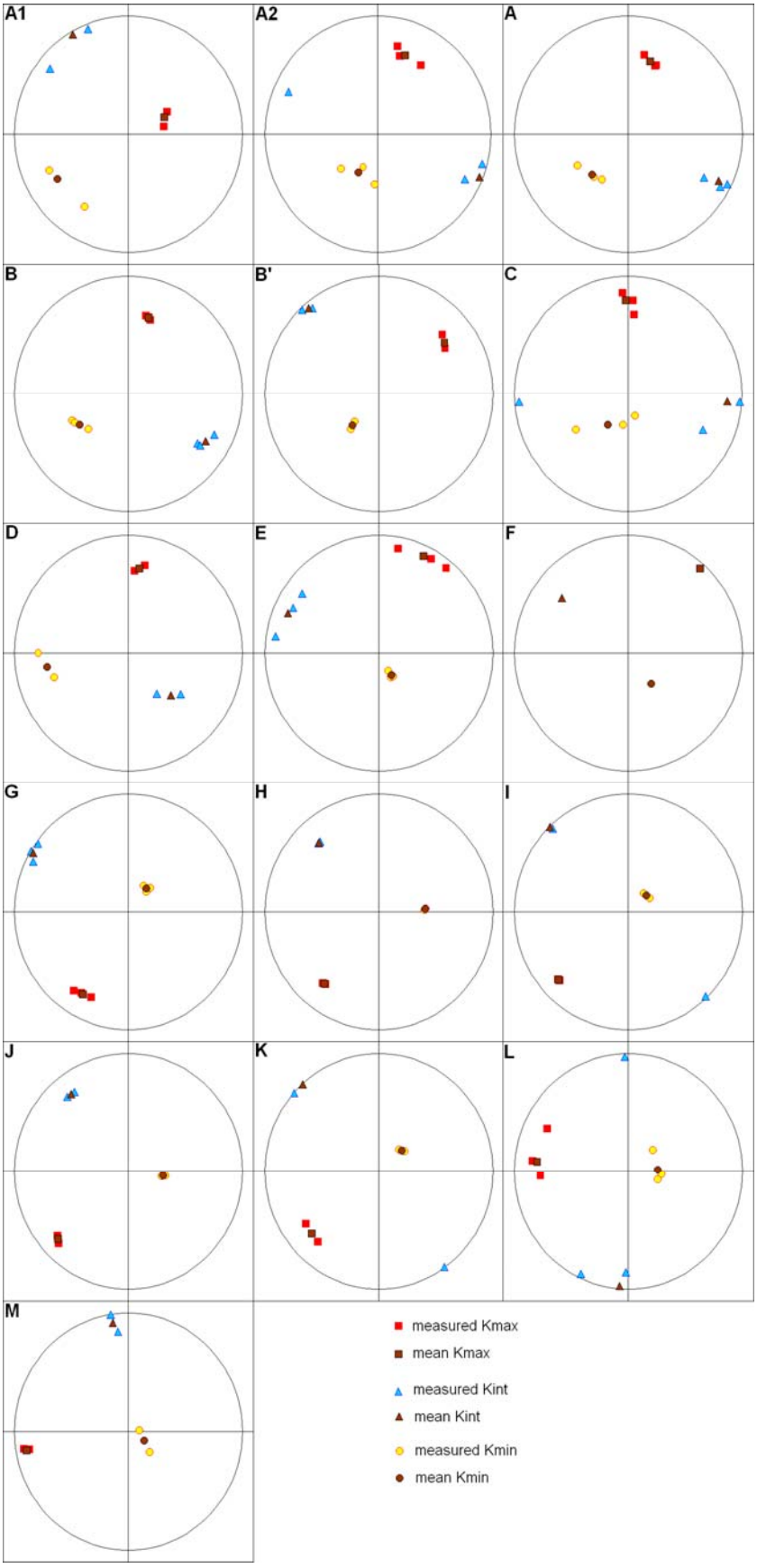

Figure 3.3.4: F3 stereograms of the anisotropy of magnetic susceptibility. Equal-area projection (lower hemisphere).

Site, n	Km 10^{-3} SI	K_{max}	ΔK_{max}	Az_{max}	Inc $_{max}$	K_{int}	ΔK_{int}	Az $_{int}$	Inc $_{int}$	K_{min}	ΔK_{min}	Az $_{min}$	Inc $_{min}$	A %	ΔA	T
A1, 2	101,61	1,014	0,008	68,7	61,3	0,999	0,067	323,8	9,2	0,987	0,069	229,1	28,1	2,038	0,311	-0,117
A2, 3	168,76	1,012	0,021	20,7	29,5	1,000	0,051	111,7	1,9	0,988	0,038	205,5	59,5	1,793	0,235	-0,026
A, 3	173,97	1,013	0,007	18,8	35,7	1,003	0,025	117,9	12,5	0,985	0,019	223,9	50,9	1,913	0,110	0,279
B, 3	150,82	1,016	0,001	15,3	33,3	1,001	0,010	121,4	22,8	0,983	0,009	239,1	47,9	2,341	0,049	0,120
B', 2	106,49	1,014	0,006	51,9	28,4	1,002	0,004	319,1	5,0	0,983	0,003	220,4	61,0	2,107	0,040	0,238
C, 3	188,23	1,012	0,019	1,5	23,4	0,999	0,097	97,2	8,2	0,988	0,103	207,4	65,9	1,811	0,431	-0,077
D, 2	121,74	1,015	0,004	8,0	28,1	0,998	0,022	134,4	48,8	0,987	0,026	261,5	27,8	2,161	0,124	-0,196
E, 3	187,34	1,014	0,042	26,8	9,3	1,003	0,042	294,3	14,6	0,983	0,002	149,6	72,7	2,085	0,262	0,327
F, 1	62,13	1,013	0,001	41,6	5,3	1,001	0,001	309,0	26,4	0,986	0,001	142,0	63,0	1,925	0,008	0,118
G, 3	199,20	1,023	0,006	210,2	20,6	1,001	0,007	301,4	3,3	0,977	0,002	39,7	69,1	3,325	0,068	0,048
H, 2	128,95	1,023	0,000	218,1	23,5	0,999	0,000	318,5	22,4	0,979	0,000	87,0	56,5	3,376	0,003	-0,094
I, 2	108,64	1,020	0,000	226,4	17,2	1,006	0,002	316,7	1,1	0,975	0,002	50,3	72,7	2,875	0,014	0,376
J, 2	116,01	1,021	0,002	226,6	16,6	1,000	0,002	322,4	18,7	0,979	0,001	97,9	64,5	3,095	0,020	0,007
K, 2	95,34	1,020	0,012	228,3	22,1	1,000	0,013	318,3	0,0	0,981	0,001	48,7	68,1	2,862	0,107	-0,036
L, 3	174,06	1,012	0,044	279,9	21,1	1,002	0,061	188,2	5,5	0,985	0,025	84,5	68,7	1,842	0,316	0,260
M, 2	93,62	1,016	0,002	260,5	10,5	1,003	0,019	352,4	8,3	0,982	0,021	119,9	76,5	2,279	0,101	0,280

Table 3.3.1 : AMS measurements on the D68 lay-by outcrop (F3)

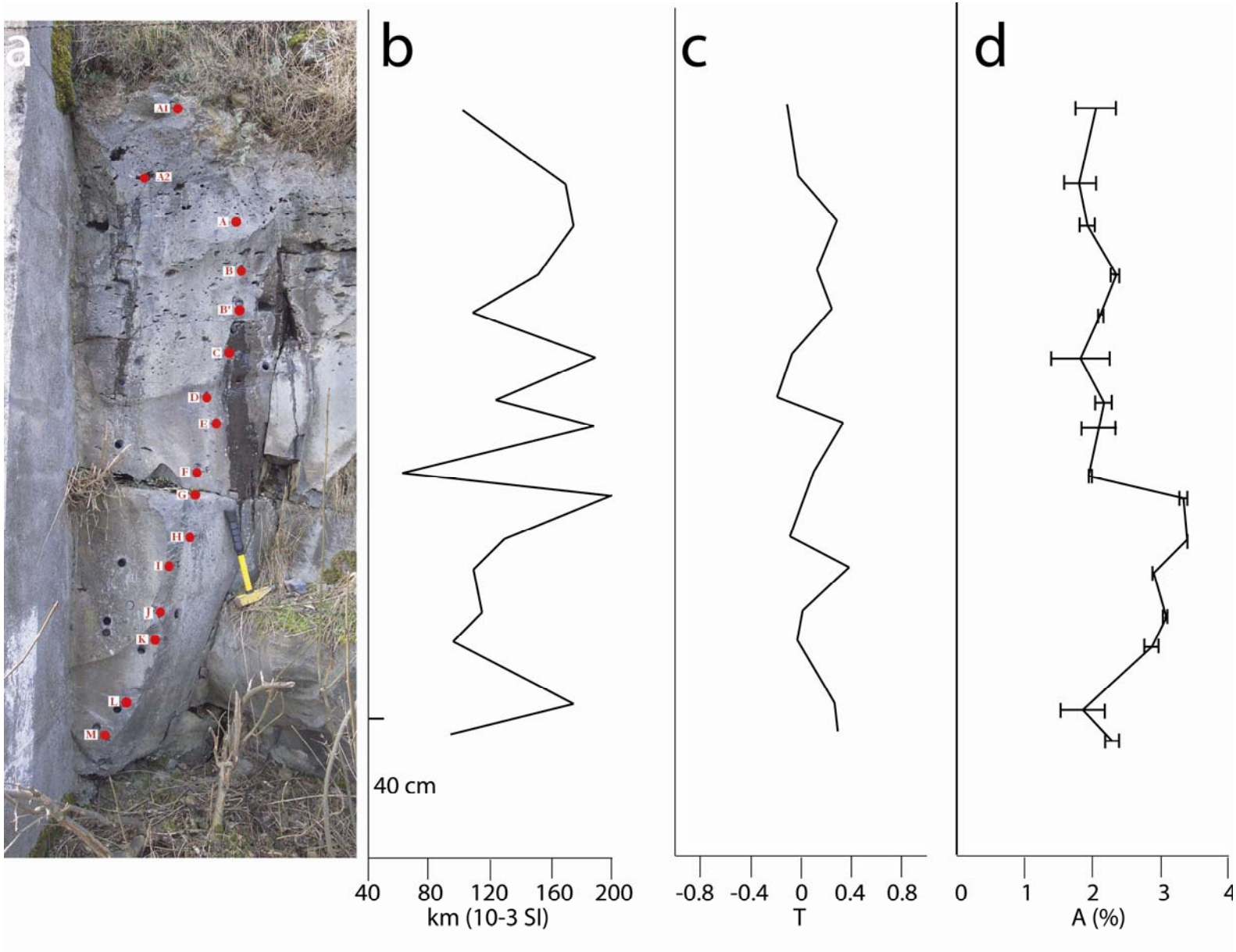

Figure 3.3.5: a. The 2m-high outcrop on F3 with core locations – **b.** Evolution of the mean susceptibility – **c.** Evolution of the magnetic shape parameter – **d.** Evolution of the magnetic degree of anisotropy

also observed on lava flow sections studied by Cañón-Tapia & al. (1997) and also in 3.2.5.2 concerning F3.

3.3.4.3: Eigenvector orientations and dip

Values of azimuths and inclinations of the eigenvectors are listed in table 3.3.1 and depicted in fig. 3.3.4. Strangely k_{max} azimuths (fig. 3.3.6) do not show an agreement with the WNW to ESE flow direction of F3 (see 3.2.1). Thus, the AMS tensor, in contrast with F2 in 3.2.5.3, has not recorded the downward flow deformation over the whole F2 section. Moreover, in spite of indicating the WNW to ESE downward movement of the flow, k_{max} azimuths (fig. 3.3.6) indicate a movement perpendicular to the main flow path (thus NNE-SSW).

This observation could be explained as an inverse magnetic signature (e.g. Rochette, 1988; Rochette & al., 1999). However, as noted in 3.1.2.1, examples of inverse fabrics in magnetic rocks are only known to be the result of SD magnetite, titanomagnetite or maghemite (Potter & Stephenson, 1988; Rochette, 1988; Borradaile & Puumala, 1989). In addition, as emphasized by our FORC measurements (see 3.3.2.3 and fig. 3.3.3) there is no evidence of SD particles.

Furthermore, the strict definition of an inverted fabric is "a fabric where k_{max} and k_{min} axes and symmetry are inverted" (Rochette, 1988) to the normal case, so in our case, if the fabric is really inverted, k_{min} should indicate the WNW-to-ESE downward flow movement which is not the case (fig. 3.3.4). So that we can clearly argue, again, that the AMS fabric is normal.

We will propose an interpretation of these unanticipated k_{max} azimuth orientations in 3.3.5.

Finally, we have nevertheless a simple k_{max} plunge imbrication with NNW to NW plunge in the upper part of the flow (samples A1 to F) and SW to W dips in the lower part of the flow (samples G to M) (fig. 3.3.6). Such a single k_{max} switch has been already observed (Bascou & al., 2005). As already evoked in 3.2.5.3., these opposing plunges are interpreted as being due to the velocity profile characteristic of a roofed lava (Cañón-Tapia, 1996). During flow cooling, the roof thickness increases and the vertical velocity profile evolves as a function of time. Modelling of strain within lava flows (Merle, 1998 & 2000), showed that for a roofed flow or a tunnel, strain evolves toward a central low strain area of highest velocity. So we can imagine that, at this outcrop location, F3 has undergone this imbricate shearing with an orientation created by a SE-to-NW movement. This point will also be discussed in 3.3.5.

3.3.4.4: Degree of Anisotropy A

The degree of anisotropy (table 3.3.1, fig .3.3.5d) is low (A varies between 1.8% in C and 3.4 in H) and could be explained by the low aspect ratio of titanomagnetites.

A well-constrained break of A is located between F and G (1.925 to 3.325% in 6 cm) with well constrained error bar. This break can also be correlated to a Km break (see 3.3.4.1) and may be due to a variation of titanomagnetite content or aspect ratio. Moreover, this break corresponds to a k_{max} plunge change (see F and G location on fig. 3.3.5).

As remarked in 3.3.4.3, this plunge change can be explained by a simple k_{max} imbrication in a lava flow having a SE-to-NW movement. This change occurs in the middle part of the flow, where it seems, according above statements, that titanomagnetites have a different mineralogy or shape, thus explaining such a break in the degree of magnetic anisotropy.

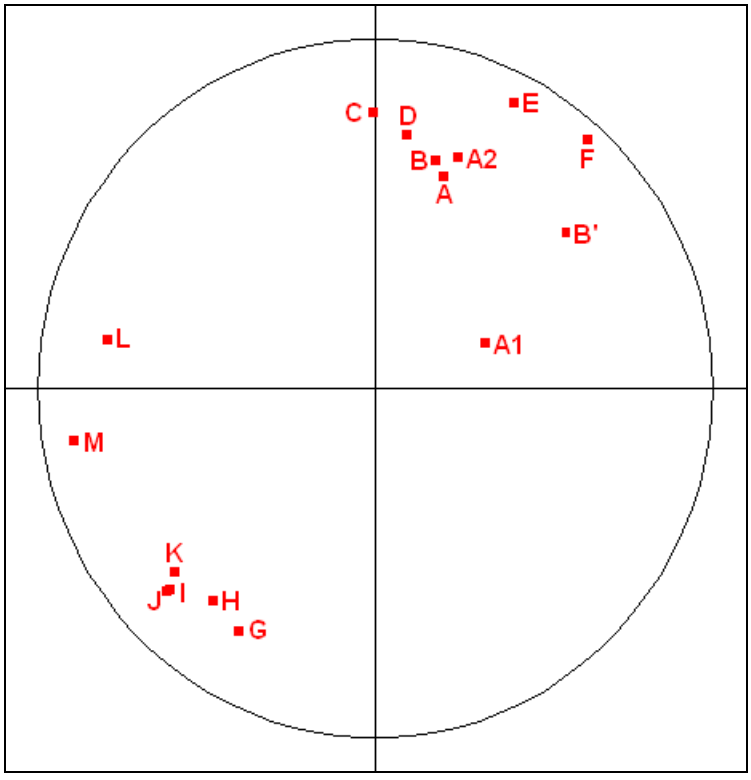

Figure 3.3.6: F3 stereogram of the k_{max} axis on the 16 samples drilled in the outcrop. Equal-area projection (lower hemisphere).

3.3.5: Interpretation

The main particularity of the F3 lava flow is to display k_{max} axes perpendicular to the apparent downward lava flow emplacement where there is no evidence of inverted magnetic fabric (see 3.3.2.3 & 3.3.4.3). In this section, we will propose an explanation based on thin section observations performed on the AMS outcrop and on the study of the surroundings outcrops.
A perpendicular to apparent flow thin section was prepared (fig. 3.3.7). Plagioclase microlites display a well defined alignment in the SW-NE plane i.e. perpendicular to the apparent downward lava flow and thus the microlite fabric is also in conformity with the AMS fabric. In fact, as there is no evidence of inverse fabric, this microlite alignment is significant in terms of flowing or stretching and thus can be linked to the SW-to-NE lava movement suggested by the k_{max} imbrication (see 3.3.4.4).

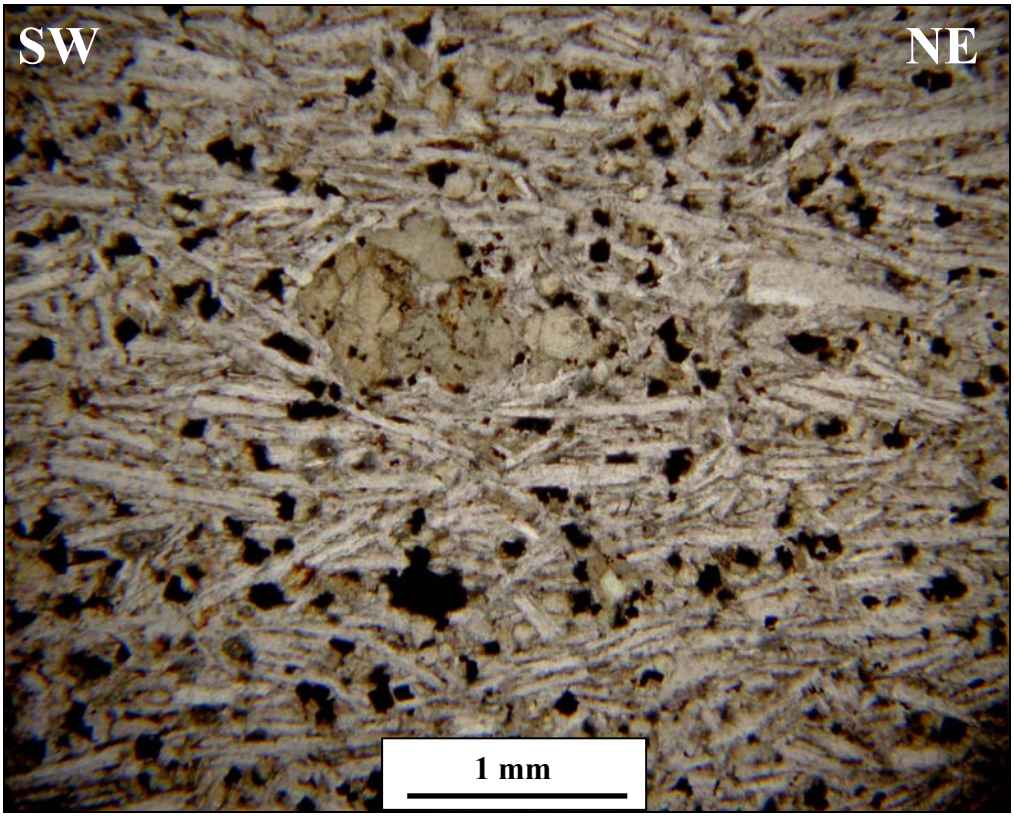

Figure 3.3.7: Thin section of F3 (D68 lay-by outcrop) perpendicular to the apparent downward movement of the lava flow.

This observation can also be related to surrounding outcrops (fig. 3.3.8) and notably to levée formation (fig. 3.3.9 and map on fig. 3.3.8b). It is well known that in order to form levees lava must have a Bingham behavior (e.g. Hulme, 1974; Sparks & al., 1976; Gregg & Fink, 2000;

Quareni & al., 2004). Hulme (1974) showed both theoretically and experimentally, (using flows of kaolin and water) that non-Newtonian fluids under a yield stress form stationary bodies of fluid at the margins of a flow and have a characteristic thickness on a given slope. The mechanism is surprisingly simple: when a fluid flows down a slope, it has a lateral velocity component. For a Bingham fluid, as lateral movement diminishes, a stage is eventually reached where the lateral boundary basal shear stress equals the yield stress and lateral motion ceases. A more recent laboratory investigation into the effects of slope on lava flow morphology was performed by Gregg & Fink (2000) using polyethylene glycol (PEG), which demonstrated that on higher slopes lavas develop levees. But, on F3, the levees are present on a constant slope, so the slope will not explain the levee formation.

We propose an explanation by linking the SW-to-NE magnetic and microlite elongation (fig. 3.3.8). When flowing down, F3 may have stopped its front in a first halt, with this stopped cooling front, the lava may has been subjected to a SW-to-NE spreading (fig. 3.3.8a), thus giving the impression that at the AMS outcrop, F3 has recorded a SW-to-NE emplacement strain. Then, with continued lava influx, lava pressure would exceed the yield strength of the lava front leading to the breakout of this first lava lobe front, leading to its deflation forming levees and to the final polylobate lava termination (fig. 3.3.8b).

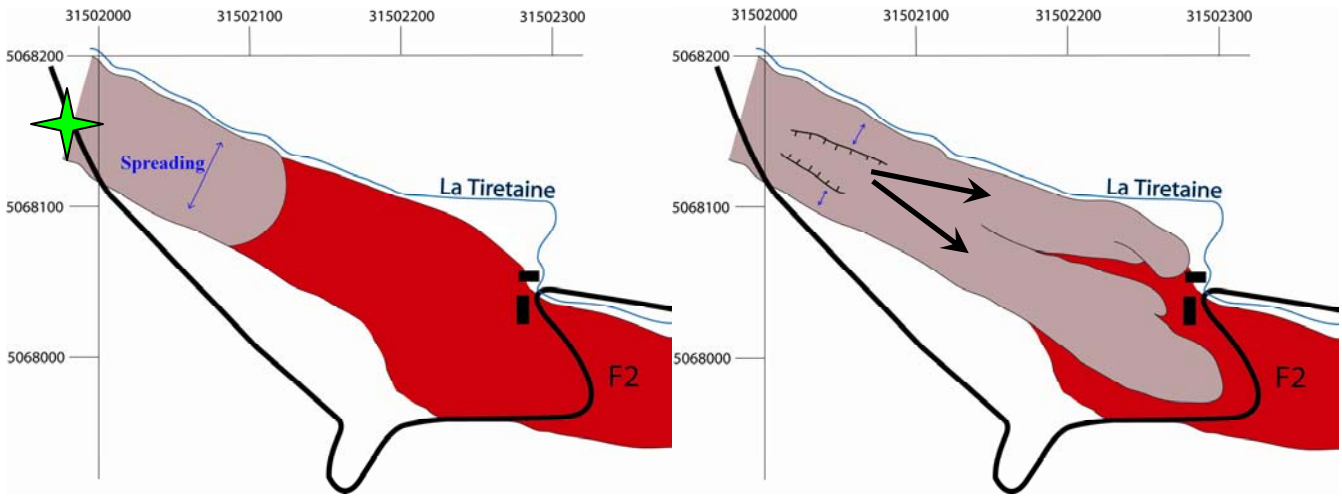

Figure 3.3.8: Possible evolution of the F3 termination. **a.** the first lobe halt of F3 inducing a perpendicular-to-flow spreading. The green star indicates the AMS sample location (D68 car park outcrop). **b.** the final halt of F3 with the wasting of the first lobe inducing the levee formation and a polylobate termination.

Figure 3.3.9: The two-levées formation in the middle part of F3 (see location on fig. 3.3.8).

3.3.6: Conclusions

In this study, we propose a methodology for the interpretation of lava flow deformation based on soundly constrained AMS and structural / textural observations.

This methodology applied to the Tiretaine F2 lava flow has allowed us to show that the main AMS carriers are MD and PSD titanomagnetites (x≈0.7) with irregular size and shape. The absence of SD particles is important; because it means no 'inverse' magnetic fabric is produced. Secondly, we have demonstrated that the AMS subfabric was acquired during the last stage of deformation of the lava flow with a comparison of fabrics in a neighbouring outcrop and a thin section on the same outcrop.

The eigenvectors of the AMS ellipsoid display a particular k_{max} orientation: perpendicular to the apparent F3 flow path. This observation cannot be linked to an inverse fabric, given the absence of SD particles. In fact, this orientation may be due to perpendicular to flow path spreading that has recorded a first stop in the lava flow emplacement.

We have also observed a simple k_{max} imbrication (in contrast to in F2, where numerous imbrications have been noted, see 3.2.5.3). This simple imbrication indicates a simple lava flow structure subjected to a roof and a basal shear. In the middle of the flow, where the imbrication occurred, a break in the bulk susceptibility and the magnetic degree of anisotropy indicate that the later-infilling lava was magnetically slightly different (different titanomagnetite compositions or shapes).

Our study of neighbouring outcrops, with the obtained AMS data, have allowed us to reconstruct the F3 lava flow emplacement with a first stop leading to the perpendicular-to-flow spreading. Then with still incoming lava, breakout occurred and deflation of this first front resulted in formation of levees and the final observed polylobate termination.

CONCLUSIONS

To promote the use of AMS in volcanology and in particular concerning lava flow emplacement, we have proposed a methodology to perform the most accurate and reliable interpretations. This methodology has been applied on two lava flows and has been field checked.

This methodology can be summed up by asking two questions:

1) Which minerals carry the AMS? This question is solved by performing Curie Temperatures, thin sections, microprobe analyses and mapping if possible. Finally, we have emphasized the importance of determining the magnetic state of the AMS carriers, as SD particles are known for their biasing of resulting ellipsoids. To solve this last point, we have made several FORC diagrams that have been interpreted and appear to be more relevant than the use of the Day plot.

2) When was the AMS acquired? It is interesting to link measured AMS ellipsoids to the lava flow emplacement, but this emplacement is time-spread and the emplacement will change while the lava flow is cooling. A way to estimate this AMS time acquisition is to compare the fabric with the microlite fabric that forms during the late stage of cooling.

The application of this methodology to two lava flows from the Chaîne des Puys: the Royat F2 and F3 flows has revealed that in both cases, the AMS fabric was carried by MD-PSD titanomagnetites without occurrence of inverted AMS fabric as SD particles are absent. The comparison of the AMS ellipsoid and microlite ellipsoid displays strong similarities arguing thus that the AMS fabric was acquired during the last stage of deformation. Therefore, our interpretation considers only elements related to this last stage of deformation.

In both lava flows, we have demonstrated the particular interest of the eigenvector orientation and plunge, in particular for k_{max}. In fact k_{max} plunges display imbrications that can be linked to lava flow models. A simple imbrication, as in F3, is typical of a single lava flow, whereas

the numerous imbrications observed in F2 indicate a more complicated lava flow emplacement composed of several stacked lava flow compartments.

In F2, values higher than 45° of k_{max} plunge suggest vertical inflation of the lava flow, not necessarily being the result of the typical pāhoehoe inflation feeding, but also being the result of variations in the width of the valley.

Concerning F2, a correlation between the k_{max} plunge changes with the degree of magnetic anisotropy has confirmed the possibility of having a lava flow being the result of stacked compartments and has allowed us, with support of modeling results, to promote a velocity profile. An explanation of multiple rheological layering was proposed in relation to AMS and the evolution in both vesicles and mafic phenocryst patterns. The patter may have formed in the lava flow by several compartments having slightly different rheologies and subjected to different shear histories. Such a process implies the existence of at least 6 different compartments in this 5m-high lava section.

Such a study should of course be performed in other lava flows to more fully investigate its significance. Nevertheless, it appears that a lava flow that in the field looks simplistic can display a complex velocity pattern and hidden layering. We stress that these interpretations are significant only for the last stage of deformation but we think that the triggering of the compartmentalization may occur early in the flow history and could be observed on active lava flows and thus may have implications for lava flow prediction and eventually hazard mitigation.

Concerning F3, displaying a normal AMS fabric, as revealed by the FORC diagram, the problem was to interpret the apparent perpendicular to flow path k_{max} orientation that suggested by its imbrication a SW-to-NE movement. This has been solved by a comparison with the microlite fabric, also displaying the same main microlite axis elongation and thus suggesting a perpendicular-to-flow stretching probably acquired during a early lobe halt. Then with continued lava influx, this first lobe broke and deflated to form levees and the presently visible polylobate termination. So in this second case, the AMS has revealed another kind of information allowing us to reconstruct, with a relatively good precision, the history of F3 emplacement.

The different results obtained in only two examples show the kind of information that can be discerned by using AMS with a careful methodology. Continuation of this methodology will certainly provide other supprised in other lava flows and can help to improve understanding of their emplacement procedure. Of particular interest, will be the study of continental flood basalt, of which the emplacement mechanisms are still subject to controversy.

REFERENCES

Ade-Hall, J.M., Palmer, H.C., Hubbard, T.P., 1971. Magnetic and opaque petrological response of basalts to regional hydrothermal alteration. Geophys. J. R. Astron. Soc. 24, 137-174.

Anderson, S.W., McColley, S., Fink, J.H.., Hudson, R, 2005. The development of fluid instabilities and preferred pathways in lava flow interiors: insights from analog experiments and fractal analysis; GSA Memoir on Lava Flow Dynamics and Kinematics.

Arbaret, L., Diot, H., 1996. Shape fabrics of particles in low concentration suspensions: 2D analogue experiments and application to tiling magma. J. Struct. Geol., vol. 18, 941-950.

Aubele, J.C., Crumpler, L.S., Elston, W.E., 1988. Vesicle zonation and vertical structure of basalt flows. J. Volcanol. Geotherm. Res. 35, 349-374.

Bascou, J., Camps, P., Dautria, J.M., 2005. Magnetic versus crystallographic fabrics in a basaltic lava flow. J. Volcanol. Geotherm. Res. 145, 119-135.

Bitter, F., 1932. On the Verification of the Theory of Magnetization of Single Crystals. Phys. Rev. 39, 371-375.

Boivin, P., Besson, J.C., Briot, D., Camus, G., De Goër de Herve, A., Gourgaud, A., Labazuy, Ph., De Larouzière, F.D., Livet, M., Mergoil, J., Miallier, D., Morel, J.M., Vernet, G., Vincent, P.M., 2004. Volcanologie de la Chaîne des Puys, 4ème édition.

Borradaile, G.J., Puumala, M.A., 1989. Synthetic magnetic fabric in plasticine. Tectonophysics 164, 73-78.

Borradaile, G.J., 1991. Correlation of strain with anisotropy of Magnetic susceptibility (AMS). Pure and Applied Geophysics 135, 15-29.

Borradaile, G.J., Henry, B., 1997. Tectonic applications of magnetic susceptibility and its anisotropy. Earth-Science Reviews 42, 49-93.

Cañón-Tapia, E., 1994. AMS parameters: guidelines for their rational selection. Pure Appl. Geophys. 142, 365-382.

Cañón-Tapia, E., 1996. Single-grain versus distribution anisotropy: a simple three-dimensional model. Phys. Earth Planet. Inter. 94, 117-131.

Cañón-Tapia, E., Walker, G.P.L., Herrero-Bervera, E., 1997. The internal structure of lavas: insights from AMS measurements II: Hawaiian pāhoehoe, toothpaste lava and ‘a‘ā. J. Volcanol. Geotherm. Res. 76, 19-46.

Cañón-Tapia, E., Pinkerton, H., 2000. The anisotropy of magnetic susceptibility of lava flows: an experimental approach. J. Volcanol. Geotherm. Res. 98, 219-233.

Cañón-Tapia, E., Coe, R., 2002. Rock magnetic evidence of inflation of a flood basalt lava flow. Bull. Volcanol. 64, 289-302.

Cañón-Tapia, E., Castro, J. 2004. AMS measurements on obsidian from the Inyo Domes, CA: a comparison of magnetic and mineral preferred orientation fabrics. J. Volcanol. Geotherm. Res. 134, 169-182.

Cañón-Tapia, E., 2004. Flow direction and magnetic mineralogy of lava flows from the central parts of the Peninsula of Baja California, Mexico. Bull. Volcanol., 66, 431-442.

Callot, J.P., Guichet, X., 2003. Rock texture and magnetic lineation in dykes: a simple analytical model. Tectonophysics 366, 207-222.

Day, R., Fuller, M. & Schmidt, V.A., 1977. Hysteresis properties of titanomagnetites: grain-size and compositional dependence. Phys. Earth planet. Inter., 13, 260–267.

DeFrates, J., Malone, D.H., Craddock, J.P., 2006. Anisotropy of magnetic susceptibility (AMS) analysis of basalt dikes at Cathedral Cliffs, WY: implications for Heart Mountain faulting. J. Struct. Geol. 28, 9-18.

Dunlop, D.J., 1986. Hysteresis properties of magnetite and their dependence on particle size: a test of the pseudo-single-domain remanence models. Journal of Geophysical Research 91, 9569–9584.

Dunlop, D. J., 1990. Developments in rock magnetism, *Rep. Prog. Phys*., *53*, 707-792.

Dunlop, D.J., Özdemir, Ö., 1997. Rock Magnetism: Fundamentals and Fontiers. Cambridge Univ. Press, Cambridge. 573 pp.

Fernandez, A., Febesse, J.L., Mezure, J.F., 1983. Theoritical and experimental study of fabrics developed by different shaped markers in two-dimensional simple shear. Bull. Soc. Géol. Fr., 7, 319-326.

Fuenten, F., 1997. A computer controlled rotating polarizer stage for the petrographic microscope. Computers and Geosciences 23, 203-208.

Gagnière G, 1980. Reconnaissance des ressources en eau souterraine des formations volcaniques à l'Ouest de Clermont Ferrand (Puy de Dôme). BRGM.

Geoffroy, L., Callot, J.P., Aubourg, C., Moreira, M., 2002. Magnetic and plagioclase linear fabric discrepancy in dykes: a new way to define the flow vector using magnetic foliation. Terra Nova, 14, 183-190.

Goër de Herve, A. de, Camus, G., Miallier, D., Sanzelle, S., Falguères, C., Faïn, J., Montret, M., Pilleyre, T., 1993. Le puy de Gravenoire et ses coulées dans l'agglomération de Clermont-Ferrand (Massif Central Français) : un modèle inhabituel d'avalanche de débris déclenchée par une éruption strombolienne en climat périglaciaire. Bull. Soc. Géol. Fr. 64, 783-793.

Gregg, T.K.P., Fink, J.H., 2000. A laboratory investigation into the effects of slope on lava flow morphology. J. Volcanol. Geotherm. Res. 96, 145-159.

Hargraves, R.B., Johnson, D., Chan, C.Y., 1991. Distribution anisotropy: the cause of AMS in igneous rocks? Geophys. Res. Letters, vol 18. 12, 2193-2196.

Hill, R., Roeder, P., 1974. The crystallization of spinel from basaltic liquid as a function of oxygen fugacity. J. Geol., 82, 709-729.

Hon, K., Gansecki, C., Kauahikaua, J., 2003. The transition from ‘a‘ā to pāhoehoe crust on flows emplaced during the Pu’u ‘O’o-Kupaianaha eruption. US Geological survey professional paper 1676.

Hrouda, F., 1982. Magnetic anisotropy of rocks and its application in geology and geophysics. Geophys. Surv., 5, 37-82.

Hrouda, F., Chlupáčová, M., Schulmann, K., Šmíd, J., Závada, P., 2005. On the effect of lava viscosity on the magnetic fabric intensity in alkaline volcanic rocks. Stud. Geophys. Geod., 49, 191-212.

Hulme, G., 1974. The interpretation of lava flow morphology. Geophys. J. R. astr. Soc. 39, 361-383.

Ildefonse, B., Launeau, P., Bouchez, J.L., Fernandez, A., 1992. Effect of mechanical interactions on the development of shape preferred orientations: a two dimensional experimental approach. J. Struct. Geol., 14, 73-83.

Krasa, D., Herrero-Bervera, E., 2005. Alteration induced changes of magnetic fabric as exemplified by dykes of the Koolau volcanic range. Earth and Planet. Sc. Let. 240, 445-453.

Launeau, P., Robin, P.Y.F., 1996. Fabric analysis using the intercept method. Tectonophysics, 267, 91-119.

Launeau, P., 2004. Mise en évidence des écoulements magmatiques par analyse d'images 2-D des distributions 3-D d'orientations préférentielles de formes. Bull. Soc. Géol. Fr., 2004, t. 75, n°4, 331-350.

Mayergoyz, I.D., 1986. Mathematical model of hysteresis, IEEE Trans.Mag., MAG-22, 603–608.

Merle, O., 1998. Internal strain within lava flows from analogue modelling. J. Volcanol. Geotherm. Res. 81; 189-206.

Merle, O., 2000. Numerical modelling of strain lava tubes. Bull. Volcanol. 62, 53-58.

Nkono, C., Féménias, O., Diot, H., Berza, T., Demaiffe, D., in press. Flowage differentiation in an andesitic dyke of the Motru Dyke Swarm (Southern Carpatians, Romania) inferred from AMS, CSD and geochemistry. J. Volcanol. Geotherm. Res.

Nishitani, T., 1981. Magnetic properties of titanomagnetites containing spinel (MgAl2O4). J. Geomagn. Geoelectr. 33 (B12), 171-179.

O'Relly, W., 1984. Rock and Mineral Magnetism. Blackie, Glasgow, 230pp.

Özdemir, Ö., Dunlop, D.J., 1993. Magnetic domain structures on a natural single crystal of magnetite. Geophys. Res. Letters, 20, 1835-1838.

Quareni, F., Tallarico, A., Dragoni, M., 2004. Modeling of the steady-state temperature field in lava flow levées. J. Volcanol. Geotherm. Res. 132, 241-251.

Pawse, A., Beske-Diehl, S., Marshall, S.A., 1998. Use of hysteresis properties and electron spin resonance spectroscopy for the identification of volcanic ash: a preliminary study. Geophys. J. Int., 132, 712-720.

Pike, C.R., Roberts, A.P.&Verosub, K.L., 1999. Characterizing interactions in fine magnetic particle systems using first order reversal curves, J. appl. Phys., 85, 6660-67.

Potter, D.K., Stephenson, A., 1988. Single-domain particles in rocks and magnetic fabric analysis. Geophys. Res. Lett. 15, 1097-1100.

Roberts, A.P., Pike, C.R. & Verosub, K.L., 2000. First-order reversal curve diagrams:Anewtool for characterizing the magnetic properties of natural samples, J. geophys. Res., 105(B12), 28461-28475.

Rochette, P., 1988. Inverse magnetic fabric in carbonate bearing rocks. Earth Planet. Sci. Lett. 90, 229-237.

Rochette, P., Jackson, M., Aubourg, C., 1992. Rock magnetism and the interpretation of anisotropy of magnetic susceptibility. Reviews of Geophysics, 30,3, 209-226.

Rochette, P., Aubourg, C., Perrin, M., 1999. Is this magnetic fabric normal? A review and case studies in volcanic formations. Tectonophysics, 307, 219-234.

Tarling, D.H., Hrouda, F., 1993. The magnetic anisotropy of rocks. Chapman and Hall, London, 217 pp.

Tauxe, L., Mullender, T.A.T., Pick, T., 1996. Potbellies, wasp-waists, and superparamagnetism in magnetic hysteresis. J. Geophys. Res., 101, 571-583.

Self, S., Keszthelyi, L., Thordarson, Th., 1998. The importance of pāhoehoe. Annu. Rev. Earth Planet. Sci. 1998. 26: 81-110.

Solana, M.C., Kilburn, C.R.J., Rodriguez Badiola, E., Aparicio, A., 2004. Fast emplacement of extensive pāhoehoe flow-fields: the case of the 1736 flows from Montaña de las Nueces, Lanzarote. J. Volcanol. Geotherm. Res. 132, 189-207.

Sparks, R.S.J., Pinkerton, H., Hulme, G., 1976. Classification and formation of lava levees on Mount Etna, Sicily. Geology. 4, 269-271.

Walker, G.P.L., Cañón-Tapia, E., Herrero-Bervera, E., 1999. Origin of vesicle layering and double imbrication by endogenous growth in the Birkett basalt flow (Columbia river plateau). J. Volcanol. Geotherm. Res. 88, 15-28.

Willis, D.G., 1977. A kinematic model of preferred orientation. Bull. Geol. Soc. Am., 88, 883-894.

CONCLUSIONS

The objective of this work was to try to better understand kinematic and deformation processes occurring in lava flows. This objective has been accomplished by associating three different approaches combining descriptive volcanology, textural petrophysical studies and magnetism.

In the first chapter, the significance of pāhoehoe and ‘a‘ā, terms originally used to describe lava flow surfaces, has been revealed to be relevant when considering rheological properties and thus emplacement of the body of the lava flow. Pāhoehoe flows are less viscous than ‘a‘ā and emplace by lobe inflation and coalescence, whereas, ‘a‘ā flows have a disrupted crust forming clinker. This falls to the flow base in a roll-over caterpillar motion.

These differences in emplacement can also be studied in cooled and old lava flows where surface features are either eroded or masked. This allows the pāhoehoe or ‘a‘ā terms to be used in such flows and thus a first determination of their emplacement mechanisms. Clinker and irregular deformed vesicles are typical ‘a‘ā features whereas, lobe stacking, inflation fissures, light deformed vesicles, vesicle pipes and zonation in phenocrysts and vesicles are pāhoehoe evidence.

Rheological properties can be qualitatively appreciated by using a shear strain rate versus apparent viscosity diagram. The observed pāhoehoe-to-’a‘ā and ‘a‘ā-to-pāhoehoe transitions can been explained according to rheological parameters. Such evolutions have explored on a recent Icelandic lava flow field: the Myvatn Fires (1724-1729). Pāhoehoe-to-’a‘ā transitions result from both increase in shear strain testifying to an increase in the ground slope and an increase in the apparent viscosity, simply as the result of the lava cooling. On the other hand, an ‘a‘ā-to-pāhoehoe transition is explained by a breakout on the ‘a‘ā lava front allowing releasing of less viscous lava core and also by lower imposed shear strain rates.

The application of the ‘a‘ā and pāhoehoe terms has been applied carefully for the first time in the French Massif Central and has revealed that most of the Chaîne des Puys lavas known by the local *cheires* term are ‘a‘ā. Nevertheless, the Royat F3 flow and the Grosliers flow have been revealed to be pāhoehoe after observing clear diagnostic internal features. The use of Anisotropy of Magnetic Susceptibility (AMS) as recorded a vertical lava fill movement in an F3 lobe, providing clear evidence of lobe inflation. In the other Massif Central volcanic provinces other pāhoehoe lava flows have been detected with the observation of similar diagnostic inner features. The Roca Neyra lava flow, Limagne volcanism, presents numerous evidence of lava lobe stacking and the Jaujac lava flow, Ardèche volcanism, displays an impressive evidence of large-scale inflation with the formation of a sill in a cooling lava.

This chapter has emphasized that whatever the age of a lava flow its type can be determined, thus providing an estimate of how the flow has been emplaced. This can be done by not only considering surface evidence but also considering inner structural features and vesicle and phenocryst zonation. The qualitative use of a shear strain rate versus apparent viscosity diagram could bebetter quantified more lava flow compositions other than the Hawaiian are included.

Textural petrophysical investigation has been done in the second chapter to study breccias associated with lava flows such as clinkers and peperites.

Clinker; scoriaceous fragments associated with lava flows, were considered to be formed only by the rupture of the ‘a‘ā crusts. Nevertheless, clinker occurrences at several pāhoehoe flow bases have forced the reconsideration of this axiom by studying clinker from different flow contexts in using SEM.

‘A‘ā clinker, from Royat F1 and the Blanzat flows, have revealed a highly deformed vesicle and dyktytaxitic textures reflecting the classical way to form clinker in ‘a‘ā lava by crust disruption.

Pāhoehoe clinker, from the Grosliers and the Roca Nera flows, displayed adhering particles (formed by marly substrata fragmentation), blocky lava shapes, conchoidal fractures, spherical structures and a strange plagioclase microphenoctyst adherence texture. Those features are also described in literature examples of phreatomagmatic ash. Thus an additional phreatomagmatic way to form clinker is thus invoked through the contact of the flowing lava with a water-saturated basement.

The Royat F3 flow presents other fine-scale features with the existence of microfaults and associated striations at the flow base and sides, suggesting that whatever the flow type, clinker can be formed simply by shearing with the basement.

Peperites associated with lava flows are quite scarce and little studied. Their occurrences in three lava flows from Auvergne (Chateaugay, Pardines and Saint Gervazy) have allowed a detailed study in the field and with the SEM to explain their intriguing formation in such a context. Occurrences of quenched lava, blocky shapes such as spherical structures like in phreatomagmatic clinker, and the occurrence of fine marly basement particles in the peperitic matrix suggest also a phreatomagmatic interaction. In this case a more explosive phenomenon is suggested and a larger water-magma ratio than in the phreatomagmatic clinker.

This second chapter has reconsidered the different ways to form clinker in a lava flow recording the classical ‘a‘ā clinker formation due to crust disruption but also promoting

phreatomagmatic fragmentation as shearing brecciation. These results will find important implications in volcanic hydrogeology, as now it has beendemonstrated that ‘a‘ā are not the only water supply aquifers. This chapter has also emphasized the widespread occurrence of phreatomagmatism in lava flows, which can lead to clinker and to peperite formation and thus explosive features different than previously described rootless cones. This phreatomagmatic impregnation in lava flows should be further explored to complete our SEM textural database and above all will help clarify our appreciation of such a hazard.

A magnetism approach was done in the third chapter via the use of AMS. In order to perform good and as accurate as possible interpretations of AMS a methodology was proposed that can be applied for lavas, but also in any AMS study.

This procedure first uses the Curie Temperature, thin sections, chemical mapping, and FORC diagrams to identify the AMS phase carrier and to check for SD particles the presence of which will alter the AMS signal. Secondly the procedure makes a direct comparison between the AMS fabric and the microlite fabric to estimate the time acquisition of the AMS fabric and thus its significance concerning emplacement. So to check the feasibility of this methodology and the quality of the interpretations reached, it has been applied to two lava flows: Royat F2 and Royat F3.

After having described the AMS carrier mineralogy and its late stage acquisition with the relationship between AMS and microlite fabric; the results obtained and the interpretations have revealed different flow emplacement histories.

Concerning the Royat F2 flow, the magnetic lineation k_{max} and the degree of magnetic anisotropy A have been revealed to be an interesting tool for proposing a qualitative velocity profile in this 45,000 years old flow. The k_{max} imbrication changes with variations of A on a vertical profile and this led us to suggest a stack of several lava flow subunits, and thus a complicated resulting velocity profile. An explanation for this intriguing velocity profile has been proposed using zonation of vesicles and phenocrysts. The profile may indicate that each compartment has particular rheological properties allowing the development of variable velocities.

Concerning the Royat F3 flow, which also has a normal fabric (without SD particles), k_{max} is perpendicular to the apparent flow path. This clearly demonstarted the importance of knowledge of the magnetic state, without which this situation could have been considered has an inverted fabric. The study of the neighboring outcrops has shown that this perpendicular k_{max} orientation was caused by a stretching occurring when the flow had first halted to form an temporary lava front subjected to lateral stretching. Then, with the still incoming lava flux,

this ephemeral lobe broke up and deflated to form levees and the new lava input formed the final polylobate termination.

The two above examples have shown the feasibility of the proposed methodology. They have also demonstrated the use of the magnetic lineation and the degree of magnetic anisotropy as a tool to propose qualitative velocity profiles. Such profiles can be applied on each lava flow with a vertical sampling and it will be particularly relevant to perform such a study on the flood basalts, the emplacement of which is still matter of debate. The determination of lava velocity profiles will also improve our knowledge in lava flow emplacement. The observation that a flow is a stack of several subunits having different rheological properties, is important for modeling lavas and such data will eventually improving our knowledge for hazard mitigation. In the other studied case, the use of AMS has allowed the reconstruction of the late stage emplacement of a lava flow in detail. Continuing the use of AMS in other lava flows, using the developed methodology, will improve our knowledge of lava flow emplacement.

The themes tackled in the three chapters have provided several elements to improve knowledge of lava flow kinematics and deformation. If a single lava flow is subjected to the three approaches, its ‘a‘ā or pāhoehoe emplacement style can be identified. Also, the way it has formed its clinker or peperite will be constrained providing information on its rheological properties or the water-magma ratio encountered. Finally, the use of AMS can provide a qualitative velocity profile and reconstruct the late stage of emplacement of the flow. These interpretations will be improved if further research is made in these three main topics in other lava flows and other contexts.

ABSTRACT

Kinematics and deformation in lava flows are addressed using three different approaches: descriptive volcanology, petrophysics and magnetism.

Pāhoehoe and ‘a‘ā are two terms used in volcanology, first used to differentiate lava surfaces, but then to describe two different emplacement styles. Pāhoehoe lavas emplace themselves as a lobe stacks that may coalesce. In contrast, ‘a‘ā lavas emplace en masse and form upper clinker by rupture crust of their. This crust can reach the flow base by roll-over caterpillar motion. As they have different modes of emplacement, they contain in their interiors several diagnostic features that make it possible to discriminate the type in old lava flows where surfaces are missing or covered. ‘A‘ā flows present clinker and highly deformed vesicles, whereas pāheohoe flows display slightly deformed vesicles, lobe stacks and particular zonations in vesicles and phenocrysts. These discriminatory characteristics allowed the attribution of lava types to several old lava flows. This has provided constraints on emplacement histories, particularly in the French Massif Central where some pahoehoe flows have been clearly identified.

Breccia associated with lava flows has been studied in detail, both in the field and in thin section. Detailed textural analysis, especially with scanning electron microscope (SEM) has revealed petrophysical information on breccia formation. These breccias include clinker (previously considered to be exclusive to ‘a‘ā lavas), fault cataclasites and peperites. The upper clinker are typical of ‘a‘ā flows, but lower clinker-like breccia can also develop in pāhoehoe flows according phreatomagmatism, or basal / lateral shearing. Peperites have phreatomagmatic features with more explosive textural patterns than clinkers. These breccia studies have revealed that phreatomagmatism is quite common during lava flow emplacement: the probability that a lava flow on its downslope movement encounters a water-saturated basement is quite high. This indicates that phreatomagmatic hazards associated with lava flows could be locally very significant.

A methodology for the correct use of Anisotropy of Magnetic Susceptibility (AMS) is proposed. This requires the determination of the AMS carriers and the AMS fabric time acquisition compared to the microlite fabric. This methodology has been applied to two lava flows to check the feasibility. The results show that AMS can be used confidently, with the methodology proposed. The results obtained are interpreted in terms of different emplacement scenarios. Interpretations include the establishment of a vertical qualitative velocity profile and the detailed reconstruction of the last emplacement stage of two lava flows.

A further improvement in understanding lava flow emplacement, with attendant hazard and aquifer knowledge improvement will be possible by continuing the investigation on the three topics on a broader range of lava flows, different compositions and environments.